University of Ioannina
Department of Chemistry
Section of Inorganic and Analytical Chemistry

Malgorzata Staninska

Synthesis, structures, spectroscopy and biological activity of metal complexes with drugs.

PhD thesis

Supervised by: Professor Dimitra Kovala-Demertzi

Ioannina 2009

Acknowledgement

The main part of research of presented PhD thesis was done in Inorganic Chemistry Laboratory of Ioannina Uiversity.

The idea of presented PhD thesis has come form Professor Dimitra Kovala-Demertzi, whom I am grateful, for giving me the opportunity to develop this work, for her support and guidance during these years.

I would like to thank Associate Professor Ioannis Plakatouras and Assistant Professor Achilleas Garoufis for valuable scientific comments.

Moreover I thank Assistant Professor Mavroudis Demertzis for his advices and help.

I highly appreciate financial support provided by State Scholarship Foundation (IKY), which gave me a scholarship for four years.

For crystal structure determinations I am grateful to Professor Alfonso Castineiras and Dr. Isabel Garcia Santos form University of Santiago de Compostela in Spain.

I also would like to thank Professor Alexandros Tselepis and Associate Professor Maria Lekka for neighbourly cooperation.

I thank NMR Center of Ioannina University, especially I like to thank Dr. Costas Tsiafoulis for 2D NMR spectra.

Furthermore many thanks go to Lector Anastasia Badeka (MS spectroscopy), Dr. Christina Papachristodoulou (XRF) and Dr. Ibrahim Ozturk (elemental analysis).

For taking care of my administrative cases, many thanks goes to Freideriki Masala.

Special thanks go to MA Alexandra Primikiri and MA Anastasia Galani who were always there for me when I needed them.

I thank to members and former members of the research group: Dr. Vasiliki Dokorou, Dr. Angeliki Galani, MA Alexandros Alexandratos, Anastasia Karagiorgou, Anastasia Purnara for any help.

Besides I would like to thank Dr. Marek Surowiec, Dr. Alexandrou Calin, Dr. Vladimiros Nikolakis, Dr. Georgos Hilas, MA Nikolaos Lekkas and MA Monica Bucsa.

Additionally I would like to thank friends of mine Aneta Bursztyka and Haris Chrysostomou.

Finally, very special thanks go to my family for very important support during these years.

Malgorzata Staninska

Ευχαριστίες

Η παρούσα διδακτορική διατριβή εκπονήθηκε στο Εργαστήριο Ανόργανης Χημείας του Πανεπιστημίου Ιωαννίνων.

Η ανάθεση του θέματος έγινε από την Καθηγήτρια κ. Δήμητρα Κόβαλα-Δεμερτζή την οποία και ευχαριστώ πολύ για την ευκαιρία που μου έδωσε, για την υποστήριξη και την συνεχή καθοδήγηση όλα αυτά τα χρόνια.

Θα ήθελα επίσης να ευχαριστήσω τον Αναπληρωτή Καθηγητή κ. Ιωάννη Πλακατούρα και τον Επίκουρο Καθηγητή κ. Αχιλλέα Γαρούφη για τις πολύτιμες επιστημονικές τους παρατηρήσεις.

Επιπλέον θα ήθελα να ευχαριστήσω τον Επίκουρο Καθηγητή κ. Μαυρουδή Δεμερτζή για τις συμβουλές του και την βοήθειά του.

Θα ήθελα επίσης να ευχαριστήσω για την οικονομική υποστήριξη το Ίδρυμα Κρατικών Υποτροφιών (Ι.Κ.Υ.) και την υποτροφία που μου χορηγήθηκε για τέσσερα χρόνια.

Για την ανάλυση των κρυσταλλικών δομών θα ήθελα να ευχαριστήσω την Καθηγητή Alfonso Castineiras και την Dr. Isabel Garcia Santos από το Πανεπιστήμιο Santiago de Compostela της Ισπανίας.

Επίσης θα ήθελα να ευχαριστήσω τον Καθηγητή κ. Αλέξανδρο Τσελέπη και την Αναπληρώτρια Καθηγήτρια κ. Μαριλέννα Λέκκα για την συνεργασία.

Θα ήθελα να ευχαριστήσω το κέντρο NMR του Πανεπιστημίου Ιωαννίνων και ειδικά τον Δρ. Τσιαφούλη Κωνσταντίνο για τα 2D φάσματα.

Επίσης θα ήθελα να εκφράσω τις ευχαριστίες μου στην Λέκτορα κ. Αναστασία Μπαδέκα (φασματοσκοπία MS), στην Δρ. Χριστίνα Παπαχριστοδούλου (XRF) και στον Dr. Ibrahim Ozturk (στοιχειακή ανάλυση).

Για την βοήθεια σε γραμματειακές υποθέσεις ευχαριστώ πολύ την κ. Φρειδερίκη Μασσαλά.

Ιδιαίτερα θα ήθελα να ευχαριστήσω την ΜΑ Αλεξάνδρα Πριμηκύρη και ΜΑ Αναστασία Γαλάνη που ήταν πάντα δίπλα μου.

Ευχαριστώ επίσης όλα τα υπόλοιπα μέλη αλλά και παλαιότερα μέλη της ερευνητικής ομάδας του εργαστηρίου: Δρ. Βασιλική Ντόκορου, Δρ. Αγγελική Γαλάνη, ΜΑ Αλέξανδρος Αλεξανδράτος, Αναστασία Καραγιώργου, Αναστασία Πουρνάρα για την βοήθειά τους.

Επίσης θα ήθελα να ευχαριστήσω τους Dr. Marek Surowiec, Dr. Alexandrou Calin, Δρ. Βλαδίμηρο Νικολάκη, Δρ. Γιώργο Χειλά, ΜΑ Νικόλαο Λέκκα και ΜΑ Monica Bucsa.

Επίσης θα ήθελα να ευχαριστήσω τους φίλους μου Aneta Bursztyka και Χάρη Χρυσοστόμου.

Τέλος, ιδιαίτερα θα ήθελα να ευχαριστήσω την οικογένειά μου για την ιδιαίτερα σημαντική υποστήριξή τους κατά την διάρκεια όλων αυτών των χρόνων.

Malgorzata Staninska

Contents

Introduction

I. Non-steroidal anti-inflammatory drugs (NSAIDs).

I.1 Classification and pharmacological profile.

Humans have been using **nonsteroid antiinflammatory drugs (NSAIDs)** in various forms for more than 3,500 years. They are still our favorite medicines.[1] Used in clinics throughout this century, NSAIDs continue to be an important therapeutic intervention for patients with disorders that cause pain, fever, or moderate inflammation.[2] The continued and widespread use of prescribed and overthe-counter (OTC) non-steroidal anti-inflammatory drugs (NSAIDs) remains an important cause of morbidity and mortality, and represents a significant and costly health problem.[3] They are called non-steroidal because their chemical structure declines from steroidal and are used to treat inflammation by suppressing the immune system (inflammation is one of the body's healing responses to trauma). All NSAIDs treat inflammation in a way similar to the mechanism of aspirin, the most well-known and oldest member of the class.[4] By the early 1900s, the main therapeutic actions of aspirin were known as the drug's antipyretic, antiinflammatory, and analgesic effects. In time, several other drugs were discovered with similar effects.[5] Despite their diverse chemical structures, these drugs share similar therapeutic properties. They alleviate the swelling, redness, and pain of inflammation; reduce a general fever; and cure a headache.[6] These are known as either ''aspirin-like drugs'' or ''NSAIDs''.[5] Some of the most widely used medicines today are aspirin and other such nonsteroidal anti inflammatory drugs (NSAIDs), which are well known for their pain-relieving, fever-reducing and anti-inflammatory effects.[7]

Non-steroidal anti-inflammatory drugs (NSAIDs) are a group of drugs of diverse chemical composition and different therapeutic potentials having a minimum of three common features: identical basic pharmacological properties, similar basic mechanism of action as well as similar adverse effects. Moreover, all drugs in this group exhibit acidic character. pK_a values are in the range of 3–5 (acids of medium strength).[1] NSAID molecules contain hydrophilic groups (carboxylic or enolic group) and lipophilic ones (aromatic ring, halogen atoms). In accordance with their acidic character, NSAIDs occur in the gastric juice in the protonated (lipophilic) form. Also in the small intestine, there are conditions favourable for absorption of weak acids. NSAID exist in highly ionized forms in plasma. Low values defining NSAIDs distribution volume (from 0.1 to 1) in tissues may be a proof of poor distribution of these drugs in extravascular systems.[1] All NSAIDs appear to be absorbed completely, have negligible first-pass hepatic metabolism, are tightly bound to albumin (all NSAIDs except piroxicam and salicylates are >98% albumin bound and have small volumes of distribution[2]. A very high degree of binding with plasma proteins is the result of favourable amiliphilic properties and accounts for the fact of displacing other drugs from protein binding of NSAIDs[1]. Patients with low levels of serum albumin (e.g., in cirrhosis or active RA) may have higher free concentrations of drug.[2] It has been suggested that the variation in both efficacy and tolerability of NSAIDs, are partly due to their differences in their physicochemical properties (e.g. ionization constants (p*K*a), solubility, partition coefficients), which determine their distribution in the body. This plethora of potential mechanisms may be, at least in part, a product of the different assay systems used to explore NSAID mechanisms (e.g., cell-free systems,

animal models, etc.) and the biochemical properties of the NSAIDs (their pKa, lipophilicity, protein binding, etc.).[8a]

Table I.1. Classification of nonsteroidal anty-inflammatory drugs proposed by Jones et all.[4]

- Carboxylic acids
  - Salicylic acids and esters
    - Aspirin
    - Aloxpirin
    - Benorylate
    - Salsalate
    - Diflunisal
  - Acetic acids
    - Phenylacetic acids
      - Diclofenac
      - Etodolac
      - Sulindac
    - Carbo- and heterocyclic acetic acids
      - Indomethacin
      - Ketorolac
      - Tolmetin
  - Propionic acids
    - Flurbiprofen
    - Ketoprofen
    - Tiaprofenic acid
    - Ibuprofen
    - Naproxen
    - Fenoprofen
    - Oxaprozin
    - Fenbufen
- Enolic acids
  - Pyrazolones
    - Phenylbutazone
    - Azapropazone
  - Oxicams
    - Piroxicam
    - Meloxicam
    - Tenoxicam
    - Lornoxicam
- Naphthylalkanone
  - Nabumetone
- Fenamates
  - Meclofenamic acid
  - Flufenamic acid
- COX-2 specific NSAIDs
  - Celecoxib
  - Rofecoxib
  - Valdecoxib/parecoxib
  - Lumiracoxib
  - Etoricoxib

In addition to an acidic group, all NSAIDs contain at least one aromatic ring system, while some NSAIDs, such as phenylbutazone, indomethacin, diclofenac, flurbiprofen and flufenamic acid, contain two aromatic rings twisted relative to each other. The enantiomeric forms of a drug refer to their optical activity. According to relatively recent convention, drugs with optically active asymmetric centers are labeled as “R” or “S” and as “(+)” or “(-)”. There are, in fact, clinically significant differences among NSAID enantiomers. Ibuprofen is marketed as a racemic mixture (half R[-] and half S[+]). Bradley et all. showed that the S(+) ibuprofen enantiomer accounts for most of ibuprofen’s analgesic potency in hip and knee osteoarthritis (OA), while the R(-) component adds little to correlations between the serum concentration of ibuprofen and the clinical response. Also of interest are the results of experiment with enantiomeric flurbiprofen. Flurbiprofen’s enantiomers were equally potent in antinociceptive animal assays, but R(-) flurbiprofen did not inhibit prostaglandin synthesis in vitro. It also caused only marginal amounts of gastric damage. Thus, R(-) flurbiprofen may be an effective analgesic without the side effect profile attendant upon cyclooxygenase inhibition. In contrast, the S(+) enantiomer may be a better antiinflammatory drug.[8]

This chemically diverse group of drugs, prototypically represented by acetylsalicylic acid (aspirin), are used for their analgesic, anti-inflammatory, anti-pyretic and cardio-protective properties[3].

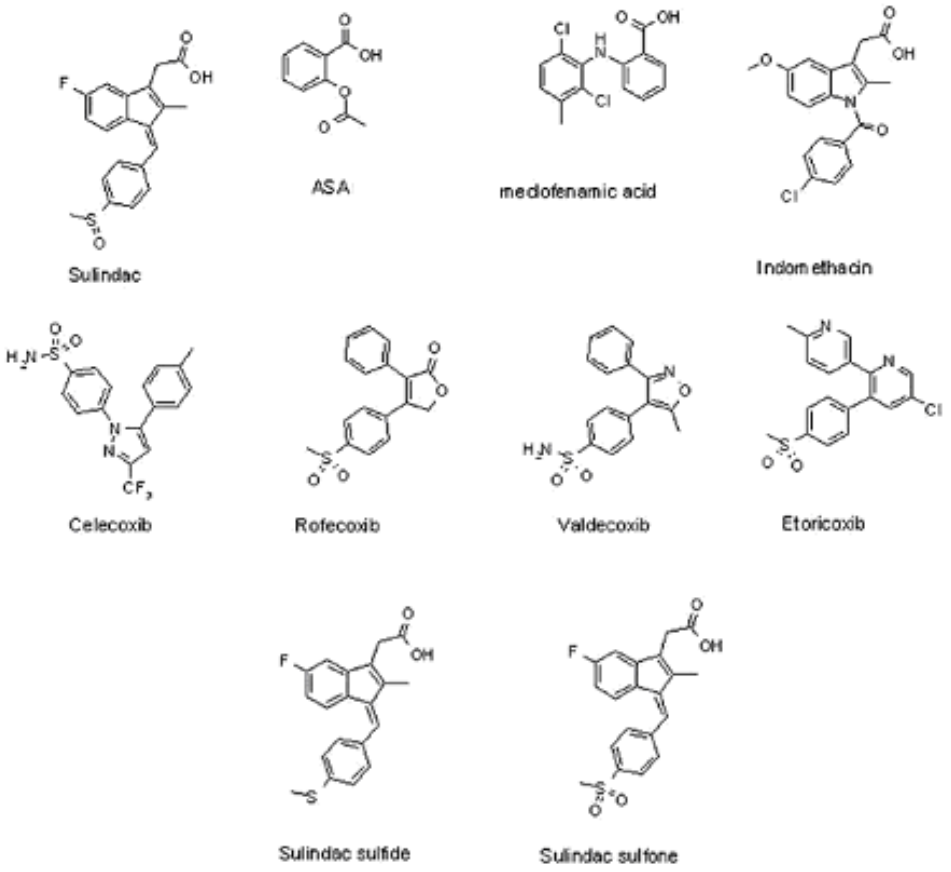

Figure I.1.. NSAIDs, COX-1/COX-2 inhibitors[sulinac].

NSAIDs can be divided into a number of groups.[4] The nonselective NSAIDs are mostly derived from carboxylic and enolic acids. The first COX-2 selective NSAIDs were celecoxib and rofecoxib, with the subsequent development of "second generation" COX-2-specific NSAIDS, including lumiracoxib and etoricoxib (**table I.1**).[4] Non-steroidal anti-inflammatory drugs, NSAIDs, from the carboxylic acid family, derivatives of N-phenylanthranilic acid, such as tolfenamic acid, diclofenac, mefenamic, flufenamic, and from the oxicam family, piroxicam, tenoxicam and lornoxicam, are widely used in inflammatory and painful diseases of rheumatic and non-rheumatic origin.[6] Non-steroidal anti-inflammatory drugs (NSAIDs) are a heterogeneous group of chemical compounds that show differences in both clinical response and pharmacokinetic profile[7]. Variability in the clinical effects of various NSAIDs has been ascribed to differences in mechanisms of action, i.e., some are more potent inhibitors of prostaglandin synthesis, and others may affect nonprostaglandin- mediated biologic events. Differential effects have also been attributed to variations in the enantiomeric state of a drug, as well as the pharmacokinetics, pharmacodynamics, and individual metabolism of specific products.[2] The principal mechanism of action of NSAIDs is cyclooxygenase inhibition and interference with the synthesis of prostaglandins. Cyclooxygenase inhibition, through actions on other mediators, may in turn have secondary effects,

including inhibition of neutrophil activation, leukotriene production, and T and B cell proliferation. Beyond that, NSAIDs have well-documented properties that are not dependent on arachidonic acid (prostaglandin) metabolis. These include inhibition of superoxide generation in neutrophils, inhibition of phospholipase C in mononuclear cells, inhibition of neutrophil aggregation, and, potentially, disruption of protein-protein interactions in the neutrophil plasmalemma.[8]

Epidemiological studies have shown that long term use of NSAIDs reduces the risk of developing Alzheimer's disease and delays its onset. Studies from the last years revealed that in addition to arthritis and pain, cancer and neurodegenerative diseases like Alzheimer's disease could potentially be treated with Cox-2 inhibitors.[10a] Certain NSAID agents have been claimed as being able in decreasing the onset of tumors in patients to whom the drugs have been administrated for prolong period of time. Recently, several other functions of this group of drugs have been identified which consist of chemoprevention, chemosupression, UV sensitization and UV-protection.[10b]

Alzheimer's disease is characterized by several changes in the brain, including the build-up of protein deposits known as amyloid plaques outside nerve cells, and the breakdown of neurons. The plaques consist of protein fibres, some 7–10 nanometres thick, that are mixed with small peptides called amyloid-b (Ab) peptides. Mature plaques also contain degenerating nerve endings, and are surrounded by active astrocytes and microglia — cells that help to clear up debris in the brain. The presence of these cells and certain inflammatory proteins has suggested that inflammation contributes to Alzheimer's disease.[10c]

Evidence from epidemiological studies has indicated a decreased risk for Alzheimer's (AD) and Parkinson's (PD) disease in patients with a history of chronic NSAID use. However, clinical trials with NSAIDs in AD patients have yielded conflicting results, suggesting that these drugs may be beneficial only when used as preventive therapy or in early stages of the disease. NSAIDs may also have salutary effects in other neurodegenerative diseases with an inflammatory component, such as multiple sclerosis and amyotrophic lateral sclerosis.[10a] Parkinson's disease has an important inflammatory component. Studies that fully explore the difference in inflammatory cascades among different neurodegenerative diseases are lacking, and could provide hints regarding the role of inflammation and the therapeutic value of NSAIDs. This cav notwithstanding, the use of nonaspirin NSAIDs has been associated with a 26% lower risk for PD. Particularly, ibuprofen users had reduced risk of PD compared with non-users. Several retrospective studies suggested that some of the drugs used to treat diseases such as rheumatoid arthritis have an unexpected benefit: they reduce the risk of Alzheimer's disease.[10a]

Several in vivo and in vitro studies in experimental models show the effects of NSAIDs on the main pathophysiological mechanisms leading to cartilage rapair and degradation in osteoarthritis (OA) and rheumatoid arthritis The articular inflammation and joint destruction that characterizes rheumatoid arthritis is the result of a complex interaction between cellular elements-that is, inflammatory cells, immunologlcally competent cells, synovial lining cells-and their soluble byproducts. The standard approach to the drug therapy of rheumatoid arthritis involves the initial use of simple analgesics and non-steroidal antiinflammatory drugs.

Some non-steroidal anti-inflammatory drugs (NSAIDs) such as acetylsalicylic acid, ibuprofen, diclofenac, naproxen sodium, mefenamic acid, tolfenamic acid and lysine clonixinate have also demonstrated efficacy in the acute treatment of migraine. Headache researchers identified the role of the prostaglandins in triggering an acute migraine attack.They also have assumed sides on whether migraine is a vascular or neurogenic disorder. The role of the vasoactive substances in migraine has also been contested. The combination of a triptan and a NSAID seems to decrease headache recurrence and increase the efficacy, being an interesting alternative in clinical practice to selected patients. The assessing the efficacy of a long-acting NSAID with proven efficacy in the acute treatment of migraine combined with Rizatriptan, as well as Rizatriptan (RI) associated with a traditionally effective NSAID was investigated. This prospective randomized study demonstrated that the combination of RI and a NSAID is associated with better efficacy, decrease of associated symptoms, and decrease on recurrence rates, compared to RI alone.

Therapeutic efficacy of NSAIDs in different types of strokes seems to be proved. The observation that NSAIDs may block thromboxame TXA_2 and prostacyclin PGI_2 synthesis with differential potencies raises the possibility of pharmacological modification of platelet-vessel wall interactions bt these drugs in cerebrovascular diseases. Topical nonsteroidal anti-inflammatory drugs have been used clinically to treat many skin conditions. Several NSAIDs are under development for the treatment of dermatological disorders.[11a]

New pilot study that the use of NSAIDs after radical retropubic prostatectomy (RRP) is a safe alternative that offers sufficient postoperative analgesia without an increased risk for postoperative hemorrhage.The analgesic efficacy of many of the current NSAIDs, such as naproxen, meloxicam, rofecoxib, acetaminophen, diflunisal, ibuprofen and ketorolac, has been documented using this pain model.since the pain is frequently confined to the surgical area with apparent inflammation. Administering the NSAIDs before surgical trauma has been proposed to be more effective in preventing the development of both peripheral and central sensitization after surgery, and many studies have been conducted to evaluate the pre-emptive analgesic efficacy of various NSAIDs zin different pain models.[11b]

I.1.1. Fenamates

Diphenylamine N-Phenylanthranilic acid

Figure I .2. Formulas of chemical compounds structurally related to diphenylamine-based NSAIDs.[7]

Fenamates are an important group of pharmaceutical compounds with anti-inflammatory and analgesic–antipyretic activity that are *N*-arylated derivatives of anthranilic acid (**Figure I.2**). Their mode

of interaction is as potent prostaglandin synthetase inhibitors. A common physical property of the fenamates is their general lack of solubility inwater and other common organic solvents which is influenced by their polymorphic form.[12a] Some of these have been characterized structurally. In all these crystal structures the molecules form hydrogen bonded dimers and the carboxylic acid group is almost coplanar with the phenyl group to which it is bonded, as observed in the two modifications of tolfenamic acid. It seems obvious that the conformation of the molecules is determined by steric interactions between the substituents on the phenyl groups. In meclofenamic acid, which has two equivalent chlorine atoms close to the amino group, the molecule is in a conformation in which the two phenyl rings are almost perpendicular, thus reducing the steric interactions.[12b] Meclofenamic acid is effective in providing temporary relief of the symptoms of arthritis, menorrhagia and it is also used to treat dysmenorrhea. The other fenamates are tolfenamic acid, niflumic acid and flufenamic acid, which are mainly used as analgesics and antipyretics and are on the market in many countries.[13] Fenamic acids are readily absorbed after oral administration and metabolized to two major and at least six minor metabolites. The drugs are metabolized by oxidation of the 3%-methyl group to a pharmacologically active 3%-hydroxymethyl metabolite, which may be further oxidized to an inactive 3%-carboxy metabolite. To a lesser extent, ring hydroxylation and monodehalogenation also occur. NSAIDs are a heterogeneous group of drugs, but many have a common carboxylic acid moiety.[14]

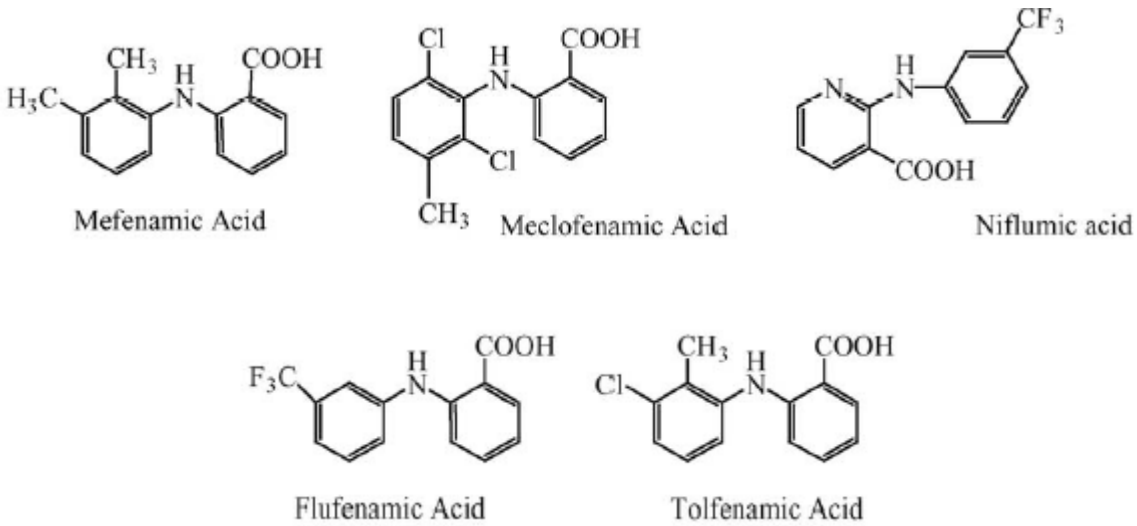

Figure I.3. Structures of fenamates.

A major biotransformation and elimination pathway for most carboxylated NSAIDs is conjugation with glucuronic acid catalyzed by the uridine diphosphoglucuronosyl transferase (UGT) superfamily of enzymes. It has been demonstrated that the N-phenylanthranilic acid derivatives flufenamic, mefenamic and niflumic acid are substrates for glucuronidation (**Figure I.4**) by human kidney cortical microsomes and recombinant human UGT1A9 and UGT2B7; NSAID- glucuronidating enzymes that are expressed in human kidney. Local formation of in particular mefenamic acid acylglucuronide, a reactive metabolite, may result in covalent binding to proteins within the renal cortex, potentially eliciting an immune response. Thus, this study has shown that human kidney metabolises mefenamic acid to an acylglucuronide. Additionally, it has been reported that mefenamic, flufenamic and niflumic acid are potent inhibitors of renal UGTs.[15] Fenamates have been shown to inhibit HL-PST (human liver phenol sulphotransferase). CYP2E1 and mycophenolic acid glucuronidation by human liver and kidney additional studies were undertaken to determine the universality of fenamates as potential inhibitors of renal glucuronidation using the UGT substrate 'probe' 4-methylumbelliferone (4-MU).[15] Mefenamic acid is the most powerful inhibitor of HL-PST. The molecular structures of mefenamic acid and tolfenamic acid differ for the substitution of a methyl group by a chlorine atom and the latter drug is a less potent inhibitor than the former one of HL-PST. The other three fenamates (nifumic acid, meclofenamic acid, flufenamic acid) have two or three atoms of chlorine or fluorine in their molecules and their IC_{50} are greater than those of mefenamic acid and tolfenamic acid.[13]

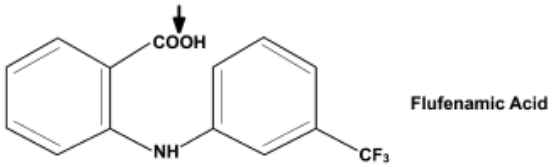

Figure I.4. Structures of N-phenylanthranilic acid derivatives showing site of glucuronidation.[15]

Substantial use of prescribed and OTC NSAIDs occurs in the treatment of heavy menstrual bleeding (menorrhagia). NSAIDs commonly used for this condition include aspirin, diclofenac, flurbiprofen, ibuprofen, indomethacin, meclofenamic acid, mefenamic acid and naproxen. Although, it is generally assumed that clinical efficacy is similar between NSAIDs, although there are individual women who seem to respond well to one agent but less well to another.[15] Mefenamic acid is one of the most effective first-line drugs with demonstrated benefit in comparison to placebo in the treatment of menorrhagia.

Recent study demonstrates for the first time that mefenamic acid and four other representatives of the fenamate NSAIDs (flufenamic, meclofenamic and mefenamic acid) are highly effective and potent modulators of native hippocampal neuron $GABA_A$ receptors as well as direct activation of neuronal $GABA_A$ receptors by mefenamic acid. Together these studies lead to the conclusion that fenamate NSAIDs should now also be considered a robust class of $GABA_A$ receptor modulators.

The wide use of Flufenamic Acid and Mefenamic Acid have prompted extensive literature on their determination in dosage forms and in biological fluids. Additionally the effects of fenamate NSAIDs on different ion channels have been studied widely. It has been shown that local administration of voltage-dependent or Ca^{2+}-activated K^+ channel blockers could prevent the fenamate- induced peripheral antinociception, suggesting that fenamate may open several K^+ channels at the primary afferent neurons. In the trabecular meshwork of the eye, flufenamic acid enhances current through maxi-K channels. Furthermore activation and inhibition of CLC-K channels (kidney CLC chloride channels) by distinct binding sites of niflumic acid and fenamate acid has been reported. However, the effect of fenamate NSAIDs on ion channels was considered to directly block ion channels, and few report were concerned with the main mechanism that mediates fenamate-induced inhibition of cyclooxygenase.[16] Fenamates represents until now the unique tool able to open and to block renal CLC-K channels and thus provides a starting point for the identification of drugs either with diuretic action or useful in the treatment of type III Bartter's syndrome, a disease characterized by severe salt wasting and hypokalemia. A number of research studies aimed provides insight into the mechanisms of activation and inhibition anion and cation chanels by fenamates[6].

Mefenamic acid

Mefenamic acid [(2-[2,3-dimethylphenyl]amino)benzoic acid], **figure I.5** is used to treat pain from rheumatic disease, soft tissue injury (Insel 1996) and dysmenorrheal as well as within ten years of marketing, cases of non-oliguric renal failure were reported with mefenamic acid.[13] Two polymorphic states of mefenamic acid are reported. Two crystalline modifications: a white form, polymorph I, and a green form, polymorph II.[12a]

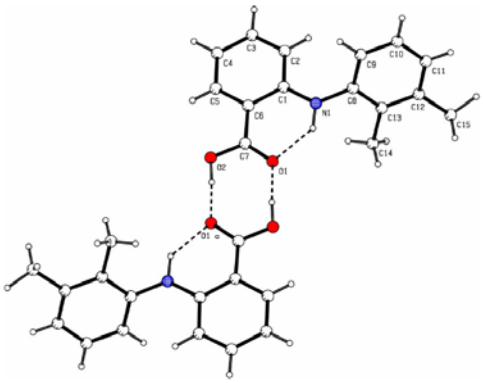

Figure I.5. . The structure of $Hmef^{mef}$

Histological examination provided evidence of renal papillary necrosis (RPN) in some individuals while in others nephrotoxicity was consistent with allergic interstitial nephritis. The latter is often characteristic of an immune mediated response to irreversible binding of either a drug or its

metabolites to various cell proteins.[15] Therapeutic potential of mefenamic acid in Alzheimer's disease and its mechanisms of action was investigated. In vitro results suggest that mefenamic acid exerts a neuroprotective effect. In addition, mefenamic acid could promote cell survival by up-regulating the expression of the antiapoptotic protein Bcl-X_L. Furthermore, it was founded that mefenamic acid improves learning and memory impairment in an $A\beta_{1-42}$ infused Alzheimer's disease rat model. Mefenamic acid (MFA) has anti-convulsant and pro-convulsant effects in vivo, and has been shown to potentiate and inhibit GABAA (g-aminobutyric acid) receptors in vitro. Finally, it was reported that mefenamic acid provided neuroprotection against b-amyloid ($A\beta_{1-42}$) induced neurodegeneration and attenuated cognitive impairments in this animal model of Alzheimer's disease. The authors proposed that neuroprotection may have resulted from inhibition of cytochrome c release from mitochondria and reduced caspase-3 activation by mefenamic acid.[17]

Tolfenamic acid

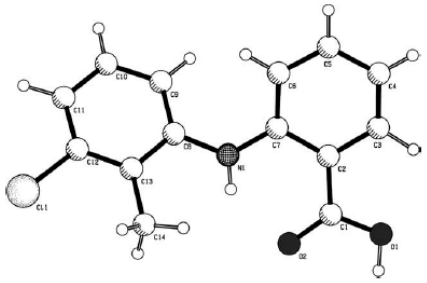

Figure I.6. The structural representation of tolfenamic acid.[18]

Tolfenamic acid (2-[bis(3-chloro-2-methylphenyl)- amino]benzoic acid or N-(3-chloro-2 methylphenyl)anthranilic acid), (**Figure I.6**) is a potent, well-tolerated non-steroidal anti-inflammatory drug (NSAID) with a low gastroulcerogenicity, a low overall toxicity and high therapeutic indices.[18]

X-ray crystal structure investigations of tolfenamic acid revealed the existence of two polymorphic forms containing the molecule as different conformers. The only significant difference between the two structures is found in the geometry of the amino group. Both modifications of tolfenamic acid form hydrogen bonded dimers in the crystal as frequently observed for carboxylic acids. In addition to this intermolecular hydrogen bond both conformers of tolfenamic acid seem to be stabilized by an intramolecular hydrogen bond between nitrogen of amino group and oxygen of carboxylic group.[12b]

It possesses analgesic and anti-pyretic properties as demonstrated in several animal models and has shown good results in long-term treatment of rheumatoid arthritis and osteoarthritis. Tolfenamic acid (TA) it is used to treat inflammatory and pain-causing diseases of rheumatic and non-rheumatic origin. Tolfenamic acid has also been used extensively in both human and veterinary medicine. Recently, its rational use in combination with the antimicrobial fluoroquinolone drug marbofloxacin has been proposed.[18] Some nonsteroidal anti-inflammatory drugs (NSAID) have also

demonstrated efficacy in treating migraine attacks. There is evidence that the combination of a triptan and a NSAID decreases migraine recurrence in clinical practice. Tolfenamic acid is a traditional NSAID with proven efficacy in the acute treatment of migraine. Its combination with effectives, fast acting drugs as rizatriptan or sumatriptan could decrease headache recurrence and increase the efficacy.[19a] Tolfenamic acid is practically insoluble in water, thereby making formulations problematic, regardless of the administration route used. Tolfenamic acid (TA)was found effective in the treatment of chronic and acute painful locomotor syndromes in the dog and in the prevention of oedema after mammectomy in bitches. The studies of the efficacy of TA in preventing postoperative pain shown significantly less postoperative pain in TA-treated animals.In an attempt to enhance its bioavailability, some results were presented. Taking into account the emerging pharmacological uses of tolfenamic acid, further investigation will be carried out in this direction.[19b] There seem to be no previous studies on the effect of fenamates on the activity of CYP enzymes. CYP1A2 is one of the major drug metabolizing enzymes in human beings, and its relative abundance in the liver is about 13% of the total cytochrome P450 (CYP) content. Typical competitive CYP1A2 (phenacetin O-deethylation) inhibitors are relatively small molecules containing, e.g., methyl and chloro substitutions, like tolfenamic acid. Recent study, tolfenamic acid was found to be a potent inhibitor of phenacetin O-deethylation in vitro when studied without albumin. The inhibition of CYP1A2 by tolfenamic acid was almost as strong as that by fluvoxamine and considerably stronger than that by ciprofloxacin both of which are also potent CYP1A2 inhibitors in humans. On the other hand, tolfenamic acid doesnot inhibits CYP1A2 when studied without albumin in vivo. This apparent discrepancy is due to the high protein binding of tolfenamic acid.[20a]

Tolfenamic acid has been the subject of several papers in the recent years dealing with its polymorphism[12a], the formation of diorgatonin derivatives and binuclear copper(II) complexes.[18]

Meclofenamic acid

Meclofenamic acid, 2-[(2,6-dichloro-3-methylphenyl)- amino]benzoic acid is a non-steroidal anti inflammatory drug (NSAID) and a structural isomer of the widely used analogue diclofenac.[21] Furthermore this agent for local and systemic application reduce the pain and swelling associated with arthritis by blocking the metabolism of arachidonic acid by the enzyme cyclooxygenase (COX) and thereby the production of prostaglandins.[7] As well as agent agent applied either topically or systemically for gout, ankylosing spondylitis, menorrhagia. Besides, drug which has been used clinically also have negative side effects such as gastrointestinal ulceration and bleeding.[21] Meclofenamic acid is a nonselective inhibitor of the COX isoforms.[15] In the quest for search of selective COX-2 inhibitors, the concept of design analogues conventionally available NSAIDs appeared. Biochemically based strategy for the facile conversion of carboxylatecontaining NSAIDs was described. The facile nature of this strategy is evident from the observation that a single chemical derivatization step (amidation or esterification) generates an impressive array of potent and highly

selective COX-2 inhibitors with oral antiinflammatory activity. Thus, studies on amide derivatives of the NSAID meclofenamic acid as COX-2-selective inhibitors were disclosed.[23a] Ion channels are also the targets of meclofenamic acid. Increase in potassium channel activity generally reduces neuronal excitability, thus making potassium channel openers potential drug candidates for the treatment of diseases linked to neuronal hyperexcitability. In all, properties of meclofenamic acid toward the brain KCNQ2/Q3 channels provide this compound potentially constitute novel drug templates for the treatment of neuronal hyperexcitability including epilepsy, migraine, or neuropathic pain.[23c] Meclofenamic acid inhibits the proliferation, clonogenic activity and migration of human aortic smooth muscle cells (haSMCs). If a sufficient dose of meclofenamic acid can be applied systemically or by local drug delivery it could be a valuable substance to prevent restenosis after angioplasty. Percutaneous transluminal angioplasty (PTA) is an established therapy for revascularization of coronary artery disease as well as for arteriosclerotic disease of the peripheral arteries.[23d] Among the NSAID, which are so called class II drugs with low solubility, Meclofenamic acid is aromatic organic compound with easily ionizables carboxylate groups, thus making it suitable for being intercalated between the hydrotalcite layers. Intercalation increases solubility and might have also beneficial effects by decreasing the side effects of the drugs.[23e]

Flufenamic acid

Flufenamic acid, (N-[3-(trifluoromethyl)-phenyl]- anthranilic acid)one of a series of N-phenylanthranilic acid derivatives synthesised during the early 1960s, was the first fenamate to undergo clinical trial as an antiinflammatory drug. It was followed closely by mefenamic acid , meclofenamic acid and niflumic acid.[15] Flufenamic acid, belongs to the class of non-steroidal anti-inflammatory drugs, NSAIDs, which are clinically used against a wide range of acute and chronic disorders. The therapeutic activity of these analgesics is believed to be due to their ability to inhibit the biosynthesis of prostaglandins by competitive interaction with the cyclooxygenase–arachidonic acid complex or by radical quenching agents that interfere with the initiation of the cyclooxygenase reaction.[24] The crystal structure of flufenamic acid and of flufenamic acid with prostaglandin D (2) 11-ketoreductase (AKR1C3) has been reported. Flufenamic acid is a compound with a large number of known polymorphs (**figure I.7**). At least eight forms are known.[24] White form I and yellow form II can be easly prepared by crystallization. Both crystal structures are known and in both forms individual molecules form dimer via hydrogen bonding. Additionally, flufenamic acid produces inhibition of a variety of ion channel responses in a range of tissues.[24] However flufenamic acid was initially identified as an anti-inflammatory drug, consequently it was also found an inhibitor of cyclooxygenase (Cox). Beyond its effects on prostaglandin synthesis, this drug has been used more recently as a cation channel antagonist. In 1989 Gogelein and Pfannmulle were the to first demonstrate that FFA inhibited nonselective cation channels, specifically in rat pancreas. Subsequently this agent has been employed as a cation channel blocker in nonneuronal preparations as well as in neurons from both vertebrates and invertebrates. A calcium-activated non-selective (CAN) cation current (I_{CAN}) plays a crucial role in

important functions in many neurons because of its involvement in generating a maintained depolarization of the cell, such as during bursting activity of pacemaker neurons. Flufenamic acid has been utilized as a blocker of (I_{CAN}) in a number of cell types. Following study examined the effects of FFA on membrane currents and intracellular Ca^{2+} in cultured bag cell neurons. Clearly FFA can alter the function of numerous membrane proteins; as such, the mechanism of FFA cation channel block in other systems may be related to how it alters plasma membrane, and perhaps intracellular, ion channels. In some ways, FFA has been seen as a gold-standard for cation channel blockers.

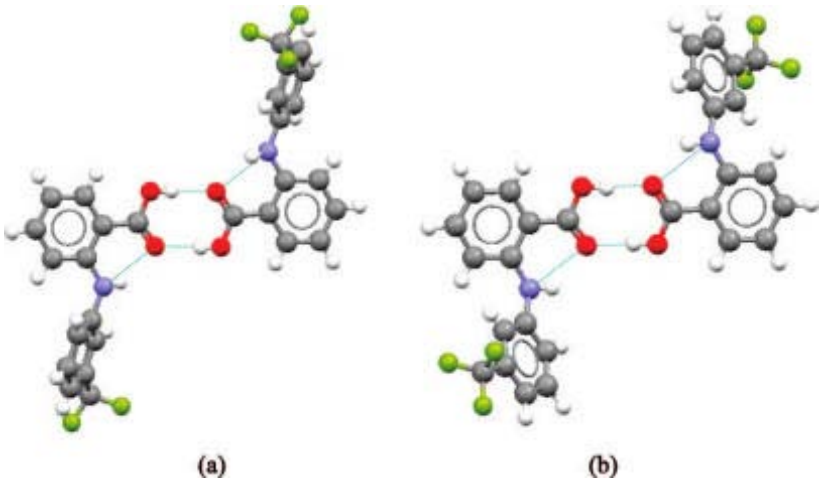

Figure I.7. Crystal packing motifs of flufenamic acid (a) form I and (b) form III, showing intra- and intermolecular hydrogen bondings[24].

However, recognizing that this drug may set off other intracellular or biophysical events, its use needs to be tempered with appropriate controls. Despite this, FFA could be employed as a tool for intentionally releasing intracellular Ca^{2+} or triggering certain currents. FFA is widely used as both a Cox inhibitor and a cation channel antagonist. Given that this drug has the potential to exert broad-spectrum effects on neuronal function, its use needs to be judicious. Alternatively, FFA may prove of value yet again as a means to activate specific conductances or cause the release of intracellular Ca^{2+} when warranted. That FFA influences a number of neuronal properties needs to be taken into consideration when employing it as a cation channel antagonist.[25] Finally, several authors have pointed out development of flufenamic acid as efficient enzyme inhibitor (beside of COX inhibitor) thus it could be a valuable way to block the potentially harmful enzymatic activity. Flufenamic acid was selected as a lead compound in a process aiming to design myeloperoxidase inhibitors. Myeloperoxidase (MPO) is a key enzyme belonging to the complex defense system against exogenous aggressions. However, MPO is liable to be released in extracellular fluids during an oxidative stress and this so-called 'circulating' MPO has been suggested to be involved in different pathogenic conditions such as those of chronic inflammatory syndromes, atherosclerosis, end-stage renal disease or neurodegenerative diseases. This drug that has anti-inflammatory properties linked to

cyclooxygenase (COX) inhibition has indeed been reported as an efficient inhibitor of the chlorinating activity of MPO at a micromolar range during the screening of compounds belonging to the same therapeutic class.[26]

I.1.2. Oxicams

Oxicams are a group of NSAIDs derived from the benzene(thieno)thiazine heterocyclic system, where the group of N-heterocyclic carboxamide include the triazine sulphur, and in position 4 there is an enolic group. Condensation of benzene ring or thiophene with the heterocyclic system as well as substitution of the amide group in position 3 imparts acidic properties to the enolic group. The structures of oxicams are illustrated in **Figure I.8**[1]. Piroxicam, and isoxicam are shown to differ only in their amide substituents, namely thiazole, pyridyl, and isoxazole ring systems, respectively. Tenoxicam, like piroxicam, has a pyridyl ring; however, the benzothiazine moiety is substituted with a thienothiazine group.[28a] The molecular structure of the oxicams consists of a co-planar arrangement with hydrophobic areas and hydrophilic centres. From a comparison of tenoxicam and piroxicam it is evident that the substitution of the benzothiazine ring by a thienothiazine ring results in a less hydrophobic (more hydrophilic) molecular structure for tenoxicam, as compared to the lipophilic character of piroxicam.[28b]

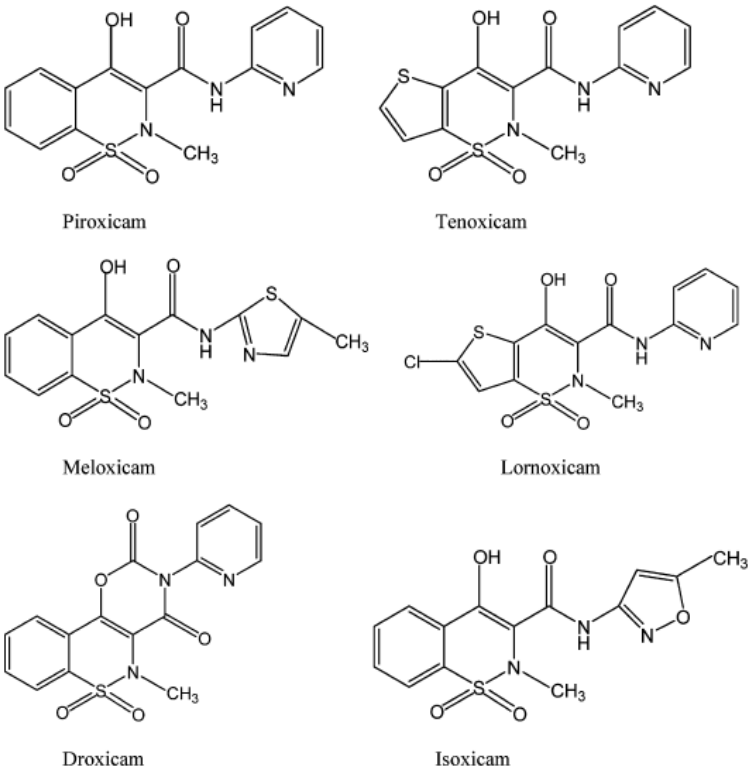

Figure I.8. Chemical structures of oxicams.[1]

Oxicams are non-steroidal antiinflammatory drugs (NSAIDs) which exhibit a specific pharmacokinetic behavior, namely a high percentage of protein binding, a low apparent volume of distribution (always lower than the volume of body-exchangeable water, 0.6 L kg^{-1}), and a long plasmatic half-life (>20 h). Piroxicam and tenoxicam are zwitterions in the pH range 2-5 and anions at pH 6 and above. Meloxicam is a zwitterion in the pH range 1-4 and an anion above pH 5. In contrast, isoxicam is mainly neutral below pH 4 and mainly anionic above. Therefore, all oxicams will be mainly anionic at physiological pH. Such properties are expected to markedly influence distribution and tissue penetration. NSAIDs seem to cause headaches and dizziness in a relatively small number of recipients. These reactions are commonly observed with indomethacin, whereas few central nervous reactions have been reported for oxicams.[28c]

More recent drugs such as several of the oxicam family (tenoxicam, lornoxicam, piroxicam and meloxicam) are nowadays rather frequently prescribed because they specifically inhibit the 2-isoform of cyclooxygenase, which could imply a lower incidence of undesirable side-effects such as gastric intolerance. It is of interest to more precisely assessing NSAID from the oxicam family capacity to interact with ROS. According to this some *in vitro* studies are reported in the literature considering the oxicams scavenging profile against superoxide anion ($O_2^{\bullet -}$), hydroxyl radical ($^{\bullet}OH$), hydrogen peroxide (H_2O_2),hypochlorous acid (HOCl) and peroxyl radicals and ($ROO^{\bullet}$) as well. Several cyclooxygenase-2 inhibitors have been developed such as celecoxib, rofecoxib or previously, meloxicam. The latter is an NSAID belonging to the enolic acid group of the oxicam family, and has been estimated to have a 3- to 77-fold greater affinity for cyclooxygenase-2 than for cyclooxygenase-1. This limited selectivity has led to meloxicam's description as a preferential cyclooxygenase-2 inhibitor.Three oxicam NSAIDs piroxicam, meloxicam and tenoxicam) can induce fusion of liposomes and lead the process to completion. This is a unique property of oxicam NSAIDs, which is not shared by NSAIDs belonging to other chemical structural groups. The three oxicam drugs used here show differential fusogenic behavior. Drugs belonging to other structural groups do not induce fusion indicating that the chemical structure plays an important role. Somet study compares the influence of the two structurally closely related NSAIDs piroxicam and meloxicam on the histamine release of mast cells from native and actively sensitized rats. Both of them could inhibit antigen-induced histamine release, with 34%, 27% inhibition , piroxicam (100 μM), meloxicam (100 μM), respectively.[29]

Lornoxicam

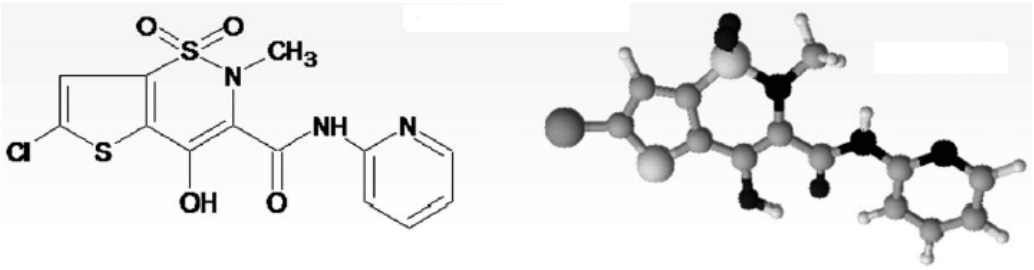

Figure I.9. Chemical and molecular 3D structures of lornoxicam.[30]

Lornoxicam, [(8-chloro-4-hydroxy-2-methyl- 2-pyridyl-2H-thieno[2, 3-*e*]-1, 2-thiazine-3- amide-1,1-dioxide] (also known as chlorotenoxicam) (**Figure I.9**) is a newly developed thienothiazine derivative of the oxicam class of NSAIDs, the use of which is increasing. Lornoxicam leads to inhibition of both COX-1 and COX-2 without a clear selectivity. Anti-inflammatory and analgesic properties of lornoxicam have greater potency, and it also prevents gastrointestinal side effects as compared to other NSAIDs . Lornoxican is a yellow crystalline substance with a dissociation constant (pKa) of 4.7. As the member of the oxicam class, it has pharmacokinetic and pharmacodynamic properties similar to those of the often-used drug piroxicam however it has with more potent clinical properties Lornoxicam has also been shown to inhibit the cyclo-oxygenase enzyme 100 times more than tenoxicam and 40 times more than piroxicam. It has been shown to be effective for joint pain and postoperative pain.Its favourable pharmacological profile: short plasma elimination half-life of 3–5 h thus it is rapidly eliminated and good gastrointestinal tolerability has fostered its increasing use also in patients with postoperative pain. Aside from analgesic, antipyretic, and anti-inflammatory effects, lornoxicam shows to be effective to various degrees in different pain models.[30]

Lornoxicam are currently available non-steroidal antiinflammatory drugs (NSAIDs) that have been shown to be effective to various degrees in pain relief when administered either pre-emptively or postoperatively. Pre-emptive administration of lornoxican proved to be effective in the management of pain following the surgical removal of impacted third molar teeth. Furthermore study revealed a significantly low incidence of adverse effects of the lornoxicam administration.[11b] It has been shown to be as effective as morphine, pethidine (meperidine), and tramadol in managing pain after several types of major surgery (eg, lumbar disk surgery, dental surgery, hysterectomy). Furthermore lornoxicam is more potent than many other nonopioid analgesics The analgesic efficacy and tolerability of lornoxicam, at differing doses and routes of administration, have been compared with other analgesics in several studies. In comparision with paracatamol, lornoxicam has the same analgesic effects after gynecologic surgery.The efficacy of lornoxicam and diclofenac were similar in postoperative pain management after cardiac surgery. Both drugs were well tolerated.[30b] It was

demonstrate the effect of preoperative administration of Lornoxicam on haemodynamic changes during laryngoscopy and tracheal intubation in the elderly.[30d] Lornoxicam may therefore be considered to be safer than the other NSAIDs regarding use in Shock wave lithotripsy (SWL). Lornoxicam is 10 times more potent than tenoxicam or piroxicam and the high GI tolerance and low side effect profile make it a good alternative to the current NSAIDs used for SWL analgesia.[30] Studies have shown that lornoxicam inhibits polymorphonuclear (PMN) leukocyte migration,superoxide release from human PMN leukocytes and nitric oxide release from macrophages. It was also demonstrated that lornoxicam can inhibit oxidative tissue damage in the trachea and the lungs.[30f]

Finally, side effects of lornoxicam (oral route) have been well documented.[30f] On the other side intravenous administration of a mixture of lornoxicam and nitroglycerin was investigated. The main result was that the chronic coadministration of lornoxicam and nitroglycerin prevents gastrointestinal and renal side effects compared to that of lornoxicam alone in rats. renal side effects compared to that of lornoxicam alone in rats. It was also been foun that nitroglycerin enhances the antioxidative effects of lornoxicam and different mechanisms might also play role to prevent side effects.[30c]

Isoxicam

Isoxicam is the product of an independent drug discovery program, set up in 1966 by Warner-Lambert, to search for novel nonsteroidal anti-inflammatory drugs (NSAIDs) of the non-carboxylic acid type.[31a] (4-hydroxy-2-methyl-N-5-methyl-3-isoxolyl-2H-1,2-benzothiazine-3-carboxamide-1,1-dioxide) is a potent , orally active, long life non steroidal anti-inflammatory drug, highly effective in relieving the symptoms of rheumatoid arthritis and degenerative joint disease.[1] In comparison with other NSAIDs, isoxicam is only a week inhibitor of cyclo-oxygenase, and demonstrates no inhibitory activity against 5-lipoxygenase.[31a] Side effects can occur with all medications, and the most important side effects that have been reported with isoxicam are hepatic toxicity and skin toxicity. The importance of sensing isoxicam might benefit for elder homecare system especially Stevens-Johnson syndrome (SJS) or toxic epidermal necrolysis (TEN). A few numbers of techniques exist for the determination of isoxicam in biological fluids, including high performance liquid chromatography and liquid chromatography–tandem mass spectrometry.[10b]

Several studies have shown the drug to be efficacious in man at a dose of 200 mg/day. Isoxicam is well absorbed orally, with peak plasma concentrations achieved at approximately 5-10 h. It is highly protein bound (ca. 98%), with a mean elimination half-life in man of 31 h. The half-life for isoxicam is somewhat shorter than that for piroxicam and tenoxicam. Elimination half-life is also prolonged in rats, dogs, and monkeys. In man and animals only small amounts of drug are excreted unchanged in urine. Administration of isoxicam to patients with various degrees of hepatic dysfunction did not significantly alter its elimination half-life. A decrease in plasma protein binding of isoxicam in patients with liver disease was observed and may explain the considerable intersubject variability observed in elimination half-lives.[28a] Initial metabolic disposition studies in rat, dog, monkey, and man resulted in

the identification of a hydroxymethyl product as the major *in vivo* metabolite. Significant quantities of a [(5-methyl-3-isoxazolyl)amino]oxoacetic acid metabolite was also detected. Identification of this metabolite led to postulate a mechanism involving oxidative cleavage of the benzothiazine ring for its formation. Later open-ring sulphonarnide, along with N-methylsaccharin and saccharin, was found as metabolites of isoxicam.[31b]

The pharmacokinetics of isoxicam have been intensively investigated in a series of single and repeated dose pharmacokinetic studies in healthy young and elderly subjects as well as elderly patients with rheumatoid arthritis. Results from these studies have indicated that the pharmacokinetic disposition of isoxicam does not alter with age. Interactions of isoxicam with oters drugs were investigated, using a variety of pharmacodynamic and pharmacokinetic designs, no clinically significant interactions have been noted with antacids, cimetidine, digoxin, propranolol, glibenclamide, phenytoin or alcohol. On the other hand, isoxicam did potentiate the anticoagulant effect of warfarin, a phenomenon common to other NSAIDs. Furthermore, the isoxicam plasma level was reduced in the presence of anti-inflammatory doses of aspirin. This also happens with other NSAIDs, but is of dubious clinical significance.[31a]

I.2. Arachidonic acid oxygenation by cyclooxygenase (COX). Mechanisms of catalysis and inhibition.

Nonsteroidal anti inflammatory drugs (NSAIDs), work mainly by inhibiting the formation of prostaglandins — potent lipid messenger molecules — and they do this by blocking cellular cyclooxygenase enzymes.[32] In addition to catalyzing a fascinating metabolic transformation, COX is an enormously important pharmacological target.[33] Back in 1971 only one cyclooxygenase was known, and Vane [34] discovered that it is inhibited by NSAIDs.It was demonstrated that their relative inhibitory potency *in vitro* correlates to their antiinflammatory activity *in vivo*. This not only explained the beneficial activity of NSAIDs but also their side effects such as gastrointestinal toxicity and bleeding because prostaglandins and related molecules (*i.e.* thromboxane) are involved in a very broad range of physiological and pathophysiological responses.[33]

The term cyclooxygenase (COX)1, 2 was coined to describe the enzyme that carried out this complex chemical transformation, and its role was confirmed by the isolation of prostaglandin endoperoxides in 1973.[33] In 1991, several research groups working independently discovered a second isoform of cyclooxygenase, namely, cyclooxygenase-2 (COX-2), which was found to have different functions and a distinct identity from cyclooxygenase-1 (COX-1).[35]

The discovery of a second gene (*COX-2*) coding for cyclooxygenase and the demonstration that its protein product is distributed differently from the originally discovered enzyme (COX-1) raised the possibility that some of the beneficial effects of NSAIDs may be separable from their side effects by development of isoform-selective inhibitors.[33] Two of cyclooxygenase enzymes have previously been discovered. It has long been a puzzle, however, that acetaminophen, otherwise known as paracetamol, works well to relieve pain and reduce fever, yet is not an effective antiinflammatory

medicine (although it is often classified as an NSAID). Also, it does not markedly inhibit the two known cyclooxygenases. This suggested the existence of yet more cyclooxygenases[32], and Simmons and colleagues[36] discovered, in cell lines, some forms of COX-2 with slightly different properties. Few years ago the Simmons group[37] has discovered an entirely new cyclooxygenase, COX-3, which they believe to be the acetaminophen-sensitive species. They have also found two smaller forms of COX 1.Recently, a COX-1 variant protein, named COX-3 (Cyclooxygenase-1b), sensitive to inhibition with acetaminophen, was characterised, cloned and expressed.[35]

Members of the cyclooxygenase (COX) family are presented in **table I.2** Cyclooxygenase (**COX**) or prostaglandin endoperoxide synthase (**PGHS**) is the key enzyme in the synthesis of prostaglandins from their precursor, arachidonic acid.[35]

The original enzyme COX-1, (dubbed COX-1), is expressed constitutively, including in platelets and the stomach and it is required for the production of PGs involved in basic housekeeping functions throughout the body. By contrast, COX-2 is generally expressed under specific circumstances, largely as a result of inflammation: it is induced by cytokine protein sassociated with inflammation, and by injury, seizures, and so on. However, in the brain, kidneys and some other tissues, COX-2 is expressed constitutively, illustrating the multifunctional nature of these enzymes. For example, the brain COX-2 gene is expressed as a result of synaptic activation in a totally physiological event.[32] COX-2 is expressed normally in several tissues, whereas elsewhere its production is increased rapidly in pathological conditions.In the brain, prostaglandin E_2 produced by COX-2 specificallyregulates the synaptic plasticity that is relevant to memory.[38] COX-2 converts anandamide and 2-acylglycerol — lipids that bind to cannabinoid receptors on specific nerve cells — into prostaglandin ethanolamines this may be involved in pain mechanisms.[32] In normal cells, COX-1 is thought to be constitutive, whereas COX-2 is up-regulated in response to inflammation or injury. However, in the spinal cord, both COX- 1 and COX-2 are present in a constitutive manner. Several splice variants of COX-1 and COX-2 enzymes have been reported. A splice variant of COX-1 was reported in human fibroblasts, another COX-1 splice variant containing an intronic sequence was described in rat tracheal epithelial cells rat stomach and rat colorectal tumors. Another COX-1 splice variant was shown to be present in endothelial cells in chicken embryo fibroblasts. As well as in human myometrium.A COX-2 splice variant was also found in platelets.[39]

In 2002, a new isoform of COX-1 that is sensitive to acetaminophen was identified in canines and designated as **COX-3** while COX-3 mRNA expression was more recently shown in rat spinal cord tissues. The discovery of COX-3 in canines seemed to offer a key to unlocking the long-sought-after mechanism of action of acetaminophen. Some findings believes that the name COX-3 should be reserved for the product of an independent third cyclooxygenase gene, which has not yet been identified. Instead of COX-3 (a splice-variant of COX-1), it is endorsed the term **COX-1b**, which better reflects the true relationships among the cyclooxygenase variants.[39]

Table I.2. Cyclooxygenases' family. The table shows the known cyclooxygenases (COXs), some of their known sites of expression and functions, and the drugs (including nonsteroidal anti-inflammatory drugs, NSAIDs) that inhibit them[7]. Data referring to COX-3 were reviewed. Furthermore the term COX-1b for COX-3 was endorsed by some groups.

Cyclo-oxygenase	Gene of origin	Expression characteristics	Functions	Inhibited by
COX-1	*COX-1*	Constitutively expressed	Involved in organ pain, platelet activation, stomach protection	NSAIDs, including aspirin; other pain-relieving drugs
COX-3	*COX-1*	Constitutively expressed, particularly highly in brain	Possibly involved in sensing pain; little involvement in inflammation	Highly sensitive to acetaminophen; also inhibited by some NSAIDs
PCOX-1a	*COX-1*	Not known	Not known	Not known
PCOX-1b	*COX-1*	Not known	Not known	Not known
COX-2	*COX-2*	Induced by growth factors, neuro-transmitters, inflammatory cytokines, oxidative stress, injury, inflammation, low oxygen levels in the brain, seizures, neurodegeneration. Constitutively expressed in brain, kidneys, and other organs	Inducible COX-2 causes inflammatory pain and fever; constitutive COX-2 is involved in synaptic plasticity	NSAIDs; COX-2-selective drugs

I.2.1. Design of enzymes.

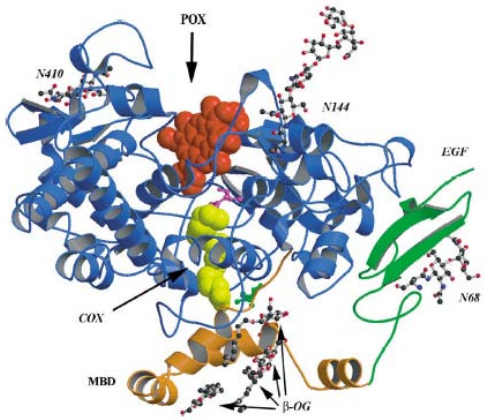

Figure I.9. Ribbon drawing of the ovine PGHS-1 monomer with bound arachidonic acid (AA) (yellow). The figure is colored to indicate the epidermal growth factor domain (green), the MBD – membrane Binding Domain (gold), and globular catalytic domain (blue). The hemes are shown in red and N-linked sugars are shown in ball-and-stick rendering.

The primary structures of COX-1 and COX-2 from numerous species are known.Two COX isoforms are encoded by distiner genes. Mature mammalian COX-1 and COX-2 contain 576 and 587 amino acids, respectively. There is a 60%–65% sequence identity between COX-1 and 2 from the same species and 85%–90% identity among individual isoforms from different species.[16] The major differences in primary structure between COX isoforms occur in four distinct areas of the sequence. First, both isoforms contain signal peptides of varying lengths. Second, an 18-amino acid insertion occurs six residues in from the C-terminus of COX-2 that are not present in COX-1. The function of this insertion in COX-2 is not known, but it may possibly be a "signal domain" for controlling protein turnover or subcellular trafficking. Elimination of this cassette by deletion mutagenesis has no apparent effect on COX-2 catalysis. Third, substantial sequence differences are found in the

membrane-binding domains (MBDs) between the two isoforms.Finally, COX-1 is *N*-glycosylated at three sites, while COX-2 is variably glycosylated at two to four sites. *N*-glycosylation of COX-1 seems to be required for enzyme folding. The high degree of sequence identity between the mature isoforms and between species allows an almost one-to-one comparison between all known sequences, aside from small insertions and deletions in COX-2.

COXs are heme-containing integral membrane proteins located on the lumenal surface of the endoplasmic reticulum (ER) and also, for COX-2 mainly, on the nuclear envelope. After post-translational processing in the ER, the mature COX-1 and COX-2 proteins have apparent molecular masses of 67 - 72 kDa and exist as homodimers which bind 1 mole of high-spin ferric heme per mole monomer. The three-dimensional (3D) structure of these two enzymes was published: ovine COX-1, recombinant human COX-2 and recombinant mouse COX-2. COX crystal structures reveal the complete dimeric form of these glycosylated, detergent-solubilized enzymes. Due to the high degree of sequence homology between COX-1 and COX-2, the tertiary and quaternary structures of those two enzymes are virtually identical. Several structures of ovine COX-1 have been determined while complexed with several different fatty acid substrates. Furthermore crystal structures of murine COX-2 complexed with AA have also been determined . COX functions as a homodimer and attempts to create monomeric species have yielded only inactive enzyme.[40]

.

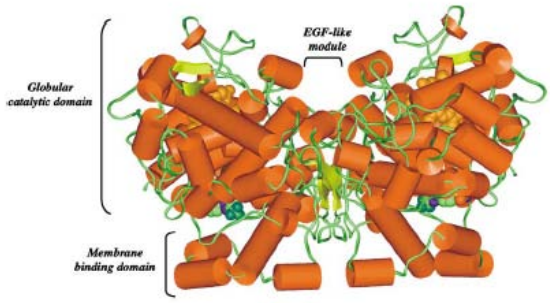

Figure I.10. Structure of mouse COX-2 homodimer, with the selective COX-2 inhibitor SC-558.

COX-1 and COX-2 exist as homodiners. Each subunit is composed of three distinct structural domains: a short N-terminal epidermal growth factor (EGF) domain; an α-helical membrane-binding motif (MBD); and a large C-terminal catalytic domain with the heme binding site facing the solvent.[41] The dimer interface is created by the **EGF domain** and catalytic domains (**Figure I.9**), which places the two MBDs in a homodimer about 25 Å apart. The EGF domains clearly make up a substantial and intimate portion of the dimer interface of COX. Whether or not the EGF domains have some functional significance is unclear. Certainly, EGF domains are common in several families of membrane proteins and secreted proteins. Typically, the EGF domain occurs at a position in the primary sequence N-terminal to a membrane anchor, such that these domains always occur on the extracytoplasmic face of the membrane. Garavito and co-workers. have suggested that the EGF domains play a role in the integration of maturing COX into the lipid bilayer. Consistent with this hypothesis, Li et al. showed that green fluorescent protein can be anchored to bilayers by fusing both the EGF domain and MBD to its

N-terminus. Interestingly, mammalian thyroid POX, which is related to COX, also uses an EGF domain and a membrane anchor to integrate the POX catalytic domain onto the membrane.[40, 41]

COX enzymes are monotopic membrane proteins; **the membrane-binding domain** consists of a series of amphipathic α helices with several hydrophobic amino acids exposed to a membrane monolayer. Three of the four helices lie in roughly the same plane while last helix merges “upwards” into the catalytic domain. The MBDs of COX-1 and -2 thus represent the first example of the monotopic” mechanism for integrating into biological membranes.The **catalytic domain** comprises the bulk of the COX isoforms.The structures of the C-terminal segments beyond Pro583 (17 amino acids in PGHS-1 and 35 amino acids in PGHS-2) have not been resolved crystallographically . Nonetheless, this region of the enzyme is of great interest as COX-1 and -2 contain C-terminal KDEL-like sequences that may target COXs to the endoplasmic reticulum and the associated nuclear envelope[34]. COX-2 appears to be relatively more concentrated within the nuclear envelope, raising the intriguing possibility that products formed via this isoform may have greater access to the nucleoplasm to affect nuclear events, perhaps via nuclear receptors.[40]

COX-1 and COX-2 are bifunctional enzymes that carry out two sequential chemical reactions in spatially distinct but mechanistically coupled active sites. Both the **cyclooxygenase** and the **peroxidase active sites (POX)** are located in the catalytic domain, which accounts for approximately 80% of the protein. The catalytic domain is highly homologous to mammalian peroxidases such as myeloperoxidase, a soluble heme-dependent POX. Structural homology between the COX catalytic domain and nonmammalian heme-dependent POXs was detectabled.The peroxidase active site is located on the surface of the protein near the heme cofactor, in a large groove on the side opposite of the MBD. The entrance to the COX active site is between the helices of the MBD.[40, 41]

The cyclooxygenase active site is located at the end of a long hydrophobic channel that is broad near the membranebinding domain (the lobby) and narrows as it extends toward the interior of the protein. A constriction composed of Arg120, Tyr355 and Glu524 separates the lobby from the cyclooxygenase active site located above it. All fatty acid substrates and NSAIDs must enter the COX active site through the MBD. The very narrow dimensions of the aperture within the COX channel clearly suggest that the MBD may undergo significant conformational changes during substrate entry and product exit.[52] The cyclooxygenase active site may be subdivided into the main (substrate-binding) channel, which is largely hydrophobic, and a smaller amphipathic side pocket. Aside from several side pockets and cul-de-sacs, the COX channel contains several water channels, including a branched water channel, which extends from the COX active site near Gly533 to the dimer interface. It is not clear if the water channels are simply structural or play some direct role in catalysis (e.g. as conduits for proton flow).[41]

Whereas the overall structures of COX-1 and COX-2 **table I.3** may diverge by as much as 1 Å rmsd, the cyclooxygenase active site is highly conserved (0.2 Å rmsd) Similarly, the peroxidase active sites of the two enzymes are also highly conserved. Consistent with these data, the two enzymes have comparable kinetic parameters (Vmax and *KM*) for the oxygenation of AA.[33]

Table I.3. Data referring to COX-1 and COX-2 were reviewed.

Parameter	Comparison of COX-3 with COX-1 and COX-2	
	COX-1 (human)	COX-2 (human)
Gene size	22 kb	8.3 kb
Chromosome	9	1
mRNA	2.8 kb	4.1 kb
mRNA regulation	Const.	Const., indu.
Amino acids	599	604
Molecular weight	70 kDa	70–72 kDa
Localization	Membrane, ER	Membrane, ER, cytoplasm
Glycolization	n-terminal	n-terminal
ASA acetylation site	Ser 529	Ser 516
Substrate specificity	AA	AA
	Gamma-linolenic acid	Gamma-linolenic acid
		Alpha-linolenic eicosapentenoic acid

Abbreviations: kb, kilobase; mRNA, messenger ribonuclein acid, const., constitutive; induc., inducible; ER, endoplasmatic reticulum; n-terminal, amino-terminus; AA, arachidonic acid; Ser, Serine.

I.2.2. Catalysis of Cyclooxygenases.

Cyclooxygenase (COX) enzymes catalyze the conversion of arachidonic acid (AA) to prostaglandin H2 (PGH2), the common biosynthetic precursor to prostaglandins and thromboxane. These bioactive lipids mediate numerous physiological and pathophysiological effects. The pharmacological effects of nonsteroidal anti-inflammatory drugs (NSAIDs) arise from their inhibition of COX enzymes.[40, 41]

The term prostanoids includes the prostaglandins (PGE_2, PGD_2, $PGF_{2\alpha}$) prostacyclin (PGI_2) and thromboxane(TXA_2).[42] Prostaglandins are a family of hormone-like chemicals, some of which are made in response to cell injury. Prostaglandins are lipid mediators made by most cells in the body except for red blood cells and released by almost any type of chemical or mechanical stimulus. They produce a remarkably broad spectrum of effects that embraces practically every biological function as well as being of prime importance as mediators of pain, fever and swelling in inflammation. Inhibition of their biosynthesis by the non-steroid anti-inflammatory drugs (NSAIDs) causes major changes to the pathophysiological functions of the organism. AA (arachidomic acid) is the most abundant polyunsaturated fatty acid found in the phospholipid cell membranes. Activation of the phospholipase A_2 (PLA_2), in response to various stimuli, releases AA, which can be further metabolised by two major enzymatic pathways: cyclooxygenase and 5-LOX, leading to pro-inflammatory mediators, prostanoids and leukotrienes (LTs), respectively. Indeed, once a prostanoid is formed, it exits the cell and then interacts with G protein-coupled receptors, either on the parent cell or on closely neighboring cells to modulate second messenger levels.[41] In the cardiovascular system, PGD_2 and PGE_2 as well as PGI_2 are potent vasodilators whereas TXA_2 displays vasoconstrictor properties. TXA_2 also plays a major role in the induction of platelet aggregation while PGI_2 presents anticoagulant properties. In the airways, $PGF_{2\alpha}$ and TXA_2 are bronchoconstrictors whereas PGI_2 and PGE_2 act as bronchodilators. In the GI tract, PGE_2 and $PGF_{2\alpha}$ as well as PGI_2 ensure the protection of the gastric mucosa by lowering acid secretions, enhancing mucosal blood flow and stimulating mucus formation and bicarbonate secretion. TXA_2 induces increased vascular permeability, leading to edema. In the compromised

kidney, PGE_2 and PGI_2, unlike TXA_2, stimulate renal blood flow and diuresis. PGE_2 and $PGF_{2\alpha}$, in contrast to PGI_2, strongly contract the uterine smooth muscle[42]. Prostanoids also mediate the body's responses to tissue injury or inflammation. PGE_2 and PGI_2 are potent vasodilators acting in synergy with other autacoids (i.e., compounds involved in inflammation) such as histamine or bradykinin. Their combined action on capillaries contributes to the redness and increased blood flow in acute inflammatory regions. They enhance vascular permeability leading to the characteristic swelling of tissues. They also produce hyperalgesia by a sensitising action on the peripheral terminals of sensory fibers. Moreover, PGE_2 acts on neurons and contributes to the systemic responses to inflammation such as fever, fatigue and pain hypersensitivity.[42] Prostaglandins are found in animals as primitive as the coelenterates and are present in a wide variety of human tissues. PGs not only play a central role in inflammation, but also regulate other critical physiological responses. In humans, prostaglandins are involved in diverse functions, including blood clotting, ovulation, initiation of labor, bone metabolism, nerve growth and development, wound healing, kidney function, blood vessel tone, and immune responses. Two classes of prostaglandin receptors exist to transduce signals upon binding of ligand, the G-coupled cytoplasmic receptor class (i.e., EP1-4 for PGE_2) and the nuclear PPAR receptor class (i.e., PPARα, PPARγ, PPARδ), which acts directly as a transcription factor upon ligand binding.[42]

Prostaglandin H_2 synthase (PGHS, also known as cyclooxygenase, COX) catalyzes the two-step conversion of arachidonic acid (or other 20 carbon fatty acids) to prostaglandin G_2 and thence to prostaglandin H_2, the first committed steps in the biosynthesis of a class of potent hormones which includes various prostaglandins, prostacyclin, and thromboxanes.[41] Prostaglandins act as potent mediators of pain, fever and inflammation. Cells synthesize prostaglandins in response to tissue injury, and inhibition of prostaglandins inhibits inflammation. Prostaglandins were discovered in human semen in 1930. Once they were identified, it was clear they arose from polyunsaturated fatty acids by a complex series of reactions involving oxygenation, cyclization, and the generation of five chiral centers from an achiral substrate. The mechanism of prostaglandin biosynthesis was outlined in 1967 by Hamberg and Samuelsson, and the basic tenets have been confirmed in subsequent studies. The key step in their proposed mechanism was the formation of bicyclic peroxides (endoperoxides) as the initial products of polyunsaturated fatty acid oxygenation.[33]

The key regulatory enzyme COX oxygenates arachidonic acid by a free radical mechanism. Thus, COX appears to have co-opted the process that gives rise to isoprostanes to generate prostaglandins. The major differences between COX-catalyzed and spontaneous oxidation of arachidonic acid are the increased rate and high degree of stereochemical control of the enzymatic reaction (1 of 64 possible isomers predominates). Thus, the overall role of COX is rather simple: stereospecifically remove the 13-pro-*S*-hydrogen and control the stereochemistry of oxygenation.[33]
The fatty acid substrate molecules are bound in an extended L-shaped conformation with two interior kinks. The carboxylate of the substrate forms an ion pair with the guanidinium group of a conserved arginine (Arg120) and a hydrogen bond with Tyr355 at the bottom of the cyclooxygenase active site. The middle portion of AA (C7–C14) adopts an S shape that meanders around the sidechain of Ser530. Sufficient space is available for the binding of molecular oxygen above C11. As many as 19

protein residues make close contacts with the substrate, the vast majority of them involving van der Waals interactions. The ω-end of the substrate, surrounded by six aromatic amino acids, binds in a narrow channel at the top of the active site that traverses the space between Tyr385 and Ser530.[41] Mutation of Gly533 in the top channel to valine or leucine seals off the channel and completely inhibits the oxygenation of AA, but not that of shorter fatty acids. A protein tyrosyl radical appears to be the *oxidizing agent* that initiates arachidonic acid oxygenation. A tyrosyl radical is formed during COX turnover. The crystal structures of both COX-1 and COX-2 reveal that Tyr- 385 is positioned perfectly to react with the fatty acid substrate. (Fig. 1 na czarnym tle) Protein radicals require an oxidant for their formation, which in most cases is a metal-containing prosthetic group. COX is a homodimer and each subunit contains one molecule of heme.[40] The productive conformation of the substrates observed in the crystal structures positions the 13-*pro(S)* hydrogen near the phenolic oxygen of Tyr385 (2.3 Å away). It is, therefore, ideally located for abstraction by the radical derivative of this tyrosine, which is the first step in AA oxygenation.[41]

The tyrosyl radical is produced by intramolecular oxidation by a ferryl-oxo derivative of the heme cofactor. The free radical thus generated on C13 of AA then migrates to C11, forming a pentadienyl radical. Subsequent attack by molecular oxygen, cyclization and the addition of a second molecule of oxygen results in the formation of PG. The sidechain of Tyr348, which forms a hydrogen bond with Tyr385, makes numerous contacts with C12–C14 of AA. Thus, Tyr348 also appears to be important for the proper positioning of C13 for hydrogen.[41]

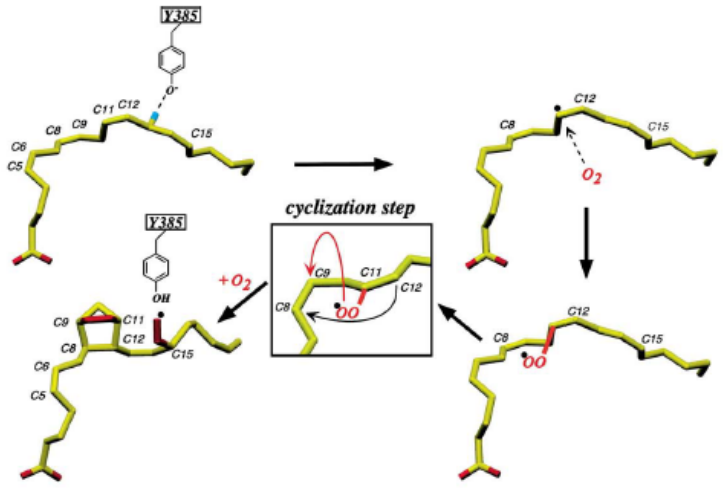

Figure I.11. A schematic presentation of the cox reactions as proposed by Malkowski and al. While the formation of the 11-peroxy-arachidonate intermediate is explained by the crystal structure for the ovine COX-1 – AA complex, its subsequent conversion to PGG_2 requires major conformational transition.[51]

Tyr-385 radical is regenerated at the end of each cyclooxygenase catalytic cycle. Thus, the final step in each round of arachidonic acid oxygenation is reduction of the peroxyl radical precursor of PGG_2 by Tyr-385, which regenerates the Tyr-385 radical for the next round of cyclooxygenase catalysis **(Figure I.11)**. This leads to multiple turnovers per activation event and allows the accumulation of PGG_2.[33] Removal of the 13-pro-*S* hydrogen followed by reaction with O_2, serial cyclization, and reaction with the second O_2 could occur with minimal motion of the reaction intermediates to produce PGG_2 with all

the correct stereocenters.[33] As expected, the carboxylate of PGH_2 is positioned near Arg120 and Tyr355. Arg-120, which plays a crucial role in binding arachidonate and arylalkanoic acid-type inhibitors[52], The identity of the species in the crystal was ambiguous. It could be either PGG_2 or PGH_2. Since no electron density was visible for the second oxygen atom at C15 of the PG, the species in the crystal was assumed to be PGH_2. The ω-end is bound in the top channel, similar to the position of the ω terminus of AA in the COX-1 complex. The bridged endoperoxide ring forms tight van der Waals interactions with the sidechains of Trp387, Tyr385, Phe381 and Leu384, all of which are conserved between COX-1 and COX-2. The indole sidechain of Trp387 provides the bulk of the interaction, which appears to be critical for positioning the 11-peroxyl radical in a conformation optimal for cyclization at C9. Some of the hydrophobic amino acids play critical roles in stabilizing the conformation of AA that leads to endoperoxide synthesis. The minor amounts of monohydroxylated products generated by native COX-1 and COX-2 probably result from the reaction of O2 with radical derivatives in different conformations in the active site.[41] The structures of AA and PGH_2 bound at the active sites of COX-1 and COX-2, respectively, provide both snapshots of a complex multistep reaction and direct support for the mechanism proposed by Samuelsson and co-workers. The intricate arrangement of protein atoms in an active site can restrain a flexible achiral substrate and cause it to adopt a conformation that will yield a product with exact stereochemistry at five nascent chiral centers.[40] COX-2 appears much more accommodating than COX-1 in that it oxidizes 18 carbon polyunsaturated fatty acids with much higher efficiency than COX-1.Also, COX-2 oxidizes the hydroxyethylamide derivative of arachidonic acid (anandamide) whereas COX-1 does not.[41]

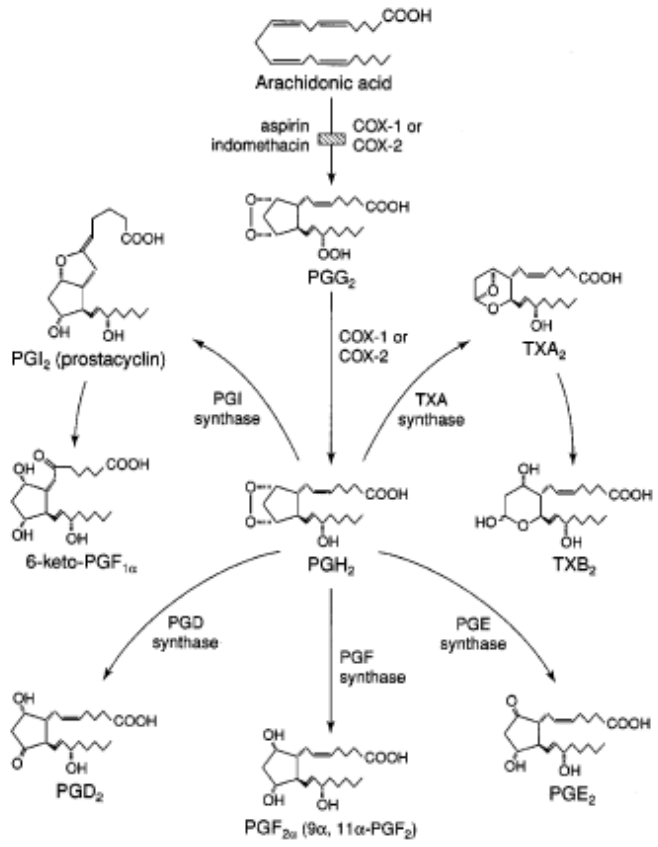

Figure I.12. The arachidonic acid cascade. The precursor of the prostaglandins, arachidonic acid, is cleaved from cell membrane phospholipids by phospholipase A2. It is then converted by COX-1 or COX-2 into unstable endoperoxides, PGG_2 and PGH_2. The endoperoxide, PGH_2 is metabolized by synthases to primary prostaglandins PGD_2, PGE_2 and PGF_{2a} as well as TXA_2 and PGI_2 (prostacyclin). TXA_2 is found mostly in platelets and PGI_2 mainly in endothelial cells and in the stomach mucosa. PGE_2 is made in the kidney and at sites of inflammation. TXA_2 is metabolised to the inactive TXB_2 and PGI_2 is converted into the inactive metabolite, 6-keto- PGF1a. (Reprinted from ''Principles of Immunopharmacology'', Nijkamp, F.P. and Parnham, M.J. eds. 2005. Birkha¨ user Verlag, Basel, Switzerland.

Thus, the precursor, arachidonic acid, is first cyclised to form the endoperoxide derivative, prostaglandin G_2 and then reduced by peroxidase to form prostaglandin H_2 (PGH_2). These two endoperoxides, which are chemically unstable, are then isomerised enzymatically or non enzymatically into different products, such as PGD_2, PGE_2 or $PGF_{2\alpha}$. Prostaglandins of the D, E and F_α series are referred to as the ''primary prostaglandins'' and they are synthesised in a stepwise manner by a complex system of microsomal enzymes beginning with COX.[15] The endoperoxide, PGH_2, is also metabolised into two unstable and highly biologically active compounds with structures that differ from those of the primary prostaglandins. One of these is thromboxane A_2 (TXA_2), formed by an enzyme, thromboxane synthase. TXA_2 has a very short chemical half-life of about 30 s; it breaks down nonenzymatically into the stable and relatively inactive thromboxane B_2 (TXB_2). The other route of metabolism of PGH_2 is to prostacyclin or prostaglandin I_2 (PGI_2), yet another unstable compound with a half-life of around 3 min, formed by the enzyme, prostacyclin synthase. PGI_2 has a double-ring structure, closed by an oxygen bridge between carbons 6 and 9. Simplify PGH_2 is subsequently converted to a variety of eicosanoids that include PGE_2, PGD_2, $PGF_{2\alpha}$, PGI_2, and thromboxane (TX) A_2 (**figure I.12**) The array of PGs (proinflammatory prostaglandins) produced varies depending on the downstream enzymatic machinery present in a particular cell type. For example, endothelial cells primarily produce PGI_2, whereas platelets mainly produce TXA_2. lung and spleen tissues are able to synthesise the whole range of products. COX-2 is an important mediator in the kidney, lung and spleen tissues are able to synthesise the whole range of products, whereas PGD_2 is made in mast cells and in the brain.[35]

While COX catalyzes both steps of this catalytic process (known as the cyclooxygenase and peroxidase steps, respectively), the reactions are carried out in two spatially distinct active sites.[40] Understanding that the NSAIDs inhibited prostanoid formation led to an appreciation of the mechanisms underlying the effects of these drugs. At sites of inflammation, the local production of prostanoids such as PGE_2 can sensitize pain nerve endings and increase blood flow, promoting feelings of pain and driving tissue swelling and redness. Inhibition of PGE_2 formation via the inhibition of local COX could therefore explain the antiinflammatory effects of NSAIDs. Similarly, prostanoids such as PGI_2 and PGE_2 were found to be protective to the stomach and so inhibition of their formation provided an explanation for the gastrointestinal toxicity associated with prolonged and high-dose use of NSAIDs. The inhibition of COX in platelets provided an explanation for the ability of aspirin to reduce blood clotting.[41]

I.2.3. Inhibition of Cyclooxygenases.

NSAIDs can be subdivided into two classes of drug behavior: (a) classical, “isoform nonspecific” NSAIDs and (b) COX-2 inhibitors. All the classical NSAIDs inhibit both COX-1 and -2 but many tend to bind more tightly to COX-1. In contrast, COX-2 inhibitors have been designed to exhibit many-fold higher selectivity toward COX-2. Second, while all NSAIDs compete with arachidonate for the COX active site, each NSAID exhibits one of three general modes of inhibition: (a) rapid, reversible

binding (e.g. ibuprofen); (b) rapid, lower affinity reversible binding followed by time-dependent, higher affinity, slowly reversible binding (e.g. flurbiprofen); or (c) rapid, reversible binding followed by covalent modification (as in the acetylation of Ser530 by aspirin). The pharmacological effects of NSAIDs are established rapidly once plasma concentrations have reached steady state. Maximal effects occur within a few days for NSAIDs with short half-lives. By contrast, NSAIDs with long half-lives accumulate and maximal efficacy of these drugs may be delayed for several days. Pain appears to respond faster than other signs of inflammation such as joint swelling and heat. Upon cessation of treatment with NSAIDs, drug effects dissipated as fast as they had appeared. The *reversibility* of action of NSAIDs is in keeping with their major mode of action, namely the reversible inhibition of cyclooxygenase, the enzyme complex involved in the synthesis of prostaglandins and other prostanoids. Aspirin is the only NSAID which is an irreversible inhibitor of cyclooxygenase, the irreversible inhibition being due to acetylation of the cyclooxygenase enzyme complex. However, irreversible inhibition is not always demonstrated in the clinical effects of aspirin, although it can be detected by the presence of prolonged inhibition of platelet function. The marked toxicity of aspirin in the stomach may also be due to acetylation of cyclooxygenase or other constituents of the gastric mucosa.[23b] NSAIDs exert their anti-inflammatory action by inhibition of cyclooxygenase activity, which transforms phospholipidderived arachidonic acid into prostaglandins. COX-1, which is not stimulated by proinflammatory cytokines such as IL-1, is a *constitutive* enzyme, present in most cells, and is associated with the regulation of hemostasis, the integrity of the gastrointestinal and renal tracts, platelet function, and macrophage differentiation. It hasbeen suggested that COX-1, is responsible for the physiological production of prostanoids.[39]

Although inhibition of COX-1 by NSAIDs may have some anti-inflammatory effect, the adverse effects of NSAIDs are predominantly related to the inhibition of the other important functions of COX-1. COX 2, by contrast, inducible under inflammatory conditions, is mainly responsible for the pathological production of prostanoids. Specific inhibition of COX-2 leads to reduction of inflammation without these adverse effects. However, all NSAIDs have some inhibitory effects on COX-1 and COX-2 activities, so that none is absolutely selective for COX-2. The adverse effects reported for COX-2 NSAIDs can occur with the older, COX-1 NSAIDs, and there also is a dose effect for the COX-2 agents, with greater COX-1 effects at higher doses. Subsequent experiments determined that most of the clinically used COX inhibitors, such as ibuprofen and naproxen, were nonselective (i.e., they blocked both COX-1 and COX-2), albeit with varying potency ratios. Consequently, the major therapeutic limitation of the nonselective COX inhibitors has been their tendency to cause gastrointestinal lesions due to reductions in gut levels of homeostatic prostanoids via COX-1 inhibition. Accordingly, significant effort has been committed to the discovery and development of selective COX-2 inhibitors that would be expected to exhibit anti inflammatory/analgesic efficacy with substantially improved gastrointestinal safety. Acetaminophen is a widely used analgesic and antipyretic drug, particularly in the treatment of certain medically compromised or vulnerable populations, such as those with gastrointestinal diseases, children, and the elderly. Devoid of the antiedema effects of the nonselective cyclooxygenase inhibitors (i.e., NSAIDs) and selective COX-2 inhibitors, the mechanism of action of

acetaminophen in the relief of pain and fever to a large extent remains unknown. Several lines of evidence have led to the hypothesis that one or more than one additional COX isoform may exist and constitute the therapeutic target of acetaminophen. Indeed, a protein comprising a third cyclooxygenase isozyme has been identified in canine cerebral cortex, and it is called COX-3 **(**Cyclooxygenases-1b).This recently described COX-3 system has opened up further avenues of therapeutic opportunity in the treatment of inflammatory conditions, not least because of the ability of paracetamol to inhibit COX-3 activity.[39]

Most NSAIDs currently in clinical use, however, are known to inhibit both isoforms of COX with little selectivity, and during extended therapy many NSAIDs cause ulcerogenic side effects most likely dueto COX-1 inhibition in the stomach. The two isoforms have been shown to differ pharmacologically, and it should prove possible to exploit these differences to target COX-2, thereby decoupling the inhibition of inflammatory prostanoid biosynthesis from the inhibition of background levels of prostanoid biosynthesis required for normal physiological functioning. All the NSAIDs are generally thought to target the cyclooxygenase activity of PGHS; however, the mechanisms by which they act vary widely. Some inhibit by covalently modifying the enzyme, some are competitive with respect to arachidonic acid, and some are slow-binding inhibitors. Information about the structural basis of NSAID binding by PGHS-1 and PGHS-2 should help to clarify why different compounds act by different mechanisms and may prove valuable in this process of designing isoform-specific inhibitors.[41]

A general model for COX inhibition is emerging in which multiple equilibria are established between free enzyme, inhibitor and two or three enzyme–inhibitor complexes (Box 1)

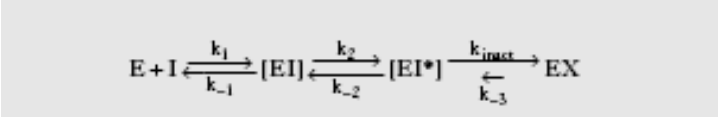

k_1, k_2 and kinact represent the forward rate constants for the three discrete steps of the overall reaction, whereas k–1 and k–2 and k–3 represent the backward rate constants. E and I represent the free enzyme and the inhibitor, respectively. The three distinct enzyme-inhibitor complexes, identified by enzyme kinetics, are represented by [EI], [EI*] and [EX]. The precise structural attributes of each of these complexes are not clear at present.[41]

The anticipated pot-of-gold at the end of the rainbow awaiting a selective COX-2 inhibitor triggered a world class race to develop candidate drugs. Some of the efforts have been been successful and are chronicled in several recent reviews. The most extensively represented class of inhibitors is diarylheterocycles; other classes of inhibitors include acidic sulfonamides, indomethacin analogs, zomepirac analogs, and di-*t*-butylphenols. All appear to be slow, tight binding inhibitors in which the selectivity is manifest in the second step (BOX 1).[41] This slow step involves the conversion of the [EI] complex to the [EI] complex, in which the inhibitor is bound more tightly to the enzyme. Formation of the [EI*] occurs in seconds to minutes and may reflect the induction of a subtle protein conformational change. The time-dependent change is not associated with covalent modification for most inhibitors.

Aspirin is the only COX inhibitor that covalently modifies the protein. It acetylates Ser-530, which is juxtaposed to Arg-120, and it is more potent against COX-1 than COX-2. Aspirin-like molecule (acetoxyphenylheptynyl sulfide) was developed that exhibits 20-fold selectivity for COX-2 and acetylates only Ser-530.[41] Crystal structures of complexes of COX-1 and COX-2 from different spicies and human with non-selective and with selective inhibitors have been solved. Indomethacin and other carboxylate-containing NSAIDs form an ion pair with guanidinium group of Arg- 120, which also form ion pairs with the carboxylate of arachidonate. Certain structural details are common to the binding of the different compounds. The carboxylic acid moieties of flurbiprofen, salicylic acid, iodosuprofen, and iodoindomethacin all form salt bridges with Arg-120, and at least some appear to form hydrogen bonds to the hydroxyl of Tyr- 355. Since many of the different classes of NSAIDs carry carboxylic acid groups, these interactions may prove to be general features of binding for these drugs. This observation also suggests that the substrate arachidonic acid may bind with its carboxylic acid group making similar contacts with Arg-120 and Tyr-355. Site-directed mutagenesis of the arginine residue in COX-1 to glutamine or glutamate renders the protein resistant to inhibition by carboxylic acid-containing NSAIDs. Arg-120 is part of a hydrogen-bonding network with Glu-524 and Tyr-355, which stabilizes substrate/inhibitor interactions and closes off the upper part of the cyclooxygenase active site from the spacious opening at the base of the channel, which we call the lobby. Disruption of this hydrogen-bonding network opens the constriction and enables substrate/inhibitor binding and release to occur. In addition, Tyr-355 sterically hinders the mouth of the COX active site, which accounts for the preferential inhibition exhibited by *S*-stereoisomers of a-methyl-substituted arylalkanoic inhibitors (*e.g.* the profens). Opening and closing of the Arg-120–Glu- 524–Tyr-355 constriction may contribute to the time dependence of all COX inhibitors. Structures of COX-inhibitor complexes presumably reflect the [EI*] complex in which the inhibitor is bound tightly to the enzyme. That COX-2-selective inhibitors, especially diarylheterocycles, bind to regions accessible in COX-2 but not COX-1 is consistent with the hypothesis that these structures reveal the molecular basis for their selectivity.[33] Several diarylheterocycles appear to be competitive inhibitors of COX-1, but display time-dependent inhibition of COX-2 that is responsible for their selectivity.[41] Comparison of the nonselective inhibitor flurbiprofen and the selective inhibitor SC-558 bound to COX-2. Both inhibitors bind in the COX-2 active site above Arg120, but the sulfonamide moiety in SC-558 wedges into a hydrophobic “side pocket” of COX-2 flanked by Val-523.and hydrogen bonds to Arg-513 and the peptide bond of Phe-518. This interaction is responsible for the stable and selective binding of diarylheterocycles to COX-2.A similar hydrophobic side pocket off the main channel in COX-1 is not accessible because of the presence of an isoleucine instead of valine at position 523, which sterically hinders inhibitor approach. Movement of Val-523 and insertion of the sulfonamide or methylsulfone moiety into the side pocket may contribute to the time dependence of inhibition by diarylheterocycles. The structural basis for selectivity by indomethacin analogs is dependent on substitutions at the top rather than the side of the cyclooxygenase active site. For example, the acetyl group introduced by bromoaspirin lies near the top of the channel, just below Tyr-385; it does not fill the channel but evidently occupies enough volume to prevent the substrate from contacting Tyr-385. On the other hand, flurbiprofen,

iodosuprofen, and iodoindomethacin are substantially larger than this acetyl group and fill the entire channel from Tyr-385 downward a distance of roughly 12- 14 Å.[41] The structure of human COX-2 complexed with a 4-bromobenzyl indomethacin analog reveals that the 4-bromobenzyl group is in van der Waals contact with Leu-503 at the apex of the COX-2 active site.5 Position 503 in COX-1 is substituted with phenylalanine, which is not as easily displaced by the bromobenzyl group as leucine. Decreased flexibility at the top of the COX-1 active site may reduce the affinity of the protein for the indomethacin analog, thereby accounting for its COX-2 selectivity.[33] The molecular basis of this puzzling difference has not been elucidated, but the observationsuggested a strategy for the conversion of certain nonselective NSAIDs to COX-2-selective inhibitors.Neutral ester or amide derivatives bind reasonably well to COX-2, but not to COX-1. This selectivity is most pronounced with indomethacin and meclofenamic acid. A model for the binding of these esters and amides is provided by the structure of an acylsulfonamide conjugate of zomepirac bound to COX-2. This compound, which is a chainextended, neutral derivative of zomepirac (zomepirac acylsulfonamide), breeches the constriction composed of Arg120, Tyr355 and Glu524 at the mouth of the COX active site and projects into the lobby. Presumably, the ester and amide functionalities of the indomethacin conjugates also project down into the lobby.[52]

References

1. Starek, M., Krzek, J*. Talanta* **77,** 925–942 (2009).
2. Simon, L. S., Strand, V. *Arthritis Rheum.* **40**, 1940-1943 (1997).
3. Pascucci, R.A. *JAOA* **102,** (2002).
4. Jones, R., Rubin G., Berenbaum, F., Scheiman, J. The American Journal of Medicine, **121**, 464-474 (2008)
5. Shahapurkar, S., Pandya, T., Kawathekar, N., Chaturvedi, S.C. Eur J Med Chem **39**, 383–388 (2008).
6. Kovala-Demertzi, D. *J. Organomet. Chem.* **691**, 1767–1774 (2006).
7. Gomez-Gaviro, M.V., Gonzalez-Alvaro, I., Domınguez-Jimenez, C., Peschon, J., Black, R.A, Sanchez-Madrid, F., Dıaz-Gonzalez F. *J. Biol. Chem*. **277**, 38212-38221 (2002).
8. a) Furst, D.E. *Arthritis Rheum* **37**, 1-9 (1994).
   b) Day, R.O., Graham, G.G., Kenneth, M.W.,CHampion, G.D.,De Jager, J. *Pharmac. Ther.* **33**, 383-433 (1987)
9. a) Kovala-Demertzi, D., Hadjipavlou-Litina, D., Staninska M., Primikiri, A., Kotoglou, C., Demertzis, M.*J Enz Inh and Med Chem* **24,** 742-752 (2009).
   b) Kovala-Demertzi, D., tolfenamic acid
10. a) Lleo, A., Galea, E., Sastre, M. *Cell. Mol. Life Sci*. **64**, 1403-1418 (2007).
    b) B. Rezaei, S. Mallakpour, N. Majidi Talanta 78) 418–423 (2009).
    c) De Stooper, B., Konig, G. *Nature* **414**, (2001).
11. a) Lewis, A.J., Furst, D.E. Second Edition *Nonstereoidal anti-inflammatory drugs. Mechanisms and clinical uses* (1994).
    b) Pektas, Z.O., Senar, M., Bayram, T., Eroglu, N., Bozdogan, A., Donmez, G., Arslan, S., Int. *J. Oral Maxillofac. Surg.* **36**, 123-127 (2007).
12. a) Gilpin, R.K., Zhou, W. J. Pharm. Biomed. Anal. **37**, 509–515 (2005).
    b) Andersen,k.L., Larsen, S., Alhede, B., Gelting, N., Buchardt, O. J*. Chem. Soc., Perkin Trans. II* 1443 (1989).
13. Vietri, M., De Saint, C., Pietrabissaoe, Mascaoe, F., Pacifici, G.M. *Xenobiotica* **30**, 111-116 (2000).
14. a) Ruiz, T.P., Lazano, C.M., Tomas, V., Carpena, J. *Talanta* **47**, 537-545 (1998).
    b) Siraki, A.G., Tatiana Chevaldina1, Peter J. O'Brien Chemico-Biological Interactions 151, 177-191 (2005).
15. Gaganis, P., Miners, J.O., Knights, K.M. 73, *Biochemical pharmacology* 1683-1691 (2007).
16. Zhao, Z.,Zhang, M., Zeng, X., Fei, X., Liu, L.,Zhang, Z.,Mei, Y.J Prarmacol Exp Ther 322,…….
17. Coyne, L., Su, J., Patten, D., Halliwell, R.F. Neurochemistry International 51, 440–446 (2007).
18. Kovala-Demertzi, D., Galani, A., Demertzis, M.A., Skoulika, S., Kotoglou, C., *J. Iorg. Biochem.* **98**, 358-…. (2004).
19. a) Krymchantowski, A.V., Bigal, M.E. *Neurology* **4**, 10-…….(2004).
    b) Cafaggi, S., Russo, E., Caviglioli, G., Parodi, B., Stefani, R., Sillo, G., Leardi, R., Bignardi, G. Eur J Pharma. Sci **35**, 19–29 (2008).
20. a) Karjalainen, M.J., Neuvonen, P.J., Backman, J.T. *Eur J Clin Pharmacol* **63**, 829-836 (2007).
    b) Ziakas, G.N., Rekka, E.A., Gavalas, A.M., Eleftheriou, P.T., Tsiakitzis, K.C., Kourounakis, P.N. *Bioorg. Med. Chem*. **13**, 6485–6492 (2005).
21. Caira, M., Miller, J.L.,Nassimbeni, L.R., *Supermolecular Chemistry* **18**, 553-229 (2006).
22. Warner, T.D., Mitchell, J.A. *PNAS* **99**, 13373-13377 (2002).
23. a) Kalgutkar, A.S., Rowlinson, S.W., Crews, B.C., Marnett, L.J. *Bioorganic Medicinal Chemistry Letters* **12**, 521–524 (2002).
    b) Boschelli, D.H., Connor, D.T., Kuipers, P.J., Wright, C.D. *Biwrganic &* Mediciml *Chemistry Letters,* **2**, 705-708 (1992).
    c) Peretz, A., Degani, N, Nachman, R., Uziyel, Y., Gibor, G., Shabat, D., Attali, B., *Mol Pharmacol* **67**, 1053–1066 (2005)
    d) Schober, W., Kehlbach, R., Gebert, R., Wiskirchen, J., Rodegerdts, E., Claussen, C.D., Duda, S.H. *Cardiovasc Intervent Radiol* **25**, 57–63 (2002).
    e) Del Arco, M., Fernandez, A., Martin, C., Rives, V. *Applied Clay Science* **36**, 133–140 (2007).

24. Kovala-Demertzi, D., Dokorou, V.N, Jasinski, J.P., Opolski, A., Wiecek, J., Zervou, M., Demertzis, M.A. *J. Organomet. Chem* **690**, 1800–1806 (2005).
25. a) Gardam, K.E., Geiger, J.E., Hickey, C.M., Hung, A.Y., Magoski, N.S., *J Neurophysiol* **100**, 38–49, (2008).
    b) Di Wang, Grillner, S., Wallen, P. *Neuropharmacology* **51**, 1038-1046 (2006).
26. Van Antwerpen, P., Neve, J., *Eur J Pharmacol* **496**, 55– 61 (2004).
27. Charlier, C., Michaux, C. Eur J Med Chem **38**, 645-659 (2003).
28. a) Woolf ,T.F, Radulovic, L.L. *Drug Metab Rev.* **21,** 255-76c (1989).
    b) Fenner, H., Scand *J Rheumatol* Suppl **65,** 97-101 (1987).
    c) Jolliet, P., Simon, N. , Bree, F., Urien, S., Pagliara, A., Carrupt, P., Testa, B., Tillement , J-P. *Pharmaceutical Research,* **14,** (1997).
29. a) Lucio, M., Ferreira, H., Lima, J.L.F.C., Reis, S., *Analytica Chimica Acta* **597**, 163–170 (2007).
    b) Villegas,I., La Casa, C., Alarcon de la Lastra, C., Motilva, V., Herrerıasb, J.M.,Martına, J.M. *Life Sciences* **74**, 873–884 (2004).
    c) Chakraborty,H., Mondal, S., Sarkar, M. *Biophysical Chemistry* xxx xxx-xxx (2008)
    d) Grosman, N. *International Immunopharmacology* **7**, 532–540 (2007).
30. a) Liu, Y-L., Zhang, W., Tan, Z-R. Ouyang, D-S., Luo, C., Liu, Z.Q., Qiu, Y., Chen, Y., He, Y-J. Zhou, G., Zhou, H-H. *Clinica Chimica Acta* **364**, 287-291 (2006).
    b) Daglar, B., Kocoglu, H., Celkan, M.A., Goksu, S., Kazaz, H., Kayiran, C. **66**, (2005).
    c) Sen, S., Doger, F.K, Sen, S, Aydın, O.N., Karul, A., Dost, T. *Eur J Pharmacol* 541 191–197 (2006).
    d) Riad, W., Moussay, A. *European Journal of Anaesthesiology* **25**, 732–736 (2008).
    e) Takmaz, S.A., Inan, N., Goktug, A., Erdogan, I., Sunay, M., Ceyhan, A.*Urology* **72**, 283-285 (2008).
    f) Ayan, E., Kaplana, M.B., Koksela, O., Tamer, L., Karabacakc, T., Ayaz, L., Ozdulger, A. *Pulmonary Pharmacology & Therapeutics* **21,** 201–207 (2008).
31. a) Downie, W.W., *Singapore Medical Journal* **26,** (1985).
32. Bazan, N.G, Flower, R.J. *Nature* **420**, (2002).
33. Marnett, L.J., Rowlinson, S.W., Goodwin, D.C., Kalgutkar, A.S., Lanzo, C.A. *J. Biol. Chem.* **274**, 22903-22903 (1999).
34. Vane, J.R., *Nature New Biol*. **231**, 232-235 (1971).
35. Botting R.M., Journal of Thermal Biology **31**, 208–219 (2006).
36. Simmons, D.L., Botting, R.M., Robertson, P.M., Madsen, M.L, Vane, J.R., *Proc. Natl. Acad. Sci.* **96**, 3275–3280 (1999).
37. Chandrasekharan, N.V.,Dai, H., Lamar, K., Roos, T., Evanson, N.K., Tomsik, J., Elton, T.S., Simmons*, D.L. Natl. Acad. Sci.* **99**, 13926–13931 (2002).
38. Bazan, N. G. *Nature Med.* **7**, 414–415 (2001).
39. a) Kis B., Snipes, J.A., Busija, D.W., . *J Pharmacol Exp Ther.* **315**, 1-7 (2005).
    b) Snipes, J.A., Kis B, Shelness G.S., Hewett JA, and Busija D.W. *J Pharmacol Exp Ther.* **313**, 668-676 (2005).
    c) Kis, B., Snipes, A., Bari, F., Busija, D.W. *Brain Res. Mol. Brain Res*. **126**, 78–80 (2004).
    d) Kis, B., Snipes, Gaspar, T., Lenzser, G., Tulbert, C.D., Busija, D.W. *Infl amm. res*. **55**, 274-278 (2006).
    e) Kis, B., Snipes, J.A., Isse, T., Nagy, K., Busija, D.W. *J Cereb Blood Flow Metab* **23**, 1287–92 (2003).
    f) Qin, N., Zhang, S.P., Reitz, T.L., Mei, J.M., Flores, C.M., *J. Pharmacol. Exp. Ther* **315**, 1298–1305 (2005).
40. a) Garavito, R.M., Malkowski, M.G., DeWitt, D.L, Prostaglandins Other Lipid Mediat. **68-69**, 129-152 (2002) .
    b) Song, I., Smith, W.L. *Arch Biochem Biophys* **334**, 67-72 (1996).
    c) Smith, W., Garavito, R., DeWitt, D. *J Biol Chem.* **271**, 33157–33160 (1996).
    d) Garavito, R.M., DeWitt, D.L. *Biochim. Biophys. Acta* **1441**, 278-287 (1999).
    e) Garavito, R.M., Picot, D., Loll, P.J. *Curr. Opin. Struct. Biol*. **4**, 529-535 (1994).
41. a) Picot, D., Loll, P.J., Garavito, R.M. *Nature* **367**, 243-249. (1994).
    b) Loll P, Picot D, Garavito R.. *Biochemistry* **35**, 7330–7340 (1996).

c) Loll, P. J., Picot, D., Ekabo, O., and Garavito, R. M. *Biochemistry* **35,** 7330–7340 (1996).

d) Laneuville, O., Breuer, D.K., Xu, N., Huang, Z.H., Gage, D.A., Watson, J.T., Lagarde, M., DeWitt, D.L., Smith, W.L. *J Biol Chem* **270**, 19330-19336 (1995).

42. a) Bazan, N. G. *Nature Med.* **7**, 414–415 (2001).

b) Chen, C., Magee, J. & Bazan, N. *J. Neurophysiol.* **87**, 2851–2857 (2002).

II.1. Transition metals: manganese copper, zinc, and cadmium in biological systems.

The medicinal uses and applications of metals and metal complexes are of increasing clinical and commercial importance. The field of inorganic chemistry in medicine may usefully be divided into two main categories: firstly, ligands as drugs which target metal ions in some form, whether free or protein-bound; and secondly, metal-based drugs and imaging agents where the central metal ion is usually the key feature of the mechanism of action.[1a]

A significant rising interest in the design is currently observed in the area of scientific inquiry appropriately termed medicinal inorganic chemistry. Investigations of metal compounds as drugs and diagnostic agents focus on speciation of metal species in biological media, based on possible interactions of these metal ions with diverse biomolecules A wide range of metal complexes are already in clinical use and encourage further studies for new metallodrugs, such as metal-mediated antibiotics, antibacterial, antiviral, antiparasitic, radiosensitizing agents, and anticancer compounds. Increasing knowledge of the biological activities of simple metal complexes may guide researchers to the development of promising chemotherapeutic compounds to target specific physiological or pathological processes. Many potential antitumoral agents have been investigated based on their anti-angiogenesis or pro-apoptotic behavior. These studies involve both designed and natural products, in association with essential metal ions (copper).[2]

It is well established that a number of metal ions are essential to life. A major determinant of their functional relevance in living systems is that a substantial fraction of enzymes require metals for their catalytic activity. A wide variety of metal-dependent enzymes are found in nature which act in fundamental biological processes, including photosynthesis, respiration and nitrogen fixation. The overall picture is that redox-inert metal ions are used in enzymes to stabilize negative charges and to activate substrates by virtue of their Lewis acid properties, whereas redox-active metal ions can be used both as Lewis acids and as redox centres. Magnesium and zinc are by far the most common ions of the first type. Magnesium, however, is most often bound to phosphate groups of substrates and interacts with the enzyme only transiently, whereas the other metals are stably bound to the enzyme. The most common metal of the second type is iron, which is prevalent in the catalysis of redox reactions, followed by manganese, cobalt, molybdenum, copper and nickel. The control of the reactivity of redox-active metal ions may involve their association with organic cofactors to form stable units.[3]

About one-third of all proteins are associated with a metal. The function of these proteins, termed metalloproteins, depends on the interaction between the proteins and the bound metals. Examination of the Protein Data Bank shows that Zn is the most abundant, while Fe, Mg and Ca are also frequently observed . Metalloproteins are one of the most diverse classes of the proteins, with the intrinsic metal atoms providing a catalytic, regulatory and structural role critical to protein function. Transition metals such as Cu, Fe and Zn play important roles in life. Zn, the most abundant transition metal in cells, plays a vital role in the functionalities of more than 300 enzymes, in the stabilization of DNA and in gene expression.[4]

Metallomics and metalloproteomics are emerging fields addressing the role, uptake, transport and storage of trace metals essential for life. Metallomics is defined as analysis of the entirety of metal and metalloid species within a cell or a tissue type, whereas metalloproteomics is focused on exploration of the function of metals associated with proteins.[4]

Metal ions are connected in several ways with inflammatory diseases. Zn(II) has been tested as an anti-inflammatory agent, and it show inhibition of Sci-7/Topoisomerase I, a DNA unwinding enzyme essential for gene transcription and for selective activation of gene clusters required for the coding of derma collagene. A collagen overproduction brings to the series of human disorders known as scleroderma. As other examples of metal-inflammation relationships, the superoxide scavenger activity of the Cu(II)/Zn(II)-superoxicie dismutase (CuZn-SOD), the anti-inflammatory activity of $[Cu_2(indo)_4(dmf)_2]$[6] and related molecules which act as drugs in dogs, and of various other Cu(II) as well as Mn(II) complexes.[5]

Metals play important roles in metabolism, biosynthesis, and many other biochemical activities, for example, iron in oxygen transportation, manganese in the synthesis of glutamine synthase, and zinc as a component of neurotransmitters in the central nervous system (CNS). In addition to their vital roles, the presence of metals is detrimental under certain circumstances; for example, the deposition of iron in the brain can initiate a series of pathophysiological progressions of chronic brain diseases. It is generally believed that the vital and detrimental roles of metals in the body are concentration- and tissue-dependent. Dietary intake is the major route through which metals enter the body; primarily, they appear in the blood as a result of digestive absorption. The circulating metals would have to extravasate from the blood vessels and enter the extracellular fluids (ECFs) of target organs before they could further enter the cells. There have been reports indicating the possibility for chronic interorgan transportation of metals; for this process to occur, the intracellular metals must reversely exit the cells and enter into the ECFs before being transported further. Therefore, profiling the time-dependent concentrations of metals in the organ ECFs would provide important information regarding the possible trafficking of metals in the body and lead to a greater understanding of the adsorption, metabolism, and excretion processes of biological metals. The brain, which is the central organ of the CNS, is compartmentalized by specialized barrier systems to prevent it from the direct assault of metals. The ECF of the brain comprises cerebrospinal fluid (CSF) and fluids extravasated from capillaries; the distribution of metals within this ECF is seriously regulated and might correlate to the neurotrophic or neurodegenerative state of brain.[7]

II.1. Copper , bioessential element.

Copper is the last member of the first transition series with configuration $3d^{10}\ 4s^1$. It is the most stable in aqueous solution. A wide range of stereochemistries are exhibited by copper(II) compounds with four, five, and six-co-ordination predominating: in each structure variations from idealized geometries occur through bond and length and bond angle distortions.[8] The d^9 configuration of Cu^{2+} in an octahedral field leads to a significant Jahn-Teller distortion that usually manifests itself as an axial

elongation, consistent with the lability and geometric flexibility of Cu(II) complexes. Hence, Cu(II) compounds commonly have square-planar or square-pyramidal geometries with ligands weakly associated in the axial position(s) at distances of 2.3-2.6 Å. In such complexes, the single unpaired electron is localized in the $d_{x^2-y^2}$ orbital. Trigonal-bipyramidal coordination of Cu(II) is also possible, in which case the electronic ground state has usually the unpaired electron in the d_{z^2} orbital. In either case, bridged compounds in which two or more Cu(II) ions are linked by anionic ligands (e.g., oxide, hydroxide) are commonplace; either an antiferromagnetic or a ferromagnetic coupling between the Cu(II) ions is observed.[9]

Copper was first shown to be an essential biological element in the 1920s when anemia was found to result from Cu-deficient diets in animals and addition of Cu salts corrected this affliction.[10] The biological activity of copper, a physiologically metal element[11] has been the subject of numerous studies[10]. Copper is a heavy metal ion found throughout in nature and essential for the development and maintenance of most, if not all, animal cells.[12]

Copper ions are cofactors for a number of metalloenzymes and, as such, are required for normal cell physiology. Copper deficiency and overload syndromes in humans that result in the decreased activity of these enzymes have severe clinical outcomes associated with the impaired function of many tissues, including the brain, liver and heart. Copper has an established role in cell growth and proliferation that may be distinct from that it serves as a catalytic moiety in relevant cupro-proteins. The properties that make copper an ideal biological cofactor also allow it to potentiate free radical generation when unbound within the cell. Therefore, cells have evolved mechanisms to balance global copper content, and to distribute copper to different subcellular compartments. These mechanisms are based primarily on the collective activity of copper transporters, chaperones and molecules that chelate copper in biologically inert complexes.[13]

Copper is a bioessential element with relevant oxidation states +1 and +2.[14] The presence of unsymmetrical metal environments in several biological systems (e.g. in copper enzymes) has been linked to their redox properties. Cu is relevant for the functionality of several enzymes (e.g., tyrosinase, superoxide dismutase, cytochrome oxidase, amine oxidase, uricase etc.).[12] It has been established that copper-dependent enzymes are required for hemoglobin synthesis, growth, keratinization, pigmentation, bone formation, reproduction, fertility, development and function of the central and peripheral nervous systems, cardiac and nerve function, cellular respiration, extracellular connective tissue formation, vascularization, mental and behavioral development, and regulation of monoamine concentrations.[15] Copper enzymes is exclusively employed as a redox-active species, occurring in oxidation states +1 and +2. The usage of the Cu^{2+}/Cu^{+} couple in catalysis involves protein sites that are designed to cope with the remarkably different coordination preferences of the two ions. Cu^{+} is a soft cation, and prefers sulfur ligation with coordination numbers from two to four, whereas Cu^{2+} is relatively harder, and better binds N-donor ligands with higher coordination numbers (up to six). At variance with iron, copper is generally not bound in organic moieties such as haem groups, but its redox properties are most commonly modulated through amino acid residues, both of the first and of the second coordination sphere. For instance, so-called blue copper sites, which function in electron

relay, are constructed in such a way as to achieve a compromise between Cu^{+} and Cu^{2+} requirements, thus minimizing the structural reorganization upon oxidation/ reduction and optimizing the rate of electron transfer. Although Cu^{2+} is a strong Lewis acid, it is never used as such in enzymes. In fact, copper is not commonly used for this role in living organisms, possibly because of the strength of Cu^{2+}–ligand bonds that would oppose a fast enzymatic turnover. With respect to iron, copper is much less frequent in enzymes. This observation can be traced back to the later appearance of copper in the course of evolution. In particular, the very same event that caused iron to become a rare element, namely the appearance of an oxidizing atmosphere, also increased the bioavailability of copper, because of the higher solubility of Cu^{2+} salts with respect to Cu^{+} ones. It is then likely that living organisms moved towards a lesser usage of iron, and employed copper as an alternative metal for redox catalysis. This evolutionary shift is reflected in the nature of the substrates of copper enzymes, most of which are either O_2 or small molecules, such as nitrogen oxides, that were scarce before the emergence of an oxygenrich environment. This scenario can also explain the appearance of a copper-dependent superoxide dismutase in eukaryotes, which replaced the structurally unrelated ironand manganese-dependent enzymes found in prokaryotes.[3]

Mitochondria contain two enzymes, Cu,Zn superoxide dismutase (Sod1) and cytochrome c oxidase (CcO), that require copper as a cofactor for their biological activity. The copper used for their metallation originates from a conserved, bioactive pool contained within the mitochondrial matrix, the size of which changes in response to either genetic or pharmacological manipulation of cellular copper status. Its dynamic nature implies molecular mechanisms exist that functionally couple mitochondrial copper handling with other, extramitochondrial copper trafficking pathways. The recent finding that mitochondrial proteins with established roles in CcO assembly can also effect changes in cellular copper levels by modulating copper efflux from the cell supports a mechanistic link between organellar and cellular copper metabolism. However, the proteins and molecular mechanisms that link trafficking of copper to and from the organelle with other cellular copper trafficking pathways are unknown. Copper trafficking to, and within, the mitochondrion for metallation of CcO and Sod1 were proposed. Copper is required within the mitochondrion for the maturation of CcO and Sod1. Apo-ligand is predominantly distributed to the cytosol. Binding of copper results in its translocation/diffusion across the outer membrane (OM) (via open channels in orange), and its protein-mediated transport (blue) across the inner membrane (IM). The anionic ligand complex (CuL) is stored in the mitochondrial matrix in an inert formt that is biologically accessible. It is mobilized in response to what remain as poorly understood signals/stimuli and transported across the IM by either the same transporter, or a second transporter, where it is transferred to COX17 or CCS for metallation of relevant targets (CcO and SOD1, respectively). CuLmay also be ‘recycled’ through the transporter for eventual release to the cytosol (indicated by dashed arrow) in the absence of the copper chaperones or under high copper conditions.[13]

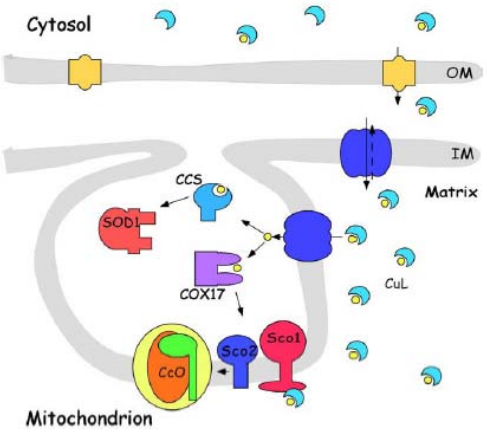

Figure II.1. Mitochondrial copper trafficking pathways.[13]

Copper dependent processes appear to be required for modulation of prostaglandin synthesis, lysosomal membrane stabilization, and modulation of histaminic activity.[15] The body of an average healthy adult male (70 kg) contains ~ 110 mg of Cu, much of which is in the skeleton (46 mg), skeletal muscle (26 mg), liver (10 mg), brain (8.8 mg) and blood (6 mg). Copper is the third most abundant transition metal element in biological systems.[10] However copper plays a crucial role in living systems, performing a wide variety of functions in the active site of proteins and enzymes involved in metabolism can also become toxic and potentially carcinogenic if not properly bound. Its redox reactivity may lead to severe injury to cells through oxidation of proteins, lipids, and nucleic acids, with generation of reactive oxygen species (ROS), that is, superoxide ion, hydrogen peroxide, and hydroxyl radical. Therefore, living cells seem to be well prepared to deal with copper ions, having an appropriate protein machinery that provide different ways for their absorption, transport, storage, and detoxification.[6]

Any essential element is classically expected to act within two distinct concentration ranges in vivo. Its very essentiality is usually expressed at trace levels within what is designated as ‘‘zone of physiological activity’’. A second range, known as ‘‘zone of pharmacotoxicological activity’’, lies at much higher concentrations at which the toxic properties of the element can be used for therapeutic purposes.[16] For some elements such as copper and iron, however, the situation may be more complicated. Copper appears to be usable for therapeutic purposes at normal physiological i.e., without needing to be administered. This occurs whenever copper is expected to catalyze chemical reactions that involve organic substances overtly perceived as the active therapeutic agents.[16]

Furthermore copper has received considerable attention with regard to its presence in normal blood plasma and serum components.[16] Research on copper metabolism in humans began after the discovery that copper was necessary for hemoglobin formation in rats.[17] In mammals, copper ions in mammals are tightly bound to protein carriers and transporters.[6] Indeed, Cu is absorbed in the gastrointestinal tract and transported in the serum bound to albumin and a-ceruloplasmin.[12] This may be important when investigating the fate of Cu-NSAIDs and the development of veterinary and pharmaceutical formulations of these complexes. Once absorbed, ~ 70-80% of plasma Cu is in a non-

exchangeable form, bound to ceruloplasmin (CP). The remainder is bound to albumin, transcuprien, metallothionein (MT) and low-molar- mass (l.m.m) complexes, e.g. L-His-Cu(II)-L-Ser, LHis- Cu(II)-L-Thr, as the exchangeable Cu fraction in blood. Albumin is the major drug binding protein in the body, particularly for acidic xenobiotics such as NSAIDs[10]. The Cu concentration range in the human serum according to the literature rent data is between 822 and 850 mg/L.[12] Copper homeostasis is a highly regulated process, and a variety of specific chaperones with high affinity for copper ensure that it is efficiently coordinated, avoiding interactions with cellular components.[6] The results of clinical studies suggest that the monitoring of the serum copper/zinc ratio may be a valuable tool, not only in determining the extent of malignancies, but also in predicting the efficacy of treatments[18] The level of Cu tends to increase in the human brain from infancy and declines gradually in all the other tissues until the tenth year of age, after which the concentration remains relatively stable.[12]

Copper is believed to possess antiinflammatory activity. The role of trace metallic elements, such as Cu in inflammation, is of great interest given their function as co-factors in metabolic processes involving articular/connective tissue and the immune system and their effect on PG synthesis.[10] Copper has been linked to RA for centuries. Folk-lore treatment of arthritis invariably involves copper, either in a copper-rich diet such as shellfish, nuts and cider vinegar, or the ubiquitous copper bangle.[19] Patients with RA and oesteoarthritis exhibit changes in the Cu distribution in the blood. For instance, there is an observed increase in total serum Cu in arthritis sufferers compared with controls. This is observed as an increase In CP-bound Cu and a decrease in albumin-bound and low-molecular-weight Cu effectively resulting in lower levels of bioavailable Cu, in the blood. Altered Cu concentrations have also been observed in the synovial fluid of RA and OA patients. A change in its metabolism is observed in acute and chronic inflammatory conditions. In acute inflammation, there are significant increases in both total Cu(II) and CP concentrations in serum, without notable changes in the Cu concentration in the liver. Likewise, in chronic inflammation, Cu serum concentrations are increased during the active phase, with appreciably higher than normal CP levels found In the synovial fluid of patients with RA and a net accumulation of Cu in inflamed areas. It is proposed that there is increased demand for Cu during inflammatory conditions, which is compensated for by enhanced intestinal absorption and/or decreased intestinal excretion of Cu. Moreover, a Cu deficiency is reported to have a pro-inflammatory effect. It has long been suggested that the mode of action of salicylates and other such anti-inflammatory drugs may involve the chelation of bioactive metal ions such as Cu(II), so facilitating the transfer of the metal to and from a site of inflammation or pain.[10]

II.2. Numerous metalloenzymes are Zn^{2+} - dependent.

Zinc is an important modulator of various cellular activities with both catalytic and structural roles. It is the cofactor of over 300 enzymes and is involved in the stabilization of the three-dimensional structure of many proteins, including more than 100 transcription factors containing zinc finger domains. Owing to these critical roles, the cellular homeostasis of zinc ions is strictly controlled at different levels by cell membrane zinc transporters, metallothionein sequestration, and storing in

intracellular compartments called “zincosomes”. Although zinc is an essential element, its excess induces apoptosis in different cell lines involving mitochondrial injury and oxidative stress production.[21]

Zinc was first shown to be required for the growth of the mold *Aspergillus niger* in 1869. Since then, zinc has been demonstrated to be essential for the growth, development and differentiation of all types of life, including microorganisms, plants and animals. After iron, zinc is the second most abundant trace metal in the human body; an average 70-kg adult human contains 2.3 g of zinc. The first zinc metalloenzyme, carbonic anhydrase II, was discovered in 1940. Since then, >300 zinc enzymes covering all six classes of enzymes and in different species of all phyla have been discovered. In most cases, the zinc ion is an essential cofactor for the observed biological function of these metalloenzymes. Furthermore, the biological functions of zinc, which are versatile and observed in many tissues, are most often associated with proteins.[22] Zinc is the second-most abundant metal ion in enzymes. The reason for the high occurrence of zinc in enzyme catalysis lies in the distinctive combination of properties displayed by this metal.[3] The inherent chemical potential and reactivity of zinc are not exceptional compared with those of other metals. However, unlike other first-row transition metals (e.g., Sc^{2+}, Ti^{2+}, V^{2+}, Cr^{2+}, Mn^{2+}, Fe^{2+}, Co^{2+}, Ni^{2+} and Cu^{2+}), the zinc ion (Zn^{2+}) contains a filled *d* orbital (d^{10}) and therefore does not participate in redox reactions but rather functions as a Lewis acid to accept a pair of electrons. This lack of redox activity makes Zn^{2+} a stable ion in a biological medium whose potential is in constant flux. Therefore, the zinc ion is an ideal metal cofactor for reactions that require a redox-stable ion to function as a Lewis acid–type catalyst, such as proteolysis and the hydration of carbon dioxide. Furthermore, due to the filled *d*-shell orbitals, Zn^{2+} has a ligand-field stabilization energy of zero in all liganding geometries, and hence no geometry is inherently more stable than another. This lack of an energetic barrier to a multiplicity of equally accessible coordination geometries can be used by zinc metalloenzymes to alter the reactivity of the metal ion and may be an important factor in the ability of Zn^{2+} to catalyze chemical transformations accompanied by changes in the metal coordination geometry. Nevertheless, in all zinc metalloenzymes studied to date, the binding geometry observed most often is a slightly distorted tetrahedral with the metal ion coordinating three or four protein side chains. However, fivecoordinate distorted trigonal bipyramidal geometry has been observed in the metal sites of Zn-substituted astacin. In addition, five-coordinate geometry has been suggested for the reaction intermediate in CA and carboxypeptidase A. A final important property of Zn^{2+} that makes it well suited as a catalytic cofactor is that ligand exchange is rapid, allowing for the rapid product dissociation required for efficient turnover.[22] Zinc is stable in the +2 oxidation state, and is redox inert. In particular, the Zn^{2+} ion has a radius (0.74 Å) similar to that of Mg^{2+}, and the electrostatic binding to negatively charged species, taking place for instance in fuculose aldolase, accounts for part of zinc functionality in the active site of enzymes. However, with respect to Mg^{2+}, Zn^{2+} has a higher electron affinity, and is thus a stronger Lewis acid. In particular, when bound to water, zinc can actually generate a hydroxide ion for attack of the substrate. Zn^{2+} is known to perform this function in a variety of enzymes (e.g. in peptide deformylase). In some enzymes, Zn^{2+} ions are involved both in generating the attacking nucleophile and in enhancing the electrophilicity of the substrate undergoing the attack, through the polarization of P–O or C–O bonds. Carboxypeptidase A

and thermolysin are well-known examples in which a single Zn^{2+} ion accomplishes both tasks. More recently, it has been proposed that the same holds also for matrix metalloproteinases. In other cases, Nature engineered dinuclear zinc sites in which one (e.g. in alkaline phosphatase) or both (e.g. in aryldialkylphosphatase and bacterial leucyl aminopeptidase) ions contribute to activate water, which bridges the two metals, and only one ion is involved in substrate binding and activation. Similar combination of roles is observed also for trinuclear zinc sites (e.g. in phospholipase C) and dinuclear mixed sites in which zinc increases substrate electrophilicity and a different metal activates water (e.g. iron in purple acid phosphatase).[3]

After an examination of a variety of small molecule coordination complexes in solution, classified zinc as a “borderline” metal, meaning that Zn^{2+} does not consistently act either “hard” (not very polarizable) or “soft” (highly polarizable) and does not have a strong preference for coordinating with either oxygen, nitrogen or sulfur atoms. In protein zinc-binding sites, the zinc ion is coordinated by different combinations of protein side chains, including the nitrogen of histidine, the oxygen of aspartate or glutamate and the sulfur of cysteine; among these, histidine is most commonly observed, followed by Other, much more rarely observed ligands include the hydroxyl of tyrosine, the carbonyl oxygen of the protein backbone and the carbonyl oxygen of either asparagine or glutamine. The varied ligands and coordination geometries in zinc metalloenzymes result in zinc-binding sites with a broad range of stability constants, reactivities and functions.[22]

A regulatory function of zinc requires a strict regulation of the cellular zinc content and its distribution. 30 to 40% of the cellular zinc is localized in the nucleus, 50% in the cytosol and cytosolic organelles and the remainder is associated with membranes. In the last few years, some of the zinc transport proteins that maintain this distribution have been identified in mammalian cells. These include plasma membrane zinc importer and zinc exporter proteins as well as transporters that mediate the sequestration of Zn^{2+} into intracellular vesicles. Most of the cellular zinc is bound to or at least associated with proteins or complexed by anions, hence the level of free intracellular zinc is very low. The major Zn^{2+} binding protein in mammalian systems is metallothionein which donates Zn^{2+} to enzymes and transcription factors with zinc finger domains wheras the apoprotein thionein accepts Zn^{2+} from binding sites in proteins with moderate affinity for Zn^{2+}. The latter authors have estimated from enzyme inhibition constants that inhibition of crucial enzymes by zinc may become significant with free Zn^{2+} above 10^{-8} M. Hence, the free cellular Zn^{2+} concentration may be estimated to be of this order of magnitude.[23]

All crucial decisions in the life of mammalian cells are involving zinc in its ionic or protein-bound form: be it cell growth and proliferation, differentiation or programmed cell death[23].The essentiality of zinc for growth and proliferation was recognized by the observation that zinc deficiency caused growth retardation in all organisms investigated. Growth and differentiation of eukaryotic cells generally are induced by growth hormones/growth factors that trigger cascades of intracellular signaling elements. These include hormone receptors, intracellular second messengers, cascades of protein kinases, protein phosphatases and transcription factors binding to promoters of the genes to be addressed. On all levels of cellular signal transduction zinc is involved, either as a structural

element or a regulatory factor or both. Thus zinc is an essential prerequisite for the progress of many signaling processes in eukaryotes. But there is also evidence for a direct signaling function of zinc: It modulates the GABA and NMDA receptors in mammalian brain cells and it binds to zinc sensing domains as in the case of the metal-regulated transcription factor MTF-1. Further, transcription factors have been detected that require zinc in the medium for binding to enhancers or their associated factors and probably are subject to modulation by zinc.[23]

Biochemical mechanisms for the function of zinc in cell proliferation were detected when zinc was shown to be a structural element in enzymes involved in DNA synthesis, transcription, aminoacyltRNA synthesis and ribosomal function . Furthermore, zinc is present in the zinc finger structures of transcription factors that control the activity of genes responding to growth factors.[23]

TFIIIA was the first transcription factor to be identified as a zinc protein. When the term DNA-binding *finger* was introduced for the nine repetitive domains in this protein, discovery followed a different path. The close spacing of metal ligands in the primary sequences of zinc finger proteins allowed recognition of recurring zinc binding motifs. Consequently, it became common practice to define any new protein with such a motif as a zinc protein, thus assuming the presence of zinc rather than determining it directly. On this basis, hundreds of zinc finger proteins were identified within about 15 years. The domains that zinc organizes in these functionally and structurally diverse proteins are key elements for the molecular recognition of nucleic acids, proteins, or lipids. With blueprints of entire genomes now in hand, we are beginning to grasp the size of the *zinc proteome*, at least with regard to the number of zinc finger proteins. Over one thousand genes in the human genome encode members of three protein families with zinc finger domains alone, i.e., C2H2 zinc fingers, RING fingers and LIM domains. In other words, the number of genes containing zinc finger domains exceeds 3% of the about 32,000 identified human genes. The set of signatures for other zinc proteins is less complete or even unknown for sites such as those between protein subunits.[28]

Figure II.2. Cartoon representation of the protein Zif268 (blue) containing three zinc fingers in complex with DNA (orange). The coordinating amino acid residues of the middle zinc ion (green) are highlighted.[42]

Zinc is not only a structural element but is also involved in regulatory mechanisms of cell proliferation. Based on observations that serum addition to mammalian cell cultures enhanced the cellular uptake of zinc, and that zinc deprivation by metal chelators caused decreased growth and DNA synthesis, zinc was proposed to be a second messenger of mitogenic signaling.[23] Zinc and

calcium synergistically stimulated DNA synthesis and mitogenic signaling in murine fibroblasts. And conversely, treatment of Swiss 3T3 cells with the zinc chelator DTPA inhibited thymidine incorporation into DNA (Chesters *et al.* 1989) and impaired the transcription of the thymidine kinase gene. The latter effect could be ascribed to the increased binding of an inhibitory transcription factor to the promoter of the thymidine kinase gene. Both zinc deficiency and zinc chelation caused impaired availability of growth hormones. In experiments with rats, zinc deficiency led to decreased secretion of growth hormone from the pituitary gland.[23]

The cellular homeostasis of zinc is at least partially controlled by metallothionein, which has been shown to play a role in the regulation of cell proliferation. MT is overexpressed in proliferating tissues, e.g. in regenerating rat liver, in developing rat liver and in various tumors. The overexpression of MT in developing tissues and at the transition from fetal to newborn rat development suggests a role for MT in differentiation, too. The differentiation ofmyoblasts to myotubeswas inhibited by the lack of zinc Generally, zinc protects from apoptosis induced by various agents. On the other hand, concentrations of extracellular zinc which exceed the capacity of homeostatic controlmay also induce programmed cell death in several mammalian cell lines.[23]

Every living organism must detoxify nonessential metals and carefully control the intracellular concentration of essential metals. Metallothioneins, which are small, cysteine-rich, metal-binding proteins, play an important role in these processes. In addition, the transcription of their cognate genes is activated in response to metal exposure. The zinc finger transcription factor MTF-1 plays a central role in the metal-inducible transcriptional activation of metallothionein and other genes involved in metal homeostasis and cellular stress response. Moreover phosphorylation of MTF-1 plays a critical role in its activation by zinc and cadmium. Inhibitor studies indicate that multiple kinases and signal transduction cascades, including those mediated by protein kinase C, tyrosine kinase, and casein kinase II, are essential for zinc- and cadmium-inducible transcriptional activation.[25]

Essential roles, organisms must maintain adequate intracellular zinc concentrations to support cell growth even when extracellular or dietary levels are low. To accomplish this feat, cells have evolved with efficient uptake systems to allow accumulation of zinc even when it is scarce. These uptake systems use integral membrane transport proteins to move zinc across the lipid bilayer of the plasma membrane. Once inside a eukaryotic cell, a portion of the zinc must be transported into intracellular organelles to serve as a cofactor for various zinc-dependent enzymes and processes present in those compartments. For example, the mitochondrial isozyme of alcohol dehydrogenase is a zinc-dependent enzyme. Therefore, transporter proteins must be present in organelle membranes to facilitate this flux of zinc. Zinc can also be stored in certain intracellular compartments when supplies are high and used later if zinc deficiency ensues. Again, zinc transporters are required to facilitate this transport in and out of organelles. Although zinc is essential, excess zinc can be toxic to cells. The mechanism of zinc toxicity is not known but the metal may bind to inappropriate intracellular ligands or compete with other metal ions for enzyme active sites, transporter proteins, etc. Therefore, while maintaining adequate levels of zinc for growth, cells must also control intracellular levels when exposed to excessive zinc concentrations. Several mechanisms exist to detoxify excess zinc including the binding of the metal to

cytoplasmic macromolecules. Metallothionein proteins may play such a detoxification role. Zinc transporters can also aid in detoxification by facilitating intracellular sequestration within organelles, or efflux of zinc across the plasma membrane. Finally,in multicellular organisms, cellular zinc efflux systems are required for the distribution of dietary zinc to other tissues. For example, in the enterocyte of the mammalian intestine, zinc transporters must take up zinc from the intestinal lumen and then efflux that zinc across the basal lateral membrane into the portal blood.[24]

Labile zinc (i.e., zinc ions that are free or only loosely bound to proteins or small molecules) is of special interest, because it can easily exchange between different compartments of the cell and bind to numerous proteins, thereby altering their biological activity. For the maintenance of the homeostasis of this labile zinc, three main mechanisms are reported, zinc can be buffered by binding to proteins, mainly at cysteine, histidine, aspartate, and glutamate residues. The major zinc buffering protein is metallothionein. Zinc transport through the plasma membrane by importers, e.g., hZip1 and hZip2 in humans or export proteins such as ZnT-1. Zinc sequestration by vesicular compartments, mediated by transporters like ZnT-2. While the amino acid sequences of the zinc transporters are known, their transport mechanisms and their driving forces remain unidentified. A major progress in the investigation of labile zinc was the development of zinc-specific fluorescent probes, e.g., TSQ or Zinquin. When investigated by fluorescence microscopy, the zinc-dependent fluorescence of these probes is not evenly distributed throughout the entire cell. Vesicles, so-called zincosomes, which can contain high amounts of labile zinc, appear as intense punctuate staining, whereas nuclear fluorescence is significantly below the cytoplasmic level.[26]

Various cellular functions are influenced by essential trace elements such as the divalent cations zinc (Zn^{2+}) and manganese (Mn^{2+}). The physiological concentrations of these cations are strictly controlled and divergence from normal levels are associated with various diseases.For instance, Zn^{2+} deficiency is mostly associated with increased apoptosis resulting in thymus atrophy, loss of splenocytes and lymphopenia, suggesting that this deficiency alters the apoptotic process involved in normal lymphopoiesis. Nevertheless, Zn^{2+}-mediated regulation of apoptosis in vivo is probably more complex. Thus, patients with Down's Syndrome, have low plasma Zn^{2+} levels and present both immature myeloid cells in peripheral blood and large numbers of apoptotic peripheral blood cells. Several studies have shown that Zn^{2+} supplementation in Down's Syndrome patients results both in the disappearance of peripheral myeloid precursor cells through an apoptotic process and the reduction of apoptotic peripheral blood cells.[27]

Zinc is also used in biological studies to gain information about non-zinc containing systems. It can be a convenient redox inactive replacement for the study of complex systems with multiple redox centers. For example, the mechanism of quenching the triplet state of zinc cytochrome c by iron(II) and iron(III) cytochrome c has been studied. Zinc insertion has been used to get around the difficulty of studying two heme proteins with the same absorption spectra and provides rate constants for iron and iron-free cytochrome c quenching.[1b] It also plays a role in the structural protection of membranes, in the neutralisation of free radicals and in the neural transmission involved in the formation of memories[29]. Investigators often use indirect measures of zinc status because only a small percentage

of the body's zinc is in plasma. Most of the body's zinc is located in muscle, bone and liver, where it turns over slowly. Biological measures of zinc status, such as plasma and hair zinc, are useful at a population level but are imperfect indicators of individual functional impairment related to zinc deficiency.[30] Several diseases have been shown to be associated with low zinc plasma levels, e.g. acrodermatitis enteropathica, alcohol-induced liver disease, sickle cell anaemia, and a variety of intestinal diseases. The latter include Crohn's disease, sprue, short bowel syndrome and the complications arising from jejunal-ileal bypass. In addition, low plasma zinc levels hale been reported in eating disorders and major depression. Zinc may function as an anti-depressant.[29] In Alzheimer's disease (AD), in addition to low plasma levels, decreased zinc concentrations have also been found in post-mortem brain samples, especially in the hippocampus, where the processing of information to be stored as memory takes place.[29] Zinc is implicated in several neuropathological conditions, including brain injury and Alzheimer's disease. Neuronal accumulation of free zinc contributed to neuronal injury induced by traumatic brain injury (TBI), seizures, and ischemia; chelating extracellular zinc dramatically reduced neuronal injury[31]. These results suggest that the elevation in the levels of MT and Zn^{2+} may be used as a helpful marker for detecting malignancy.[18]

II.3. Manganese ions, are important modulators of cell activation.

Manganese is more electropositive than any of its neighbours in the periodic table and the metal is more reactive. For manganese the +2 oxidation state, represented by the high-spin Mn^{II} cation is the most stable. This may be taken as an indication of the stability of the symmetrical d^5 electron configuration.[71] Manganese, with an electronegativity of 1.55, has a preference for bonding of predominately ionic character to oxide, hydroxide and carbonate ligands. The electron configuration of Mn^{2+} has five unapired electrons in almost all of its complexes, providing no ligand field stabilization energy (LFSE) and resulting in complex of usually lower stability compared to those of the other bivalent 3d transition metal ions.[79] Manganese is an essential element in many biological processes. Two functional values can be distinguished: the Mn^{2+} as a Lewis acid, like divalent ions Magnesium, Calcium, Zinc and in higher oxidation states (Mn^{3+}, Mn^{4+}) as an oxidation catalyst, like Copper, Iron, Cobalt.[32] Mn is one of the most abundant naturally occurring elements in the earth's crust; it does not occur naturally in a pure state. Oxides, carbonates and silicates are the most important Mn-containing minerals. Depending on its oxidation state, Mn is utilized in countless industrial processes, such as the production of dry cell batteries, steel, fuel oil additives and antiknock agents.[33]

Manganese is an essential metal cofactor in enzymes (transferases, hydrolases, lyases, glutamine synthetase and integrins) that cover the entire range of enzyme functionality.[1c] In many manganoproteins the manganis is in II oxidation state and can often be replaced by magnesium(II) without loss of function. In other cases, where redox activity is involved, some naturally occurring forms containing either manganese or iron are known.[34] The most well known Mn(II) proteins are: *Arginase*, containing 4 Mn(II) ions per enzyme; an enzyme present in lipids that is required for ammonia elimination, *Concanavalin A*, a manganese-calcium metalloprotein; *Glutamine-Synthatase*, requiring two Mn(II) ions; *Phosphoenolpyruvate Carboxykinase*, converting irreversible cytoplasmic

oxaloacetate to phosphoenolpyruvate; a *manganese ribonucleotide reductase* isolated from B ammoniagemes; *Mn Thiosulfate Oxidase* containing a binuclear Mn(II) site; *Isopropylmalate Synthase*, with the Mn bound to the S-H group near site; *Pyruvate carboxylates*, the first metalloenzyme shown to contain manganese. Manganese redox enzymes with manganese in oxidation states 3+ and 4+ are: *Manganese SOD* catalyzing the dismutasion of superoxide radicals to oxygen and hydrogen peroxide with a single Mn(III) center; enzyme typically found in the mitochondria. The manganese *Peroxidase (MnP)* is one of the two known enzymes capable for thr oxidative degradation of lignin containing protoporphyrin IX heme prosthetic group; non heme manganese catalase containing two manganese per subunit and the *Oxygen Envolving Complex*, catalyzing one of the most important reactions occurring in the plants, the light driven oxidation of water to oxygen and protons,containing four manganese atoms while the presence of calcium and chloride ions is required for proper functioning.[32] Although manganese is relatively common, manganese-containing enzymes, generally do not have an absolute requirement for this metal. Rather, manganese appears to be interchangeable with other metals, in particular with magnesium and zinc. In fact, manganese is always present in the +2 oxidation state even though other states are possible in biological systems (e.g. +3 in manganese catalase), and its functional importance is, similarly to the other divalent cations, as a Lewis acid and electrostatic stabilizer. The exchangeability of Mn^{2+} with Mg^{2+}, Ca^{2+} and Zn^{2+} depends on the intermediate properties of Mn^{2+} relative to these ions, including the in-between length of its radius (0.83 Å) and its borderline hard–soft character, and may occur, at least in principle, also in living cells. However, the intracellular concentration of Mn^{2+} is considered to be in the micromolar range, and the other ions are expected to outperform Mn^{2+} in the competition for both oxygen-donor sites (where Mg^{2+} comes first because is more abundant) and nitrogen- and sulfur-donor sites (where Zn^{2+} and Cu^{2+} prevail according to the Irving–Williams series), unless relatively high manganese concentrations are attained in specific compartments. Genuine manganese enzymes, therefore, are characterized by specifically designed active sites, which typically contain a combination of hard and soft donors and rely on ion size as a key factor for selection.[3]

Moreover, Mn plays a role in the modulation of the immune system, and in protein, lipid and carbohydrate metabolism. Evidence also corroborates the involvement of Mn in the stellate process production in astrocytes, as well as in the metabolism of brain glutamate to glutamine, a step carried out by the astrocyte-specific enzyme, glutamine synthetase.[33]

Manganese is an essential element with a recommended daily intake by humans of between 2 and 5 mg.[55c] Tracts of manganese are found in many plants and bacteria, and a healthy human adult contains about 10-20 mg of Mn^{2+} distributed approximately equally between the soft tissue and bone.[1c] Tissues with high levels of mitochondria tend to have high manganese concentrations, as the concentration of manganese in mitochondria is higher than in cytoplasm.[35] The distribution of manganese within the body is not uniform; the concentration within the central nervous system is orders of magnitude greater than in most other organs.[1c] Manganese absorption is thought to occur throughout the small intestine The efficiency of enanganese absorption is typically reported to be low, and it is not thought to be under homeostatic controls that are specific for manganese.[1c]

Mn plays an important role in the development and functioning of the brain, particularly in some neurodegenerative diseases and lead to a neurological disorder resembling Parkinson's disease (PD)[12], a disease known as manganism. Patients suffering from manganism exhibit a signature biphasic mode of physical decline, which comprises of an initial phase of psychiatric disturbance and neurological deficits which are followed by motor defects such as akinetic rigidity, dystonia and bradyskinesia.[33]

Mn deficiency may result in birth defects, poor bone formation and an increased susceptibility to seizures. The basis of Mn neurotoxicity lies on the ability of bivalent form Mn^{2+} to oxidize to the trivalent form Mn^{3+}, a powerful oxidizing species. This finding further supports the hypothesis that high doses of Mn can induce manganism, and chronic exposure of low doses can accelerate the physiological aging of neurological function[12]. Dietary manganese deficiency is rare in humans, its uptake is tightly regulated, and any excess of ingested Mn is readily excreted via the bile; in animals it results in impairment in oxidant defences, cardiovascular and insulin production systems, altered lipoprotein metabolism, arteriosclerosis, and diabetes. If the deficiency occurs during early development, there are pronounced skeletal abnormalities and an irreversible ataxia. Manganese toxicity in humans occurs in individuals with exposure to high levels of airborne manganese or where manganese excretory pathways are compromised. The levels of manganese intake associated with adverse effects are uncertain.[1c]

Due to the delicate relationship between Mn's essentiality and toxicity,Mn homeostasis is vital for the optimal functioning of any organism. Although some research has focused on mechanisms associated with the transport of Mn across the blood–brain barrier (BBB), the exact identity of the carrier(s) involved in Mn trafficking into the brain is still controversial. During the past two decades, various transportmechanisms have been identified, including active transport and facilitated diffusion. More recently, it has been established that Mn can also be transported via high affinity metal transporters such as calcium (Ca) and iron (Fe) transporters. Some of these transporters include the divalent metal transporter (DMT1), which belongs to the family of natural resistance-associated macrophage protein (NRAMP). Contribution of each of these transporters remains unknown, it is likely that optimal tissue Mn concentrations are maintained by the involvement of all of these transporters.[33]

II.4. Cadmium – architecture of coordination.

The presence of a filled d-shell for cadmium means that this metal are flexible for its coordination geometries; there is no ligand field stabilization effect.[36] The most invariable oxidation state of this elelent is +2. Cadmiu (likewise Zn^{II}) favour 4-coordinate tetrahedral complexes though Cd^{II}, being larger, forms 6-coordinate octahedral complexes more readily than dose Zn^{II}. Cd has no known beneficial biological role and are amongst the most toxic elements. Cadmium is extremely toxic and accumulates in humans mainly in the kidneys and liver, prolonged intake, even of very small amounts, leads to dysfunction of the kidneys.[34] Cadmium is generally regarded to be far more toxic than lead. Chronic cadmium poisoning can cause embrittlement of bones and extremely painful deformations of the skeleton. In its ionic form, Cd^{2+} (ionic radius 95 pm) shows great chemical

similarity with two biologically very important metal ions, viz. the lighter homologue Zn^{2+} (74 pm), and Ca^{2+} (100 pm) which comes very close in size. Accordingly, cadmium as the 'softer' and more thiophilic metal may displace cysteinate-coordinated zinc from its enzymes and even replace it in special cases, while it can also substitute for calcium, e.g. in bone tissue[41]. It can inhibit the action of zinc enzymes by displacing the zinc. It acts by binding to the –SH group of cysteine residues in proteins (e.g., matallothioneins) and so inhibits SH enzymes.[34]

These 'metallothionein' proteins feature a highly conserved sequence homology, in particular with regard to the cysteine residues, it can thus be assumed that they had been optimized early in the evolution and that they possess an essential function. In addition to the liver and kidneys, the small intestines, the pancreas and the testicles of mammals contain larger amounts of these proteins. It was found that a total of seven metal centers, each of them four-coordinate, can be bound in two clusters by nine and eleven cysteinate residues, respectively. Peptide synthesis of the cysteine-rich domains of metallothioneins has demonstrated that such small synthetic oligopeptides can similarly bind metals like Cd^{2+} and can thus indicate approaches toward modified metallothioneins. Crustaceans and microorganisms such as yeast contain metallothioneins with slightly different cluster compositions and metal selectivities.[41]

In particular, cadmium is an environment pollutant chich inhibits RNA polymerase activity in vivo, and reacts readily with proteins and other biological molecules.[37] Cadmium is well established as a human carcinogen. Occupational exposure correlates with increased frequencies of prostate, skin, lung, oesophageal, nasal and lung cancers in particular, for which a dose response relationship has been demonstrated for excess human mortality. In fact all cadmium compounds are classified as potential human carcino- gens. However, the underlying biochemical mechanism(s) of these effects are not fully understood.[38] Therefore, it is worth investigating the influence of toxic metal ions such as cadmium especially, on the copper homeostasis because in recent years studies have shown that cadmium can invoke some effects on cellular redox systems. As cadmium does not participate in the Fenton reaction directly only indirect generation of free radicals is possible. Cadmium enhanced ROS via suppression of free radical scavengers (e.g., glutathione) or by inhibition of detoxifying enzymes (such as SOD). Another possible mechanism which helps to explain the increase in ROS caused by cadmium is the displacement of copper from various intracellular sites. This increases the concentration of ionic copper, which can then cause oxidative stress via the Fenton reaction.[39] The coordination chemistry of cadmium(II) has received increased attention lately, in part due to concerns regarding its impast on the environment and its toxicological effects on heath.[40]

In contrast to many other heavy metals and toxic elements, cadmiurn *does not* easily pass into the central nervous system or the fetus because, in its ionized form and under physiological conditions, it cannot be bioalkylated to form potentially membrane-penetrating organometallic compounds such as R_2Cd or RCd^+.The instability of such species in aqueous media is related to the electropositive character of Cd as reflected by the rather low oxidation potential.[4]

References

1. a) McCleverty, J., Meyer, T.J. **9**, *Comprehensive coordination chemistry* (2005).
   b) McCleverty, J., Meyer, T.J. **6**, *Comprehensive coordination chemistry* (2005).
   c) McCleverty, J., Meyer, T.J. **5**, *Comprehensive coordination chemistry* (2005).
2. Vinod, M., Keshavayya, J., Vaidya, V.P., Khan, M.H., *Journal of Coordination Chemistry* **61**, 2629–2638 (2008).
3. Andreini, C.,Bertini, I.,Cavallaro G., Holliday, L. ,Thornton, J.M., *J Biol Inorg Chem* **13,** 1205–1218 (2008.)
4. Shi, W., Chance, M.,R. *Cell. Mol. Life Sci.* **65**, 3040 – 3048 (2008).
5. Cini, R. *Comments on Inorganic Chemistry* **22,** 151 — 186 (2000).
6. Cerchiaro, G., Costa Ferreira, A.M. *J. Braz. Chem. Soc.,* **17,** 1473-1485, (2006).
7. Chung, Y.T., Ling, Y.C., Yang, C., S., Sun, Y.C., Lee, P.L., Lin, C.Y., Hong, C.C., Yang, M.H., *Anal. Chem.*, **79,** 8900-8910 (2007).
8. Nicholas, D. *Complexes and first-row transition elements* (1974).
9. Mirica, L.,M., Ottenwaelder, X., Stack, T.D., *Chem. Rev.* **104,** 1013-1045 (2004).
10. Weder, J.E., Dillon, C.T., Hambley, T.W., Kennedy, B.J., Lay, P.A., Biffin, J.R., Regtop, H.L., Davies, N.M. *Coord. Chem. Rev.* **232,** 95-126 (2002).
11. Hernández-Gil, J., Perelló L., Ortiz, R., Alzuet, G., González-Álvarez, M., Liu-González, M. *Polyhedron* **28,** 138–144 (2009).
12. Zatta, P., Drago, D., Zambenedetti, P., Bolognin, S., Peruffo, N.A., Cozzi, B. *Journal of Chemical Neuroanatomy* **36,** 1–5 (2008).
13. Leary, S.C., Winge, D.R., Cobine, P.A. *Biochimica et Biophysica Acta* **1793**, 146–153 (2009).
14. Patel, R.N., Singh, N., Gundla, V.L.N., Chauhan, U.K. *Spectrochimica Acta Part A* **66,** 726–731 (2007).
15. Theodorou, A., Demertzis, M.A., Kovala-Demertzi, D., Lioliou, E., Pantazaki, A.A., Kyriakidis, D.A., *BioMetals* **12,** 167–172 (1999).
16. Halova-Lajoie, B., Brumas, V., Fiallo, M.M.L., Berthon, G., *Journal of Inorganic Biochemistry* **100**, 362–373 (2006).
17. Hart, E.B, Steenbock, J., Waddell, J., Elvehjem, C.A. *J Biol Chem* **77,** 797–812 (1928).
18. Ebadp, M., Iversen, P.L. *Gen. Pharmac.* **25,** 1297-1310 (1994).
19. Jackson, G.E., Mkhonta-Gama, L., Voye, A., Kelly, M., *Journal of Inorganic Biochemistry* **79,** 147–152 (2000).
20. Walker, W.R., Reeves, R.R., Brosnan, M., Coleman, G.D., *Bioinorg. Chem*. **7,** 271 (1977).
21. Donadelli, M., Pozza, E.D., Scupoli, M.T., Costanzo, C., Scarpa, A., Palmieri, M. *Biochimica et Biophysica Acta* **1793**, 273–280 (2009).
22. McCall, K.A., Huang, C.C., Fierke, C.A. *J. Nutr.* **130,** 1437S—1446S (2000).
23. Beyersmann, D., Haase, H. *BioMetals* **14,** 331–341 (2001).
24. Gaither, L.A., Eide, D.J. *Biometals* **14** , 251–270 (2001).
25. Saydam, N., Adams, T.K., Steiner, F., Schaffner, W., Freedman, J.H.,*J. Biol. Chem.* **277,** 20438–20445 (2002).
26. Haase, H., Beyersmann, D. *Biochem. Biophys. Res. Commun.* **296**, 923–928 (2002).
27. Schrantz, N., Auffredou, M.T., Bourgeade, M.F., Besnault, L., Leca, G., Vazquez, A. *Cell Death and Differentiation* **8,** 152-161 (2001).
28. Maret, W. BioMetals **14,** 187 (2001).
29. Potocnik, F.C.V., Rensburg, S.J., Hon, D., Emsley, R.A., Moodie, I.M., Erasmus, M. *Metab Brain Dis* **21,** 139–147 (2006).
30. Black, M.M. *J. Nutr*. **133,** 1473S–1476S (2003).
31. Hellmicha H.L., Fredericksonb, C.J., DeWitta, D.S., Sabanc, R., Parsleya, M.O., Stephensona, R., Velascod, M. Uchidae, T., Shimamura, M., Prough, D.S. *Neuroscience Letters* **355,** 221–225 (2004).
32. Kessissoglou, D.P. (editor) *Bioinorganic Chemistry. An Inorganic Perspective of life.*1995.
33. Au, C., Benedetto, A.,, Aschner, M. *NeuroToxicology* **29,** 569–576 (2008).
34. Greenwood, N.N. Earnshaw, A. Chemistry of the Elements (1997).
35. Sigel, A., Sigel, H. *Metal ions in biological systems* vol. 37 (2000).
36. Housecroft, C.,E. The heavier d-block metals: Aspects of inorganic and coordination Chemistry 2006

37. Fernández-Fernández, C., Bastida, R., MacíasP A. Pérez-Lourido, P.,
38. O'Brien, P., Salacinski, H.J., *Arch Toxicol* **72,** 690-700 (1998).
39. Barszcz, B., Jabłonska-Wawrzycka, A., Stadnicka, K., Jezierska, J. *Polyhedron* **27,** 3500–3508 (2008).
40. Pons, J., García-Antón, J., Font-Bardia, M., Calvet, T., Ros, J. *Inorganica Chimica Acta* xxx, xxx–xxx (2009).
41. Kaim, W., Schwederski, B. *Bioinorganic Chemistry: Inorganic Elements in the Chemistry of Life*. Wiley (1994).
42. http://encyclopedia.thefreedictionary.com/Zinc+finger

III Nonsteroidal anti-inflammatory drugs' complexes with transitions metals: Mn(II), Cu(II), Zn(II) and Cd(II).

It is well established that metal ions play a wide range of important roles in biological systems. The presence of drugs that can compete with other biological molecules for the metal ions, changes the distribution of these ions in blood plasma and other fluids. On the other hand, presence of these metal ions can affect the bio-availability of these drugs. Knowledge of the species formed by combining a metal ion with a drug provides useful information to approach the mechanisms of action of the drug for a disease under treatment and ultimately this can also diminish collateral effects and enhance the efficacy of the parent drug.[1] Synthesis and study of metal complexes with active drugs as ligands is a research area of increasing interest for inorganic, pharmaceutical and medicinal chemistry and has concentrated much attention as an approach to new drug development.[2]

The search of new metal based pharmaceutical compounds has acquired new impetus during the last few years with the aim to find species that have high activity, low toxicity and with the goal to circumvent the drug resistance. Cancers, inflammations, and diseases of the immune system are often related each other and attract much research efforts. It has been reported by that treatments with non-steroidal-anti-inflammatory drugs (NSAIDs) protect against lung cancers and breast cancer. The interest on metal complexes with drugs as ligands has much increased because of the improved activities of the complexes when compared to the free ligands and because multi-therapies can stem from the same coordination molecule. Different active functions can be combined in the same molecule through coordination chemistry. Some advantages that can come from coordination compounds are: (a) synergistic effects of the ligands and the coordination residue, (b) protection from the enzymatic degradation of the drug, (c) tuning of the hydrophobicity/ hydrophilicity, (d) superior transport process through cell membranes.[3]

Combined therapies are nowadays very often administered in many diseases with the aim of increasing efficacy and circumventing drug resistance.Different active functions can be successfully combined in the same molecule through coordination chemistry.[2] Metal-binding compounds are being explorer as potential anticancer agents Metals are involved in a variety of biological processes, and until recently, it has been assumed that the cytotoxicity of metal-binding compounds was due entirely to their ability to remove the metal in question from key biological reactions.[4]

Results from in vitro studies on novel classes of metal complexes with NSAIDs showed a potent oxygen radical scavenger activity, and selective cytotoxic activity on cancer cell lines, lung (NCI-H23, HOP-92), central nervous system (SNB-19, XF-498), melanoma (SK-MEL-5, UACC-62), ovarian (SK-OV-3) cells when analyzed for administration [Cu(HPIR)2(DMF)2].[3]

The synthesis of metal complexes with nonsteroidal anti-inflammatory drugs (NSAIDs) as ligands has acquired new impetus in the past decade. First, on the basis of pure co-ordination chemistry NSAIDs are very versatile ligands and show a huge variety of ligating modes as function of the metal and the environmental conditions. The information collected from the preparative, structural and reactivity studies have high significance for several fields which span from the bio-sciences to the

material sciences. Second, NSAIDs have numerous applications as pharmaceutical agents. Third, for this type of drugs the complex formation with specific metals may improve the activity towards certain diseases and hopefully may increase the activity spectrum. The combination of two or more different species into the same compound may bring to a multitherapeutic agent which can be expanded by the synergic action of the metal residue once the coordination compound dissociate inside the target tissue. The coordination chemistry of non-steroidal anti-inflammatory drugs (NSAIDs) has been studied by several groups worldwide. Some complexes have increased pharmaceutical or biological activity with respect to the drug, or are interesting from a purely chemical point of view. Most of the NSAIDs, including aspirin, possess a carboxylate group, which is able to coordinate metal ions.[5] Metal complexes of NSAIDs with interesting structures and pharmacological profile have been reported.[2,5,6] The antiinflammatory activity of NSAIDs and most of its other pharmacological effects are related to the inhibition of the conversion of arachidonic acid, AA, to prostaglandins, which are mediators of the inflammatory process. The enzymes cycloxygenase, COX and lipoxygenase, LOX, which catalyze the oxidative metabolism of AA, are useful targets for the design and the development of new drugs that substantially inhibit the generation of the final inflammatory products and the propagation of inflammation.[5] It has long been suggested that the mode of action of many anti-inflammatory drugs may involve the chelation with some bioactive metals such as Cu(II), Zn(II), Cd(II) and it facilitates the transfer of the metal to and from a site of inflammation or pain.[1]

The past decade has seen an upsurge of interest in metal ion therapeutics for both diagnosis and treatment of diseases. Important in this regard is the ability of metal ions to bind proteins and peptides in vivo. Of particular interest, Cu(II) chelating agents have been observed to reduce inflammation associated with rheumatoid arthritis (RA).[7] Some of the earliest trials of the efficacy of Cu complexes followed on from the hypothesis that arthritis was bacterial in nature and may respond to treatment with heavy metals, e.g. Cu and Au. Promising evidences of the benefit of copper complexes were reported afterwards. There was a decline in experimental work on Cu antiinflammatory agents from the 1950s, which is attributed to the appearance of the corticosteroids and later the NSAIDs.[8] However for the design of Cu(II) chelating agents targeting at inflammation , the Cu(II) would have to be bio-available, and compounds possessing the potential of facilitating transport of Cu(II) in human blood plasma to sites of inflammation have to be developed. Although Cu(II) complexes under physiological conditions administered orally and intravenously have been reported to increase the bio-availability of Cu(II) in vivo, it is difficult to move the coordinated metal ion through a series of body compartments without binding to proteins. One essential requirement for the Cu(II) complexes is the formation of electrically neutral species at physiological pH so as to enable easy perfusion into tissues with minimal renal loss.[7] The biological role of copper(II) and its synergetic activity with drugs have been the subject of a large number of research studies. The antifungal and antibacterial properties of a range of Cu(II) complexes have been evaluated against several pathogenic fungi and bacteria.[9] Several reviews have been published on the anti-inflammatory activity of copper complexes. In clinical studies on mice, reduction in inflammation was achieved. There are several possible mechanisms for the anti-inflammatory activity of copper complexes. The copper may induce lysyl oxidase activity,

modulate prostaglandin synthesis, induce or mimic superoxide dismutase activity, decrease the permeability of human synovial lysosomes and modulate the physiological effects of histamine.[7]

Reports abound in the literature concerning the active role of copper complexes in the control of inflammatory diseases.[10] A variety of recent observations indicate that copper when co-administered with anti-inflammatory drugs exhibit synergistic activity. It is also reported that there is an increased demand for Cu(II) during inflammatory conditions, which is compensated for by enhanced intestinal absorption and/or decreased intestinal excretion of Cu(II)[1]. The proposed curative properties of Cu-based NSAIDs have led to the development of numerous Cu(II) complexes of NSAIDs with enhanced anti-inflammatory activity and reduced gastrointestinal, GI, toxicity compared with their uncomplexed parent drug. These low toxicity Cu drugs have yet to reach an extended human market, but are of enormous interest, because many of today's anti-inflammatory drug therapies, including those based on the NSAIDs, remain either largely inadequate and/or are associated with problematic renal, GI and cardiovascular side effects.[5] Besides the role of copper complexation in enhancing the pharmacological profile of NSAID activity and reducing toxicity, other pharmacological activities of copper complexes, and their potential as antiarthritic, antiulcer, anticancer, antidiabetic and antiepileptic drugs, have been reported. Sorenson found that the copper*(II)* complex of 3,5-diisopropylsalicylic acid, $[Cu(II)(3,5\text{-}Dips)_2]_2$, attracts much interest because of its radioprotectant, radiorecovery, anti-inflammatory, antiulcer, antineoplastic, anticarcinogenic, anticonvulsant, antidiabetic, and analgetic activities. The binuclear copper*(II)* complex of diclofenac, $[Cu(L)_2(H_2O)]_2 \cdot 2H_2O$, was found to have an antiinflammatory profile superior to diclofenac when inhibiting inflammationsdue mainly to the activation of lipooxygenase and/or to the complement systems. The metal–ligand association seems to play a specific role, which sustains the hypothesis advanced by Sorenson[11] that copper complexes are the active forms of these drugs. In these drugs, either the ligand simply behaves as a carrier that brings copper to the target or the complex interfering with the inflammatory process acts as catalyst.[5] The synthesis and crystal structures of copper(II) complexes of NSAIDs piroxicam, meloxicam, indomethacin, niflumic acid and diclofenac were reported. Other proposed modes of action of Cu-NSAIDs include stabilization of polymorphonuclear leukocytes (PMNL), which are part of the immune system and exert phagocyte activity, down-regulation of phosholipase A_2, inhibition of lipid peroxidation and microsomal NADPH oxidation[5]. Moreover Sorenson discussed modes of anti-inflammatory action of the Cu complexes, including gastric sparing activities due to inhibition of SOD activity. SOD activity, redox behavior, lipophilicity and stability constants may be useful parameters in evaluating the biological activity of these Cu compounds A review of the synthesis and crystal structures of a number of anti-inflammatory compounds as ligands in metal complexes and a review of copper complexes with NSAIDs have recently been reported[2,5,6,8]. The superoxide radical anion has been demonstrated to be a mediator of ischemia, injury, inflammatory and vascular diseases. Superoxide dismutase, SOD, catalyses the dismutation of superoxide radical anions to the non-radical products oxygen and hydrogen peroxide and protects living cells against the toxicity of hyperoxia. The application of superoxide dismutase as a pharmaceutical has attracted considerable attention. However, SODs have molecular weights too high

to cross cell membranes and can only provide extracellular protection. In order to circumvent this difficulty, a stable non-toxic, low molecular-weight metal complex that catalyses the dismutation of superoxide anion might be a suitable alternative to superoxide dismutase in clinical applications with the desirable qualities of low cost, cell permeability and non-immunogenicity.[10] The Cu(II)–NSAID complexes have also been implicated to have better anti cancer effect. Piroxicam and meloxicam exist as anion near physiological pH that makes their approach to the poly-anionic backbone prohibitory.[1]

III.1. Coordination architectures of Cu-NSAIDs. Copper complexes of fenamates.

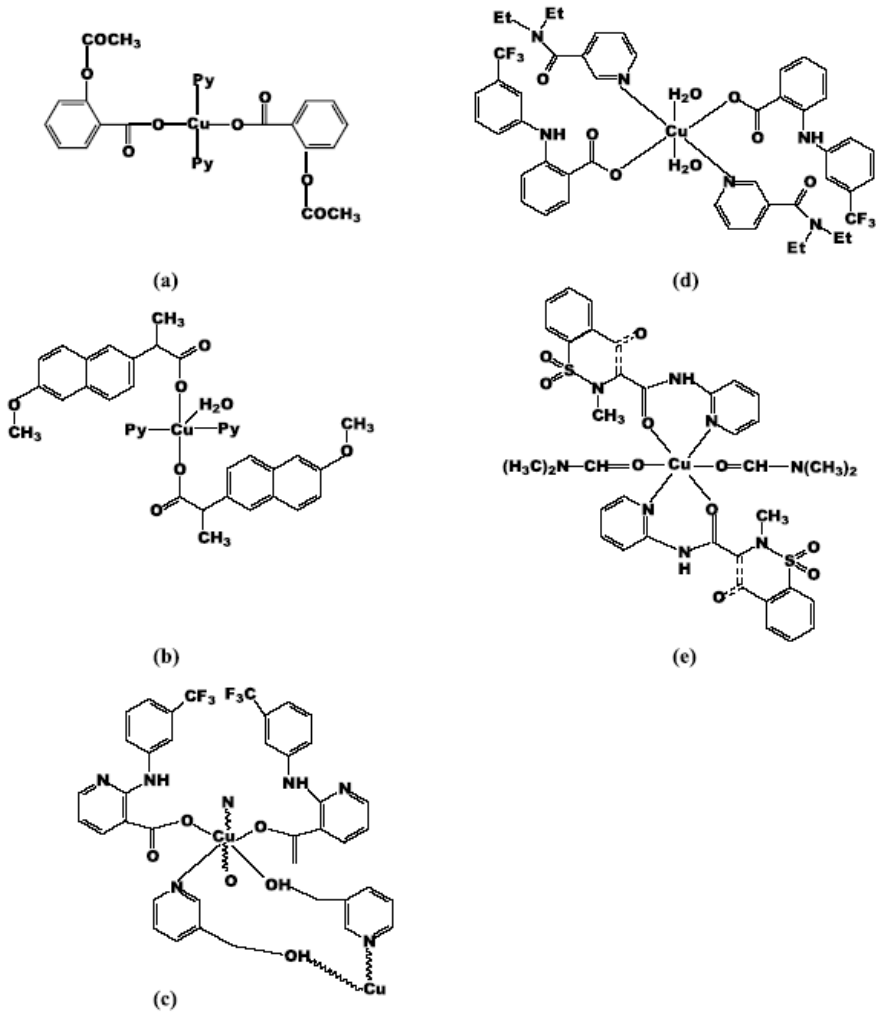

Figure III.1. The unidentate Cu(II) monomer structures of (a) aspirin ([Cu(Asp)$_2$(Py)$_2$] Py pyridine),(b) naproxen (Nap),(c) niflumic acid (Nif), (d) flufenamate (Fen)and (e) piroxicam (Pirx) .[61]

Analysis of the structures of the metal-complexes with NSAIDs both from the oxicam and the carboxylic acid family reveals that in the case of Cu(II) the formation of stable chelates prevails.[2] The structure of the Cu-NSAID is likely to be an important factor for its biological activity. For example, the anti-tumor activity of the monomeric Cu(II) complex of aspirin ([Cu(Asp)$_2$(Py)$_2$]) is reportedly more

effective than the dimeric $[Cu_2(Asp)_4]$ complex.[12] In the solid-state, Cu-NSAIDs (arylalkanoic NSAIDs) are typically monomeric or dimeric, with bonding to the Cu(II) ion via the carboxylato group. The structure of the Cu(II) complexes of the arylalkanoate NSAIDs is dependent upon the electronic properties of the carboxylate groups and the coordinating and steric properties of the added base.[8]

The coordination of the Cu center in the Cu(II) dimers of the NSAIDs of the general formula ($[Cu_2(RCOO)_4L_2]$ (R = aryl/phenyl alkanoic acid), (**Figire III.2**) containing either CuO_4O' or CuO_4N' coordination environments (L = O' or N' axial adduct), is characteristically octahedral and is typified by the Cu(II) acetate structure ($[Cu_2(CH_3COO)_4(OH_2)_2]$) The carboxylato ions act as bridging ligands (exhibiting a center of symmetry idway between the Cu atoms) and the solvent used In the synthesis binds in the position trans to the Cu···Cu axis. To date, there are ~ 147 CuO_4N" and ~ 188 CuO_4O' acetate-type structures deposited in the Cambridge Crystallographic Database. This 'paddle-wheel' dimeric Cu(II) structure typically has a Cu···Cu distance of ~ 2.64 Å ; with an octahedral stereochemistry tetragonally elongated along the Cu-Cu-O_L axis due to the Jahn-Teller effect. The rigid gometry of the acetate-type Cu(II) dimers is due to the estricted bite of the bidentate carboxylate bridge and llows little variation (~ 0.3 Å) in the Cu-Cu distance of these carboxylato-bridged dimers. The Cu- Cu distances in the dimeric Cu(II)-NSAIDs are only slightly longer than that in Cu metal (2.56 A°); consistent with a significant Cu-Cu bonding interaction. Hydrogen-bonding between the bridging carboxylate oxygens of neighboring dimers may, however, distort the inverted center of symmetry, making the four carboxylate oxygens coordinated to the Cu(II) ions non-equivalent.[8]

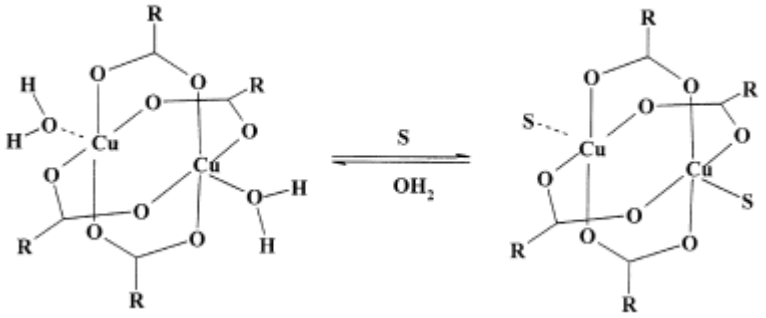

Figure III.2.. Structural representation of the complexes $Cu_2(RCOO)_4S_2]$, where S is the axially bonded solvent molecules.[13]

The structure consists of two Cu atoms linked by four tolf groups in a fashion similar to that of Cu(diclofenac) $_2(DMF)]_2$,[14] $[Cu(niflumato)_2(DMSO)]_2$, $[Cu(mef)_2(DMSO)]_2$. The crystal and molecular structure of tolfenamic copper(II) complexes with formula $[Cu(tolf)_2(DMF)]_2$ (where L is H_2O or DMF, N,N-dimethylformamide) was reported by our group.The complex is self-assembled via C–H–π intermolecular stacking interactions. The molecular structure of the binuclear complex is presented in **Figure III.3**. This structure consists of a quadruply bridged neutral molecule lying on a crystallographic mirror. A DMF molecule is bound trans to the Cu–Cu vector on each of the Cu atoms. The individual Cu atoms have a Jahn–Teller distorted, octahedral geometry, with four short Cu–ORCOO (1.944(6)–1.951(5) Å) bond lengths and a long solvent Cu–O (2.140(5)Å) bond length. The two copper atoms in

each dimeric unit are separated by a distance of 2.6074(18) Å. The Cu–Cu distance of 2.6075(19) Å is the shortest among the carboxylatobridged binuclear copper(II) complexes. X-ray structure of the DMF dimer does not exhibit strong intermolecular interactions due to the hydrophobic nature of the exterior. This may be important In facilitating its dissolution in micelles and transport through membranes.The structure of copper complex of tolfenamic acid in a fashion similar to that of $[Cu(diclofenac)_2(DMF)]_2$, $[Cu(niflumato)_2(DMSO)]_2$.[10]

The electronic properties and stereochemistry of mononuclear Cu(II) complexes of carboxylato-complexes were reviewed as early as the 1970s[8], with a number of subsequent studies that describe the factors that influence monomer over dimer formation in Cu(II) carboxylate complexes. Increasing the acid strength of the carboxylate groups, e.g. halogenation of the alkyl group, and increased basicity, e.g. pyridine and imidazole, of the other coordinating ligands, favors the formation of the Cu(II) monomer over the Cu(II) dimer[15], with steric effects reportedly playing a less important role. Cu(II) carboxylate monomers can exist as cis or trans adducts. The crystal structures of the monomeric Cu(II) arylalk- anoic-type NSAIDs typically display a trans unidentate bis (carboxylato) binding. Likewise, a structure with a trans bidentate bis(ligand) binding has been reported for the enolic-NSAID piroxicam. The coordination number around the Cu(II) center in the unidentate bis(carboxylato) Cu- NSAID ranges from four to six.[16]

Monomer and dimer Cu-NSAID complexes may occur for a given NSAID, depending upon the electronic properties of the added solvent. Both monomer and dimer complexes of aspiryn have been reported and this may explain their different anti-tumor effects. The nature and structure of dimeric Cu-Asp are typical of Cu(II) acetate monohydrate ($[Cu_2(CH_2COO)_4(OH_2)_2]$) with, a somewhat longer Cu-O_L = 2.24(2) Å coordination to a neighboring acetyl residue, compared with $[Cu_2(CH_2COO)_4(OH_2)_2]$ (Cu-O_L = 2.156(4) Å). The crystal structure of the Cu(II) monomer of aspirin ($[Cu(Asp)_{2(}Py)_2]$) displays a CuN_2O_2 core in a trans square-planar arrangement with the N atoms of the two pyridine molecules (Cu-N = 2.003(4) Å) and a carboxylate oxygen from each of the two Asp moieties (Cu-O = 1.949(3) A°.[15]

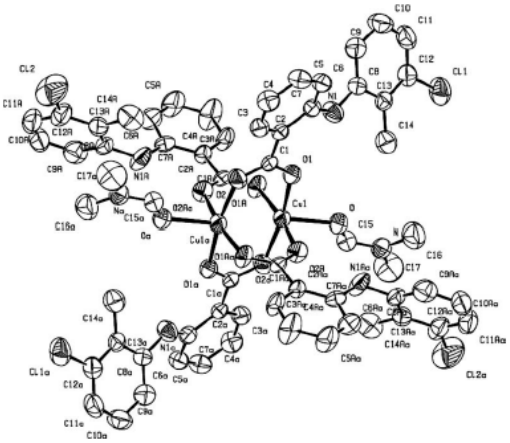

Figure III.3. The structure of $[Cu_2(tolf)_4(DMF)_2]$[10].

Recently, a number of Cu(II) monomer and dimer complexes of Indo have been prepared, including Cu(II) dimer complexes of the metabolites of IndoH, i.e. desmethyl- and desbenzoyl-IndoH. d investigation of the structure-activity relationship of these Cu(II) monomer and dimer complexes Indo is yet to be undertaken.[8] Synthesis, spectroscopic and electrochemical studies and the crystal structure of $[Cu(tolf)_2(DMF)]_2$ was reported.[10] The binuclear copper(II) complex of diclofenac, $[Cu(L)_2(H_2O)]_2 \cdot 2H_2O$ was found to have an anti-inflammatory profile superior to diclofenac when inhibiting inflammations due mainly to the activation of lipooxygenase and or to the complement systems.[17]

III.2. Structures of Mn(II) and Zn(II) complexes with NSAIDs from fenamates family.

New manganese and zinc complexes of mefenamic acid with potentially interesting biological activity wer described.[5] Infrared spectral data of $[Zn(mef)_2]$ $[Mn(mef)_2(H_2O)_2]$ were reported. The medium bands at ~ 400 cm^{-1} is attributed to the $\nu(M\text{-}O_{H2O})$ stretching mode, while the bands at 250-210cm21 to the $\nu(M\text{-}O_{oco})$ stretching mode.Optical and Monomeric six-coordinated species were isolated in the solid state for Mn(II) and monomeric four-coordinated for Zn(II). In DMF or CHCl3 solution the coordination number is retained and the coordinated molecules of water are replaced by solvent molecules.[5]

III.3. Structures of Cu(II) complexes with NSAIDs from oxicams family.

NSAIDs from the “oxicam” family (**Figure I.8**) have several potential donors towards metal ions, and at least three different co-ordination modes have been found for piroxicam (H_2pir) in the solid state *via* X-ray diffraction. H_2pir reacts as a singly deprotonated chelating ligand *via* pyridyl nitrogen and amide oxygen towards Cu(II) and Cd(II), as a mono-dentate ligand *via* pyridyl nitrogen towards Pt(II), and as a di-anionic tri-dentate ligand *via* amide oxygen and nitrogen, and pyridyl nitrogen towards Sn(IV). It is therefore worth investigating the co-ordinating ability of other NSAIDs from the “oxicam” family. The search for molecular modelling tools to gain an insight into the structure of co-ordination molecules and metal complex–biomolecule systems is a fast expanding area because of the advances in bio-co-ordination and medicinal inorganic chemistry as well as in computers and computational methods. Molecular mechanics, semi-empirical quantum mechanics, density functional and *ab initio* quantum mechanics methods can be used to investigate a large variety of structural, electronic, spectroscopic and thermodynamic properties at different degrees of accuracy, depending on the size of the system investigated, on the power of the computer and program capabilities. Several possible choices of method and computer programs are available to most inorganic chemistry laboratories; the selection of the optimal computational strategy for each type of complex molecule is often crucial.[18]

Piroxicam has several possible conformational rotamers with EZE and ZZZ (**figure III.5**). Piroxicam when deprotonated can form conformational rotamers and the most stable rotamer is the ZZZ, the one with the intramolecular H-bond.[20]

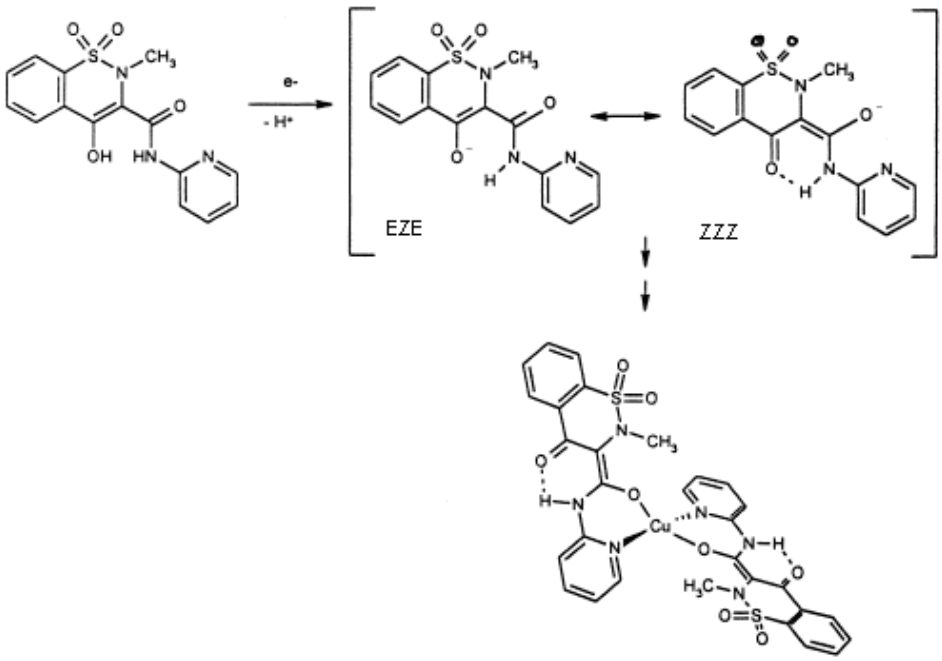

Figure III.4. Intramolecular hydrogen bond in the piroxicam ligand.[19]

Strong hydrogen bond is formed between the hydrogen in the amide group N(16) and the oxygen in the ketone functionality formed after ligand reduction and complexation, O(17). Whipple's study of conformational rotamers of piroxicam supports the hypothesis that this conformation is the most stable rotamer. Enol tautomers of b-dicarbonyls exhibiting keto-enol tautomerism are known to be stabilized by strong intramolecular OHO hydrogen bonding.[20]

This is the first structure of an isoxicam-metal compound reported was $[Cu(HISO)_2] \cdot 0.5DMF$, $2 \cdot 0.5DMF$. The metal center has a square planar coordination arrangement. Interestingly, the two $HISO^-$ anions behave differently as chelating agents towards the metal. One of them has a ZZZ conformation and links the copper(II) center via amide oxygen (O15) and isoxazole nitrogen (N10) whereas the second one has a EZE conformation and chelates through enolate oxygen (O17) and amide oxygen (O15). The orientation of the two ligands is such to have enolate oxygen from the EZE conformer trans to amide oxygen from the ZZZ one, and the amide oxygen from EZE trans to nitrogen (isoxazole) from ZZZ. Meloxicam produced $[Cu(HMEL)_2(DMF) \cdot 0.25H_2O$, $3 \cdot 0.25H_2O$ The coordination sphere has also a square-pyramidal arrangement, with the two $HMEL^-$ anions chelating at equatorial positions, whereas the apical site is occupied by the oxygen atom from DMF. The two $HMEL^-$ anions are in the ZZZ conformation and link the metal through the thiazole (N10) nitrogen atom and the amide (O15) oxygen atom; they assume a trans arrangement with respect to each other.[21]

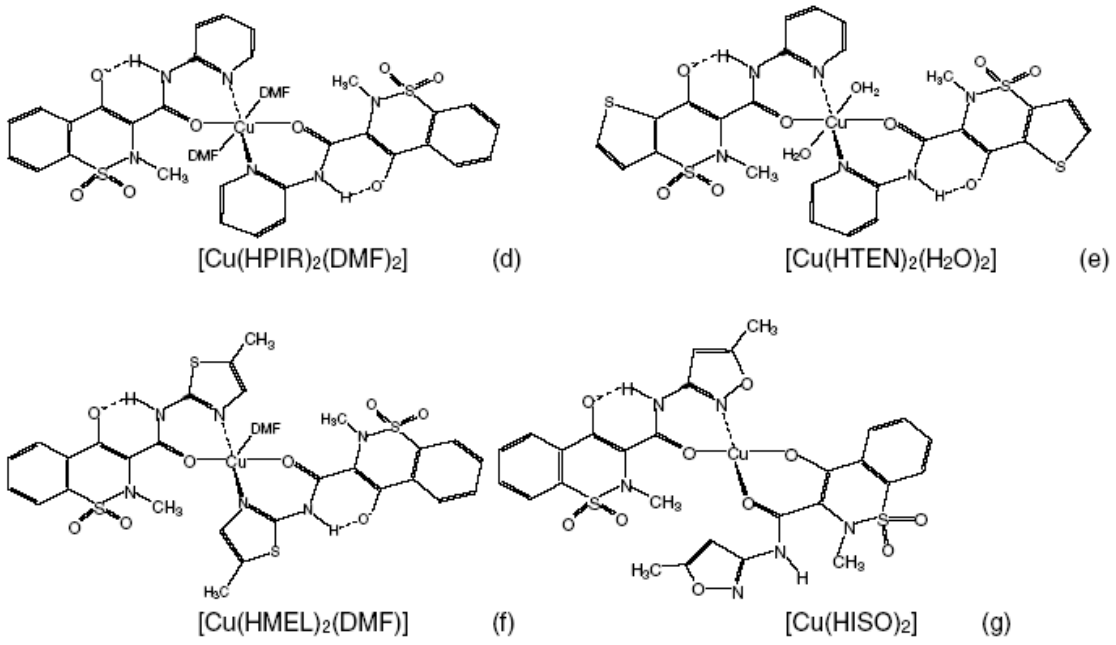

Figure III.5. Structural formula for $[Cu(HPIR)_2(DMF)_2]$ (d), $[Cu(HTEN)_2(H_2O)_2]$ (e), $[Cu(HMEL)_2(DMF)]$ (f), $[Cu(HISO)_2]$ (g).[3]

The molecular structure of $[Cu(HPIR)_2(DMSO)_2]$ (**Figure III.6**) and the selected crystallographic data, and geometrical parameters were by Tamasi et al. The coordinate molecule has a pseudo-octahedral arrangement, where the metal atom is linked to two apical oxygen atoms from DMSO, and is chelated by two $HPIR^-$ molecules in a ZZZ conformation in the equatorial positions via the amide oxygen and the pyridine nitrogen atom. The metal centers lies in an inversion center. The compound is therefore isostructural with the corresponding complex with DMF previously reported. Furthermore, the structure for the DMSO derivative produced much better crystals than the DMF species and refinement converged to much better parameters in the presented work (R1 agreement factor is 0.0341 and 0.0591 for DMSO and DMF respectively). However, crystals for DMSO derivative are not isomorphic with those for DMF species. For the structure the Cu–O15, Cu–N10 and Cu–O(apical) bond distances are 1.9422(14), 2.0494(17) and 2.4092(19) Å, respectively and have to be compared to 1.92(1), 2.05(1), 2.43(1) Å for DMF derivative. The bond distances and angles for the $HPIR^-$ chelating ligand are also much better defined for DMSO species than for the DMF one, even though the trends do not change significantly. It has also to be noted that the structure is isomorphic with those previously found $[M(HMEL)_2(DMSO)_2]$ (M = Co, Zn, Cd). Therefore, it was confirmed that even for crystals obtained from DMSO solutions the bis-chelate molecules for $HPIR^-$ have the same structure as those from DMF, the chelating mode for $HPIR^-$ and $HMEL^-$ are the same in DMSO solution at least for Co(II), Cu(II), Zn(II) and Cd(II) cations. It is reasonable that the arrangement for these bis-chelates is the same also in the solution phases.[3]

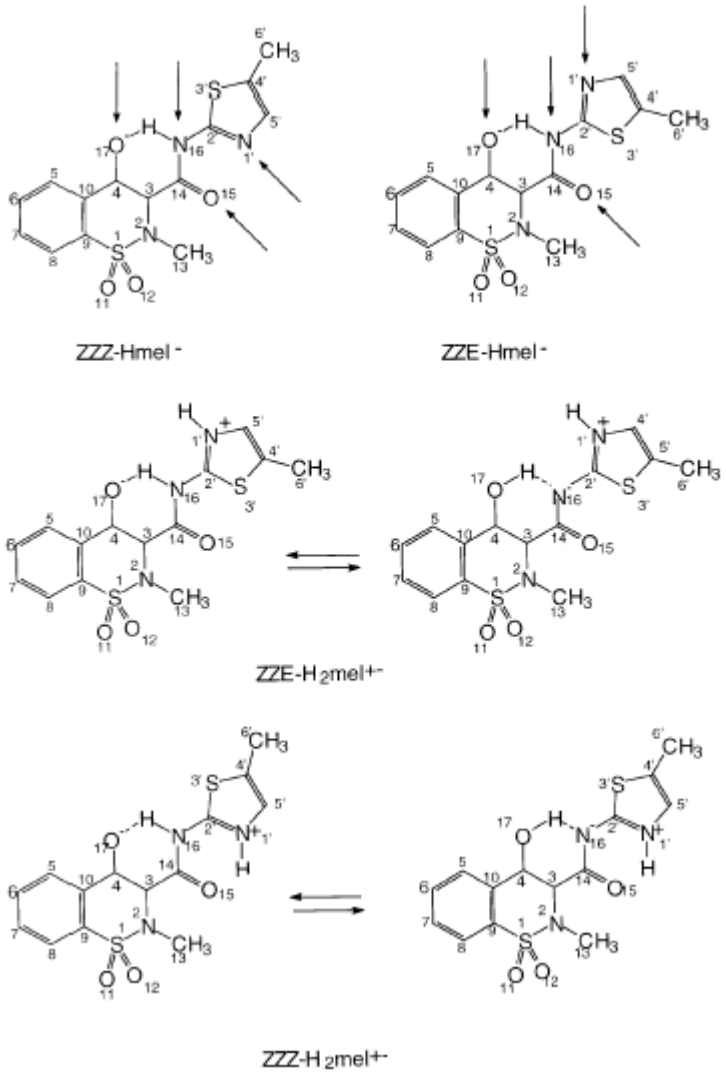

Figure III.10. Selected conformations for $Hmel^-$ and H_2mel^{--}.[18]

The molecular structure for the compound obtained from THF solution[$Cu(HISO)_2(THF)_2$] is new both as regards the apical and the equatorial positions when compared to that obtained from DMF solution. In the presented compound two solvent molecules occupy the apical position of the pseudo-octahedron through the oxygen atoms. Furthermore, $HISO^-$ in the ZZZ conformation chelate through O(amide) and N(isoxazole) and the enolate oxygen atom does not interact with the metal; it is instead involved in the common intra-molecular N–H···O hydrogen bond. It has to be recalled that for [$Cu(HISO)_2$] · 0.5 DMF an ambidentate behavior was revealed for the ligand. The Cu–O15, N1' and Cu–O(apical) bond distances are 1.960, 1.950 and 2.509 Å, respectively, in the presented structure. Corresponding distances for the O,N1' chelate for [$Cu(HISO)_2$] · 0.5DMF are 1.918 and 1.915 Å.[3]

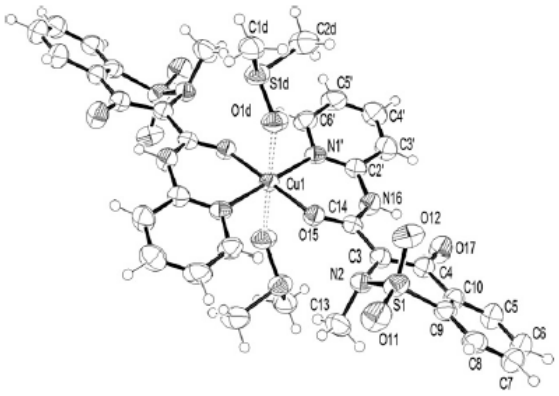

Figure III.6. Ortep style drawing for the molecule of $[Cu(HPIR)_2(DMSO)_2]$. Ellipsoids enclose 50% probability. The weak apical Cu···O bonds are represented as dashed lines, all other bonds are full lines.[3]

III.4. Structures of Mn(II), Zn(II) and (Cd) complexes with NSAIDs from oxicams family.

The interaction of other first-row transition-metal ions as Mn(II), Zn(II) and (Cd) with a widely used antiinflammatory drugs from the carboxamide family,was undertaken.[16]

The synthesis and characterization of Cu(ll), Zn(ll), and Cd(II) complexes with piroxicam [4-hydroxy-2-methyl-N-2-pyridyl-2H- 1,2-benzothiazine-3-carboxamide 1 ,1 -dioxide] were described. The crystal and molecular structures of $M(Pir)_2(DMF)_2$, (M = Cu, Cd; Pir piroxicam; DMF = N,N-dimethylformamide) are also reported (**Figure III.9**)[16].The presented study demonstrates that several first-row transition-metal ions are capable of forming stable chelates with piroxicam by employing the amide oxygen and pyridyl nitrogen atoms of the drug molecule. Previous spectroscopic studies[22] on metal complexes with some other enolizable amides like isoxicam and tenoxicam suggested that these antiinflammatory agents can act as chelate ligands with coordination involving the enolate oxygen atom and the oxygen atom of the amido group. Piroxicam, however, clearly does not follow the postulatem pattern, adopting coordination mode employing the pyridyl group of the side chain and the amide oxygen atom. Although an ambivalent ligating behavior cannot be excluded, it should be noted that the observed N,O chelation could be a reflection of the preference of transition-metal ions to form intramolecular mixed-ligand complexes by binding to ligands with heteroaromatic N residues and 0 donors.[16]

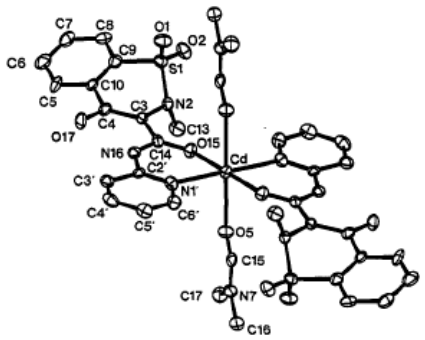

Figure III.8 . ORTEP drawing of the $Cd(Pir)_2(DMF)_2$ molecule showing the atom-labeling scheme.[17]

The Cu complex is isostructural with and shows geometrical features similar to the Cd complex. The molecular structure of the Cd complex is presented in Figure. The six-coordinate metal ion sits upon crystallographic centers of symmetry with the piroxicam ligand chelated through its carbonyl oxygen atom of the amido group and the pyridyl nitrogen atom. The arial positions are occupied by two DMF molecules bonded to the metal through their carbonyl oxygen atoms. The geometry of the five-membered chelate ring resembles closely those found in the octahedral complexes of Ni and Zn with N-(2-pyridyl)acetamide where the amide nitrogen atom is protonated. The axial Cu-0 bonds are weaker than the corresponding bonds in the Cd complex, as indicated by the long Cu-O distances of 2.43 Å**.** Potentially, piroxicam may act as a multiple-site ligand and various schemes of its bonding to metal ions could be considered. The neutral piroxicam molecule undergoes several structural changes upon its complexation to the metal ions. Piroxicam has five known forms, namely the free neutral molecule, the free zwitterion, the free anion, and the Cd and Cu complexes. As evidenced by the X-ray analysis, the deprotonation occurs at the enol oxygen site, while the amide nitrogen atom remains protonated.[17]

The meloxicam investigated by Defazio et al. were *EZE*-, *EZZ*- and *ZZZ*-H_2mel (**Figure III.10**) for selected forms and conformations), and *trans*-Zn$(Hmel)_2$ (a planar arrangement of the co-ordination sphere atoms was used for the bis-chelate). The meloxicam ligand is deprotonated at O(17) and adopts the 17,1'-*ZZZ* conformation. The chelating anion is stabilised by a strong intramolecular hydrogen bond which involves the O(17) and the N(16) atom It has to be noted that the conformation for free H_2mel is a screw halfchair. This means that the thiazine moiety of the oxicam class of drugs is flexible at least upon deprotonation at O(17) and metal co-ordination at O(15) and N(1').The X-ray diffraction analyses showed that complexes of [M$(Hmel)_2$(*O*-dmso$)_2$] (M = Zn, Cd,) are isomorphous and isostructural.The co-ordination spheres are pseudooctahedral and the metal ions sit on the inversion centres. Th $Hmel^-$ anions act as chelators through the N(1') nitrogen atoms of the thiazole moieties and through the O(15) amidic oxygen atoms at the equatorial positions (with a *trans* arrangement). The apical co-ordination sites are occupied by the O(1D) oxygen atoms of the two dmso ligands. The equatorial bond distances found for [Cd$(Hmel)_2$(*O*-dmso$)_2$] agree well with the values previously found for the octahedral [$Cd^{II}$$(Hpir)_2$(dmf $)_2$] (dmf = *N*,*N*-dimethylformamide) complex.[18]

Mn^{2+} complexes with deprotonated piroxicam have been prepared and characterized with the use of infrared, UV–Vis, nuclear magnetic resonance and electron paramagnetic resonance spectroscopies. The experimental data suggest that piroxicam acts as a deprotonated bidentate ligand and is coordinated to the metal ion through the pyridine nitrogen and the amide oxygen.[20]

The preparation, spectroscopic and magnetic properties were reported for complex of manganese-(II) with tenoxicam Mn$(TENOX)_2 \cdot 3H_20$. Tenoxicam acts as a chelate monoanionic ligand with coordination involving the enolate oxygen atom and the carbonyl oxygen atom of the amide group. The complex appear to have an octahedral stereochemistry involving two chelate tenoxicam ligands.[22b]

III.5. Biological assays of manganese, copper, zinc complexes with NSAIDs from fenamates and oxicams family.

The application of inorganic compounds to medicine requires detailed examination of the fundamental aqueous chemistry of the proposed drug, including its pharmacokinetics, the metabolic fate in blood and intracellularly, and the effects of the drug on the target of choice. Coordination and complexes present a wide variety of coordination spheres, ligand designs, oxidation states, and redox potentials, giving the ability to systematically alter the kinetic and thermodynamic properties of the complexes toward biological receptors. The toxicology of inorganic compounds in medicinal use, especially those containing the heavymetals, confronts the ‘‘stigma’’ of heavy metal toxicity; but therapeutic windows are rigorously defined to minimize such side effects—the usefulness of any drug is a balance between its toxicity and activity. The toxicity of a compound may derive from its metabolism and unwanted ‘‘random’’ protein interactions. Human serum albumin is of fundamental importance in the transport of drugs, metabolites, endogenous ligands, and metal ions. The crystal structure, combined with physical and biophysical studies, allows visualization of likely binding sites of many potential inorganic drugs. The nature of the target to be attacked by any drug obviously depends on the specific application. Many cytotoxic metal complexes target DNA because of its importance in replication and cell viability. Coordination compounds offer many binding modes to polynucleotides, including outer-sphere noncovalent binding, metal coordination to nucleobase and phosphate backbone sites, as well as strand cleavage induced by oxidation using redox-active metal centers. The accessibility of different oxidation states of metals such as Fe, Cu, Co, Ru, Mn, etc. may allow for redox chemistry resulting in strand breakage. Cytotoxic agents reduce the proliferation of a tumor but lack of selectivity between normal and malignant tissue may render many agents of little clinical utility. Drug discovery in general has been transformed by rapid advances in the understanding of the cell’s molecular biology coupled with information sciences. Cancer treatment strategies especially have evolved in favor of agents targeted toward specific pathways, notably those involved in cell signaling. A challenge for the medicinal inorganic chemist is the placement of coordination chemistry within this new paradigm.[23] The goal is to define the probability to extend the pharmacological profile of “parent drug”, in order to discover new properties such as antioxidant and anti-cancer activity. New complexes with essential metal ions, which would exhibit improved or different biological behaviour compared to the “parent drug.”[5] Cu-NSAIDs do exhibit a marked SOD-mimetic activity and this is commonly proposed to account for their modes of antiinflammatory action[61].Other proposed modes of action of Cu-NSAIDs include down-regulation (and stabilization) of polymorphonuclear leukocytes (PMNL), which are part of the immune system and exert phagocyte activity, (including inhibition of $O_2^{-\bullet}$ synthesized by PMNLs), down-regulation of phosholipase A_2 (which activates/releases membrane-bound arachidonic acid prior to its conversion by COXs and lipoxygenases to, e.g. PGs and leukotrienes, respectively), inhibition of lipid peroxidation and microsomal NADPH oxidation], and modulation of nitric oxide synthetase (NOS) activity.[8]

Transition matal aspirinates (mononuclear and binuclear transition matal ([Cu(II), Zn(II)] acetylsalicylates) shered the activity pattern in antiinflamation.[24] It has been demonstrated that the

Zn(II) complex of aspirin has a better therapeutic index than aspirin itself and has improved physicochemical characteristics. Furthermore, the Zn-aspirin complex displays more favorable therapeutic properties, is more effective, and less ulcerogenic than aspiryn alone.[25]

Cobalt and zinc complexes of meloxicam as well as the model bis-chelates are highly hydrophobic in the exterior surface; this suggests a facile cell membrane permeability and an inertness towards dissociation in aqueous media for the potential anti-inflammatory drugs. Furthermore, the formation of stable bischelates protects the drug molecules from enzymatic degradation.[18]

Some of the Cu(II) complexes have shown oxygen radical scavenger activity *in vitro* whereas certain others are clinically used to treat animals.The SOD-like activity exerted by the Cu(II) complexes or by some of their Cu(II)-containing metabolites, added to the COXs-enzyme inhibitory activity by the released ligands or by the complexes themselves, can explain the beneficial effects on the organisms, The metal-piroxicam and metal-carboxylic acid family drug complexes so far characted are usually highly hydrophobic neutral molecules. This property should facilitate passage of the complex molecule through the membranes. The weakly apically bound ligands of most of the Cu(II) complexes can easily dissociate and the 0_2^- radicals can interact with the metal via the free sites: in this way the SOD-like activity is readily rationalized[2]. Recently the superoxide dismutase activity of copper complexes with tolfenamic acid and diclofenac was measured. $[Cu(tolf)_2L]_2$ was showed as good superoxide scavenger and $[Cu(dicl)_2(H_2O)]$ was also found as potent superoxide dismutase mimics[10]. The manganese(I1) and copper(I1) complexes of tenoxicam $Mn(TENOX)_2 \cdot 3H_20$ and $Cu(TENOX)_2 \cdot 2H_20$ exhibit marked superoxide dismutase activity in the nitroblue tetrazolium assay.

Manganese complexes exhibit interest due to their catalytic antioxidant activity, in blocking oxidant stress in vitro. Manganese, copper and zinc complexes of mefenamic acid $[Mn(mef)_2(H_2O)_2]$, $[Cu(mef)_2(H_2O)]_2$ and $[Zn(mef)_2]$ were been studied with regard to their antioxidant ability as well as their inhibition of LOX, of b-glucuronidase and of trypsin- induced proteolysis. The complex $[Mn(mef)_2(H_2O)_2]$ exhibits the highest antioxidant activity and the highest inhibitory effect against the soybean lipogygenase (LOX), properties that are not demonstrated by mefenamic acid. Their anti-inflammatory effects on rat paw edema induced by Carrageenan was studied and compared with those of mefenamic acid. The complex $[Zn(mef)_2]$ exhibited a strong in vivo inhibitory effect, superior than the inhibition induced by mefenamic acid at the same molar dose. These compounds may prove useful for treating a variety of inflammatory diseases and may lead to the development of new drugs.[5]

The design and development of small- or medium-sized potential therapeutic agents, particularly those designed to target nucleic acids site-specifically or to mimic the function of enzymem can lead to safer and more rational approaches to novel therapeutic agents for cancer, viral diseases and tools for molecular biology. Complexes of first row transition elements showing photocleavage activity could find better application at the cellular level.[26] Some stydy shows for the first time that these Cu(II)–NSAID complexes can bind directly with the DNA-backbone. Cu(II)–piroxicam and Cu(II)–meloxicam complexes, which show chemopreventive and chemosuppressive effects in different cancer cell lines and animal models were studied. In an effort to explain their anti-cancer effects, researchers have pointed out that inhibition could be both at the level of protein and/or transcription.[1]

Formation of the uncharged Cu-piroxicam species is of particular interest, since it has been shown that such neutral Cu drug complexes are essential for effective distribution of the pharmacoactive agents and maintaining the copper balance In blood plasma.[16] N-pyridinobenzamide-2-carboxylic acid (PBCA) Comparative studies of ulcerogenic damage in the rat stomach were performed for a number of metal (Cu(II), Zn(II), and Mn(II) complexes of PBCA(N-pyridinobenzamide-2-carboxylic acid), and it was found that the Cu(II) complex exhibited the lowest ulcerogenic effects. This was also observed for a number of monomeric and dimeric complexes of indomethacin whereby copper complex exhibited the lowest ulcerogenic damage in both the stomach and small intestine of all the complexes studied.[8]

References

1. Roy, S., Banerjee, R., Sarkar, M. *Journal of Inorganic Biochemistry* **100,** 1320–1331 (2006).
2. Cini, R. *Comments on Inorganic Chemistry* **22,** 151 — 186(2000).
3. Tamasi, G., Serinelli, F., Consumi, M., Magnani, A., Casolaro, M., Cini, R. *Journal of Inorganic Biochemistry* **102,** 1862–1873 (2008).
4. Ding, W-Q., Yu, H-J., Lind, S,E. *Cancer Letters* xxx (2008).
5. Kovala-Demertzi, D., Hadjipavlou-Litina, D., Staninska M., Primikiri, A., Kotoglou, C., Demertzis, M.*J Enz Inh and Med Chem* **24,** 742-752 (2009).
6. a) Kovala-Demertzi, D., tolfenamic acid Kovala-Demertzi, D., Hadjipavlou-Litina, D., Primikiri, A., Staninska M., Kotoglou, C., Demertzis, M. *Chemistry& Biodiversity* **6,** 948 (2009).
   b) Kovala-Demertzi, D. *J. Organomet. Chem.* **691**, 1767–1774 (2006).
7. Zvimba, J.N., Jackson, J.E. *Journal of Inorganic Biochemistry* **101,** 148–158 (2007).
8. Weder, J.E., Dillon, C.T., Hambley, T.W., Kennedy, B.J., Lay, P.A., Biffin, J.R., Regtop, H.L., Davies, N.M., *Coord. Chem. Rev.* **232,** 95-126 (2002).
9. Psomas, G., Tarushi, A., Efthimiadou, E.K., Sanakis< Y., Raptopoulou, C.P., Katsaros, N. *Journal of Inorganic Biochemistry* **100,** 1764–1773 (2006).
10. Kovala-Demertzi, D., Galani, A., Demertzis, M.A., Skoulika, S., Kotoglou, C., *J. Iorg. Biochem.* **98**, 358 (2004).
11. Sorenson,J.R., *J. Med. Chem.* **19,** 135 (1976).
12. Oberley, L.W., Buettner, G.R. *Cancer Res.* **39,** 1141 (1979).
13. Kovala-Demertzi, D. *Journal of Inorganic Biochemistry* **79,** 153–157 (2000).
14. Kovala-Demertzi, D., Theodorou, A., Demertzis, M.A., Raptopoulou, C., Terzis, A., *J. Inorg. Biochem.* **65,** 151 (1997).
15. Greenaway, F.T., Pezeshk, A. Cordes, W., Noble,M.C., Sorenson, J.R.J. *Inorganica Chimica Acta*, **93,** 67-71 (1984).
16. Cini, R., Giorgi, G., Cinquantini, A., Rossi, C., Sabat, M., *Inorg. Chem.* **29,** 5197 (1990).
17. Kourkoumelis, N., Demertzis, M.A. Kovala-Demertzi, D., Koutsodimou, A., Moukarika, A. *Spectrochimica Acta Part A* **60,** 2253–2259 (2004).
18. Defazio, S., Cini, R., *J. Chem. Soc. Dalton Trans.* 1888–1897 (2002).
19. Mendez-Rojas, M.A., Cordova-Lozano, F., Gojon-Zorrilla, G., Gonzalez-Vergara, E., Quiroz, M.A. *Polyhedron* **18,** 2651–2658 (1999).
20. Christofis, P., Katsarou, M., Papakyriakou, M., SanakisN Y., Katsaros, Psomas, G. *Journal of Inorganic Biochemistry* **99,** 2197–2210 (2005).
21. Cini, R., Tamasi, G.,Defazio, S., Hursthouse, M.B. *Journal of Inorganic Biochemistry* **101,** 1140–1152 (2007).
22. a) Harrison, D. 0.; Thomas, R.; Underhill, A. E.; Fletcher, J. K.; Gomm, P. *S.;* Hallway, F. *Polyhedron* **4,** 681 (1985).
    b) Bury, A.; Underhill, A. E.; Kemp, D. R.; O'Shea, N. J.; Smith, J. P.; Gomm, P. *S.;* Gomm, P. S. *Inorg. Chim. Acra* **138 ,** 85 (1987).
23. McCleverty, J., Meyer, T.J. **9**, *Comprehensive coordination chemistry* (2005)
24. Yun, Y *The Pharmaceutical society of Japa* **127,** 1869-1875 (2007).
25. Zhou, Q., Hambley, T.W., Kennedy, B.J., Lay, P.A., Turner, P., Warwick, B., Biffin, J.R., Regtop, H.L. *Inorg. Chem.*, **39,** 3742-3748 (2000).
26. Rupesh, K.R., Deepalatha, S., Krishnaveni, M., Venkatesan, R., Jayachandran, S. *European Journal of Medicinal Chemistry* **41,** 1494-1503 (2006).

IV Nonsteroeidal anti-inflamatory drugs' complexes with metals (cobalt, nickiel and tin).

IV.1. Cobalt(II), Nickiel(II) and Iron(III) complexes with members of fenametes and oxicams family. Structural characterization and biological activity.

Living organisms transport and store transition metals (TMs). Although TM are present in small concentration ranges in biological systems, their importance is capital as they are bound to proteins or found in cofactors such as porphyrins or cobalamins. Iron, well-known for reversible binding of dioxygen (hemoglobin or hemerythrin), copper which participates in activation of dioxygen, cobalt found in vitamin B12 or molybdenum proteins catalyzing the reduction of nitrogen and nitrate are just a few examples which illustrate the importance of TM complexes in biological systems. TMs are also important in a wide range of fields such as catalysis, material synthesis, photochemistry, bioinorganic chemistry and even cancer treatment, as is the case for *cis*-platinum which was shown, in 1965, to prevent cell division. In addition, TM complexes are appealing to the chemists due to the variety of colors exhibited in comparison with complexes formed by the main metals, which are usually white.[1]

Traditionally, the design and development of small molecules that can selectively bind to nucleic acids centred upon organic chemistry; however, through the pioneering work of Dwyer, Lippard, Nordén, Barton and others, there is now considerable interest in utilising transition metal complexes as nucleic acid binding agents. Metal complexes can interact with nucleic acids through a variety of modes, are amenable to modular assembly and have favourable spectroscopic, photophysical and electrochemical properties that allow a detailed examination of their binding and the potential to regulate DNA/RNA function.[2]

Metal complexes containing non-steroidal anti-inflammatory drugs are among those compounds which have received much attention and increasing interest from a medicinal inorganic chemistry viewpoint in the field of co-ordination compounds with active drugs as ligands, during the last decade.The case of indomethacin and its metal complexes can be considered as a typical example of how much the co-ordination compounds of certain metals can improve the overall quality of the drug by reducing the damaging effects on the gastro-intestinal system and increasing the anti-inflammatory action, when compared to the uncomplexed drug. Certain metal complexes of indomethacin are now being prepared in millions of doses as veterinary pharmaceuticals. Metal complexes of anti-inflammatory drugs can also be potentially active against other diseases such as cancer and bacterial infections, as is the case when the co-ordination residues contain metals like Pt(I), Pt(II), Ru(II), Ru(III), Rh(II), Rh(III), Ag(I), Au(I).[3]

Monomeric six coordinated species of complexes of mefenamic acid $[Co(mef)_2(H_2O)_2]$, $[Ni(mef)_2(H_2O)_2]$ were reported.In DMF or $CHCl_3$ solution the coordination number is retained and the coordinated molecules of water are replaced by solvent molecules.[4] In vitro biological studies. In this investigation all compounds were studied in order to gain insight into their biological response. The metal complexes and the parent drug were studied with regard to their antioxidant ability as well as to the inhibition of a) soybean lipoxygenase, b) b-glucuronidase and c) of trypsin- induced proteolysis.

Cobalt and nickiel complexes of mefenamic acid complexes present very low interactions (8 and 6.2%) with the stable free radical DPPH (**Table IV.1**). It seems that interaction increases with the time and the concentration. Compounds show potent inhibition in the evaluation of their hydroxyl radical scavenging activity. Furthermore both complexes were found to inhibit signifi- cantly high β-glucuronidase and cobalt complex was found to inhibit trypsin in vitro (**Table IV.2**).[4]

Table IV.1. Interaction % with DPPH- Reducing ability (RA %).[4]

Compounds	RA % 0.1 mM		RA % 0.5 mM	
	20 min	60 min	20 min	60 min
Mefenamic	2.1	2.6	7.5	8.3
$[Co(mef)_2(H_2O)_2]$	8.0	10.2	9.1	10.1
$[Ni(mef)_2(H_2O)_2]$	6.2	8.1	13.0	13.1

Table IV.2. Competition% with DMSO (0.1mM) for hydroxyl radical HO·, inhibition of LOX and antiproteolytic activity of mefenamic acid and its metal complexes.[4]

Compounds	Competition % with DMSO (0.1 mM)	Inhibition of LOX at 5 min (0.033 mM)	% Inhibition of Glucuronidase (0.1 mM)	% Inhibition of trypsin (0.3 mM)
Mefenamic acid	99.7	No	91.8	NA
$[Co(mef)_2(H_2O)_2]$	61	12.5	94.3	58.2
$[Ni(mef)_2(H_2O)_2]$	67.7	39.4	78.3	34.4

The synthesis and the structural characterization of cobalt(II) complex with the widely used anti-inflammatory drug meloxicam (mono-anionic form) was repoted. The Co(II) derivatives are themselves potential anti-inflammatory drugs. Two complex were obtained at high yield through simple reaction of the relevant metal acetate and the drug in methanol produced micro-crystalline solids which were recrystallized from dimethylsulfoxide (dmso) solution to give crystals of *trans*,*trans*-$[M^{II}(Hmel)_2(O\text{-dmso})_2]$ (M = Co) (**Figure IV.1**). The X-ray diffraction analyses showed that cobalt complex is isomorphous and isostructural with reported Zn and Cd complexes. The meloxicam molecule acts as a mono-anionic chelating ligand, the two $Hmel^-$ anions chelate the metal centre through the nitrogen atom from the thiazole ring and the amide oxygen atom at the equatorial positions, whereas the two dmso molecules link the metal at the apical sites through their oxygen atoms. The metal atom is pseudo-octahedrally co-ordinated, the M–O(amide) bond distances being 2.083(3), 2.081(4) and 2.269(2) Å, and the M–N(thiazole) lengths 2.088(3), 2.060(4) and 2.254(2) Å for cobalt complex, respectively. The $Hmel^-$ ligand adopts a *ZZZ*-conformation which is stabilised by a strong intramolecular O···H–N hydrogen bond and the conformation of the thiazine ring changes from a half-chair to an envelope. The ambidentate dmso ligand co-ordinates the metal centre through the oxygen atom (O(1D)). The preference for the *O*-dmso co-ordination mode over the *S*-dmso one can be explained by the relatively hard character of the cation and on the basis of steric reasons. The O(1D)–S(1D) bond distance ranges 1.512(4)–1.521(3) Å for the three complexe, whereas it is 1.46(1) Å

(average) for *trans*-[$PtCl_2$(N1'-H_2pir)(*S*-dmso)]. Therefore the change of thiazolyl (meloxicam) for pyridyl (piroxicam) does not alter the co-ordination mode of this class of ligand and the enolate oxygen atom is still not active as a donor, at least for Co(II), Zn(II) and Cd(II). The cobalt complex have no strong intermolecular contacts in the unit cell and have no co-crystallised water molecules even though the crystal growth procedures were carried out in air. This confirms the hydrophobic character of the complex molecule which is important for the potential pharmacological properties. The hydrophobicity of metal based pharmaceuticals is desired to help prevent their decomposition in biological buffer solutions and is believed to facilitate their transport through the cell membranes.[3]

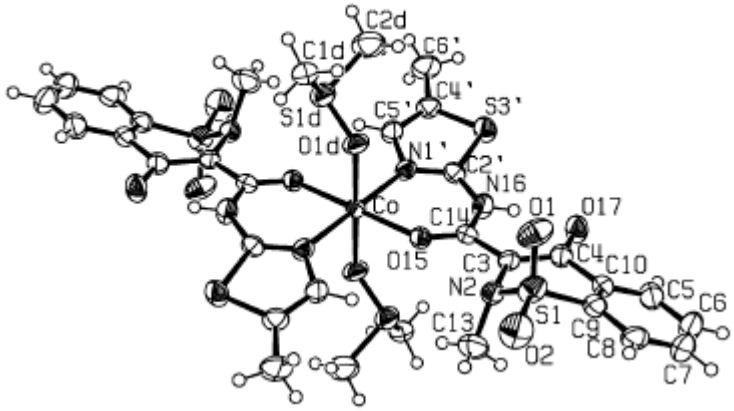

Figure IV.1. Drawing of the complex molecule for [Co^{II}(Hmel)$_2$(*O*-dmso)$_2$].[3]

One solid complex of Fe(III) with isoxicam, which shows a 1 : 3 Fe(III) : isoxicam stoichiometry, was reported, isoxicam acts as a monoanionic chelate with coordination that involves the oxygen belonging to the enolate and the oxygen of amide. Later, a solid complex of Fe(III) with tenoxicam with the same kind of coordination, 1 : 3 Fe(III) : tenoxicam was reported. The same stoichiometry for the solid complex formed between Fe(III) and piroxicam was found. A spectrophotometric study of the chemical coordination of two nonsteroidal anti-inflammatory drugs (tenoxicam and piroxicam) with Fe(III) was been undertaken in methanol in order to confirm the formation of the red species Fe(tenox)$_2$ so far. The Fe(III)–tenoxicam and Fe(III)–piroxicam systems in acetone give formation of three red dimers: Fe_2(oxicam), Fe_2(oxicam)$_2$ and Fe_2(oxicam)$_3$[5].

IV.2. Organotin(IV) complexes with NSAIDs from the fenametes family.

Organotin compounds are of interest in view of their considerable structural diversity. Among the compounds, the most ubiquitous are the carboxylates. The increasing interest in organotin(IV) carboxylates that has arisen in the last few decades is attributed to their significantly important biological properties.[6] They are often used as catalysts and stabilizers, biocides, anti-fouling agents and wood preservatives[7].Several di- and tri-species have shown potential as anti-neoplastic and anti-tuberculosis agents. Some of the organotin complexes exhibit very promising anti-tuberculosis and anti-proliferative activity in vitro.[6]

Information on the structures of organotin carboxylates continues to accumulate, and, at the same time, new applications of such compounds are being discovered, which are relevant for industrial and medicinal applications.[7]

NSAIDs from the carboxylic acid family such as mefenamic, tolfenamic, flufenamic were used as ligands in order to synthesize organotin complexes in our laboratory.[6] The dimeric ladders $[R_2LSnOSnLR_2]_2$, are tetranuclear, centro-symmetric and features a central rhombus Sn_2O_2 unit with two additional tin atoms linked at the O atoms. The ''external' tin atoms have their coordination geometry completed by a bridging bidentate carboxylate ligand or by a monodentate carboxylate ligand. Five rings, each containing two tin atoms, are present in the dimeric tetraorganodistannoxanes and the geometry around the four tin centers is distorted octahedral or distorted trigonal bipyramidal. The overall geometry found in these structures, allowing for differences in chemistry, is similar to that found in the common motif adopted by compounds with the general formula $[R_2LSnOSnLR_2]_2$. In the dimeric distannoxane of tolfenamic the dihedral angles between the aminobenzoate aromatic ring and the other ring are 78.0(3)° and 47.8(2)°, respectively. Remarkably, these are comparable to the angles of 73° and 46°, respectively, found in the two white and yellow forms of free tolfenamic acid. Significant π→π stacking interactions, C–H– π interactions and intramolecular hydrogen bonds stabilize these structures and the organotin complexes are self-assembled via C–H– π and π→π stacking interactions (**Figure IV.2**).[6]

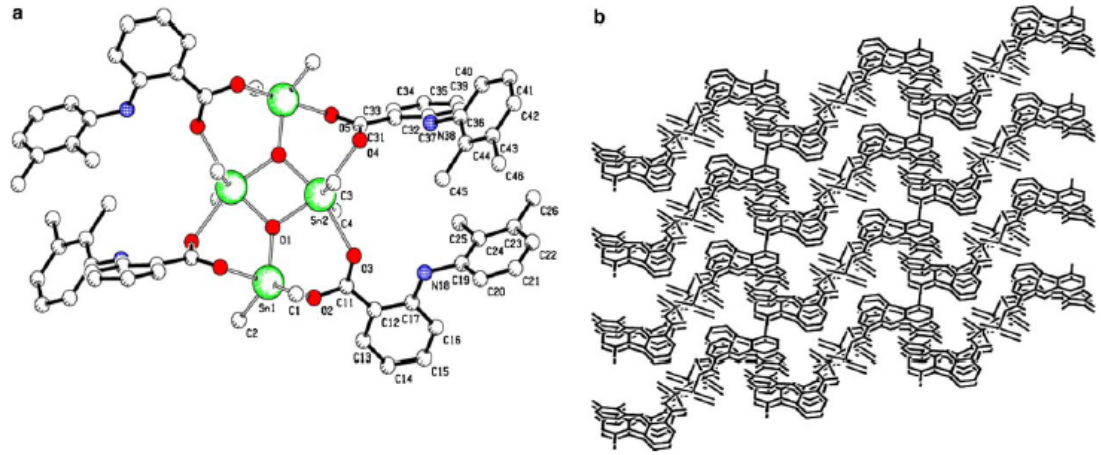

Figure IV.2. (a) Perspective view of $[Me_2Sn(mef)O(mef)SnMe_2]_2$. (b) Packing diagram of the complex of $[Me_2Sn(mef)O(mef)SnMe_2]_2$ viewed along the b-axis[6]

The organotin flufenamates $[Me_2(flu)SnOSn(flu)Me_2]_2$, $[Bu_2(flu)SnOSn(flu)Bu_2]_2$ and $[Bu_2Sn(flu)_2]$ were reported. The crystal and molecular structure of $[Me_2(flu)SnOSn(flu)Me_2]_2$ (**Figure IV.3**) with six-coordinated tin centers are presented in the dimer distannoxane is described. Three distannoxane rings are present to the dimeric tetraorganodistannoxane of planar ladder arrangement. The structure

is centro-symmetric and features a central rhombus Sn_2O_2 unit with two additional tin atoms linked at the O atoms, two endo-cyclic and one exo-cyclic. The distance between the endocyclic and exocyclic tin atoms is 3.732(1) and the distance between the two endocyclic tin centers is 3.290(1). The additional links between the endo- and exo-cyclic Sn atoms are provided by bridging carboxylato ligands that form asymmetrical bridges (Sn(1A)–O(1B) 2.340(5) Å and Sn(1B)–O(2B) 2.204(5) Å). Each exocyclic Sn atom is also coordinated by an anisobidentate chelating carboxylato ligand. The crystal structure shows ring-stacking interactions. The monomers are stacked by a strong p interaction and weaker C–H→p interactions. This structure is self-assembled via p→p and C –H→p stacking interactions. C–H→p, p→p stacking and intramolecular hydrogen interactions stabilize this structure.[6]

Recently crystal structure of organotin meclofenamic complexes $[Me_2(Meclo)SnOSn(Meclo)Me_2]_2$ and $[Ph_3Sn(Meclo)]$, where HMeclo is meclofenamic acid were determined by X-ray crystallography and reported by our group.[7] Three distannoxane rings are present to the dimeric tetraorganodistannoxane of planar ladder arrangement of $[Me_2(Meclo)SnOSn(Meclo)Me_2]_2$. The structure is centro symmetric and features a central rhombus Sn_2O_2 unit two additional tin atoms linked at the oxygen atoms. The coordination number is five and six for Sn(1) and Sn(2), respectively. The metal coordination geometry for Sn(1) is described as intermediate between square pyramidal and cis-trigonal bipyramidal, in which the carboxylato ligand spans equatorial and axial sites and for Sn(2) as distorted octahedral. Distortions from the ideal geometries may be related to the approach 3.075(7) Å of the O(2a) atom to Sn(1). This distance is long for primary Sn–O bonding, but represent a type of secondary interaction. The dihedral angles between the planes of the phenyl rings for 2 are 81.0(2)° and 67.3(1)° for the bidentate bridging and the anisobidentae chelating ligands, respectively, while in meclofenamic perpendicular, the corresponding angle being 81°. The aminobenzoate portion of each carboxylato ligand is effectively planar which facilitates the formation of intra-molecular N(1)–H···O(4) and N(2)–H···O(3) interactions of 2.632(6) and 2.647(5) Å, respectively. The overall geometry found, allowing for differences in chemistry, is remarkably similar to compounds with the general formula $[R_2(R'CO_2)SnOSn(O_2CR')R_2]_2$. Five- and six-coordinated tin centers are present in the dimer distannoxane. X-ray analysis of $[Ph_3Sn(Meclo)]$ **figure IV.3** revealed a penta-coordinated structure containing Ph_3Sn coordinated to the chelated carboxylato group. The polar imino hydrogen atom participates in intra-molecular hydrogen bonds. The intra-molecular Hbond formed from the amino group [O(2)···N(1) 2.660(6) Å] contributes to an elongated Sn–O(2) bond. A similar H-bonded situation was found in mefenamic acid compound [Ph3Sn[(mef)].[7]

The geometry at the Sn atom is represented as intermediate between square pyramidal and cis-trigonal bipyramidal, in which the carboxylato ligand spans equatorial and axial sites. The dihedral angle between the planes of the phenyl rings of Meclo is 65.9(3)°. The polar amino H-atom participates in an intra-molecular H-bond. Both complexes are self-assembled via p→p, C–H–p, stacking interactions and intra-molecular hydrogen bonds.[7]

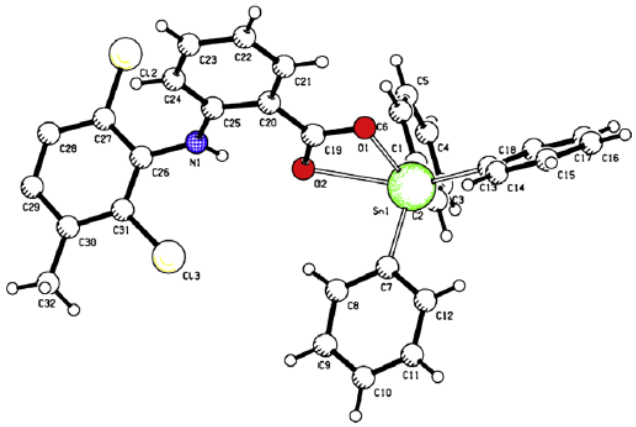

Figure IV.3. Perspective view of $[Ph_3(Meclo)Sn]$[7].

IV.3. Organotin(IV) complexes with NSAIDs from the oxicams family.

Tenoxicam, piroxicam and lornoxicam were used as ligands to synthesize organotin complexes.[6] The stoichiometries of the complexes indicate that organotin(IV) is coordinated by the singly charged anion in $[SnR_2(HL)_2]$ and by the doubly charged anion in $[SnR_2L]n$. In $[SnR_2L]n$ the doubly deprotonated ligand is coordinated as a tridentate ligand via the enolic oxygen O, the amide and pyridyl nitrogen atoms. Two carbon atoms complete the fivefold coordination at the diorganotin(IV) fragments. The di-anionic, tridentate ligand has an EZZ configuration and the metal coordination geometry is therefore described as distorted square pyramidal with the amide nitrogen occupying the apical position. Molecules of $[SnR_2L]$ are joined into dimers in a head-to-tail fashion by intermolecular bonds between tin and the neighbouring ketonic oxygen atom, with distances of Sn–O 2.971–2.611 Å. The dimers are arranged in polymers with a stacking of alternate parallel chains. Extended networks of Sn–O–Sn, C–H–O and C–H–π contacts lead to aggregation and a supramolecular assembly, (**Figure IV.4**).[6]

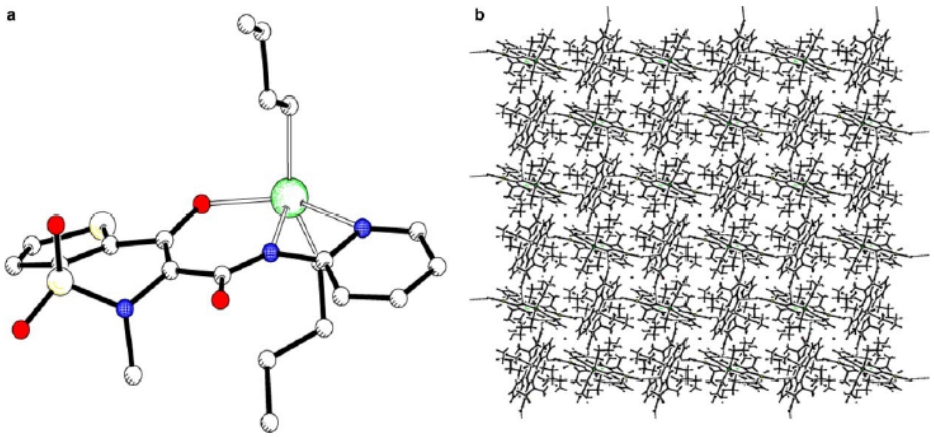

Figure IV.4. (a) Perspective view of $[Bu_2Sn(tenox)]n$. (b) Packing diagram of the complex $[Bu_2Sn(tenox)]n$ viewed along the c-axis.[6]

The crystal structure of $[Ph_2Sn(Hpir)_2]$ (**Figure IV.5**) was solved. The tin atom is coordinated in a very distorted octahedral configuration through its enolate and amide oxygen atoms in a trans-$O_{enolate}$-cis-O_{amide}-cis-C_2 configuration. The two phenyl groups are cis but the C–Sn–C angle is much greater than 90°; indeed, it is closer to the tetrahedral value. In the present structure, the amide nitrogen atoms remain protonated, as they are not coordinated. This is in sharp contrast to the behaviour of piroxicam with di-*n*-butyltin, which forms $[Bu_2Sn(pir)]n$ with doubly deprotonated, tridentate piroxicam. Spectral solution studies suggest that the diorganotin adducts 1:2 lose one ligand and after rearrangement, give the 1:1 adducts.[6]

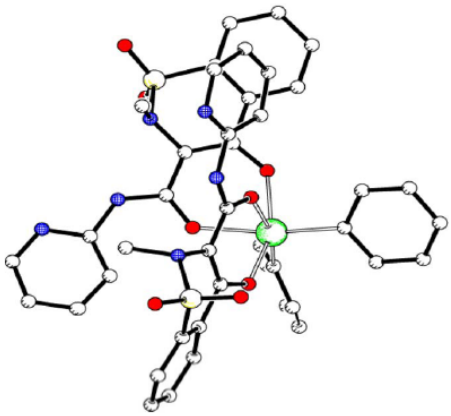

Figure IV.5. Perspective view $[Ph_2Sn(Hpir)_2]$.[6]

The synthesis and spectral characterisation of novel organotin complexes with a 1:1 Sn/lornnoxicam stoichiometry, $[SnMe_2(lorn)]$ and $[SnBu_2(lorn)]$, (**Figure IV.6**) were reported by our group. Crystal structure determinations of both complexes showed that the ligand is doubly deprotonated at the oxygen and amide nitrogen atoms and is coordinated to the SnR_2 fragment via four- and six-membered chelate rings. The monomers of $[SnMe_2(lorn)]$ are linked through intermolecular hydrogen bonds of C H···O type and through C−H−π intermolecular interactions. Interactions and intramolecular hydrogen bonds stabilize the structure. Although the numerous contacts, of many different types, are remarkable, the interactions themselves are consistent with known guidelines for hydrogen bond formation.There are two similar molecules in the asymmetric unit of $[SnBu_2(lorn)]$.The metal coordination geometry is therefore described as square pyramidal with N(31) occupying the apical positions. The donors N(31) are chosen as apices by the simple criterion that neither should be any of the four donor atoms that define the two largest angles, α and β. Molecules of $[SnBu_2(lorn)]$ are joined into dimers in a head-to-tail fashion by intermolecular bonds between tin and the neighbouring ketonic oxygen atom. Intermolecular distances for Sn·· O of 2.61-3.02 Å have been confidently reported for intramolecular bonds, indicating Sn-O bonding. The dimers of second complex are arranged in polymers with a stacking of alternate parallel chains and are linked through intermolecular hydrogen bonds of C H···O type, and through HC π intermolecular interactions. An extended network of SnO−Sn, C− H···O and C−H--π contacts lead to aggregation and a supramolecular assembly. The negative charge on the atoms in a molecule with several donor

centres can be used to study its formation of a donor-acceptor bond with a metal. In H_2lorn the four oxygen atoms exhibit the maximum electron density and negative charge. The highest effective charge and the highest electron density values for the four oxygen atoms and for the pyridyl and imine nitrogen in both complexes evidently show strong electron-donor properties and could rationalize the coordination scheme and the extended network of inter-, intra- hydrogen, and non-hydrogen bonding.[8]

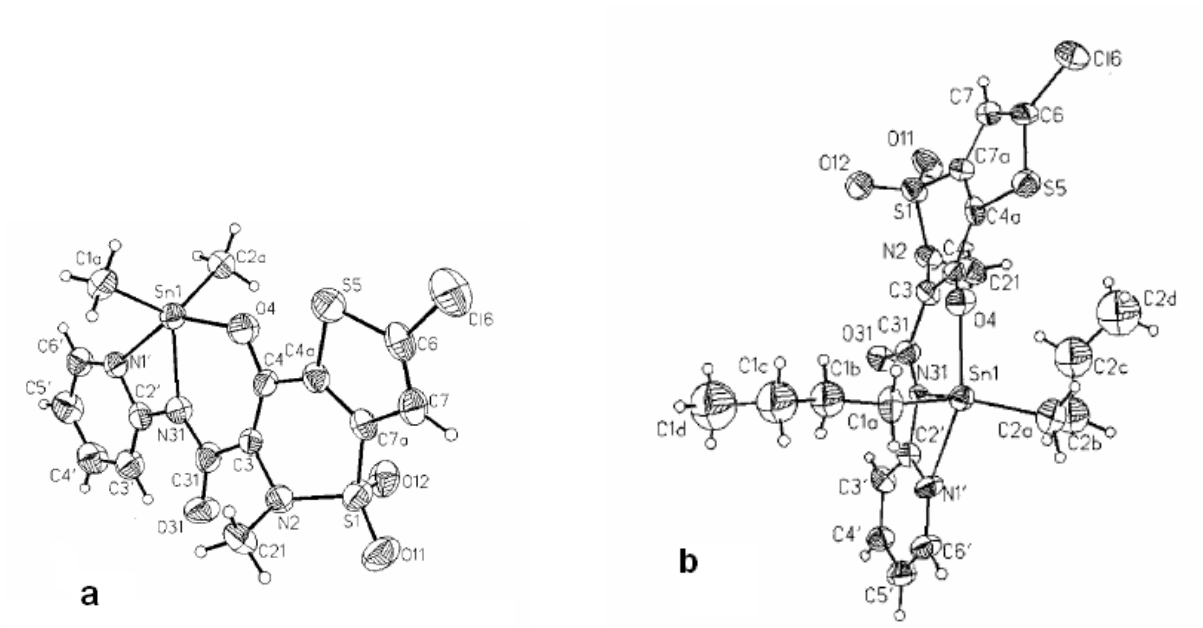

Figure IV.6. ORTEP representation of [$SnMe_2$(lorn)] (a) and [$SnBu_2$(lorn)] (b).[8]

IV.4 Biological activity of organotin complexes with NSAIDs, derivatives of the carboxylic acid family and oxicam family.

Tuberculosis (TB) caused by *Mycobacterium tuberculosis* remains a leading cause of mortality worldwide into 21st century. The mortality and spread of this disease has further been aggravated because of synergy of this disease with HIV. A number of anti-TB drugs are ineffective against this disease because of development of resistance strains. Internationally efforts are being made to develop new anti-tubercular agents Selected NSAIDs and organotin complexes were screening against *Mycobacterium tuberculosis* H37Rv in BACTEK 12B medium using the BACTEC 460-radiometetric system at the single concentration of 6.25 µg/ml. Rifampicin, RMP, was included as a positive drug control (**Table IV.3**).[6]

Table IV.3. Biological activities of NSAIDs and organotin complexes of NSAIDs towards *Mycobacterium tuberculosis* H37Rv[6].

Compound	Inhibition (%)	MIC (μg/ml)	IC_{50} (μg/ml)	SI
H_2tenox	21	>6.25		
H_2pirox	11	>6.25		
H_2lorno	2	>6.25		
Hfluf	0	>6.25		
HDMAB	0	>6.25		
[Me_2(dicl)SnO-Sn(dicl)Me_2]$_2$	0	>6.25		
[Ph_2(dicl)SnO-Sn(dicl)Ph_2]$_2$	0	>6.25		
[Sn(Ph)$_3$(Flu)]	0	>6.25		
[SnPh$_3$(mef)]	98	0.39		
[SnBu$_2$(mef)$_2$]	92	>6.25		
[SnMe$_2$(dicl)$_2$]	100	3.13		
[SnBu$_2$(dicl)$_2$]	100	3.13		
[SnPh$_3$(pirox)]	100	1.56	0.07	0.04
[SnPh$_3$(lorno)]	100	3.13	0.19	0.06
[SnPh$_3$(indo)]	100	0.78	0.07	0.09
[SnPh$_3$(tenox)]	100	0.78	0.08	0.10
[Sn(Ph)$_3$(DMAB)]	100	0.78	1.89	2.42
Rifampicin	95	0.25	113.6	

Alamar assay; drug concentration 6.25 μg/ml.

The parent drugs, the dimeric tetraorganostannoxanes, and the triphenyl ester of flufenamic did not exhibit any inhibitory effect and were not screened further. The rest of the organotin compounds exhibited highest inhibitory activity of 92–100%, respectively, and considered as active compounds. The column labeled MIC, lists the measured minimum inhibitory concentration. The MIC values are in the range of 3.13–0.78 μg/ml. The significance of this value depends on several factors such as compound structure, novelty, toxicity, and potential mechanism of action, though generally an MIC ≤ 1 μg/ml in a novel compound class is considered as an excellent lead. The triphenyl esters of NSAIDs were also tested for cytotoxicity (IC_{50}) in Vero cells at concentrations equal to and greater than the MIC value *Mycobacterium tuberculosis* H37Rv. The IC_{50} value was found to a concentration level of 1.89 μg/ml for [Sn(Ph)$_3$(DMAB)]. The selectivity index (SI = IC_{50}/MIC) was calculated to be 2.42, showing that this compound not only displaying a considerable activity, but also had increased cytotoxicity. The triphenyl esters of anthranilic acids are considered excellent lead compounds and the results of this study represent the discovery of triphenyl derivatives as a potential new class of anti-tuberculosis agent. Flufenamic acid and organotin adducts were evaluated for anti-proliferative activity in vitro in our laboratory. Among the compounds tested [Bu_2(flu)SnOSn(flu)Bu_2]$_2$ and [Bu_2Sn(flu)$_2$] exhibited high cytotoxic activity against the cancer cell line A549 (non-small cell lung carcinoma). The ID_{50} value for Bu_2(flu)SnOSn(flu)Bu_2]$_2$, and [Bu_2Sn(flu)$_2$] is 0.24 ± 0.1 and 0.35 ± 0.1, respectively (where ID_{50} is the dose of compound (in μg/ml) that inhibits a proliferation rate of the tumor cells by 50% as compared to control untreated cells). The ID_{50}values for [Bu_2(flu)SnOSn(flu)Bu_2]$_2$ and [Bu_2Sn

$(flu)_2$] are lower to the international activity criterion for synthetic agents (4 μg/ml). Thus, these compounds are considered as agents with potential anti-tumor activity, and can therefore be candidates for further stages of screening in vitro and/or in vivo.[6]

New organotin meclofenamic complex [SnPh3(Meclo)] was tested for its antiproliferative activity in vitro against the cells of three human cancer cell lines: MCF-7 (human breast cancer cell line), T24 (bladder cancer cell line), A-549 (non-small cell lung carcinoma) and a mouse fibroblast L-929 cell line (**Table IV.4**) and reported by our group. The IC_{50} values for complex against A-549 and T-24 cell lines are 0.42 and 3.23 μM, respectively, and against MCF-7 and L-929 cell lines are 0.43 μM and 0.18 μM, respectively. Complex is 3.56 and 1.64 times more active than cisplatin against A-549 and L-929 cell lines, respectively. Complex is 44.44 and 41.70 times more active than cisplatin against MCF-7 and T24 cell lines, respectively, and exhibited high activity against all cell lines, more active to cisplatin against the four cell lines. The cytotoxic activity shown by SnPh3(Meclo)] against L-929, A-549, MCF-7 and T24 cell lines indicate that coupling of meclofenamic acid to $SnPh_3$(IV) metal center result in a metallic complex with important biological properties and remarkable cytotoxic activity, since it displays IC_{50} values in a μM range better to that of the anti-tumor drug cisplatin. Thus, the complex is considered as agent with potential anti-tumor activity, and can therefore be candidate for further stages of screening in vitro and/or in vivo. Moreover [SnPh3(Meclo)] was screened against *Mycobacterium tuberculosis* H37Rv and it was found to be a promising anti-mycobacterial lead compound, displaying high activity against M. tuberculosis H37Rv.[7]

References

1. Matito, E., Solà, M. *Coordination Chemistry Reviews* **253**, 647–665 (2009).
2. Keenea, F.R., Smitha, J.A. Collins, J.G. *Coordination Chemistry Reviews* xxx (2009).
3. Defazio, S., Cini, R. *J. Chem. Soc. Dalton Trans.* 1888–1897 (2002).
4. Kovala-Demertzi, D., Hadjipavlou-Litina, D., Staninska, M., Primikiri, A., Kotoglou, Demertzis, M.A. *Journal of Enzyme Inhibition and Medicinal Chemistry* **24,** 742-752 (2009).
5. Moya-Hernández, R., Gómez-Balderas, R., Mederos, A., Domínguez, S., Ramírez-Silva, M. T. Rojas-Hernández, A. Journal of Coordination Chemistry **62,** 40 — 51 (2009).
6. Kovala-Demertzi, D. *Journal of Organometallic Chemistry* **691,** 1767–1774 (2006).
7. Kovala-Demertzi, D., Dokorou, V., Primikiri, A., Vargas, R., Silvestru, C., Russo, U., Demertzis, M.A. *Journal of Inorganic Biochemistry* xxx (2009).
8. Galani, A., Demertzis, M.A., Kubicki, M., Kovala-Demertzi, D. *Eur. J. Inorg. Chem.* 1761-1767 (2003).

V Cephalosporins: β-lactam agents

Cephalosporins are a major group of semisynthetic β-lactam antibiotics used in clinical medicine. They are closely related in the fundamental structure and in antibactericidal action mechanism to penicillins. They are used for the treatment of infections caused by both gram-negative and gram-positive bacteria. Cephalosporins are among the oldest and most frequently prescribed of naturally occuring antimicrobial agents.[1] Several classifications of the cephalosporins have been proposed with the most practical and commonly used being based on the timing of introduction for the parenteral agents in clinical practice, which usually corresponds to their advancing antibacterial spectrums. Using this approach, many publications classify the orally administered cephalosporins by generations, similar to the parenteral cephalosporin classification ("1st-, 2nd-, and 3rd-generation" agents). However, it is difficult or impossible to classify several of these oral compounds based on variations in In vitro potency and the limitations imposed on levels achievable in vivo with oral administration. Using an alternative approach, one can simply divide these agents between "older cephems", which include compounds with more limited potencies and spectrums, and "advanced-generation cephems", which include more potent compounds with expanded antibacterial spectrum against some respiratory tract pathogens (**table V.1**). Group I includes cephalosporins with more limited spectrums, but that also include *Neisseria gonorrhoeae* and a few enteric Gram-negative bacilli, such as *Escherichia coli*, *Proteus mirabilis*, and *Klebsiella pneumoniae.* Groups II and III include compounds with more extended or potent antibacterial activity targeting *Enterobacteriaceae*; however, compounds in group II show limited activity against *Staphylococcus aureus* and penicillin-nonsusceptible *Streptococcus pneumoniae* (**table V.1**).[2]

Table V.1. Older and modern orally administered cephalosporins available in the United States.[2]

Older cephems of comparable spectrum	So-called advanced-generation cephems		
	Group I	Group II	Group III
Cefodroxil	Cefaclor	Cefixime	Cefdinir
Cephalexin	Cefprozil	Ceftibuten	Cefditoren
Cephradine	Cefuroxime		Cefpodoxime
	Loracarbef[c]		

Brotzu discovered cephalosporins in the late 1940's as naturally occurring substances produced by the fungus *Cephalosporium acremonium*, now known as *Acremonium chrysogenum*. Later on, a research team from Oxford university isolated the 1st compound (cephalosporin C). The first widely used cephalosporin was cephalothin, introduced to the market in 1962 and was available only for parenteral use. Among the first semisynthetic modifications of the C-7 side chain of the cephem nucleus was the addition of a D-phenylglycyl moiety that produced cephalexin, the first oral cephalosporin. Side chain modifications continued to appear, which expanded spectrums of activity and/or enhanced bioavailability either by the oral or parenteral routes. With the discovery of very

potent parenteral 2-amino-5-thiazolyl cephalosporins, efforts were further directed to develop orally delivered counterparts in that series. The existing so-called 2nd-generation parenteral compounds were among the first targets for development of orally active agents. Two compounds were esterified and have come to be widely used, cefuroxime axetil and cefotiam axetil (Europe). The α-aminocephalosporin compounds that were also developer included cefaclor, cefprozil, and an aminocarbacephem, loracarbef, that very closely resembled cefaclor.[2]

The chemical structures of cephalosporins is shown in **Figure V.1**. The basic nucleus is the 7-amino cephalosporanic acid (7-ACA), which is formed by the hydrolysis of cephalosporin C produced by fermentation. It is seen that the structures consist of a β-lactam ring fused with a dihydrothiazine ring, but differing in the nature of substituents attached at the 3- and/or 7-positions of the cephem ring (R2 and R4). The substitution at the 3-position affects the pharmacokinetic properties, while the substitution at the 7-position affects the antibacterial spectrum of the cephalosporins.[1]

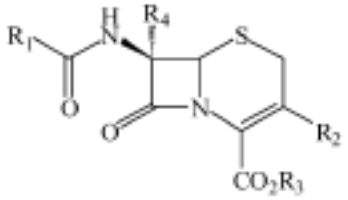

Figure V.1. The chemical structure of cephalosporins (7-Amino cephalosporanic acid 7-ACA).[1]

Since modern antibiotic therapy was started, the abuse of antibacterial agents in many fields of human medicine and of zootechnic activities has promoted the progressive development of bacterial resistance. In the case of Gram-positive bacteria, for example, some cocci, such as *Staphylococcus aureus* (*S.a*.) and *Streptococcus pneumoniae* (*S.p*.), once very sensitive to the action of penicillins (*S.a*. pen-S or *S.p*. pen-S), have become very resistant to these antibiotics (*S.a*. pen-R or *S.p*. pen-R) or, in the case of some strains of *S.a*. also to methicillin (*S.a*. met-R). Some of these cocci, once sensitive to vancomicin or to its associations with rifampicin or cephotaxime , are now resistant also to this antibiotic.[3]

In general, at present, bacterial infection caused by pen-R Gram-positive cocci is treated with the more recent β-lactam antibiotics and/or macrolides, but it is beginning to appear evident that there is a need for new antibiotics, in order to overcome the multi-drug resistance shown by these infectious agents. In the field of cephalosporin β-lactam antibiotics, the antimicrobial properties of the new compounds essentially depend on their ability to interact more or less strongly with the bacterial penicillin-binding proteins (PBPs), which appear to be mutated in the resistant pathogens. These interactions are essentially linked to the nature of the substituents bound to the C-3 and C-7 atoms of the cephem nucleus. In particular, as regards the C-7 position, there is good evidence that appropriate variations in the steric hindrance and/or lipophilicity of the substituent R_1 on the amido side-chain can modify the affinity and the selectivity of new cephalosporins against the mutated PBPs of the Gram-positive pen-R and met-R strains. In the more recent cephalosporins which possess a good activity

against resistant Gram-positive cocci, the C-7 acylamido side-chain is characterised by the presence of a bulky heteroaromatic portion, in its structure which is probably able to give the drugs better molecular characteristics for their interaction with the PBPs.[3]

The effectiveness of cephalosporins against Gram-negative bacilli is due to a combination of the ability to penetrate the outer membrane, the stability to β-lactamase hydrolysis in the periplasmic space, and affinity for penicillin binding proteins (PBPs)[7]. Cephalosporins exert their antibacterial activity by inhibiting bacterial cell wall biosynthesis. B-lactams bind to proteins on the inert surface of the bacterial cell membrane. These proteins, penicillin binding proteins (PBPs) are of 3 classes: transpeptidases, carboxypeptidases, and endopeptidases. These enzymes are responsible for the final assembly of newly synthesized cell wall, external to the cell membrane. Cephalosporins inhibit the transpeptidase enzyme responsible for cross-linking nascent peptidoglycan. The cephalosporin β-lactam ring sterically mimics the D-ala-D-ale amino acid sequence of the pentapeptide precursor, covalently binding at the transpeptidase active site, rendering the enzyme and the cephalosporin inactive.[4]

V.1. The second-generation cephalosporin: Cefaclor.

Cefaclor (**Figure V.2**) is in the class cephalosporins, and has the same fundamental structure as penicillin. Cefaclor became available in the United States in 1979 for the treatment of upper and lower respiratory tract infections.[2,6]

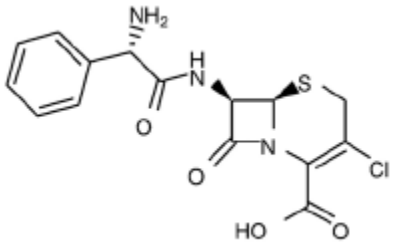

Figure V.2. Chemical structure of cefaclor.[2]

Cefaclor is a β-lactam antibiotic widely used for the medical treatment of microbial infective diseases caused by bacteria, such as pneumonia and infections of the ear, lung, skin, throat and urinary tract. Moreover, cefaclor is one of ‘‘the top antibiotics by mass” produced and prescribed in many countries, and has also been detected at a level of several μg/ls in sewage treatment plants.[6]

After 2 decades of widespread use, cefaclor remains clinically effective for the management of pharyngitis and tonsillitis, acute bacterial exacerbations of chronic bronchitis (ABECB), and secondary bacterial infections of acute bronchitis.Between 1979 and 1990, there were no increases in the incidence of bacterial strains resistant to cefaclor. In the 1990s between 89.4% and 99.6% of isolates of *Haemophilus injluenzae* and *Moraxella catarrhulis* identified as susceptible to cefaclor remained so.Cefaclor retains its excellent safety profile, which is especially distinguished by its low incidence of gastrointestinal adverse events.[7]

Table V.2. Bactericidal activity of extendedrelease cefaclor against respiratory tract pathogens: in vitro evidence.[7]

Gram-positive pathogens
Staphylococcus aureus
Streptococcus pneumoniae
Streptococcus pyogenes
Gram-negative pathogens
Haemophilus influenzae
Moraxella catarrhalis

Cefaclor has chemical structure being similar to that of cephalexin but with a substitution of a halogen atom (chlorine) for the methyl group in the 3 position of the dihydrothiazine ring, which increases the lipophilicity of the molecule. This substitution gave cefaclor greater antibacterial activity, especially against *Haemophilus influenzae.*[2] Cefaclor has a highly stable zwitterionic molecule (ie, a molecule with a positive and a negative charge). As a zwitterionic compound, cefaclor diffuses into external membranes more rapidly than does a monoanionic compound such as cefuroxime or a dianionic compound such as cefonicid. This characteristic contributes to its excellent penetration rate. The bactericidal action of cefaclor its their inhibition of cell-wall synthesis as a result of binding to and inhibiting penicillin-binding proteins. Cefaclor as second-generation cephalosporins are active against both gram-positive and gram-negative bacteria, including the most common respiratory tract pathogens- *Streptococcus pneumoniae*, *H influenzae*, and *M catarrhalis.* Cefaclor attains 90% to 95% bioavailability which is greater than other oral cephalosporins. Peak serum concentration is attained ~ 1 hour after dosing in fasted subjects. Approximately 85% of administered cefaclor undergoes rapid renal excretion, and ~ 15% undergoes spontaneous degradation, with little or no hepatic metabolism. Because of this rapid and high level of absorption (cefaclor reaches maximum plasma concentration within 1 hour compared with other drugs), cefaclor has a high tissue concentration and a low risk of gastrointestinal adverse effects.[7]

The efficacy of cefaclor compares favorably with that of other cephalosporins in the treatment ofvrespiratory tract infections. In few separate studies conducted within the past decade, cefaclor has been shown to be as effective as other cephalosporins. None of the studies showed any statistically significant differences in clinical or bacteriologic response rates between cefaclor and the other cephalosporins. In addition, cefaclor has been compared with the carbacephem loracarbef in the treatment of acute bacterial bronchitis. The clinical responses were almost the same for cefaclor and loracarbef (94.7% and 95.3%, respectively), and the bacteriologic responses were similar (92.8% and 90.4%, respectively). A number of attributes of cefaclor make one of the most effective and well tolerated choices for the management of respiratory tract infections. These attributes include its molecular stability, excellent activity against most gram-positive and gram-negative respiratory tract pathogens, rapid absorption, >90% bioavailability, and mucosal penetration.[7]

V.2. Metal complexes of cephalosporins.

β-lactam antibiotics interact with metal ions and this interaction is of a complex nature. The investigations show that metal(II) ions catalyze hydrolysis of some penicillins and cephalosporins and the saturation kinetics from the concentration of metal ions was observed. In the presence of an excess of metal ions, an antibiotic/metal ion complex was formed. It was found also, that the ratio metal: penicillin was 1:1 and the great catalytic effects of Cu^{2+} ions was established in the case of hydrolysis of benzylpenicillin. It was supposed that the metal ion stabilizes the tetrahedral transition complex formed during the hydroxide-ion catalyzed hydrolysis of benzylpenicillin and that the site of, coordination with Cu(II) ion is the β-lactam nitrogen and carboxylate group. It was also investigated the rate of hydrolysis of natural penicillins and their investigation suggests that the nitrogen substituent on the 6 position is involved in a transition complex prior to the ring opening. Literature data for the metal complexes of semisynthetic penicillins, especially cephalosporins are scarce. Fazakerley and Jackson have examined the interaction between ampicillin and cephalexin with Cu(II) and Mn(II) ions using 1H NMR and it was found that the metal ion is coordinated through the carbonyl and amino group in the side chain. Coordination between metal ions and cephalexin, which takes place through the side chain, has been also confirmed using infrared spectroscopy and magnetic measurements. The metal complexes of semisynthetic penicillins and cephalosporins and their stability constants have been determined mainly by electroanalytical methods, spectrophotometric and other methods. The formation of complex ions between cefaclor and Cu^{2+} has been investigated by ultraviolet spectroscopy. The conditions of formation of complex ions were studied in weak acidic, neutral and alkaline medium in the pH range from 5.60 to 11.05. The interaction between cefaclor and Cu(II) ion in acidic medium results in the formation of $Cu(CEF)^{+}$ complex and it is supposed that the ligand acts as zwitterion which is coordinated to the metal ion. This complex easily hydrolyzes giving a hydroxo complex Cu(OH)(CEF). The hydroxo complex dominates at pH > 7.50. This complex species at pH = 8.00 shows absorption band in the range from 400 to 282 nm, with a maximum at 300 nm. It was found that the stoichiometric ratio of cefaclor to Cu(II) is 1:1.[8]

The serious medical problem of bacterial resistance and the rate at which it develops have led to increasing levels of resistance to classical antibiotics among Gram positive organisms such as *Pneumococci, Enterococci* and *Staphylococci.* The actual mechanism involved is the release of relatively large amounts of β-lactamase into the surrounding medium and thus the destroying of the p-lactamic antibiotics by hydrolysis of the lactam ring has become the most predominant mechanism of resistance. Several *in vivo* studies have indicated that metal complexes possess interesting toxicological and pharmacological properties. However, a significant problem is that some of them lose their activity upon exposure to proteins, and appear to have better affinities than the ligands/compounds studied for metal ions, which are deactivated once again when embedded in the proteins. We have previously the coordination chemistry of some antibiotics and/or antibacterial compounds with transition metals to examine the modes of binding and to study their effect on biological activity. Consequently investigations on the interaction of metal ions with antibiotics, it was

report the synthesis and characterization of kefzol (**Figure V.3)** metal complexes and their antibacterial properties against various pathogenic bacterial strainsof *Staphylococcus aureus, Klebsiella pneumoniae, Pseudomonas aeruginosa, Escherichia coli* and *Proteus mirabilis.*[9]

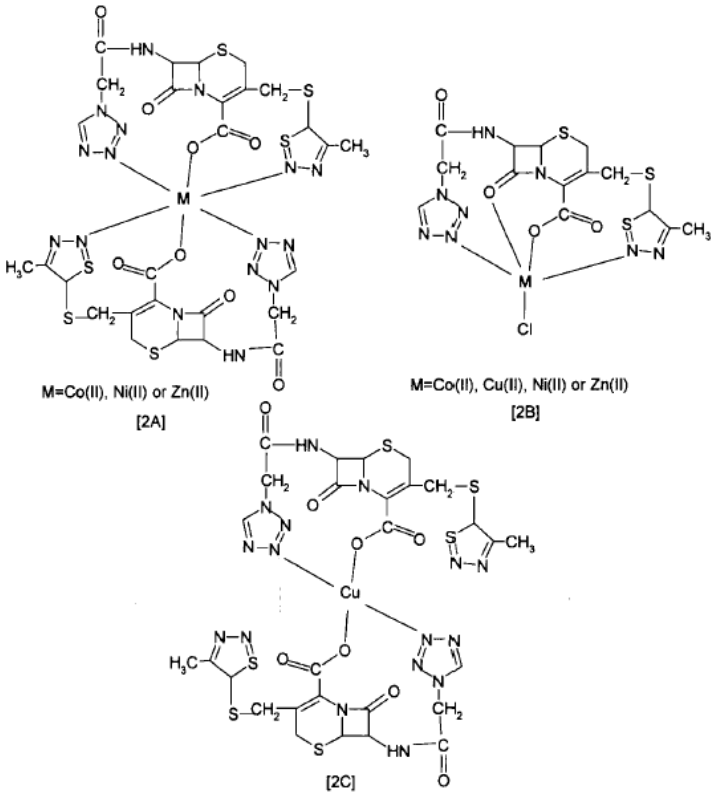

Figure V.3. Proposed Structure of the metal complexes of kefzol.[9]

All the newly synthesized complexes of kefzol coordinated with the metals Co (II), Cu (II), Ni (II) and Zn (II) were screened for their antibacterial activity against *S. aureus, E. coli, P. ueruginosa, K. pneumoniue and P rnirabilis.* The metal(II) complexes exhibited a marked enhancement in kefzol activity against tested bacterial strains. The metal complexes with two kefzol molecules coordinated to the one central metal atom were more antibacterial than the complexes having one kefzol molecule attached with the metal atom.This enhancement in activity may be due to an efficient diffusion of the metal complex into the bacterial cell and/or interaction with the bacterial cell. It has been further suggested that ligands having nitrogen and oxygen donor systems might inhibit those enzyme which require these groups for their activity to be especially more susceptible to deactivation by the metal ions upon chelation.[9]

Chelation/coordination also reduces the polarity of the metal ion mainly because of the partial sharing of its positive charge with these donor groups and possibly the π-electron delocalization within the whole chelate ring system. This process of chelation thus increases the lipophilic nature of the central metal atom, which in turn**,** favors its permeation through the lipoid layer of the thus causing the metal complex to cross the membrane of the microorganism cell wall and hence increases the bioavailability

and activity of the drug.[9] The synthesis and characterization of cloxacillin (clox) complexes with divalent metal ions [Co (II), Cu (II), Ni (II) and Zn (II)] was described (**Figure V.4**). The nature of bonding of the chelated cloxacillin and the structures of the metal complexes have been elucidated on the basis of their physical and spectroscopic data. In all the complexes, the cloxacillin acts as a uninegatively charged bidentate ligand with coordination involving the carboxylate-O and endocyclic-N of the b-lactam ring. The new compounds have been screened for in-vitro antibacterial activity against *Escherichia coli* (a), *Klebsiella pneumonae* (b), *Proteus mirabilis* (c), *Pseudomonas aeruginosa* (d), *Salmonella typhi* (e), *Shigella dysentriae* (f), *Bacillus cereus* (g), *Corynebacterium diphtheriae* (h), *Staphylococcus aureus* (j) and *Streptococcus pyogenes* (k) bacterial strains. The brine shrimp bioassay was also carried out to study their in-vitro cytotoxic properties. All compounds, respectively, showed a promising activity (90%) against five bacterial species at 10 µg/ml concentration and a significant activity (52%) against the same test bacteria at 25µg/ml concentration.[10]

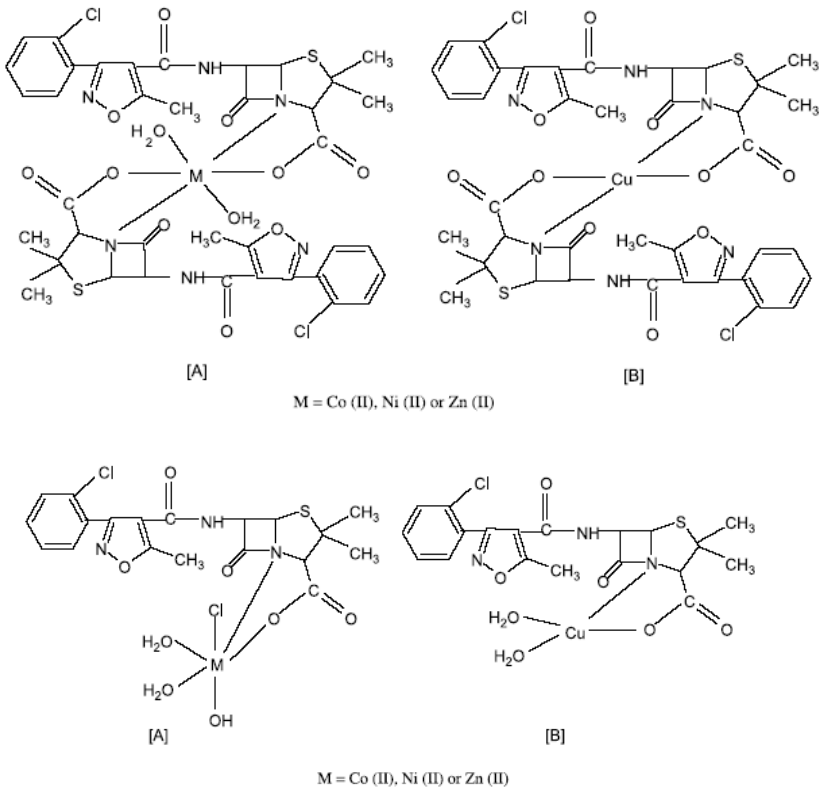

Figure V.4. Proposed structure of cloxacillin metal (II) complexes.[10]

References

1. Thongpoon, C., Liawruangrath, B., Liawruangrath, S., Wheatley, R.A., Townshend, A., *Analytica Chimica Acta* **553,** 123–133 (2005).
2. Sader, H.S., Jacobs, M., Fritsche, T.R. *Diagnostic Microbiology and Infectious Disease* **57**, 5S–12S (2007).
3. Rossello, A., Orlandini, E., Nuti, E., Rapposelli, S., Macchia, M., Di Modugno, E., Balsamo, A., *IL FARMACO* **59,** 691–696 (2004).
4. Bryskier, A., *Clinical Microbiology and Infection* **3,** s1-s6 (1997).
5. Scott, D.L., *Center for drug evaluation research application number: nda 50739. Microbiology reviews*. (1997).
6. Yu, S., Lee, B., Lee, M., Cho I-H., Chang, S-w., Chemosphere **71,** 2106–2112 (2008).
7. Meyers, B.R., *Clin Therr* **22,** 154–166 (2000).
8. Dimitrovska, A.,, Andonovski, B., Stojanoski, K. *International Journal of Pharmaceutics* **134,** 213-221 (1996).
9. Chohan, Z-H., Supuran, C.T., Scozzafav, A. *Journal of Enzyme Inhibition and Medicinal Chemistry* **19,** 79 — 84 (2004).
10. Chohan, Z-H. Supuran, C.T., *Journal of Enzyme Inhibition and Medicinal Chemistry* **21,** 441 — 448 (2006).

VI Superoxide dismutase (SOD) enzymes and SOD mimetics.

VI.1. Metabolites of molecular oxygen known as reactive oxygen species.

Nearly a century ago it was noted that animals with higher metabolic rates often have shorter life spans. These observations led to the formulation of 'the rate-of-living hypothesis', which states that the metabolic rate of a species ultimately determines its life expectancy. Initially, the mechanistic link between metabolism and ageing was unknown. In the mid-1950s, Denham Harman articulated a 'free-radical theory' of ageing, speculating that endogenous oxygen radicals were generated in cells and resulted in a pattern of cumulative damage. Although the concept of endogenous oxidants was at first controversial, the identification a decade later of **superoxide dismutase (SOD)**, an enzyme whose sole function seemed to be the removal of superoxide anions, provided mechanistic support for Harman's hypothesis. Given that the mitochondria produce most of the energy in the cell, and correspondingly consume the bulk of intracellular oxygen, the free-radical theory of ageing is now often thought of synonymously with the rate-of-living hypothesis; the higher the metabolic rate of an organism, the greater the production of reactive oxygen species (ROS) and hence the shorter the life span.[1]

In humans, several pathologies involve the overproduction of reactive oxygen species. Metal-containing catalytic antioxidants have emerged as a novel class of potential therapeutic agents that scavenge a wide range of reactive oxygen species. Cardiovascular, neurodegenerative and inflammatory lung disorders are all potentially important targets for catalytic antioxidant therapy.[2]

Reactive oxygen species (ROS), such as the superoxide radical anion ($O_2^{-\bullet}$) and hydrogen peroxide (H_2O_2), are formed in biological systems by the partial reduction of molecular oxygen (**Figure VI.1**). $O_2^{-\bullet}$ is produced from the one-electron reduction of molecular oxygen. Reduction of $O_2^{-\bullet}$ with a second electron generates H_2O_2, which can also be formed from a two-electron reduction of molecular oxygen. Formation of the hydroxyl radical (HO•), another ROS, is thought to occur through the one-electron reduction of H_2O_2, a reaction that is facilitated by transition metals that are in a reduced valence state (e.g. reduced copper or iron). Four electrons and two protons are required to reduce molecular oxygen to water (H_2O). Additionally, there are a large number of other reactive species that are formed from the reaction of ROS with biological molecules [e.g. polyunsaturated lipids, thiols and nitric oxide (NO)].[2]

$O_2^{-\bullet}$ is generated from the uncoupling of the mitochondrial electron transport chain during oxidative phosphorylation and also by the catalytic action of a variety of intracellular and extracellular oxidases. The production of $O_2^{-\bullet}$, which occurs during host defense responses, is either beneficial or detrimental depending upon the site of formation, the amount generated and the prevalence of antioxidant defenses. $O_2^{-\bullet}$ is thought to act as a cell-signaling molecule and to contribute to the killing of foreign bacteria. However, during acute and chronic inflammation, the overproduction of $O_2^{-\bullet}$ has been shown to contribute to tissue damage and injury. H_2O_2 is generated directly from $O_2^{-\bullet}$ through a

rapid dismutation reaction that can occur either enzymatically (rate of 10^{-9} M^{-1} s^{-1}) or non-enzymatically (rate of 10^{-5} M^{-1} s^{-1}).[2]

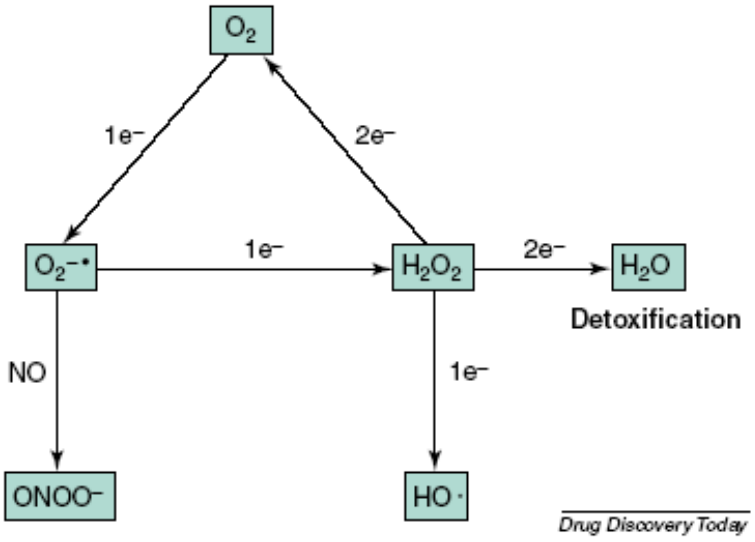

Figure VI.1. The generation of reactive oxygen species. Oxygen (O_2) is partially reduced by either one electron to form the superoxide radical anion ($O_2^{-\bullet}$) or two electrons to generate hydrogen peroxide (H_2O_2). In addition, further reduction of $O_2^{-\bullet}$ and H_2O_2 produces other reactive species. H_2O_2 can be reduced to form the hydroxyl radical (HO•). $O_2^{-\bullet}$ readily reacts with nitric oxide (NO) to form peroxynitrite ($ONOO^-$), which is unstable at physiologic pH and readily decomposes into potent oxidizing and nitrating species that damage cellular macromolecules such as proteins, DNA, lipids and sugars. Antioxidants detoxify these reactive species to water (H_2O)[2].

In addition, H_2O_2 is formed enzymatically as a byproduct of lipid metabolism in peroxisomes. H_2O_2 is stable at biological pH, but can participate in HO• formation in the presence of reduced transition metals. H_2O_2 readily reacts with the thiol functional group and this type of reaction is proposed to be one of the key mechanisms through which ROS participate in cell signaling. Several phosphatases contain sensitive thiol residues; the oxidization of this functionality results in inactivation of the phosphatase. In addition, H_2O_2 participate in the formation of several reactive species that have been directly implicated in tissue damage, for example, HO•. $O_2^{-\bullet}$ effects the release of iron from iron-containing proteins, thus increasing the concentration of the transition metal that is available to reduce H_2O_2 to HO•. HO• is an extremely reactive species that readily oxidizes all cellular macromolecules, including proteins, sugars, lipids and DNA. In addition, $O_2^{-\bullet}$ readily reacts with NO to form peroxynitrite ($ONOO^-$), which is unstable at physiological pH and rapidly decomposes to form potent nitrating and oxidizing species. Cellular damage by oxidative modification of cellular macromolecules ensues when ROS are generated in excess of endogenous defenses. ROS are implicated in several pathological processes including tissue injury, inflammatory disorders, cardiovascular disease, pulmonary disease and neurodegenerative diseases.[2]

The concentrations of these metabolic intermediates are actually kept under strict control by the activity of a complex defence system including enzymes (superoxidedismutase, catalase, glutathione peroxidase) and non-enzymatic species such as glutathione, ascorbate, tocopherol or retinol. However, an uncontrolled production of reactive oxygen species is liable to occur in several conditions leading to a situation known as ‘‘oxidative stress’’ where the highly reactive species can attack many essential biomolecules (protein, DNA, RNA, lipids) and even cell structures, causing oxidative

damages. As a matter of fact, many pathological processes are initiated or aggravated bysuch. For several years, pharmacological investigations of exogenous compounds or therapeutical agents have focused on a possible interaction with reactive oxygen species in order to assess their capacity to prevent or minimize free radical damages to biological targets.[3]

VI.2. Superoxide dismutases enzymes.

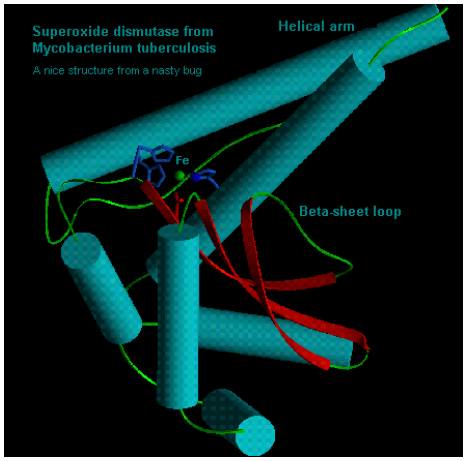

Figure VI.2. The overall structure of the Fe-superoxide dismutase.[4]

Four different types of SOD are known, a **Cu/Zn-containing SOD** (**Figure VI.4**), a **FeSOD** (**Figure VI.2**), a **NiSOD**, and **MnSOD**.[5a] Distinct types of SOD have been isolated from various species of organisms, and each of them contains different transition metals as the prosthetic group: Cu/Zn, Fe and Mn. The metal ligands are in all cases aminoacid residues, varying in composition according to the type of species or even subspecies considered. Maybe the most widely present in different organisms is the homodimeric[6] copper-zinc superoxide dismutase (CuZnSOD), an enzyme found in relatively high concentration in the cytoplasm of all or nearly all eukaryotic cells. CuZnSODs from different organisms are very similar, particularly in the regions of their metal-binding sites, as judged from a high degree of homology in their amino acid sequences and the resemblance of the spectral properties of the native enzymes and metal-substituted derivatives from different organisms. Several CuZnSODs have been extensively studied, most notably bovine, human, and yeast. Eukaryotic cells also have a mitochondrial Mn-containing SOD, and prokaryotes often have Fe- and Mn-containing SODs. The Fe and Mn enzymes are structurally related to each other. Neither the Mn- nor the Fe-containing SOD is structurally related to CuZnSOD. All of the SODs are believed to function as intracellular antioxidant enzymes by reducing the steady-state level of superoxide present in the cell[7]. Superoxide dismutases, found in virtually all areobic organisms, catalyze the disproportionation of superoxide ($2\ O_2^- + 2\ H^+ \rightarrow O_2 + H_2O_2$) into hydrogen peroxide (H_2O_2) and elemental oxygen (O_2)

which diffuses into the intermembrane space or mitochondrial matrix (**Figure VI.3**), and thus, SODs provide an important defense against the toxicity of superoxide radicals.[7]

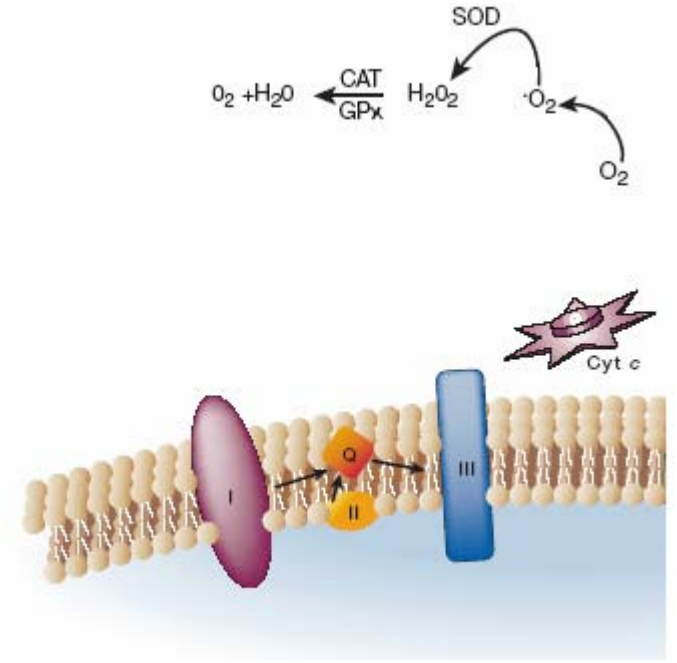

Figure VI.3. Most estimates suggest that the majority of intracellular ROS production is derived from the mitochondria. The production of mitochondrial superoxide radicals occurs primarily at two discrete points in the electron transport chain, namely at complex I (NADH dehydrogenase) and at complex III (ubiquinone–cytochrome *c* reductase). Once generated, the superoxide can be enzymatically dismutated by SOD to form hydrogen peroxide that in turn is metabolized by enzymes such as catalase (CAT) and glutathione reductase (GPx) regenerating water and molecular oxygen. The generation of superoxide is nonenzymatic and hence the higher the rate of metabolism, the greater the production of ROS.[1]

The enzyme superoxide dismutase (SOD), either as the manganesecontaining MnSOD (present in the mitochondrion) or the dinuclear Cu/Zn-SOD (present in the cytosol and extracellular space), performs the role of superoxide detoxification in normal cells and tissue.[5b] They catalyze the dismutation of superoxide to dioxygen and hydrogen peroxide, in a 'ping-pong' fashion, cycling between oxidised and reduced forms during each half cycle of the $O_2^{-\bullet}$ disproportionation reaction.[8]

VI.2.1. Relationship between the structure of CuZnSOD and the enzymatic mechanism.

The x-ray crystal structures of the oxidized form of **CuZnSOD** show it to consist of two identical subunits held together almost entirely by hydrophobic interactions. Each subunit consists of a flattened cylindrical barrel of P-pleated sheet from which three external loops of irregular structure extend. The metal-binding region of the protein binds Cu^{2+} and Zn^{2+} in close proximity to each other, bridged by the imidazolate ring of a histidyl side chain. The Cu^{2+} ion is coordinated to four histidyl imidazoles and a water in a distorted square pyramidal geometry. The Zn^{2+} ion is coordinated to three histidyl imidazoles (including the one shared with copper) and an aspartyl carboxylate group, forming a distorted tetrahedral geometry around the metal ion. One of the most unusual aspects of the structure of this enzyme is the occurrence of the bridging imidazolate ligand, which holds the copper and zinc ions 6.3 Å apart. Such a configuration is not unusual for imidazole complexes of metal ions, which sometimes form long polymeric imidazolate-bridged structures. The role of the zinc ion in CuZnSOD appears to be primarily structural. There is no evidence that water or other ligands can bind to the zinc, and it is therefore highly unlikely that superoxide would interact with that site. The copper site is clearly the

site of primary interaction of superoxide with the protein. The x-ray structure shows that the copper ion lies at the bottom of a narrow channel which is large enough to admit only water, small anions, and similarly small ligands. In the lining of the channel is found the positively charged side chain of an arginine residue, 5 Å away from the copper ion and situated in such a position that it could interact with superoxide and other anions when they bind to copper. Near the mouth of the channel at the surface of the protein, are located two positively charged lysine residues, which are believed to play a role in attracting anions and guiding them into the channel.[7]

Figure VI.4. In the native enzyme CuZnSOD, copper(II) is coordinated by three imidazole residues (His_{44}, His_{46} and His_{118}) and a water molecule, while two imidazoles (His_{69} and His_{78}) and a carboxylate of an aspartyl residue (Asp_{81}) are the binding sites of zinc(II) ion.[9]

In the case of superoxide dismutase enzymes CuZnSOD, mechanism is believed to be operating, with the copper center undergoing changes in redox state.[7]

$$O_2^- + Cu^{II}SOD \rightarrow O_2 + Cu^{I}SOD$$

$$O_2^- + 2H^+ + Cu^{I}SOD \rightarrow H_2O_2 + Cu^{II}SOD$$

It is important to note that the spectroscopic properties of CuZnSOD are unchanged over the same pH range wherein the rate of superoxide dismutation is unchanged by pH, i.e. pH 5 - 9.5. This property is unusual because the oxidized form of CuZnSOD contains a water molecule bound to Cu^{II} and water molecules bound to Cu^{II} either in a protein or in a coordination complex generally ionize well below pH 9.5 to give Cu^{II}-hydroxide complexes.[7]

VI.2.2. Mitochondrial mandanese superoxide dismutase (MnSOD).

Crystal structure determinations of **MnSODs** from organisms ranging from E. coli to humans have been reported. The coordination sphere of the Mn in the active site of these MnSODs is illustrated in **Figure VI.6.**[5a] Human manganese superoxide dismutase is a homotetramer of 22-kDa subunits found in mitochondria that also catalyzes the disproportionation of superoxide to O_2 and H_2O_2. This catalytic decay of superoxide competes in cells with the reaction at diffusion-controlled rates of superoxide with NO, the product of which is peroxynitrite. In mechanisms that often involve species of CO_2, peroxynitrite nitrates tyrosine and tryptophan residues, among other reactions. The presence of nitrated proteins is associated with a number of pathological states and with certain diseases characterized by inflammatory processes. Human MnSOD in the presence of peroxynitrite is nitrated at a number of sites, but the observed near complete inhibition of catalysis is associated with the nitration of Tyr34 Tyr34 in human MnSOD is an active-site residue the side chain of which is close (5.5 Å) to the catalytic manganese but not directly bound to it. Tyr34 is highly conserved in eukaryotic and bacterial MnSODs sequenced to date, as well as in the bacterial FeSODs. The phenolic side chain of Tyr34 is hydrogen-bonded with the side-chain carboxamide of Gln143 which, in turn, forms a hydrogen bond with the metalbound solvent.[10]

One area of research interest has been the metal ion specificity of the MnSOD and FeSOD molecules. The tertiary structures of these molecules are very similar and the ligands coordinated to the metal ions are identical. Many organisms contain both forms of the enzyme and each form has an absolute specificity forits metal ion, the enzyme is completely inactive if the wrong metal ion is present.[5a]

VI.3. Development of catalytic antioxidants: SOD mimetics.

Superoxide dismutases (SODs) and catalase are metalloproteins that catalyze 'dismutation' reactions, which detoxify ROS. A dismutation reaction is defined as a reaction in which two like-molecules react to produce two different products (i.e. $A + A \rightarrow B + C$). SODs catalyze the formation of oxygen and H_2O_2 from two $O_2^{-\bullet}$, whereas catalase metalloproteins catalyze the reaction of two H_2O_2 to produce oxygen and water. Because these efficient reactions do not require additional reducing equivalents, no energy is taken from the cell to drive these transformations. The overall goal of cellular antioxidant defenses is to reduce ROS to water. The overexpression of these metalloproteins in cell culture and in whole animals has provided protection against the deleterious effects of a wide range of oxidative stress paradigms. The use of SOD and catalase as therapeutic agents to attenuate ROS-induced injury responses has had mixed success. The principal limitations of using these proteins are their large sizes, the consequences of which are low cell permeability, a short circulating half-life, antigenicity and high-manufacturing costs. To overcome many of these limitations, an increasing number of low molecular-weight catalytic antioxidants have been developed.[2] So far, the superoxide dismutases (SODs), from the family of metalloenzymes**,** catalyze the dismutation of superoxide to dioxygen and hydrogen peroxide. However, the natural enzymes show some drawbacks as therapeutic agents for treating the disease states connected with the overproduction of $O_2^{-\bullet}$ immunological problems, short half-lives *in vivo*, cost of production, solution instability, reduced

efficacy due to the large size and inability to access the target tissues, *etc.* This has motivated inorganic chemists to synthesize different redox active metal complexes, with the ability to efficiently remove $O_2^{-\bullet}$ in a catalytic manner.[8] The majority of catalytic antioxidants are designed with redox-active metal centers that catalyze the dismutation reaction of $O_2^{-\bullet}$ and/or H_2O_2 by a mechanism that is similar to the mode of action of the active-site metals of SOD and catalase. An ideal **mimetic** is stable and non-toxic. Furthermore, the size and charge of a mimetic can be exploited to target crucial cellular sites of oxidative stress. For many years, it has been recognized that simple metal chelates react with $O_2^{-\bullet}$ and H_2O_2. However, the rates of reaction of chelates with these particular ROS are low and the complexes formed are unstable. The finding that structurally different classes of catalytic antioxidants are effective in similar oxidative stress models confirms the basic concept that small, efficient, catalytic antioxidants show promise in the treatment of ROS-mediated injuries.[2]

A number of Cu-containing SOD mimics have been developed to try to improve the efficiency of the natural enzyme. For example, the compounds can be modified to: (i) possess the required chemical stability in vivo; (ii) provide access to intracellular space; and (iii) facilitate oral administration. Furthermore, some drugs are more advantageous than SOD itself, because they do not pose potential immunogenetic complications and, depending on the drug, may be financially competitive SOD.[12]

VII.3.1. SOD activities of some Cu-NSAIDs.

Non-steroidal anti-inflammatory drugs (NSAID) act principally by inhibiting prostaglandin and leukotriene synthesis, mediated by cyclooxygenase (COX) and lipoxygenase enzymes, respectively . However, NSAID also possess free radical scavenging properties which could act in addition to the inhibition of COX. Such additional antiradicalar effects of NSAID could be of interest in the treatment of chronic inflammatory diseases and lead to the development of more active compounds. NSAID from the oxicam family (tenoxicam, lornoxicam, piroxicam and meloxicam) are nowadays rather frequently prescribed because they specifically inhibit the 2-isoform of COX, which could imply a lower incidence of undesirable side-effects such as gastric intolerance. It is therefore of interest to more precisely assessing their capacity to interact with ROS. According to this some *in vitro* studies are reported in the literature considering the oxicams scavenging profile against superoxide anion ($O_2^{\bullet -}$), hydroxyl radical (•OH), hydrogen peroxide (H_2O_2) and hypochlorous acid (HOCl).[13]

Whatever the proposed mode of action of the Cu-NSAIDs, they display a superior anti-inflammatory and anti-ulcerogenic effect compared with the parent drug. The use of SOD as a pharmaceutical has been proposed for treatment of a number of diseases including, hyperoxia, reperfusion injury, auto-immune bronchopulmonary dysplasia in premature neonates, as well as inflammation and inflammation-associated diseases, such as RA and OA. $O_2^{-\bullet}$ was implicated in the promotion of arthritis due to its ability to degrade hyaluronic acid (HA). HA is an important component of synovial fluid that maintains internal joint homeostasis by acting as a lubricant. It assists with the nutrition of articular cartilage and provides direct anti-inflammatory action.[12]

When $O_2^{-\bullet}$ is added to synovial fluid, the viscosity decreases, indicating depolymerisation of HA Introduction of SOD provides complete protection against this degradation by removing potentially damaging $O_2^{-\bullet}$ from cells. An increase in SOD activity has been found in the synovial fluid of RA and OA patients compared with controls, with increased SOD activity occurring with the progression of the disease. While it has been suggested that injection of SOD into arthritis patients may have anti-inflammatory effects, there have been conflicting results. Unsurprisingly, as the catalytic role of SOD is based on the cyclic Cu(II)-Cu(I) redox reactions, it has been shown that many Cu containing complexes also exhibit SOD activity.[12]

Table shows the IC_{50} results of the SOD studies performed for a number of Cu-NSAID complexes using the xanthine-xanthine-oxidase-generated $O_2^{-\bullet}$ in the NBT reduction assay. A number of papers have been published on the $O_2^{-\bullet}$ scavenging activity of Cu(II) complexes of aspirin and salicylate compounds The SOD activity of the Cu(II) salicylate decreased in the order of: $[Cu(salicylate)_2]$ > $[Cu(acetylsalicylate)_2]$ > $[Cu(p\text{-}aminosalicylate)_2]$ > $[Cu(DIPS)_2]$. As shown in **Table VI.1** , all four complexes exhibited SOD activity with IC_{50} values ranging from ca. 1 to 28 μM. In the reported study, a number of different assays were performed, including the NBT reduction assay using KO_2 as a source of $O_2^{-\bullet}$ and the inhibition of cytochrome c reduction using xanthine_/xanthine oxidase as the source of $O_2^{-\bullet}$. All complexes exhibited SOD activity in these assays but, interestingly, the order of activity of the complexes was not preserved across the different assays.[12]

Table VI.1. SOD activity of Cu-NSAID complexes.

Complex	IC_{50} (μM)
Cuprein	0.04
Cuprein	0.06
Cuprein	0.5–18 (solvent dependence study)
$[Cu(salicylate)_2]$	16
$[Cu(salicylate)_2]$	1.3
$[Cu(acetylsalicylate)_2]$	23
$[Cu(acetylsalicylate)_2]$	2.15
$[Cu(acetylsalicylate)_2]$	11–60 (solvent dependence study)
$[Cu(p\text{-}aminosalicylate)_2]$	28
$[Cu(p\text{-}aminosalicylate)_2]$	3.0
$[Cu(DIPS)_2]$	73 (extrapolated value)
$[Cu(DIPS)_2]$	2.85
$[Cu(DIPS)_2]$	8.9
$[Cu_2(Indo)_4(DMF)_2]$	2–25 (solvent dependence study)
$[Cu_2(Indo)_4(DMF)_2]$	0.23

DIPS - diisopropylsalicylate.
Indo - indomethacin.

The SOD activity of $[Cu_2(Indo)_4(DMSO)_2]$ was first reported by Weser et al. using pulse radiolysis and the NBT reduction assay using KO_2 as the superoxide source. The values obtained and compared with values of spontaneous superoxide dismutation, IndoH and SOD, indicating that $[Cu_2(Indo)_4(DMSO)_2]$ did, indeed, exhibit high SOD activity. The IC_{50} values of $[Cu_2(Indo)_4(DMSO)_2]$

ranged from 25 μM in acetonitrile to 2 μM in DMSO solutions. SOD activity of $[Cu_2(Indo)_4(DMSO)_2]$ was also observed in the NBT assay employing xanthine-xanthine oxidase as the $O_2^{-\bullet}$ source, whereby 3 μM inhibited NBT reduction by 60%. This was consistent with the IC_{50} value of 0.23 μM obtained using the NBT assay with xanthine-xanthine oxidase. It was noted that the IC_{50} value for $[Cu_2(Indo)_4(DMF)_2]$ lies at the high activity region of the spectrum exhibited by these Cu- NSAID complexes.[12]

SOD activity was also observed for other Cu- NSAIDS although IC_{50} values were not determined. It was showed that suprofen exhibited an absorbance increase of 27% at 560 nm due to the reduction of NBT, whereas the monomeric Cu(II) complex of Sup exhibited an increase of only 18% in the absorbance at this wavelength compared with the control. Furthermore studies of SOD activity of a number of monomeric metal tenoxicam complexes and showed that the monomeric Cu(II) complex exhibited the greatest activity (2% absorbance increase at 540 nm), followed by Mn(II) (19%), Co(II) (57%), Ni(II) (74%), Fe(III) (78%) and finally the free ligand (79%).[12]

The superoxide dismutase activity of free tolfenamic acid related copper complexes was measured and compared with those of superoxide dismutase enzyme, SOD. IC_{50} value was measured by the Fridovich test (1.97± 0.17 μM), which showed that $[Cu(tolf)_2L]_2$ is a good superoxide scavenger. These value indicate that potent superoxide dismutase mimics. The inhibition of the NBT reduction by superoxide in the presence of 3 reached a maximum value of about 85% concentration 10 μM.[14]

References

1. Finkel,T.,Holbrook, N.J. *Nature* **408,** 239-247 (2000).
2. Day, B.J. DDT **9,** 557-566 (2004).
3. Van Antwerpen, P., Neve, J. *European Journal of Pharmacology* **496,** 55– 61 (2004).
4. http://www.cryst.bbk.ac.uk/recent_structures/sod/sod.html
5. a) McCleverty, J., Meyer, T.J. **5**, *Comprehensive coordination chemistry* 93-94 (2005).
   b) McCleverty, J., Meyer, T.J. **9**, *Comprehensive coordination chemistry* (2005).
6. Rodrıguez-Ciria, M., Sanz, A.M., Yunta, M.J.R., Gomez-Contreras, F., Navarro, P., Sanchez-Moreno, M., Boutaleb-Charki, S., Osuna, A., Castineiras, A. Pardo, M., Cano, C., Campayo, L. *Bioorganic & Medicinal Chemistry* **15,** 2081–2091(2007).
7. Kessissoglou, D.P. (editor) *Bioinorganic Chemistry. An Inorganic Perspective of life. (*1995).
8. Ivana Ivanovic-Burmazovic, I., Van Eldik, R., 39, 8 Dalton Transactions 4952-5388 (2008).
9. Boka, B., Myari, A., Sovago, I., Hadjiliadis, N*. Journal of Inorganic Biochemistr* **98,** 113–122 (2004).
10. Quint, P., Reutzel, R., Mikulsk, R., McKenna, R., Silverman, D.N. Free Radical Biology & Medicine 40 453 – 458 (2006).
11. http://www.chem.uky.edu/research/miller/sod_projects2.html
12. Weder, E., Dillon, C.T., Hambley, T.W., Kennedy, B.J., Lay, P.A., Biffin, J.R., Regtop, H.L., Davies, N.M. *Coord. Chem. Rev.* **232,** 95-126 (2002).
13. Lucio, M., Ferreira, H., Lima, J.L.F.C., Reis, S. *Analytica Chimica Acta* **597,** 163–170 (2007).
14. Kovala-Demertzi, D., Galani, A., Demertzis, M.A., Skoulika, S., Kotoglou, C., *J. Iorg. Biochem.* **98**, 358 (2004).

VII Cancer cells.

VII.1. The biological basis of cancer.

About 140 years ago Johannes Mueller, showed that cancers were made up of cells, a discovery that began the search for changes that would help to pin-point the specific differences between normal and cancer cells. Cancer is a disorder of cells and although it usually appears as a tumour (a swelling) made up of a mass of cells, the visible tumour is the end result of a whole series of changes which may have taken many years to develop.[1] The human body is made of millions of cells, each one containing 23 pairs of chromosomes. Chromosomes carry genetic information that directs cellular growth and functioning. In normal cells development cells have the ability to reproduce themselves through a process called mitosis. This process allows new cells to replace old cells, with a turnover rate of more than a billion cells a day. Cancer is a disease that originates from normal, healthy cells that lose their ability to control their growth and proceed to divide without control or order. When mutations in cellular division and chromosomal reproduction occur, the abnormal cell loses its ability to grow in an orderly fashion, and a mass or lump can result from the excessive cell division.[2]

Cancer cells are defined by two heritable properties: they and their progeny (1) reproduce in defiance of the normal restraints on cell division and (2) invade and colonize territories normally reserved for other cells. It is the combination of these actions that makes cancers peculiarly dangerous. An isolated abnormal cell that does not proliferate more than its normal neighbors does no significant damage, no matter what other disagreeable properties it may have; but if its proliferation is out of control, it will give rise to a tumor, or *neoplasm* — a relentlessly growing mass of abnormal cells. As long as the neoplastic cells remain clustered together in a single mass, however, the tumor is said to be **benign.** At this stage, a complete cure can usually be achieved by removing the mass surgically. A tumor is considered a cancer only if it is **malignant,** that is, only if its cells have acquired the ability to invade surrounding tissue. Invasiveness usually implies an ability to break loose, enter the bloodstream or lymphatic vessels, and form secondary tumors, called metastases, at other sites in the body. The more widely a cancer spreads, the harder it becomes to eradicate.[3]

Cancers are classified according to the tissue and cell type from which they arise. Cancers arising from epithelial cells are termed **carcinomas;** those arising from connective tissue or muscle cells are termed **sarcomas.** Cancers that do not fit in either of these two broad categories include the various **leukemias,** derived from hemopoietic cells, and cancers derived from cells of the nervous system. Each of the broad categories has many subdivisions according to the specific cell type, the location in the body, and the structure of the tumor; many of the names used are fixed by tradition and have no modern rational basis.[3]

In parallel with the set of names for malignant tumors, there is a related set of names for benign tumors: an *adenoma,* for example, is a benign epithelial tumor with a glandular organization, the corresponding type of malignant tumor being an *adenocarcinoma,* similarly a *chondroma* and a *chondrosarcoma* are, respectively, benign and malignant tumors of cartilage. About 90% of human cancers are carcinomas, perhaps because most of the cell proliferation in the body occurs in epithelia, or because epithelial tissues are most frequently exposed to the various forms of physical and chemical damage favor the development of cancer. Each cancer has characteristics that reflect its origin. Thus, for example, the of an epidermal *basal-cell carcinoma,* derived from a keratinocyte stem cell in the skin, will generally continue to synthesize cytokeratin intermediate filaments, whereas the cells of a *melanoma,* derived from a pigment cell in the skin, will often (but not always) continue to make pigment granules. Cancers originatig from different cell types are, in general, very different diseases**.** The basal-cell carcinoma, for example, is only locally invasive and rarely forms metastases, whereas the melanoma, if not removed promptly, is much more malignant and rapily gives rise to many metastases The basal-cell carcinoma is usually easy to remove by surgery, leading to complete cure; but the malignant melanoma, once it has metastasized widely, is often impossible to eliminate and consequently fatal.[3]

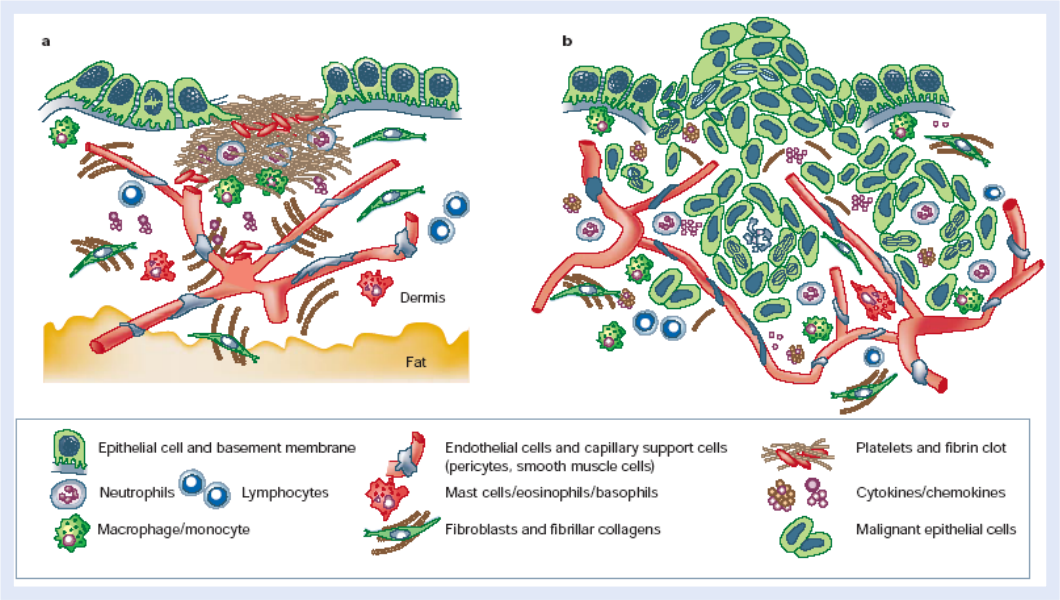

Figure VII.1. Wound healing versus invasive tumour growth. **a**, Normal tissues have a highly organized and segregated architecture. Epithelial cells sit atop a basement membrane separated from the vascularized stromal (dermis) compartment. **b**, Invasive carcinomas are less organized. Neoplasia-associated angiogenesis and lymphangiogenesis produces a chaotic vascular organization of blood vessels and lymphatics where neoplastic cells interact with other cell types (mesenchymal, haematopoietic and lymphoid) and a remodelled extracellular matrix. Several factors potentiate tumour growth, stimulate angiogenesis, induce fibroblast migration and maturation, and enable metastatic spread via engagement with either the venous or lymphatic networks.[4]

VII.2. The process of carcinogenesis.

Carcinogenesis is a multistage process. The application *of* a cancer-producing agent (carcinogen) does not lead to the immediate production of a tumour. There are a series of changes after the initiation step induced by the carcinogen. The subsequent stages—tumour promotion—may be produced by the carcinogen or by other substances (promoting agents) which do not themselves produce tumours. Initiation, which is the primary and essential step in the process, is very rapid, but once the initial change has taken place the initiated cells may persist for a considerable time, perhaps the life span of the individual. The most likely site for the primary event is in the genetic material (DNA), although there are other possibilities. The carcinogen is thought to damage or destroy specific genes probably in the stem cell population of the tissue involved.[1]

Initiated cells remain latent until acted upon by promoting agents. Many of these 'transformed' cells may not grow at all or grow very slowly. It is at this stage that the influence of growth appears. Promoting agents are not carcinogenic in themselves but they do induce initiated cells to divide. Many agents will induce cell division, but only promoters will induce tumour development, so that although cell growth is necessary for tumour development there must also be other factors involved. The suggestion is that promoting agents may interfere with the process of differentiation that normally takes place when cells move from the dividing stem cell population into functioning, and usually non-dividing, cells. Even though these growth-promoting stimuli are acting on the cells, they may still be sensitive to the normal growth-inhibiting factors in the body so that the final outcome depends on the balance between the factors and the extent of the changes in the initiated cells. This explains why preneoplastic, or even apparently fully transformed tumours, can be found but do not appear to be growing, and sometimes even regress. The whole sequence of events in the process *of* tumour formation is almost certainly a consequence of gene changes, although gene expression max be influenced by the host. Those gens have been localized to specific chromosomes abnormalities in tumours.[1]

VII.3. Molecular biology of cancer.

At the level of individual cells cancer is a genetic disease. The crucial events in tumorigenesis involve rearrangement of the genetic material, of the DNA molecule itself. Rapid progress in molecular biology and gene mapping has greatly advanced understanding of the significance of chromosome aberrations in cancer. It is known that they directly affect the functioning of two broad classes of genes: *cellular oncogenes* and tumor *suppressor genes* (antioncogenes). Cellular oncogenes generally promote cell growth and division, inhibit differentiation, or block apoptosis (programmed cell death). They transmit signals to the genome by means of multiple relentlessly, forming a tumor. Tumor suppressir genes, on the other hand, normally constrain cell growth and division. Their removal or inactivation from the genome also results in relentless cell multiplication.[1]

Finally, third, a very heterogeneous group of modulating genes can be recognized.They influence modifying the interaction between the neoplastic cells and the host organism, for examole, by altering immune responses or the neoplastic cells' resistance to immunological rejection or the tumor's ability

to grow invasively. Althought clearly important for the spread of cancer once it is established, the effects of modulating genes in carcinogenesis are only indirect; these genes go not themselves have transforming capacity.[8]

Tumor formation results, at least partly, from mutations of *proto-oncogenes* and tumor suppressor genes. Proto-oncogenes are genes whose protein products deliver signals leading to cell proliferation. Proto-oncogene products participate in all levels of the signaling pathways that fuel cell growth and can usually categorized into four types: growth factors, growth factor receptors, intracellular signal transducers, and transcription factors. Mutations in proto-oncogenes often result in a gain of function that manifests itself in the unceasing stimulation of cell growth. Typically, such mutated proto-oncogenes, now referred to as oncogenes, functionally dominate the wild-type allele at the molecular level. More than 50 proto-oncogenes have been described to date. Almost invariably, these genes become involved in cancer pathogenesis through somatic mutations that strike cells within target tissues. Only one example of mutant proto-oncogene (*ret*) inherited through the germ line currently exists. The most common and instructive oncogenetic alleles seen in human cancer: oncogene activation by pointmutation (H-ras, K-ras and N-ras, chromosomal translocation (myc, bcl-2, CYCD1, E2A-pbx1, and bcr-abl), and gene amplification (myc, N-myc, L-myc, neu, EGFR,CYCD1)[9]. Bcr-abl oncogene encoded by translocation between chromosomes 9 and 22 (the Philadelphia translocation) and frequently present in chronic myelogenous leukemia.[6] For some genes, such as retinoblastroma (Rb-1), p53, and adenomatous polyposis coli (APC) genes, much is know about the inherited and somatic mutations in the genes and the spectrum of human cancers in which mutations are most frequently found. For others, like the neurofibromatosia type 1 (NF-1), neurofibromatosia type 2 (NF-2), VHL, and P16/MTS1 genes, much less is know about the nature and prevalence of mutations in various tumor types[9].P53 is one of those multifunctional proteins for whichnumerus different tumor suppression mechanism are possible.[6]

VII.4. Basic steps in the metastatic cascade.

Malignant cells have a capacity to grow along tissue spaces, nerves, and vessels, and finally penetrate lymphatics, venules, and capillaries as well as the body cavities. Single or small clumps of tumor cells then break away from the original mass and are carried to distant organs, where they implant. This process of dissemination of malignant cells is called metastasis. The original tumor is called the primary tumor, and the process of metastasis establishes secondary tumors in distant organs where they incite the development of a stroma and develop into new tumors, which in turn invade and metastasize. The most important rule to remember about metastasis is that secondary tumors are almost always multiple and therefore not amenable to surgery or irradiation as curative procedures. Currently the only hope for prolonging useful life or obtaining cure for the person with metastasis is chemotherapy[5].From clinical, anatomic, and pathologic observations of metastasis, a picture of the steps involved in a metastatic cascade emerges. Numerous prerequisites and steps can be envisioned.[6]

Invasion and motility. Normal tissue requires proper adhesions with basement membrane and/or neighboring cells to signal to eatch other that proper tissue compartment size and homeostasis is being maintained. Tumor cells display diminished cellular adhesion, allowing them to become motile, a fundamental propertv of metasiatic cells. Tumor cells use their migratory and invasive properties in order to burrow lthrough surrounding extracellular stroma and to gain entry into blood vessels and lymphatics.[6]

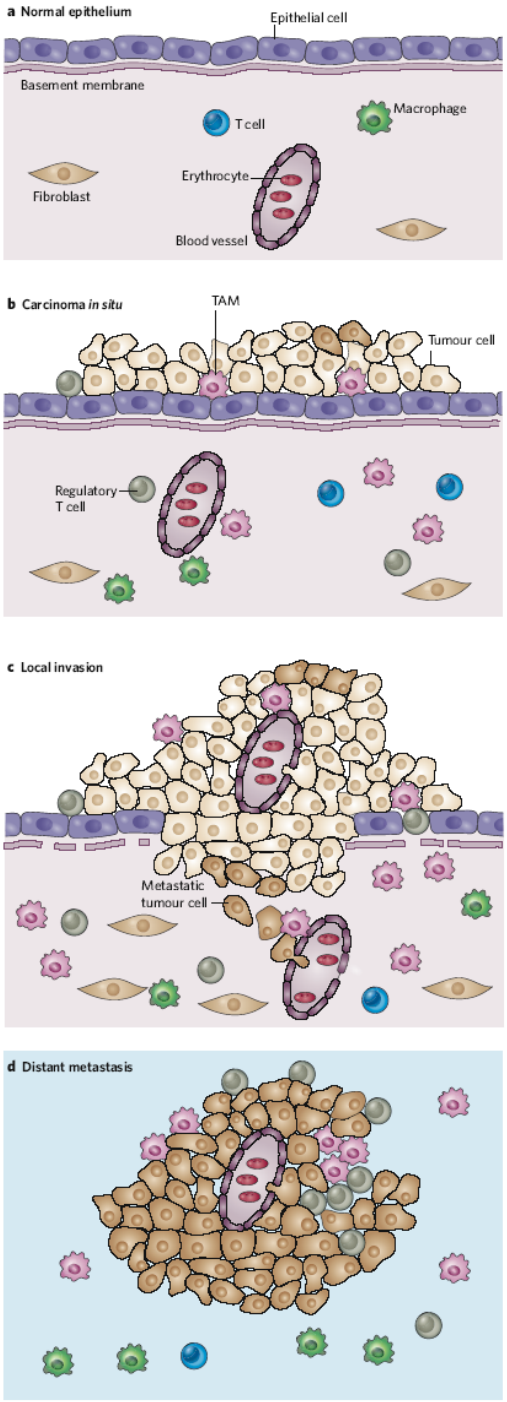

Figure VII.2. Inflammation and the malignant progression of epithelial tumours. a, Normal epithelium. b, Carcinoma *in situ*. The extrinsic (inflammatory) pathway and the intrinsic (oncogenic) pathway induce the production of chemokines and cytokines. These factors attract a tumour-promoting infiltrate (which contains, for example, TAMs and regulatory T cells, as shown here), and they also promote angiogenesis. The expression of chemokine receptors can be induced on initiated cells (that is, early tumour cells). These receptors then aid in tumour cell survival and might be necessary (but are not sufficient) for invasion across the basement membrane. Both autocrine and paracrine networks of cytokines and chemokines are involved in these processes. c, Local invasion. The chemokines and cytokines continue to attract and modulate a tumourpromoting infiltrate. They also promote angiogenesis and control tissue remodelling (for example, changes in the basement membrane), these factors induce the expression of genes associated with survival, invasion and migration in cells that have enough oncogenic changes to allow them to invade the basement membrane. The chemokines and cytokines are also involved in the intravasation of tumour cells into blood vessels and in lymphatic spread. d, Distant metastasis. chemokine- and cytokine-mediated signaling promotes the survival of malignant cells in distant organs, again attracting a tumour-promoting infiltrate and stimulating angiogenesis.[7]

Intravasation and survival in the circulation. Once tumor cells enter the circulation, or intravasate, they must be able to withstand the physical shear forces and the hostility of sentinel immune cells. Solid tumors are not accustomed to surviving as single cells without attachments and often interact with each other or blood elements to form intravascular tumor emboli.[6]

Arrrest and extravasation. Once arrested in the capillary system of distant organs, tumor cells must extravasate. or exit the circulation , into foreign parenchyma. This may happen by physical means whereby intravascular growth causes eventual.disruption of small capillaries, or escape may be more regulated via invasive properties that the tumor has acquired.[6]

Growlh in distant organs. Successful adaptation to the new microenvironment results in sustained growth. Of all the steps in the metastatic cascade, the

ability to grow in distant organs has the greatest clinical impact. However, accomplishing this may be rate-limiting. Clinically, manv patients treated by local excision of a primary cancer but with micrometastatic disease at the time of diagnosis will show a long latency period before distant disease develops. The ability of the tumor to adopt or to co-opt new growth signals mav determine whether distant relapse occurs rapidlv or dormancy ensues. How and if extravaseted tumor population grows in a distant organ lies at the core of the seed and soil hypothesis.[6]

VII.5. Description of selected cancers and cancer cell lines.

VII.5.1. Breast cancer.

Benign epithelial lesions with no significant tendency to malignant transformation include: adenoma (ductal, lactating, tubular), adenosis (apocrine, blunt duct, microglandular, sclerosing), fibroadenoma, radial scar/complex sclerosing lesions.[10]

Invasive breast carcinomas are divided into two major categories on the basis of their cytoarchitectural features: Invasive ductal carcinomalo and labular carcinoma.[10]

The recognized precursor lesions of invasive breast carcinoma are :intraductal proliferative lesions: (atypical ductal hyperplasia, ductal carcinoma in situ, florid, usual), lobular neoplasia/atypical lobular

The terminology Invasive ductal/lobular carcinoma does not imply an origin form ducts and lobules, respectively, but the presence of cytoarchitectural and phenotypical features of ductal-type and lobular-type, respectively. Ductal adenocarcinoma is the most common. Lobular carcinoma is the second malignant breast tumour. Medullary carcinoma is rare. Hyperplasia is a proliferation without criteria of malignancy.Fibroadenomas are benign breast tumours.[10]

The etiology is multifactorial. It involves diet, genetic and reproductive factors, and related hormone imbalances.[10]

The main factors of risk are: gender (women's risk for the development of invasive breast carcinoma is approximately 400 times that of men), age (breast cancer incidence increases rapidly with age), genetic factors.[10]

The most common histologic type of invasive breast carcinoma is designated as ductal, NOS (not otherwise specified). It comprises about 80% of all cases. It is a proliferation of epithelial cells from galactophoral ducts; it may be preceded and accompanied by an in situ component characterized by a proliferation of cells within the ducts without interuption of the basal membrane; when this membrane is altered, the carcinoma is invasive. It can be graded on the basis of the architecture (amount of tubule formations), nuclear atypia and mitotic activity.[10]

Many morphologic variants of invasive ductal carcinoma exist, some of them extremely rare. They include: tubular, cribriform, medullary, mucinous, neuroendocrine, papillary, micropapillary, apocrine, metaplastic, lipid-rich, secretory, oncocytic, adenoid cystic, acinic cell, glycogen-rich (clear cell), sebaceous, and inflammatory carcinoma. The prognosis of these subtypes varies, some of them having a better and some a worse outcome than invasive ductal carcinoma, NOS.[10]

Invasive lobular carcinoma is the second major type (5-10%) of breast cancer. Like its ductal counterpart, it may be preceded or accompanied by an in situ component. It is histologically more homogeneous than ductal carcinoma, but some morphologic variation exist, such as pleomorphic and signet ring cell.[10]

Medullary carcinoma, as a rare subtype of invasive ductal carcinoma (1%) with a better prognosis, it has a very distinctive form: sharply circumscribed, accompanied by a heavy lymphoid infiltrate, of high nuclear grade, with a syncytial pattern of growth, and lacking in situ or microglandular features. When one of these features is lacking, the tumor is referred to as Òatypical medullary carcinoma". A high frequency of medullary carcinoma has been reported in patients with BRCA1 germ line mutation. The different steps in the progression of breast cancer are not well individualized.[10] Hyperplasia is a proliferation of ductal or lobular epithelial cells, without criteria of malignancy; in contrast, atypical hyperplasia has incomplete malignant features and can be difficult to distinguish from in situ carcinoma.Fibroadenomas are the most common form of benign breast tumors.[10]

VII.5.2. Human breast cancer cell line MCF-7.

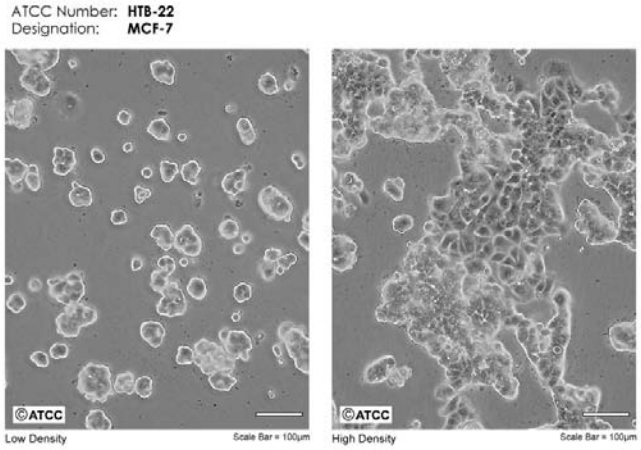

Figure VII.3. Human breast adenocarcinoma cells.[11,12]

Cell line: MCF-7

Cell type: Human breast adenocarcinoma

Orgin: established from the pleural effusion of a 69-year-old Caucasian woman with metastatic mammary carcinoma (after radio- and hormone therapy) in 1970; cells were described of being positive for cytoplasmic estrogen receptors and having the capability to form domes

Morphology: epithelial-like cells growing as monolayers.[11,12]

VII.5.3. Cancer of the lung.

The overwhelming majority of lung tumors are carcinomas. Most commonly, they arise from the pseudo-stratified epithelial lining of the bronchial airways but they can also arise from the epithelia of the smaller terminal airways and alveoli. Worldwide, lung cancer is the most common cause of

cancer-related death. Lung tumors are divided into two broad categories of: small cell carcinoma (SCLC 20-25% of cases) and non-small cell lung cancer (NSCLC 70-80% of cases) based on clinical behaviour and histological appearance. Other rarer tumour types include: carcinoids (typical or atypical), carcinosarcomas, pulmonary blastomas, giant and spindle cell carcinomas. Tumors are classified primarily on their cytological appearance. The relative frequency of subtypes varies in different regions and the figures cited therefore represent broad approximations. Clinically, the most important division is between SCLC and NSCLC. Small cell tumors metastasis very early in the course of the disease but are relatively responsive to chemotherapeutic drugs: they are therefore managed in a different way to non-small cell lesions. Lung cancers are generally heterogeneous, consisting frequently of cells of different histological subtypes. Pathological classifications therefore emphasise the major cell type present in the tissue analyzed and may note significant minor components. When components are roughly equal, designations such as adenosquamous carcinoma may be used. This common intra-tumor heterogeneity has led to the suggestion that lung carcinomas arise from a multipotent stem cell-like (or stem cell) component of the bronchial epithelium. Whilst microarray analyses have shown that gene expression can be used effectively to subdivide disease into existing or novel subtypes, it has also highlighted the similarity that lies between these subtypes at the level of gene expression. Such observations are consistent with a common stem cell progenitor.[13]

Lung tumors generally show complex karyotypic changes which involve multiple chromosomes. However, one of the most consistent alterations seen in both SCLC (approaching 100%) and NSCLC (approaching 90%) is a loss of coding potential from the short arm of chromosome 3. Loss of chromosome 3 sequence appears to occur frequently at the very earliest stages of neoplastic transformation, when epithelial cells may show no evidence of morphological alteration. The loss of p53 function, generally through mutation of the coding sequence is seen in the majority of lung carcinomas. Less dramatically, mutation of KRAS2 occurs in approximately 20% of NSCLC lesions and may indicate a poor prognosis when it is detected in small adenocarcinomas.[13]

Non-small cell lung cancer (NSCLC) is further divided histologically into three main disease subtypes of: squamous cell carcinoma, adenocarcinoma and large cell carcinoma[13].

However, many if not most tumors are composed of multiple histological types. Such variation in a presumably clonal lesion has led to the suggestion that lung cancers arise from a multi-potential stem cell component of the normal tissue. It is very likely that transcript profiling will lead to further subdivisions within these overall classes of disease, some which mirror preexisting pathological classes and some which are novel Whilst such classification regimes may be very important in understanding disease biology and may become critical in the future with respect to assessing lung cancer prognosis and directing subsequent therapeutic practice, such uses are perhaps currently secondary to the need for improved diagnostic and therapeutic agents[14].

Squamous cell carcinoma. Approximately 30% of lung tumours are classified as squamous cell carcinomas (SCC). Whilst this was the most common sub-type seen in the past, the incidence of SCC appears to be decreasing relative to adenocarcinoma, probably as a consequence of historical changes in the way that cigarettes are smoked (lower tar and filter tips promoting deeper inhalation).

SCC cells are large, flattened and stratified with a high cytoplasm to nucleus ratio. Key diagnostic features include the presence of intracytoplasmic keratin which may be linked to the presence of intercellular bridges and squamous pearl formation. Most SCC arise centrally within the main, lobar, segmental or subsegmental bronchi but some occur more peripherally. The tumour mass generally extends into the lumen of the airway with invasion into the underlying wall[15].

Adenocarcinoma: A further 30-50% of tumours are defined as adenocarcinomas (ADC). This tumour type is the most common in non-smokers and women and it is more frequently associated with pleural effusions and distant metastases. ADC may be further sub-classified into: acinar (gland forming), papillary, bronchioalveolar (BAC), solid with mucin and mixed. As most ADC are histologically heterogeneous, they generally fall into the mixed category. The tumours usually arise in the smaller peripheral airways (as distinct from the cartilage bearing bronchi) but they can be found more centrally. The key diagnostic features of ADC include gland formation - where the tumour cells are arranged around a central lumen - and/or mucin production. ADC is the tumour type most commonly found associated with fibrotic scars, which are thought to be caused in some way by the tumour. BAC, which represents 2-6% of total lung cancer is distinct from other sub-types both in terms of its growth pattern, which is lepidic (typically arising beyond the terminal bronchioloes, where it spreads along the alveolar septa causing minimal structural damage) and by the fact that it is non-invasive[15].

Large cell carcinoma. Approximately 10% of NSCLC are defined as large cell carcinomas (LCC). This is a diagnosis of exclusion. Where a poorly differentiated tumor has none of the defining features of SCLC, SCC or ADC it may be classified as LCC: that is, where the cells of the lesion are not-columnar in shape, do not contain mucous, do not show squamous differentiation, and do not have neuroendocrine properties or small cell characteristics. Tumors tend to consist of large cells with abundant cytoplasm, large nuclei and prominent nucleoli and they may occur peripherally or centrally. Variants of LCC include clear cell carcinoma, giant cell carcinoma and large cell neuroendocrine carcinoma (LCNEC)[15].

Pre-invasive lesions. The bronchial epithelium of the larger airways is a pseudo-stratified epidermal layer. The most frequent cell types present are ciliated columnar cells, interspersed mucous-producing goblet cells and, lying closely against the basement membrane, multi-potent basal epithelial cells. The basal (or reserve) cell has a repair capacity in that it is able to differentiate, as required, into the other mature cells of the larger conducting airways. In the smaller terminal and respiratory bronchioles, basal cells are not present. The reserve cells of these epithelia are the cuboidal, non-ciliated Clara cells. It has been suggested that the multi-potent basal cell or a stem cell precursor of such cells may represent a common lung cancer progenitor. Lung carcinomas represent the end-stage of the neoplastic transformation of a stem (or stem-cell like) cell that has been repeatedly exposed over many years to high levels of multiple carcinogens. It is therefore not surprising that the genetic and epigenetic lesions seen in lung cancer cells are complex. Correspondingly, frequent numerical and structural chromosomal alterations are reported in NSCLC. Whilst many changes are common, some perhaps occurring more often in one histological class over another, few if any have been shown to be exclusive to particular sub-types of disease or prognostic groupings. At the molecular level, highly

complex patterns of allelic imbalance (LOH) have been observed in primary tumours. Again, few if any of these have been strongly related to diagnosis or prognosis. No balanced chromosomal translocations have yet been associated characteristically with NSCLC[15].

VII.5.4. Human cancer cell line A-549 (non-small cell lung carcinoma).

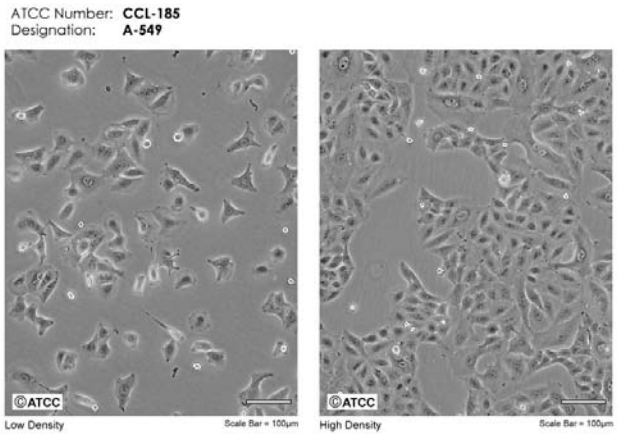

Figure VII.4. Human lung carcinoma cells.[16,17]

Cell line: A-549

Cell type: human lung carcinoma

Origin: established from an explanted lung tumor which was removed from a 58-year-old Caucasian man in 1972; cells were described to induce tumors in athmyic mice and to synthesize lecithin

Morphology: epithelial cells, growing adherently as monolayer.[16,17]

VII.5.5 Bladder cancer

Bladder cancer is two and one-half times more common in males than in females and more common in whites than in blacks. There are approximately 53,000 new cases per year, which is a 20% increase from 20 years ago. The incidence increases with age and peaks in the sixth, seventh, and eighth decades of life[6].

Transitional cell carcinomas (TCCs) constitute 90% to 95% of all the urothelial tumors diagnosed in North America and Europe. TCCs occur throughout the lining of urinary tract from the renal calyceal system to the proximal two thirds of the urethra, at which point squamous epithelium predominates. Approximately 90% of the urothelial cancers of the renal pelvis, ureter, and bladder are transitional cell cancers, all of which share similarities in epidemiology, pathology, biology, patterns of spread, molecular tumor markers, and treatment[6].

One of the risk factors involving genetic abnormalities include protooncogene expression, tumor suppressor gene mutation, and abnormalities of specific cell cycle regulatory proteins. Protooncogencs that have been implicated in bladder cancer include the Ras p21 proteins. The tumor suppressor genes that have been associated with an altered biology of the disease include p53, p21, p27 and retinoblastoma gene (Rb)[6].

More than 90% of the TCCs throughout the lining of the urinary tract occur in the urinary bladder, and of the remaining 10%, most are in the renal pelvis and fewer than 2% are in the ureter and urethra. Squamous cell carcinomas, defined bv the presence of keratinization, account for 5% of bladder tumors. Other even less-common bladder tumors include adenocarcinoma and undifferentiated carcinoma variants such as small cell carcinoma, giant cell carcinoma, and lymphoepitheliomas. Tumors of mixed origin are quite common and consist of TCC; within which squamous and adenocarcinomatous elements are also identified[6].

VII.5.6. Human bladder cancer cell line T24,

Figure VII.5. Human urinary bladder carcinoma.

Cell line: T-24
Cell type: human urinary bladder carcinoma
Origin: established from the primary tumor of an 81-year-old Caucasian woman with urinary bladder carcinoma (transitional cell carcinoma, grade III) in 1970; described to produce a variety of cytokines (e.g. G-CSF, IL-6 and SCF) and to carry a p53 mutation
Morphology: epitheloid adherent cells growing in monolayers

VII.5.7. Fibroblasts in cancer.

Genetic and cell-biology studies indicate that tumour growth is not just determined by malignant cancer cells themselves, but also by the tumour stroma. Tumour progression is clearly dependent on angiogenesis, and inflammatory cells also contribute to tumour growth. It is becoming increasingly clear that fibroblasts are also prominent modifiers of cancer progression. Evidence is increasing that a subpopulation of fibroblasts — the so-called cancer-associated fibroblasts (CAFs) — are important promoters of tumour growth and progression[20].
The important functions of fibroblasts include the deposition of extracellular matrix (ECM), regulation of epithelial differentiation**,** regulation of inflammation, and involvement in wound healing[20].
Fibroblasts are elongated cells with extended cell processes that show a fusiform or spindle-like shape in profile. Fibroblasts are widely distributed and easy to culture *in vitro*. They are often identified by their spindle-shaped morphology, their ability to adhere to plastic, and their lack of markers that indicate other cell lineages. Nevertheless, they remain poorly defined in molecular terms. The lack of a

reliable and specific molecular fibroblast marker is a limiting factor in studying fibroblasts *in vivo*. There are several well-established indicators of fibroblast phenotype, but none of them are both exclusive to fibroblasts and present in all fibroblasts (see table). Among all of the known markers, fibroblast specific protein 1 (FSP1) seems to provide the best specificity for detecting fibroblasts *in vivo*[20].

In the early growth of tumours, cancer cells form a neoplastic lesion that is embedded in the microenvironment of a given tissue (usually epithelium) but separated from the surrounding tissue and contained within the boundary of a basement membrane. This is called the carcinoma *in situ* (CIS). The basement membrane, immune cells, capillaries, fibroblasts and ECM surrounding the cancer cells constitute the tumour stroma. CIS is associated with a stroma similar to that observed during wound healing, and it is commonly referred to as 'reactive stroma'. The influence of such reactive stroma on cancer cells and *vice versa* in the setting of CIS is still debated, but there is evidence that they can communicate with each other through the basement-membrane[20].

Normal stroma in most organs contains a minimal number of fibroblasts in association with a physiological ECM. Reactive stroma is associated with an increased number of fibroblasts, enhanced capillary density, and type-I-collagen and fibrin deposition[20].

During cancer progression from CIS to invasive carcinoma the tumour cells invade the reactive stroma. **Figure** exemplifies tumour development in the setting of mammary ductal carcinomas. Although the ductal epithelium and the underlying myoepithelial cells are separated from the surrounding connective tissue by a basement membrane in both normal female breast and in ductal carcinoma *in situ* (DCIS), the basement membrane in DCIS, although intact, is altered. During invasive ductal carcinomas the basement membrane is degraded and the activated stroma (previously outside the basement-membrane zone), which contains myofibroblasts, inflammatory infiltrate and newly formed capillaries, comes into direct contact with the tumour cells[20].

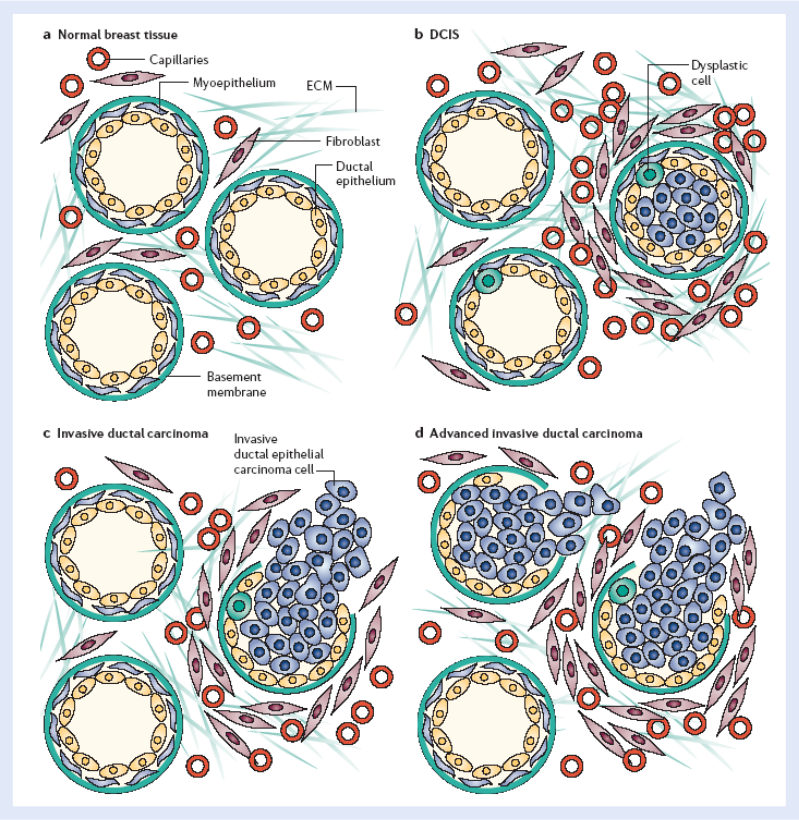

Figure. VII.6. Tumour stroma interactions during different stages of mammary ductal carcinoma progression. **A** In the normal female breast, the ductal epithelium and the underlying myoepithelial cells are separated by a basement membrane from the surrounding connective tissue by fibrillar extracellular matrix (ECM), capillaries and fibroblasts. **b** In ductal carcinoma in situ (DCIS), the lumen contains carcinoma cells owing to the proliferation of transformed epithelia. The wall of the duct is irregular in outline, the myoepithelial cell layer is indistinct and areas of altered yet intact basement membrane can be observed. The surrounding tissue is fibrotic and characterized by deposition of fibrillar ECM and fibroblast accumulation. **c** During invasive ductal carcinomas the basement membrane is ruptured and the tumour cells often form irregular duct-like areas without a defined basement membrane. The stroma surrounding the tumour cells contains myofibroblasts, inflammatory infiltrate and newly formed capillaries. **d** Advanced breast carcinoma. Irregular nests and cords of cancer cells invade the dense and fibrous stroma[20]

VII.5.8. Mouse L-929 cancer cell line (a fibroblast-like cell line cloned from strain L).

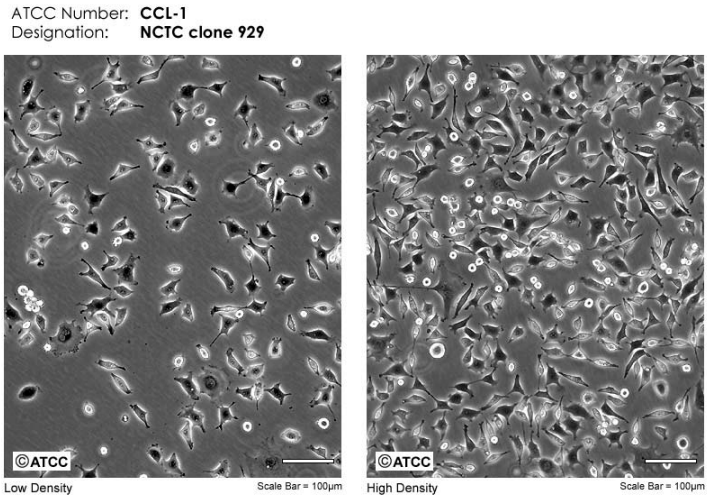

Figure VII.7. Mouse connective tissue fibroblast cells[22,23].

Cell line: L-929

Cell type: mouse connective tissue fibroblast

Origin: established from the normal subcutaneous areolar and adipose tissue of a male C3H/An mouse; used as target in TNF detection assays

Morphology: fibroblasts growing as monolayer[22,23].

VII.6. NSAIDs, metal complexes with NSAIDs and chemotherapy.

VII.6.1. NSAIDs for chemotherapy.

Cancer represents perhaps the defining medical challenge of our times. The search for pharmacological agents that can control cancer, either as chemotherapeutic or as chemopreventive agents is intense and to date has yielded significant results. Nevertheless, as the continuing morbidity and mortality form cancer indicate, there is a pressing need to identify new agents. Rational design of pharmacological agents includes, among others, modification of known agents in order to optimize their pharmacological properties, mainly their safety and efficacy.[23]

The genetic events associated with cellular progression from differentiated function to neoplastic transformation present opportunities for intervention in order to delay or reverse these processes. Drugs with demonstrated efficacy or potential efficacy to delay or reverse the carcinogenesis process at common epithelial sites target three key internal or external homeostatic processes that are associated with neoplastic transformation. Inflammation with associated enhanced cellular oxidative stress; over-or underexpression of intracellular signal transduction pathways that control cellular proliferation apoptotic events; and epigenctic modulation.[6]

Despite demonstrated success in translating preclinical data to reduction in cancer incidence at important epithelial targets (breast, colon, prostate), safty concerns have limited chemopreventive drug entry into clinical practice. Long-term administration of drugs to health populations imposes more

stringent safety thresholds than treatments of clinical conditions that cause symptomatic reduction of quality of lile. The risk-benefit ratio varies based on the long-term risk of developing a cancer.[6]

Nonsteroidal anti-inflammatory agents (NSAIDs) represent a class of drugs that reduce cellular inflammation through modulation of eicosanoid. Prostaglandins play crucial roles in controlling cellular proliferation, apoptosis, cellular invasiveness, angiogenesis, and in modulating immunosuppression. Since PGE_2 is the most abundant PG in tumors, reducing local concentrations of PGE_2 may be a pivotal colorectal cancer preventive maneuver. PGHS-independent mechanism of NSAIDs action may, at leats in part explain NSAID preventive efficacy. NSAIDs inhibit nuclear factor (NF)-$_k$B at pharmacologic concentrations and key cellular proliferation signaling intermediates, The impact of NSAIDs on carcinogenesis events driven by these upstream pathways remains unclear.[6]

An inverse relationship with NSAIDs use is seen consistently esophageal squamous, esophageal adenocarcinoma, and gastric adenocarcinoma. Somee reduction in breast cancer risk among women who use NSAIDs have been found, although two large prospective studies have not found an inverse asscciation between NSAID use and breast cancer incidence or mortality. Several of the cohort studies of NSAIDs use in relation to bladder and kidney cancer suggest that NSAIDs use may be associated with a small increase in risk of cancer. The relationship between NSAIDs use and cancer of the pancreas, lung, bladder and prostate is inconsistent.[6]

NSAIDs, including aspirin, indomethacin, piroxicam, sulindac, ibuprofen and ketoprofen, suppres colonic tumorigenesisinduced chemically or trangenically. The selective COX-2 inhibitors were the most efficacious colon tumorigenesis inhibitors in both chemical and transgenic rodent models.

NSAIDs effect the onsetand progression of cancers at a variety of other sites, although the evidence is more limited than the data for colon cancers. NSAID inhibit chemical carcinogenesis models for stomach, skin, breast, lung, prostate and urinary bladder. Sulindac and the selective COX-2 inhhibitor celecoxib are in clinical trials for the prevention of colorectal cancer.[6]

Aspirin suppresses adenoma recurrence in patients previously treated for adenomas or for cancer. Nither sulindac or piroxicam su8ppressed adenoma formation in high-risk sporadic populations at tolerable doses. Selective COX-2 inhibitors (celecoxib, rofecoxib)reduce the reccurrence of adenomas.[6]

NSAIDs may have unacceptable toxicity profiles for daily prescription to otherwise healthy populations. In addition to the anti-tumor activity of NSAIDs as single agents, there is interest in the effects of a combined therapy of chemotherapy with NSAIDs. Mixed COX inhibitors (piroxicam, indomethacin, aspirin) have sufficient gastrointensial toxicity to reduce their acceptability as chronic cancer preventive interventions.[6]

VII.6.2. Metal complexes of NSAIDs and antiproliferative activity in vitro.

Although metal complexes have been used as therapeutic agents since early history, organic drugs have dominated pharmacology since its beginnings in the 19th century. However, the comeback of ‘forgotten’ inorganic drugs was triggered in the 1960s by the development and success of the anticancer agent cisplatin {cis-[$PtCl_2(NH_3)_2$]}. Since then, medicinal inorganic chemistry has become a

rapidly growing field of research with numerous applications in many branches of medicine. In the treatment of cancer three platinum compounds, viz. cisplatin, carboplatin, and oxaliplatin, have achieved worldwide approval to date (Fig. 1) . Today, cisplatin is used in one of two cancer patients (usually in combination with other drugs), and has a cure rate for testicular cancer of over 90%, showing high activity against ovarian, cervical, head and neck, and bladder carcinoma. Carboplatin shows a reduced toxicological profile (in particular lacking nephrotoxic properties in usual doses) compared to cisplatin, yet has a similar spectrum of activity. Oxaliplatin is active against metastatic colorectal cancer. Beside the successful implementation of platinum compounds, nephro- and neurotoxicity during administration and acquired drug resistance are serious problems of platinum-based drugs. Therefore, with the aim of reducing toxic side effects, and improving their pharmacological pro- file and therapeutic efficacy, a series of non-platinum-based anticancer drugs is in current development.[24]

A wide range of metal complexes are already in clinical use and encourage further studies for new metallodrugs, such as metal-mediated antibiotics, antibacterial, antiviral, antiparasitic, radiosensitizing agents, and anticancer compounds. Mechanisms of action are often still unknown, but recently, more than a thousand potential anticancer metal compounds, from the National Cancer Institute (NCI) tumorscreening database, were analyzed based on putative mechanisms of action, and classified into four broad classes according to their preference for binding to sulfhydryl groups, chelation, generation of reactive oxygen species, and production of lipophilic ions. Increasing knowledge of the biological activities of simple metal complexes may guide researchers to the development of promising chemotherapeutic compounds to target specific physiological or pathological processes. Many potential antitumoral agents have been investigated based on their anti-angiogenesis or pro-apoptotic behavior.[25]

It has been found that mefenamic acid induces apoptosis in human liver cancer cell-lines through caspase-3 pathway. Cytotoxic activities of mefenamic acid and its Mn(II), Co(II), Ni(II), Cu(II) and Zn(II) complexes have been evaluated for antiproliferative activity in vitro against the cells of three human cancer cell lines: MCF-7 (human breast cancer cell line), T24 (bladder cancer cell line), A-549 (non-small cell lung carcinoma) and a mouse L-929 (a fibroblast-like cell line cloned from strain L). The IC50 value for for the complex $[Cu(mef)_2(H_2O)]_2$ against the T24 cell line is 7.77×10^{-6} M. The IC_{50} values shown by $[Cu(mef)_2(H_2O)]_2$ against MCF-7 and L-929 cancer cell lines are in a μM range similar to *cis-platin* 2.8 times and 8.0 times less cytotoxic against L-929 and MCF-7 cancer cell lines respectively. These results indicate that coupling of mefenamic acid to Cu(II) metal center result in ametallic complex with important biological properties. The cytotoxic activity shown by $[Cu(mef)_2(H_2O)]_2$ against T24, MCF-7 and L-929 cancer cell lines indicates that coupling of mefenamic acid to Cu(II) metal center result in metallic complexes with important biological properties since it displays IC_{50} values in a M range similar or better to that of the antitumor drug *cis-platin.*[26]

Recently Cini et all. submitted copper(II)–''oxicam'' showed the cytotoxic activity in vitro by copper complex of piroxicam $[Cu(HPIR)_2(DMF)_2]$, was tested for anti-proliferating activity against a series of 56 different human tumor cell lines. Metal complex Has GI_{50} values for many of these cells are 20 μM,

significantly smaller than those found for carboplatin that was selected as reference in this study. The activity opf complex is larger against ovarian cancer cells, non-small lung cancer cells, melanoma cancer cells, and central nervous system cancer cells[99]. Potential anticancer cytostatic and cytotoxic effects of piroxicam complexes with Mn^{2+} on human promyelocytic leukemia HL-60 cells have been investigated. Cellular proliferation was found to be inhibited in the case $Mn(pir)_2(H_2O)_2$ in a time-dependent manner. $Mn(pir)_2(H_2O)_2$ enhanced the density of cells undergoing necrosis, especially after 48 h incubation with the complex.

References

1. Franks, L.M., Teich, N.M., *Introduction to the cellular and molecular biology of cancer* 1-2, 4-6, 205 (1997)
2. Veach,T., Nicholas, D., Barton, M. CANCER AND THE FAMILY LIFE CYCLE: A Practitioner's Guide (2002), 2
3. Alberts, B., Johnson, A. Lewis, J., Raff, M., Roberts, K., Walter, P. *Molecular biology of the cell* Fourth edition (2002)
4. Coussens, L.M., Werb, Z., *Nature* **420,** 19 - 26 (2002).
5. McKinnell, R.G, Parchment, R.E., Perantoni, A.O., Pierce, G.B. *The biological basis of cancer* 27, (1998).
6. DeVita, V.T., Lawrence, T.S., Rosenberg, S.A.*Cancer rinciples and practice of oncology* Volume 1, 8th edition, 626-630, 1358-1359 (2008).
7. Mantovani, A., Allavena, P., Sica, A., Balkwill, F., Nature **454,** (2008).
8. Heim, S., Mitelman, F. *Cancer cytogenetics* 266 (1989).
9. Bishop, J.M., Weinberg, R.A. (editors) *Scientific American molecular oncology* 111, 147, 157 (1996).
10. http://atlasgeneticsoncology.org/Tumors/breastID5018.html
11. http://www.lgcpromochematcc.com/common/catalog/numSearch/numResults.cfm?atccNum=HTB-22
12. http://www.dsmz.de/human_and_animal_cell_lines/info.php?dsmz_nr=115&from=cell_line_index&select=M&term=&preselect=human;hamster;mouse;rat;insect;other&firstload=0
13. http://AtlasGeneticsOncology.org/Genes/LungTumOverviewID5030.html
14. Heighway, J., Knapp, T., Boyce, L., Brennand, S., Field, J.K., Betticher, D.C., Ratschiller, D., Gugger, M., Donovan, M., Lasek, A., Rickert, P. *Oncogene* **21,** 7749 – 7763 (2002).
15. http://AtlasGeneticsOncology.org/Genes/LungNonSmallCellID5141.html
16. http://www.dsmz.de/human_and_animal_cell_lines/info.php?dsmz_nr=107&from=cell_line_index&select=A&term=&preselect=human;hamster;mouse;rat;insect;other&firstload=0
17. http://www.lgcpromochematcc.com/common/catalog/numSearch/numResults.cfm?atccNum=CCL-185
18. http://www.lgcpromochematcc.com/common/catalog/numSearch/numResults.cfm?atccNum=HTB-4
19. http://www.dsmz.de/human_and_animal_cell_lines/info.php?dsmz_nr=376&from=cell_line_index&select=T&term=&preselect=human;hamster;mouse;rat;insect;other&firstload=0
20. Kalluri, R., Zeisberg, M. *Nature* **6,** 392 (2006).
21. http://www.lgcpromochematcc.com/common/catalog/numSearch/numResults.cfm?atccNum=CCL-1
22. http://www.dsmz.de/human_and_animal_cell_lines/info.php?dsmz_nr=2&from=cell_line_index&select=L&term=&preselect=human;hamster;mouse;rat;insect;other&firstload=0
23. Rigas, B., Williams, J.L. *Nitric Oxide* **19,** 199–204 (2008).
24. Reisner, E., Arion, W.B., Keppler, B.K. *Inorganica Chimica Acta* **361,** 1569–1583 (2008).
25. Vinod M., Keshavayya, J., Vaidya, W.P., Khan, M.H., *Journal of Coordination Chemistry* **61,** 2629–2638 (2008).
26. Kovala-Demertzi, D., Hadjipavlou-Litina, D., Staninska, M., Primikiri, A., Kotoglou, Demertzis, M.A. *Journal of Enzyme Inhibition and Medicinal Chemistry*, **24,** 742-752 (2009).

Aim of study

Chemistry

Complexes of drugs with most of d-block metals have been synthesized and reported. The synthesis, crystal structure and spectroscopic properties of coordination complexes is an extremely important area in both inorganic and organometallic chemistry. A variety of coordination arrangements and chemical reactivity of metal complexes with drugs is interesting even from a basic coordination chemistry stand-point. These facts reinforced the will to synthesize and characterize other new copper(II), manganese(II), zinc(II), cadmium(II) NSAIDs (meclofenamic acid, flufenamic acid, lornoxicam) and cephalosporins (cefaclor) complexes.

- For the reasons of this PhD thesis, we have undertaken to study **three NSAIDs drugs**: two members of the fenamates family meclofenamic acid (N-(2,6-dichloro-3-methylphenyl) anthranilic acid), flufenamic acid (N-[3-(trifluoromethyl)-phenyl]-anthranilic acid), one member of the oxicams family lornoxicam (6-chloro-4-hydroxy-2-methyl- 2-pyridyl-2*H*-thieno[2,3-*e*]-1,2-thiazine-3- amide-1,1-dioxide) and **one cephalosporin**, from the β-lactam antibiotics, cefaclor [7-(D-2-amino-2-phenylacetamido)-3-chloro-3-cepham-4-carboxylic acid].
- Furthermore, we have chosen four transitions metals: Mn(II), Cu(II), Zn(II), bioessential elements, present in the body and Cd(II), coordination architecture.
- As part of our investigation, the simple synthesis of Mn(II), Cu(II), Zn(II), Cd(II) complexes with meclofenamic acid, flufenamic acid, lornoxixam and cefaclor.
- We attempt to isolate crystals, from prepared metal complexes, suitable for X-ray diffraction analysis.
- Characterization of the compounds accomplished by means of elemental analysis, XRF and spectroscopic techniques ^{1}H-NMR, ^{13}C-NMR, 2D ^{1}H–^{1}H COSY, ^{1}H–^{13}C HSQC, ^{1}H–^{13}C HMBC NMR, DEPT-135, IR, UV-vis and mass spectroscopy (ESI-MS, APCI-MS).

Biological studies

The study of the interactions between drugs and transition metals is an important and active research area in bioinorganic chemistry. Many drugs possess modified pharmacological and toxicological potentials when administered in the form of metallic compounds. The widely studied metallic ions in this respect are manganese(II), copper (II), and zinc (II) because they form low molecular weight complexes which are proved to be more beneficial against several diseases. Experimental evidences collected during decades of research work by several teams all over the world proved that the coordination of bioessential metal ions by NSAIDs and cephalosporines improves the pharmaceutical activity of the drugs themselves and reduce their undesired toxicity effects in human and veterinary medicine. The new compounds deserve subsequent experimental work aimed to determine cytotoxic activity against tumor cell lines *in vitro* and biological activity like oxygen radical scavenger activity. These facts reinforced the will to

determind cytotoxic activity by series new copper(II), manganese(II) zinc(II), cadmium(II) of meclofenamic acid, flufenamic acid, lornoxicam and cefaclor complexes against selected human tumor cell lines and mouse fibroblast-like cell line. The application of superoxide dismutase as a pharmaceutical has attracted considerable attention. However, SODs have molecular weights too high to cross cell membranes and can only provide extracellular protection. In order to overcome many of these limitations, a stable non-toxic, low-molecular-weight metal complex that catalyses the dismutation of superoxide anion might be a suitable alternative to superoxide dismutase in clinical applications with the desirable qualities of low cost, cell permeability and non-immunogenicity.

The aim of this research was to extend the pharmacological profile of selected drugs, in order to search for new properties such as antioxidant and anticancer activity, to prepare new compounds, complexes of meclofenamic acid, flufenamic acid, lornoxixam and cefaclor with essential metal ions, which probably would exhibit improved or different biological properties compared to parent drugs. The complexes of manganese , copper and zinc may lead to the development of **an antitumor drug**. Moreover copper complexes may lead to the development of **SOD mimics.**

- Part of this project including studies aimed to test **anti-proliferative activity *in vitro*** of Mn(II), Cu(II), Zn(II), Cd(II) complexes with meclofenamic acid, flufenamic acid, lornoxixam and cefaclor against the cells of three human cancer cell lines, MCF-7 (breast cancer cell line), T24 (bladder cancer cell line), and A-549 (non-small-cell lung carcinoma), and a mouse fibroblast L-929 cell line.
- We wish to find new compounds with IC_{50} values (for tested cancer cell lines) smaller than those of well known cisplatin that is selected as references in this study.
- The superoxide dismutase activity is measured, and IC_{50} value is determined by the Fridovich test. According to the usual criteria we wish to find new complexes with **SOD (superoxide dismutase) activity**, considered as potent **SODmimics**.

Results and discussion

VIII Synthesis and characterization of manganese(II), copper(II), zinc(II) and cadmium(II) complexes with (N-(2,6-dichloro-3-methylphenyl) anthranilic acid), meclofenamic acid (1).

VIII.1. General

Meclofenamic acid (Hmcfa) **1** was synthesized according to a published procedure, condensation with (2-carboxyphenyl)phenyliodonium, inert salt.[1]

The synthesis of first and second row-block-d divalent metal ion complexes with ''fenamates'' family anti-inflammatory drugs were previously reported.[2,3] The reactions of manganese(II)-, copper(II)-, zinc(II)-, cadmium(II)-acetates and/or cadmium(II)-chloride with the anti-inflammatory drug meclofenamic acid, (Hmcfa), (N-(2,6-dichloro-3-methylphenyl) anthranilic acid) in methanol produced micro-crystalline solids powder-like solids, **table VIII.1** (metal to ligand molar ratio 1:2), (**table VIII.2**) (metal to ligand molar ratio 1:1). Further recrystallization from dimethylsulfoxide (dmso) solution of complex **3** gave crystals of $[Cu_4(MCFA)_6(OH)_2(DMSO)_2]$.2DMSO (**3a**).The X-ray diffraction analyses showed that **3a** is tetranuclear molecule.

Table VIII.1. Analytical and physical data of the meclofenamic acid complexes.

	Compounds	M.W g/mol	mp (˚C)	Colour	C%	H%	M%
1	Hmcfa	296.15	256-257°C	off white			
2	$[Mn(MCFA)_2]$	645.187	250°C	off white	52.13 (52.29)	3.12 (3.12)	8.52 (10.3 ±1.4)
3	$[Cu(MCFA)_2(H_2O)]$	671.803	191°C (dec)	green	50.06 (50.31)	3.30 (3.22)	9.46 (7.11 ±1.7)
4	$[Zn(MCFA)_2(H_2O)_4]$	727.661	141-142°C	off white	46.22 (46.28)	3.87 (3.44)	8.98 (9.8±1.6)
5	$[Cd(MCFA)_2(H_2O)_2]$	738.675	190-192°C	off white	45.53 (45.64)	3.27 (3.33)	15.22 (17.4 ±2.1)

Results of elemental analysis: calculated, (found).

Table VIII.2. Analytical and physical data of the meclofenamic acid complexes.

	Complexes	M.W g/mol	mp (˚C)	Colour	C%	H%	M%
6	$[Mn(AcO)(MCFA)]^a$	409.094	>300°C (dec)	brown			13.43 (14.4±1.2)
7	$[Cu(AcO)(MCFA)]^a$	417.702	>300°C (dec)	green			15.21 (16.9 ±2.1)
8	$[Zn(AcO)(MCFA)(H_2O)_4]^a$	419.536	250°C	off white	39.09 (39.23)	4.30 (3.39)	13.13 (12.0 ±1.5)
9	$[Cd(AcO)(MCFA)(H_2O)_4]^a$	538.588	>300°C (dec)	off white	35.68 (34.60)	3.93 (3.11)	20.87 (20.6 ±2.9)

Results of elemental analysis: calculated, (found).

[a] Ac = CH_3CO

The complexes $[Mn(MCFA)_2]$ **2**, $[Cu(MCFA)_2(H_2O)]$ **3**, $[Zn(MCFA)_2(H_2O)_4]$ **4**, $[Cd(MCFA)_2(H_2O)_2]$ **5**, were synthesized according to the reactions (a) – (d). The complexes [Mn(AcO)(MCFA)] **6**, [Cu(AcO)(MCFA)] **7**, $[Zn(AcO)(MCFA)(H_2O)_4]$ **8**, $[Cd(AcO)(MCFA)(H_2O)_4]$ **9**, were synthesized according to the reactions (e) – (h). All complexes are stable in the air. All the complexes are insoluble in water, except of **5** and **9** which is slight soluble in water. All the complexes are soluble in polar solvents as DMFand DMSO, except of **8** and are slightly soluble in nonpolar solvents as $CHCl_3$, CH_2Cl_2.

$Mn(AcO)_2 + 2\ Hmcfa \rightarrow [Mn(mcfa)_2] + 2\ AcOH$ (a)

$Cu(AcO)_2 \cdot H_2O + 2\ Hmcfa \rightarrow [Cu(mcfa)_2(H_2O)] + 2\ AcOH$ (b)

$Zn(AcO)_2 \cdot 2\ H_2O + 2\ Hmcfa \rightarrow [Zn(mcfa)_2(H_2O)_4] + 2\ AcOH$ (c)

$Cd(AcO)_2 \cdot 2\ H_2O + 2\ Hmcfa \rightarrow [Cd(mcfa)_2(H_2O)_2] + 2\ AcOH$ (d)

$Mn(AcO)_2 + Hmcfa \rightarrow [Mn(AcO)(mcfa)] + AcOH$ (e)

$Cu(AcO)_2 \cdot H_2O + Hmcfa \rightarrow [Cu(AcO)(mcfa)] + AcOH + H_2O$ (f)

$Zn(AcO)_2 \cdot 2\ H_2O + Hmcfa \rightarrow [Zn(AcO)(mcfa)(H_2O)_4] + AcOH$ (g)

$Cd(AcO)_2 \cdot 2\ H_2O + Hmcfa \rightarrow [Cd(AcO)(mcfa)(H_2O)_4] + AcOH$ (h)

Table VIII.3. Solubility test of **2** – **9** complexes and parent drug **1**.

	H_2O	n-pentane	n-hexane	Et_2O	CH_3NO_2	CH_3CN	cyclohexae	methanol	ethanol	acetone	toluene	benzene	THF	DMF	DMSO	CH_2Cl_2	$CHCl_3$
1	-	-	-	-	+/-	+/-	-	+	+	+/-	+/-	+/-	+/-	+	+/-	+/-	+/-
2	-	+/-	+/-	+/-	+/-	+/-	+/-	+	+/-	+	+	+	+	+	+	+	+
3	-	+/-	+/-	+/-	+	+	+/-	+	+	+/-	+	+	+	+	+	+/-	+/-
4	-	-	-	-	-	-	-	-	-	-	-	-	-/+	+	+	+/-	+/-
5	+/-	-	-	-	-	-	-	-	-	-	-	-	+/-	+	+	+/-	+/-
6	-	+/-	+/-	+/-	+/-	+/-	+/-	+/-	+/-	+/-	+/-	+/-	+	+	+	+/-	+/-
7	-	-	-	-	+/-	+/-	-	+	+/-	+/-	+/-	+/-	+/-	+	+	+/-	+/-
8	-	-	-	-	-	-	-	-	-	-	-	-	-	+/-	+	+/-	+/-
9	+/-	-	-	-	-	-	-	-	-	-	-	-	+/-	+	+	+/-	+/-

+ soluble; +/- slightly soluble; - insoluble.

VIII.2. X-Ray crystallography

VIII.2.1. X-Ray structure of $[Cu_4(MCFA)_6(OH)_2(DMSO)_2].2DMSO$ (3a).

Table VIII.4.1. Selected bond lengths [Å] and angles [º] for $[Cu_4(MCFA)_6(OH)_2(DMSO)_2].2DMSO$.

Vector	Length	Vector	Angle
Cu(1)-O(52)#1	1.929(3)	O(52)#1-Cu(1)-O(11)	86.28(13)
Cu(1)-O(11)	1.934(3)	O(52)#1-Cu(1)-O(1)#1	92.58(12)
Cu(1)-O(1)#1	1.959(3)	O(11)-Cu(1)-O(1)#1	175.78(12)
Cu(1)-O(1)	1.960(3)	O(52)#1-Cu(1)-O(1)	167.60(12)
Cu(1)-O(10)	2.266(3)	O(11)-Cu(1)-O(1)	95.92(12)
Cu(1)-Cu(1)#1	2.9045(10)	O(1)#1-Cu(1)-O(1)	84.34(12)
Cu(1)-Cu(2)	3.0987(7)	O(52)#1-Cu(1)-O(10)	113.24(11)
Cu(1)-Cu(2)#1	3.3278(7)	O(11)-Cu(1)-O(10)	92.94(11)
Cu(2)-O(31)	1.936(3)	O(1)#1-Cu(1)-O(10)	91.24(11)
Cu(2)-O(1)	1.944(3)	O(1)-Cu(1)-O(10)	78.90(11)
Cu(2)-O(51)	1.990(3)	O(31)-Cu(2)-O(1)	176.11(12)
Cu(2)-O(12)	1.991(3)	O(31)-Cu(2)-O(51)	87.74(12)
Cu(2)-O(10)	2.277(3)	O(1)-Cu(2)-O(51)	93.18(12)
Cu(2)-O(32)	2.684(3)	O(31)-Cu(2)-O(12)	87.79(12)
O(1)-Cu(1)#1	1.959(3)	O(1)-Cu(2)-O(12)	92.38(12)
O(51)-C(50)	1.252(5)	O(51)-Cu(2)-O(12)	163.07(12)
O(52)-C(50)	1.280(5)	O(31)-Cu(2)-O(10)	97.18(11)
O(11)-C(10)	1.271(5)	O(1)-Cu(2)-O(10)	78.94(11)
O(12)-C(10)	1.261(5)	O(51)-Cu(2)-O(10)	106.36(11)
		O(12)-Cu(2)-O(10)	90.40(11)
		O(31)-Cu(2)-O(32)	54.43(11)
		O(1)-Cu(2)-O(32)	129.45(11)
		O(51)-Cu(2)-O(32)	75.50(11)
		O(12)-Cu(2)-O(32)	88.64(11)
		O(10)-Cu(2)-O(32)	151.61(10)
		Cu(2)-O(1)-Cu(1)#1	117.00(14)
		Cu(1)#1-O(1)-H(1)	109.6
		Cu(1)-O(1)-H(1)	110.1
		Cu(1)-O(10)-Cu(2)	86.02(10)

Table VIII.4.2 Selected hydrogen bonds for $[Cu_4(MCFA)_6(OH)_2(DMSO)_2].2DMSO$.

Atoms D,H,A	Dist. D, H [A]	Dist. H, A [A]	Dist. D,A [A]	Angle D,H,A [º]
O1—H1—O20^{I}	0.7400	1.9000	2.640(4)	176.900
N17—H17A—O12	0.9300	2.0500	2.669(5)	123.300
N37—H37A—O32	0.9400	1.8000	2.606(5)	142.800
N57—H57A—O52	0.9200	1.9300	2.698(5)	139.500

The molecular structure of complex $[Cu_4(MCFA)_6(OH)_2(DMSO)_2].2DMSO$ (**3a)** is depicted in **figure VIII.1.1** Selected interatomic distances and angles for compound are listed in **table VIII.4.1** Selected hydrogen bonds are given in **table VIII.4.2** Complex **3a** crystallizes in the monoclinic space group P 21/n.The tetranuclear molecule is held together by six ligands and two DMSO groups. Meclofenamic acid acts as a deprotonated bidentate ligand and it is coordinated to the metal ions through the oxyxens of the carboxyl group. The new core consists of two, 5-coordinate Cu^{II} atoms Cu(1) and two, 6-coordinate Cu^{II} atoms Cu(2). The structure of the complex consists of two centrosymmetrically related Cu(1) ions bridged by the oxygen O(1) atoms which present μ^3 coordination mode. A chelating two oxygen atoms O(52) and O(11) that belong to the two different meclofenamate anions as ligands and dmso molecule complete five-coordination around each Cu(1) atom. The ambidentate dmso ligand co-ordinates the metal Cu(1) through the oxygen atom O(10).The O(10)–S(1) bond distance is 1.518(3) Å, whereas the O(10)–S(1)–C(1) and O(10)–S(1)–C(2) bond angles 104.4(2) and 107.7(2) respectively.The coordination geometry about each metal ion Cu(1) is well described as square pyramidal with dmso oxygen O(10) atom occupying the apical positions for the two Cu(1) centres. Cu(2) atoms are bridged by oxygen atoms originating from the DMSO in the μ coordination mode. In addition to the one μ-oxygen atoms O(10) of DMSO ligand, each Cu(2) center is coordinated to two oxygen atoms belonging to two different MCFA ligands and to two oxygen atoms belonging to the same MCFA ligand. The coordination polyhedron can be described as a distorted octahedron and two apical positions are occupied by two oxygen atoms [Cu(2)–O(10) 2.277(3) Å, Cu(2)–O(32) 2.684(3) Å] of dmso O(10) and meclofenamate anion as ligand O32. Bond distance of Cu(2)–O(10), Cu(2)–O(32) involving the oxygens of the same corboxylate group differ by 0.407 Å, while bond distance Cu(1)–O(52), Cu(2)–O(51) and Cu(1)–O(11), Cu(2)–O(12) involving the oxygens of the same corboxylate group coordinated to different metal cente differ by only 0.061 Å, 0.057 Å.The carboxylate group has a difference of 0.045 Å, 0.028 Å and 0.010 Å between its [C(30)–O(31) 1.289(5) Å, C(30)–O(32) 1.244(5) Å], [C(50)–O(52) 1.280(5) Å, C(50)–O(51) 1.252(5) Å] and [C(10)–O(11) 1.271(5) Å, C(10)–O(12) 1.261(5) Å bonds.

Two oxygen atoms that belong to the same meclofenamic acid ligand are bidentaly coordinated to two different metal centers Cu(1) and Cu(2) give rise to remarkable six-membered Cu(1) – O(1) – Cu(2) – $O(51)_{carboxylate}$ – C(50) – O(52) chelating ring or Cu(1) – O(1) – Cu(2) – $O(12)_{carboxylate}$ – C(10) – $O(11)_{carboxylate}$ chelating ring.

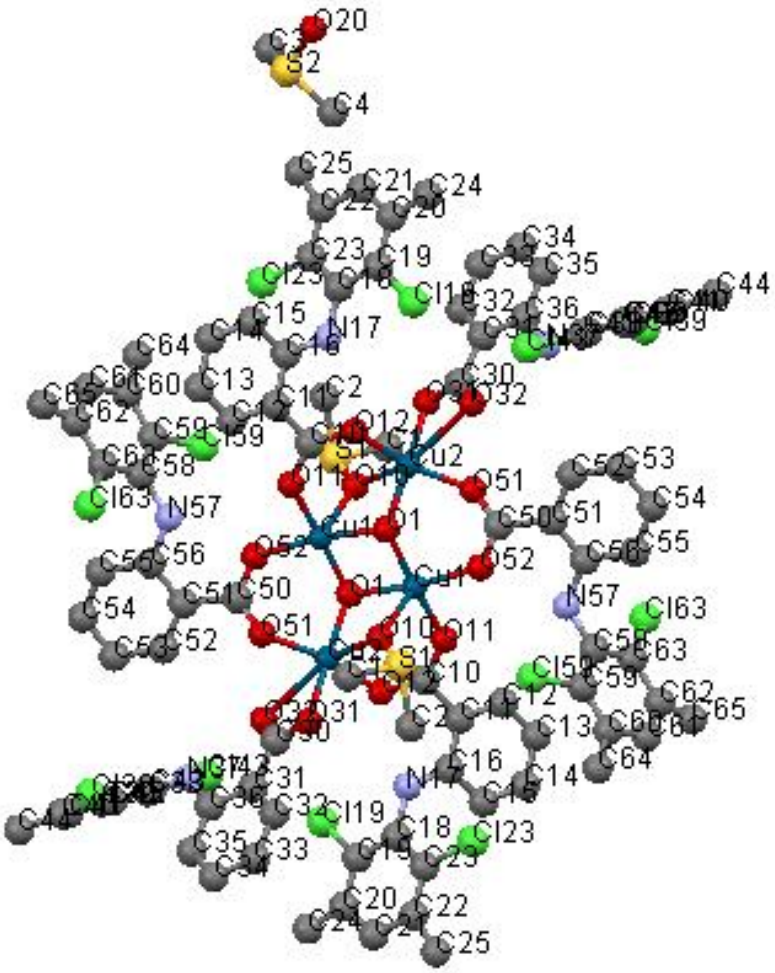

Figure VIII.1.1. The crystal structure of $[Cu_4(MCFA)_6(OH)_2(DMSO)_2].2DMSO$ (**3a)**.

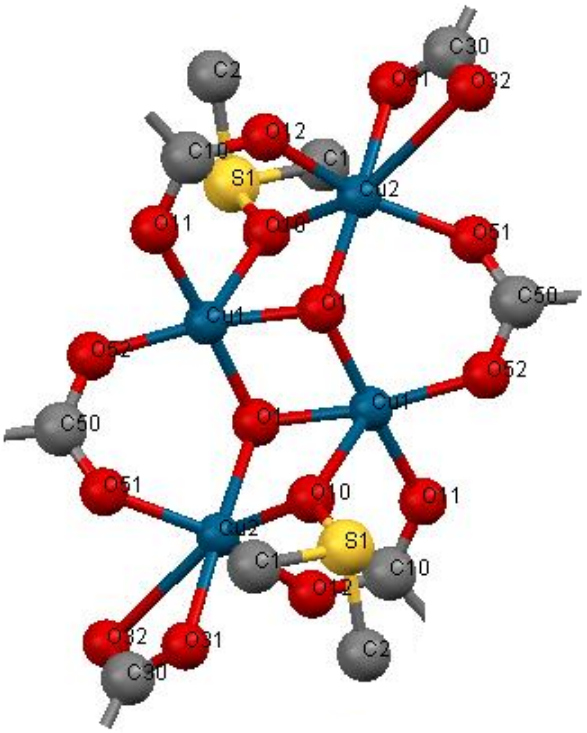

Figure VIII.1.2 The core of the complex molecule for$[Cu_4(MCFA)_6(OH)_2(DMSO)_2]$.2DMSO (**3a)**.

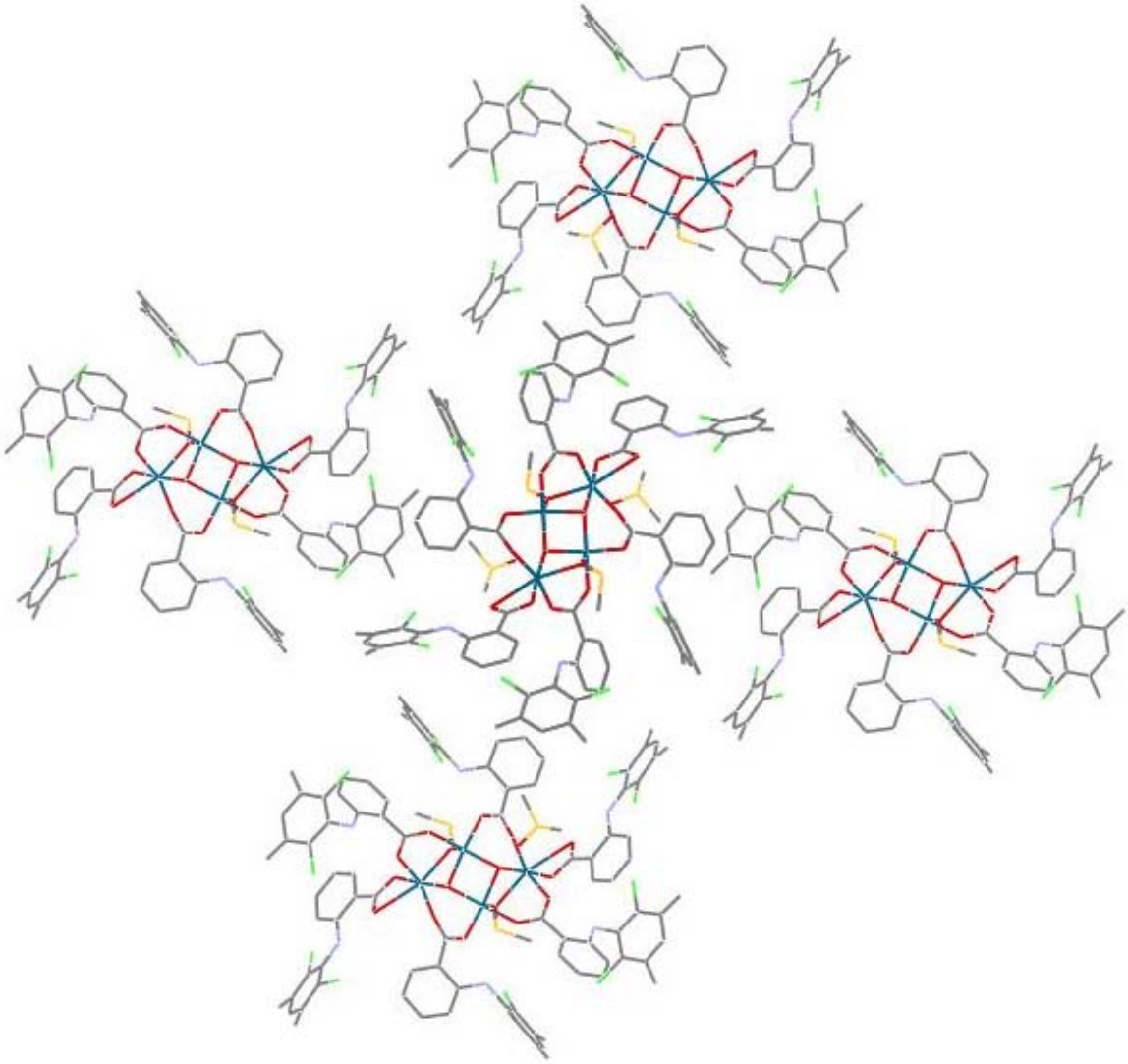

Figure VIII.2. Packing diagram of the complex[$Cu_4(MCFA)_6(OH)_2(DMSO)_2$].2DMSO (**3a)**.

VIII.2.2. X-Ray structure of $[Cd(MCFA)_2(DMSO)_2]$ (5a).

Table VIII.5.1. Selected bond lengths [Å] and angles [º] for $[Cd(MCFA)_2(DMSO)_2]$ (5a).

Vector	Length	Vector	Angle
Cd(1)-O(31)	2.270(3)	O(31)-Cd(1)-O(11)	159.88(13)
Cd(1)-O(11)	2.352(3)	O(31)-Cd(1)-O(12)	138.55(12)
Cd(1)-O(12)	2.377(4)	O(11)-Cd(1)-O(12)	55.51(12)
Cd(1)-O(1)	2.389(4)	O(31)-Cd(1)-O(1)	82.83(13)
Cd(1)-O(2)	2.396(4)	O(11)-Cd(1)-O(1)	84.71(13)
Cd(1)-O(32)	2.418(4)	O(12)-Cd(1)-O(1)	85.62(13)
		O(31)-Cd(1)-O(2)	79.63(14)
		O(11)-Cd(1)-O(2)	120.45(14)
		O(12)-Cd(1)-O(2)	76.87(13)
		O(1)-Cd(1)-O(2)	128.35(15)
		O(31)-Cd(1)-O(32)	55.76(12)
		O(11)-Cd(1)-O(32)	108.53(12)
		O(12)-Cd(1)-O(32)	163.67(12)
		O(1)-Cd(1)-O(32)	89.60(13)
		O(2)-Cd(1)-O(32)	117.86(13)

Table VIII.5.2. Selected hydrogen bonds for $[Cd(MCFA)_2(DMSO)_2]$ (5a).

Atoms D,H,A	Dist. D, H [A]	Dist. H, A [A]	Dist. D,A [A]	Angle D,H,A [º]
N17—H17A—O11	0.81	1.91	2.630(5)	147.3
N37—H37A—O31	0.73	2.03	2.630(5)	140.3

The molecular structure of the complex $[Cd(lorn)_2(DMSO)_2]$ **5a**, is depicted in **Figure VIII.3.1.** Selected interatomic distances and angles for compound are listed in **Table VIII.5.1** Selected hydrogen bonds are given in **Table VIII.5.2** Complex crystallize in the triclinic space group -1. Metal center is coordinated by two ligands and two DMSO groups. Meclofenamic acid acts as a deprotonated bidentate ligand and it is coordinated to the metal ion through the oxygens of the carboxyl groups at the equatorial positions [Cd(1)-O(31) 2.270(3) Å, Cd(1)-O(11) 2.352(3) Å]. The coordination polyhedron can be described as a distorted octahedron and the apical positions are occupied by two dmso oxygen atoms. The ambidentate dmso ligand co-ordinates the metal centre through the oxygen atom. M–O(apical) bond distances are Cd(1)-O(1) 2.389(4) Å, Cd(1)-O(2) 2.396(4) Å.

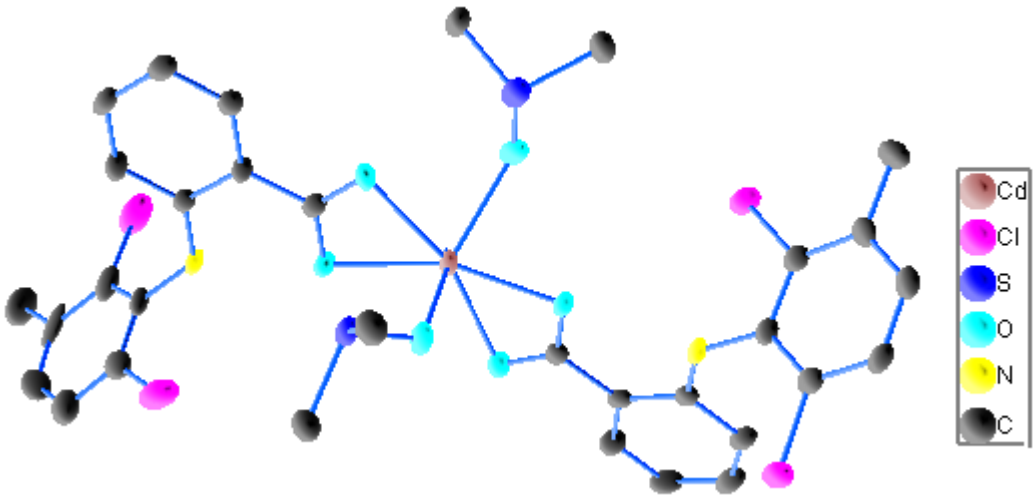

Figure VIII.3.1. Crystal structure of $[Cd(MCFA)_2(DMSO)_2]$ (**5a)**.

VIII.3. Spectroscopic characterization of Mn(II), Cu(II), Zn(II) and Cd(II) complexes with meclofenamic acid.

VIII.3.1. Nuclear Magnetic Resonance

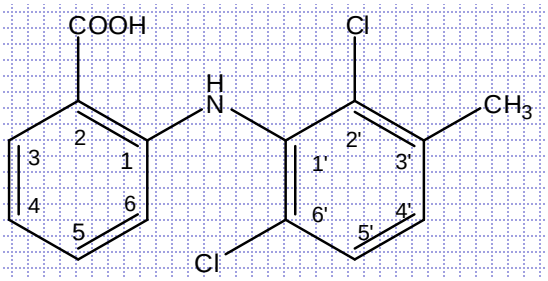

Figure VIII.4. Structural formule of meclofenamic acid, **1**.

The ^{1}H and ^{13}C signals were assigned using one- and two-dimensional $^{1}H–^{1}H$ COSY, $^{1}H–^{13}C$ HSQC, $^{1}H–^{13}C$ HMBC spectra. The $^{1}H–$ and $^{13}C–$NMR data for meclofenamic acid (**figure VIII.4**.), zinc complexes **4**, **8** and cadmium complexes **5**, **9** are summarized in **table VIII.6. and table VIII.7.** These results, together with the published data on meclofenamic acid[2] allowed complete assignment of all signals in the spectra of both the meclofenamic acid and its zinc and cadmium complexes. In order to investigate the behaviour of the compounds in solution similar to those, used for the biological studies, all solutions were prepared mostly in DMSO-d_6. In all ^{1}H-NMR spectra of complexes one singlet appear in the region of methyl group resonance and it is shifted upfield for **4**, **8**, **9**, while it is not changed for **5**, when compared to that found for free drug Hmcfa. Small perturbations of the chemical shifts (ca. 0.03 – 0.08 ppm), **4**, **8**, **9**, are observed for methyl proton, which lie far away from the coordination center of the ligand. The methyl group is also confirmed by ^{13}C-NMR spectra. The NH peak is a sharp singlet at approximately 9.2 ppm in the $^{1}H–$NMR spectra of meclofenamic acid.The existence of the HN resonance indicates that the nitrogen atoms remain protonated in **4**, **8** and **5**, **9**.The small downfield shift (0.21ppm) of the NH resonance in $CDCl_3$ solution suggests that no significant participation in intermolecular hydrogen-bonding takes place. The greatest downfield shift occurs of the NH resonance in DMSO-d_6 solution for **4**, **8** and **5**, **9**, respectively. The furthest downfield peak is assigned as H-3 due to its proximity to the carboxylic acid group in the ^{1}H spectrum of free drug. In ^{1}H-NMR spectra of **4**, **8** and **5**, **9** H(4), H(5), H(6), H(4'),H(5') shifts are upfield except for that due to H(3) which is shifted downfield. For **8** and **9** one singlet appears at ca. 1.85 ppm, thus in the region of proton of acetate group. Two resonances attributed to the acetate carbons are found at 22.3 ppm and 176 ppm in ^{13}C-NMR spectrum of **8** and 22.0 ppm and 178 ppm in ^{13}C-NMR spectrum of **9**. Involvement of the carboxyl group in bonding to Zn and Cd atoms is confirmed by the resonance ascribed to C2, which either disappears for **5** and **9** cadmium complexes or exhibits the greatest shift upon coordination for **4** and **8** zinc complexes.[4b] The remaining resonances due to the aromatic carbon atoms for **4**, **8** and **5**, **9** do not shift considerably after binding to Zn and Cd, respectively. In all ^{1}H-NMR spectra of zinc and cadmium complexes with meclofenamic acid one triplet appear at ca. 1.0 ppm and one quartet at

ca. 2.5 ppm. These peaks are assign to protons of triethylamine (CH_3 and CH_2), respectively. The presence of triethylamine is confirmed by two peaks ca. at 12 ppm and 46 ppm in ^{13}C-NMR of complexes.

Table VIII.6. ^{1}H NMR shifts of **4**, **5**, **8**, **9** complexes and parent drug **1** (δ in ppm and *J* in Hz).

	1[a]	**1**[b]	**4**[a]	**4**[b]	**8**[a]	**5**[a]	**9**[a]
OH	13.14s	c	-	-	-	-	-
NH	9.15s	9.21s	10.23s	9.42s	10.21s	10.33s	10.30s
H – C(3)	7.90dd J(3-4)=8.0 J(3-5)=1.0	8.07d J(3-4)=6.7	8.00d J(3-4)=9.0	8.00d	7.95d J(3-4)=6.6	8.02dd J(3-4)=7.4	7.98d J(3-4)=7.4
H – C(4)	6.77t J(4-5)=8.0	6.79t J(4-5)=7.6	6.69t J(4-5)=7.4	6.63t J(4-5)=7.2	6.70t J(4-5)=7.3	6.74t J(4-5)=7.1	6.69t J(4-5)=7.3
H – C(5)	7.31m	7.22m	7.16m	7.17d J(5-4)=8.1	7.18t J(5-4)=7.6	7.21t J(5-4)=7.4	7.16t J(5-4)=7.4
H – C(6)	6.19d J(6-5)=8.4	6.33d J(6-5)=8.4	6.12d J(6-5)=8.2	6.25d J(6-5)=8.3	6.12d J(6-5)=8.1	6.15d J(6-5)=8.1	6.10d J(6-5)=8.1
H –C(4')	7.35d J(4'-5')= 8.3	7.14d J(4'-5')= 8.3	7.19d J(4'-5')= 8.3	6.97d J(4'-5')= 8.3	7.26d J(4'-5')= 8.4	7.32d J(4'-5')= 8.2	7.27d J(4'-5')= 8.3
H –C(5')	7.50 d J(5'-4')= 8.3	7.32t J(5'-4')= 8.2	7.38d J(5'-4')= 8.3	7.21d J(5'-4')= 8.2	7.44d J(4'-5')= 8.3	7.48d J(4'-5')= 8.2	7.43d J(4'-5')= 8.2
CH_3 – C(3')	2.38s	2.41s	2.30s	2.28s	2.35s	2.38s	2.33s
CH_3COO	-	-	-	-	1.84s	-	1.86s

[a] Spectrum recorded in DMSO-d_6
[b] Spectrum recorded in $CDCl_3$
[c] Carboxyl proton exchanged in $CDCl_3$

Table VIII.7. ^{13}C NMR shifts (ppm) of **4**, **5**, **8**, **9** complexes and parent drug **1**.

	1[a]	**1**[b]	**4**[a]	**4**[b]	**8**[a]	**5**[a]	**9**[a]
COOH	170.0	172.1	173.6	175.2	173.6	173.9	174.1
C1	147.1	148.5	146.2	147.2	146.2	146.1	146.3
C2	111.7	110.4	-	113.6	116.4	-	-
C3	131.5	132.3	132.0	131.1	132.0	131.9	131.9
C4	117.3	117.4	116.7	117.1	116.7	116.7	116.8
C5	134.6	134.9	135.5	135.9	135.5	135.5	135.5
C6	112.9	113.1	112.3	115.2	112.3	112.2	112.2
C1'	134.1	135.2	133.3	134.3	133.3	133.3	133.3
C2'	133.5	134.7	132.1	133.3	134.6	132.4	132.4
C3'	130.5	131.6	130.2	129.1	130.2	130.2	130.3
C4'	129.3	128.8	128.5	127.0	128.4	128.6	128.6
C5'	128.8	127.8	127.9	127.9	127.9	128.0	128.0
C6'	136.4	136.6	136.2	136.2	136.2	136.3	136.3
CH_3	20.1	20.6	20.1	20.5	20.1	20.2	20.2
CH_3COO	-	-		-	22.3 176.9	-	22.0 177.9

[a] Spectrum recorded in DMSO-d_6
[b] Spectrum recorded in $CDCl_3$

Figure VIII.5. ^{1}H-NMR spectrum of $Zn(MCFA)_2(H_2O)_4]$, **4** recorded in $CDCl_3$.

Figure VIII.6. ^{13}C-NMR spectrum of $Zn(MCFA)_2(H_2O)_4]$, **4** recorded in $CDCl_3$.

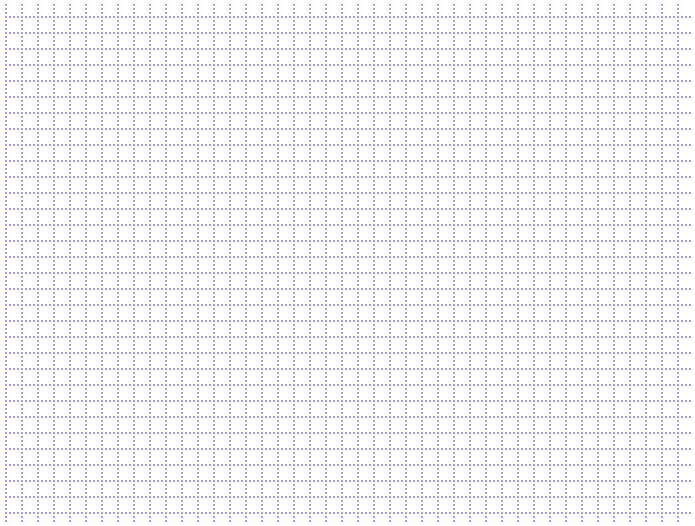

Figure VIII.7. ^{1}H-NMR spectrum of [Zn(AcO)(MCFA)], **8** recorded in dmso-d_6.

Figure VIII.8. ^{13}C-NMR spectrum of [Zn(AcO)(MCFA)], **8** recorded in dmso-d_6.

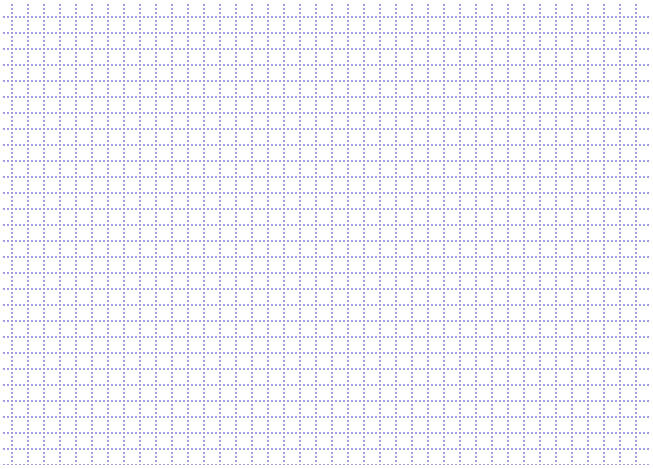

Figure VIII.9. ^{1}H-NMR spectrum of [Cd(MCFA)$_2$(H$_2$O)$_2$], **5** recorded in dmso-d_6.

Figure VIII.10. ^{13}C-NMR spectrum of [Cd(MCFA)$_2$(H$_2$O)$_2$], **5** recorded in dmso-d_6.

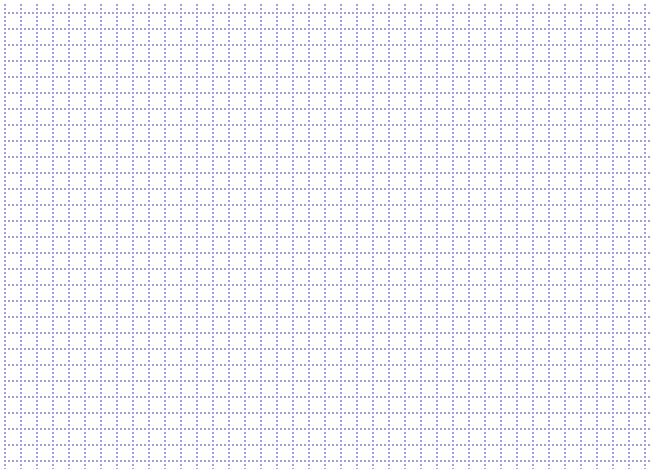

Figure VIII.11. ^{1}H-NMR spectrum of [Cd(AcO)(MCFA)], **9** recorded in dmso-d_6.

Figure VIII.12. ^{13}C-NMR spectrum of [Cd(AcO)(MCFA)], **9** recorded in dmso-d_6.

2D $^{1}H–^{1}H$ shift correlated spectra (COSY), 2D cross-peaking of heteronuclear single quantum correlation (HSQC) and heteronuclear multiple bond correlation (HMBC) gradient-assisted spectra of **4** were performed in order to completely assign the resonances in zinc complex of meclofenamic acid. 2D $^{1}H–^{1}H$ (COSY), 2D $^{1}H–^{13}C$ (HSQC), 2D $^{1}H–^{13}C$ (HMBC) data for complex **4** are summarized in **tables VIII.8**, **VIII.9**, **VIII.10**.

The ^{1}H-NMR spectra of **4** shows seven distinct signals, respectively. H(CH_3) resonance is appeared as a singlet. The methyl group is also confirmed by ^{13}C-NMR spectra. In complex, there is one signal due to the imine proton NH resonance at ca. 10.2 ppm in ^{1}H NMR spectrum. In the region characteristic of aromatic protons (6.00–8.00 ppm) five signals are found. In the region corresponding to the signals of aromatic rings carbons (110-150 ppm) signals are observed. However it was not possible to assign explicitly the signals to each of all aromatic systems present in the molecule.

2D $^{1}H–^{1}H$ (COSY) spectrum shows correlation between coupled protons thus give rise to off-diagonal or cross-peaks for all protons that have significant(measurable) J-J coupling. In the COSY spectrum of **4**, interestingly the protons of the methyl group are coupled to H(4'). As expected, the aromatic protons show ortho coupling between H(6) and H(5), H(5) and H(4), H(4) and H(3), H(5') and H(4').[3c]

2D $^{1}H–^{13}C$ (HSQC) spectrum shows correlation between directly attached (one-bond) proton-carbon. In the 2D $^{1}H–^{13}C$ (HSQC) spectrum of **4** the ^{13}C signal of the methyl carbon atom is detected at ca. 20 ppm and assigned through the shift correlation peaks with CH_3 protons. Moreover correlation peaks of C6 and H(6), C4 and H(4), C4' and H(4'), C5' and H(5'), C5 and H(5), C3 and H3 are observed.

2D $^{1}H–^{13}C$ (HMBC) spectrum shows correlation between long-range (two, three and four-bonds) proton-carbon couplings.[3c] In the 2D $^{1}H–^{13}C$ (HMBC) spectrum of **4** carbon atom (at ca. 175 ppm) of the carboxylic group displayed a coupling to H(3), H(4), H(6) protons of the carboxyl-bearing ring. Imine proton NH connect through aromatic ring to the carbons C1, C2, C3, C6,additionally to the carbon C2' of methyl-bearing ring. Proton signal of the methyl group is detected at ca. 2.30 ppm and assigned through the shift correlation peaks with C1', C2', C4' fron the aromatic ring followed on the basis of coupling patterns The remaining carbons of the aromatic rings may then be assigned to protons in the fashion described above.In general, the carbons of each aromatic ring showed connectivity to protons of each aromatic ring **table VIII.10**.

Table VIII.8. 2D^{1}H,^{1}H-COSY NMR data of $Zn(MCFA)_2(H_2O)_4]$, **4**[a].

1	2	3	4	5
H6 – H5	H5 – H4	H4 – H3	H5' – H4'	H(CH_3) – H4'

[a]Spectrum recorded in DMSO-d_6

Table VIII.9. 2D^{1}H,^{13}C-HSQC NMR data of Zn(MCFA)$_2$(H_2O)$_4$], **4**[a].

1	2	3	4	5	6	7
C(CH_3) – H(CH_3)	C6 – H6	C4 – H4	C4' – H4'	C5' – H5'	C5 – H5	C3 – H3

[a]Spectrum recorded in DMSO-d_6

Table VIII.10. 2D^{1}H,^{13}C-HMBC NMR data of Zn(MCFA)$_2$(H_2O)$_4$], **4**[a].

1	C(CH_3) – H4'	14	C2' – H(NH)
2	C2 – H4	15	C3 – H(NH)
3	C2 – H5	16	C1 – H(NH)
4	C2 – H3	17	C1 –H3
5	C2 – H(NH)	18	C1 – H5
6	C6 – H(NH)	19	C1 – H4
7	C6 – H3	20	C1 – H6
8	C6 – H5	21	C(COO) – H3
9	C6 –H4	22	C(COO) – H4
10	C4' – H5'	23	C(COO) – H6
11	C2' – H5'	24	C4' – H(CH_3)
12	C5' – H1'	25	C2' – H(CH_3)
13	C2' – H4'	26	C1' – H(CH_3)

[a]Spectrum recorded in DMSO-d_6

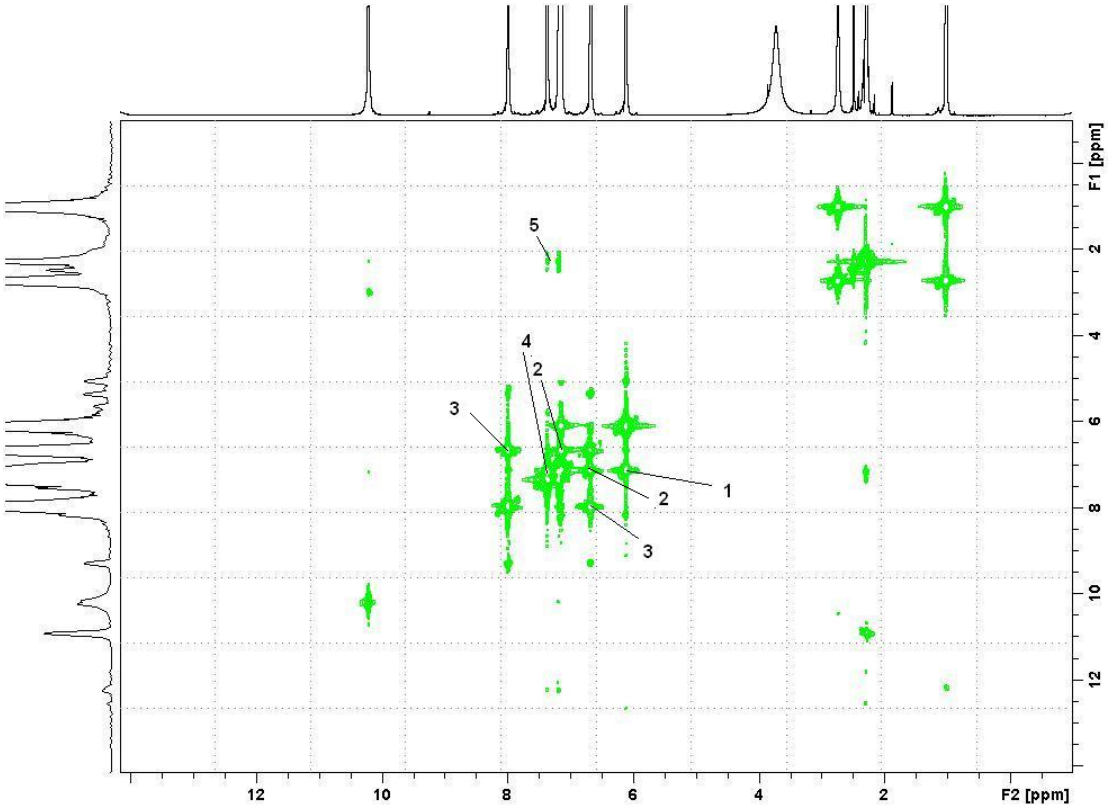

Figure VIII.13. 2D^{1}H,^{1}H-COSY NMR spectrum of Zn(MCFA)$_2$(H_2O)$_4$], **4** recorded in dmso-d_6.

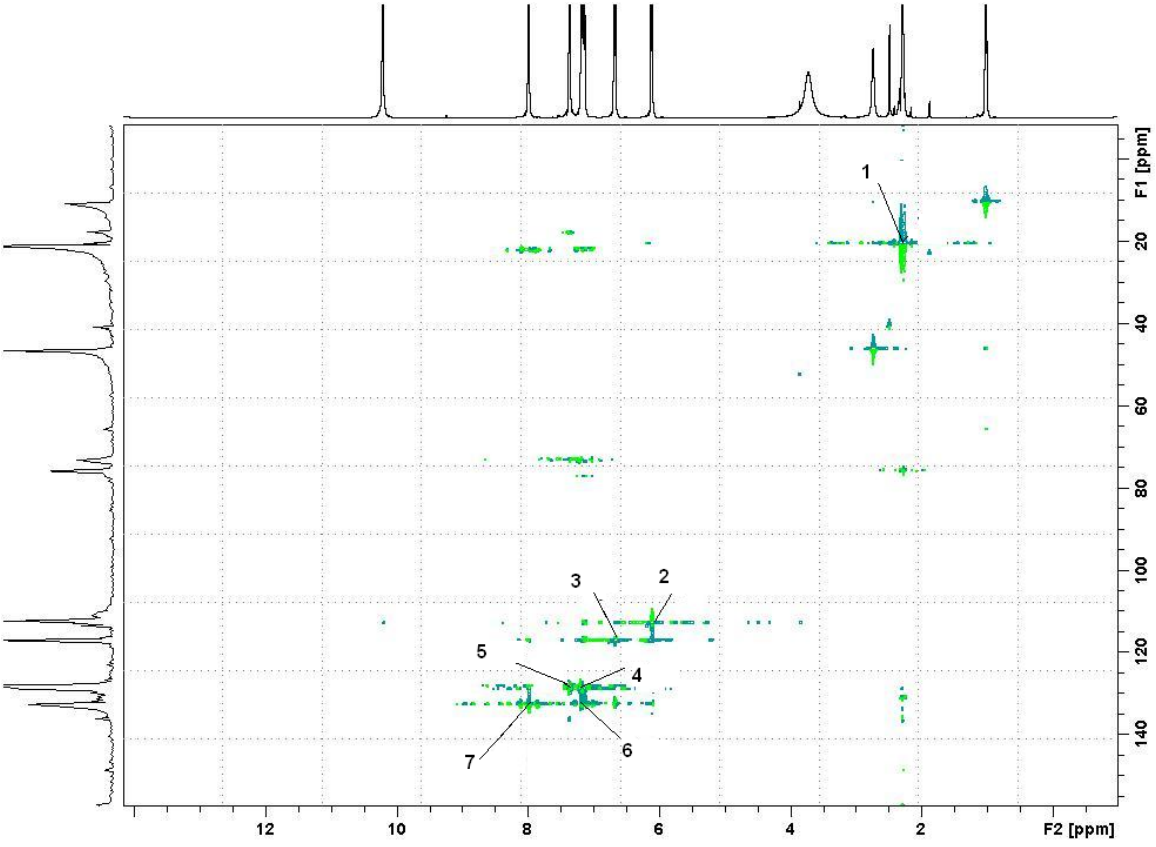

Figure VIII.14. 2D^{1}H,^{13}C-HSQC NMR spectrum of $Zn(MCFA)_2(H_2O)_4]$, **4** recorded in dmso-d_6..

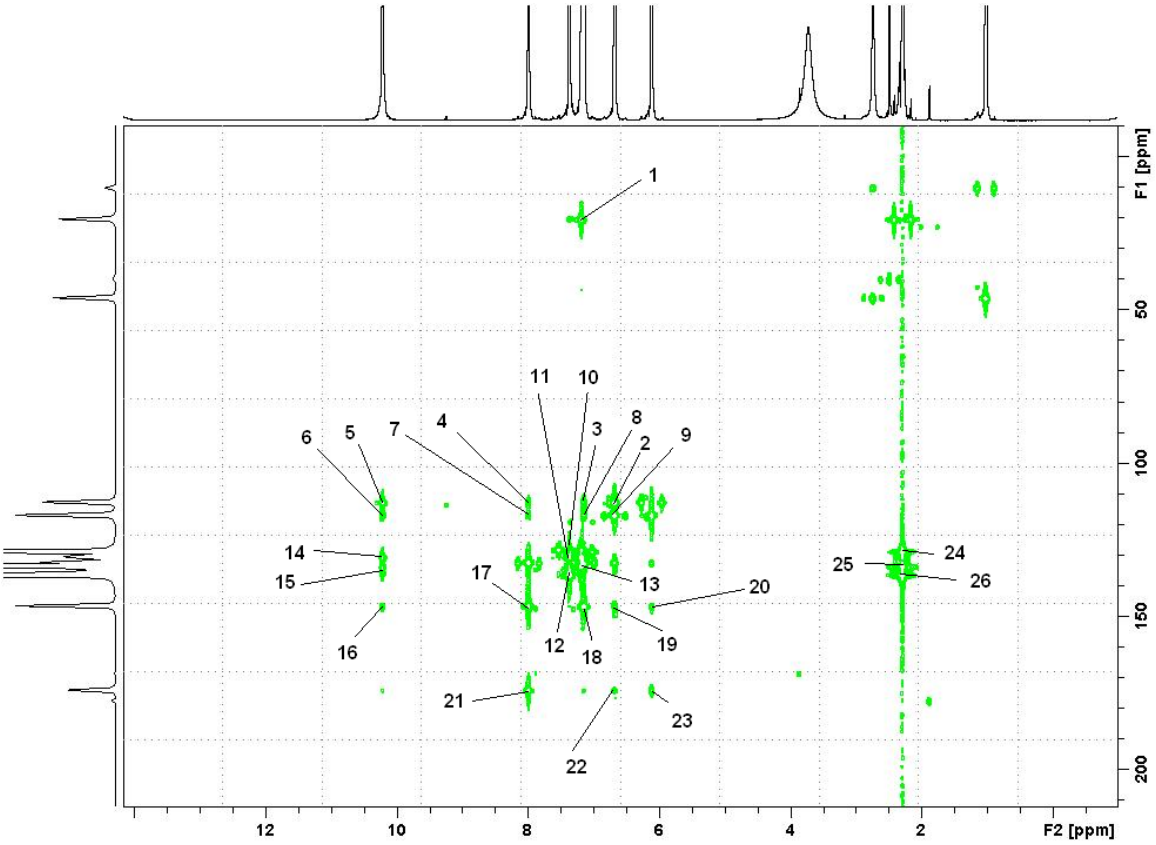

Figure VIII.15. 2D^{1}H,^{13}C-HMBC NMR spectrum of $Zn(MCFA)_2(H_2O)_4]$, **4** recorded in dmso-d_6.

VIII.3.2. Infrared spectroscopy.

Table VIII.11. IR-data (cm^{-1}) for the prepared complexes **2 – 5** and the parent drug.

Compounds	νNH	Carboxylic groups		Δν	νM - O_{OCO}	νM – O_{H20}
		ν_{asym} (COO^-)	ν_{sym} (COO^-)			
Hmcfa	3290s	1656s	1502s	154	-	-
$[Mn(MCFA)_2]$	3226m	1581s	1456s	125	281ms	438ms
$[Cu(MCFA)_2(H_2O)]$	3310m	1583s	1455s	128	246m	375m
$[Zn(MCFA)_2(H_2O)_4]$	3295m	1583s	1457s	126	289sh	438m
$[Cd(MCFA)_2(H_2O)_2]$	3251m	1580s	1455s	125	246m	430m

s = strong, m = medium, w = weak, sh = sharp, br = broad

Table VIII.12. IR-data (cm^{-1}) for the prepared complexes **6 - 9**.

Compounds	νNH	Carboxylic groups		Δν	νM - O_{OCO}	νM – O_{H20}
		ν_{asym} (COO^-)	ν_{sym} (COO^-)			
[Mn(AcO)(MCFA)]	3279m	1580s	1455m	125	246m	398m
[Cu(AcO)(MCFA)]	3271m	1576s	1448m	128	246m	394mw
[Zn(AcO)(MCFA)]	3337m	1581s	1458m	123	247ms	399mw
[Cd(AcO)(MCFA)]	3524m	1579s	1455m	124	251ms	397mw

s = strong, m = medium, w = weak, sh = sharp, br = broad

IR data of meclofenamic acid **1** and its metal Complexes **2 – 5** and **6 – 9** are reported in **table VIII.11. table VIII.12.** A comparison between the IR spectra of drug alone and those of its complexes provides evidence regarding the bonding sites. Meclofenamic acid has two strong potential donor sides: oxygens atoms of the carboxyl group and nitrogen atom of imino group. As the carboxyl hydrogen is more acidic than the amino hydrogen the deprotonation occurs in the carboxylic group. This is confrmed by the IR spectra of the complexes, showing the characteristic bands for the secondary amino groups and for the coordinated carboxylato group.[3] The absence of large systematic shifts of the ν(NH) and δ(NH) bands in the spectra of the complexes **2 – 5** compared with those of the ligand **1** indicates that there is no interaction between the NH group and the metal ions.[3] The IR spectra of **2 – 5** show a broad absorption bands at ca. 3400 - 3500 cm^{-1}. These bands correspond to the antisymmetric and symmetric OH stretch and confirm the presence of water in the complex. Moreover, the IR spectra exhibit characteristic bands at approximately 860–855 and 580–550 cm^{-1} assigned to the rocking and wagging mode of the coordinated water molecule.[7] Each complex showed carboxylate stretching frequencies, $\nu_{asym}(COO^-)$ and $\nu_{sym}(COO^-)$ are in the expected region[7].The $\nu_{as}(COO^-)$ and $\nu_s(COO^-)$ bands of the prepared complexes **2 – 5 and 6 – 9** are at 1618-1583 and at 1501- 1450 cm^{-1} respectively. The difference between the asymmetric and symmetric stretching vibration $\Delta\nu = [\nu_{asym}(COO^-) - \nu_{sym}(COO^-)]$ gives information on the carboxylate bonding mode. However, splitting of the bands assigned to $\nu_{sym}(COO^-)$ indicates that the meclofenamate anion as a ligand in **2 – 5 and 6 – 9** complexes is coordinated through bidentate carboxyl group. Δν value for **2 –**

5 complexes is significantly less than the ionic value (for sodium mefenamic the Δν value is 180cm^{-1}), as expected for the bidentate chelating mode of carboxylate ligation. The medium bands at approximately 400 cm^{-1} is attributed to the ν(M-O_{H2O}) stretching mode, while the bands at 250-280cm^{-1} to the ν(M-O_{oco}) stretching mode.

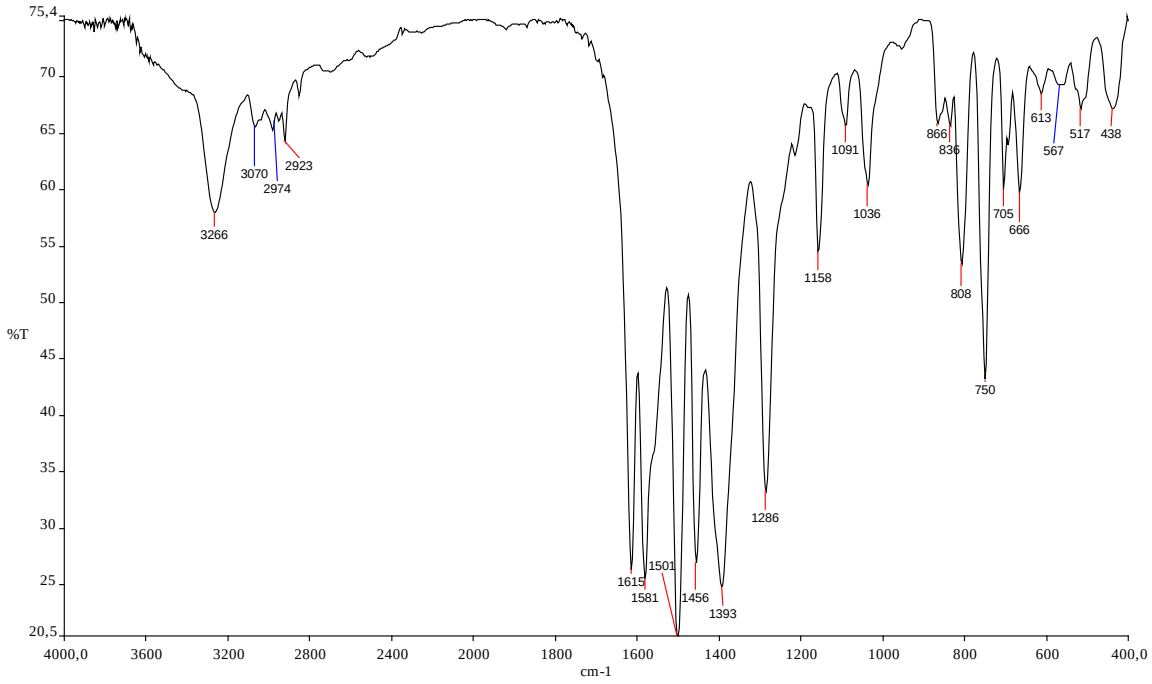

Figure.**VIII.16.** Infrared spectrum of Mn(MCFA)$_2$], **2**.

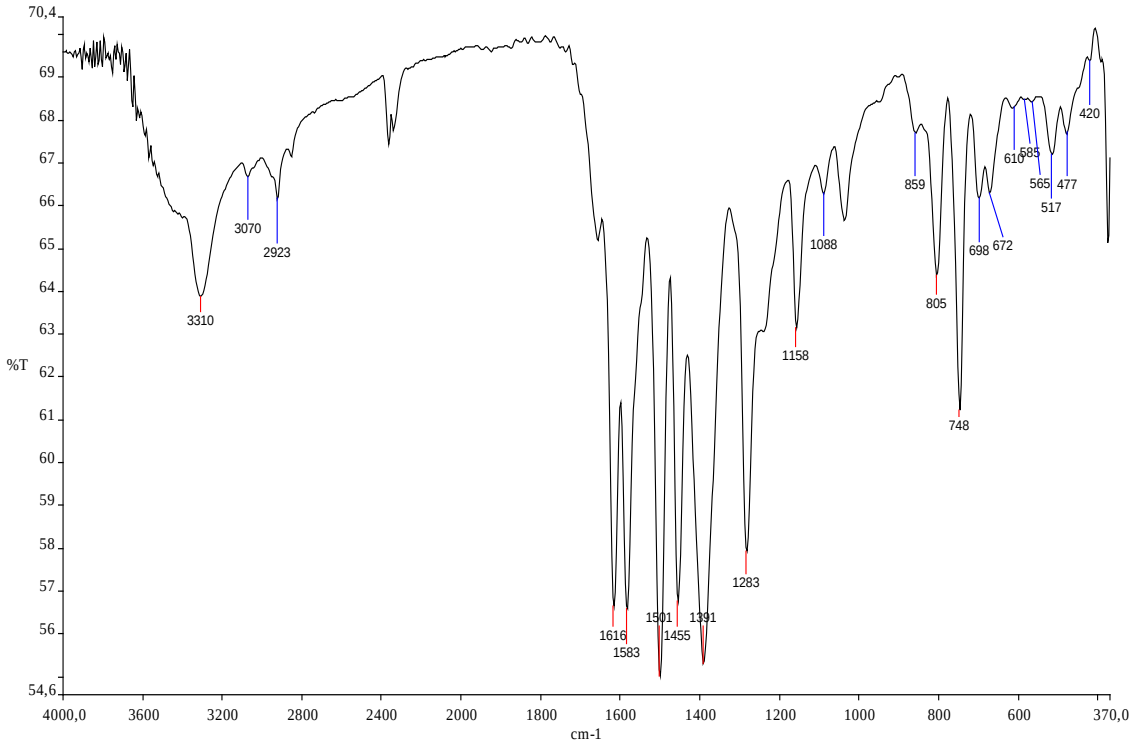

Figure VIII.17. Infrared spectrum of [Cu(MCFA)$_2$(H_2O)], **3**.

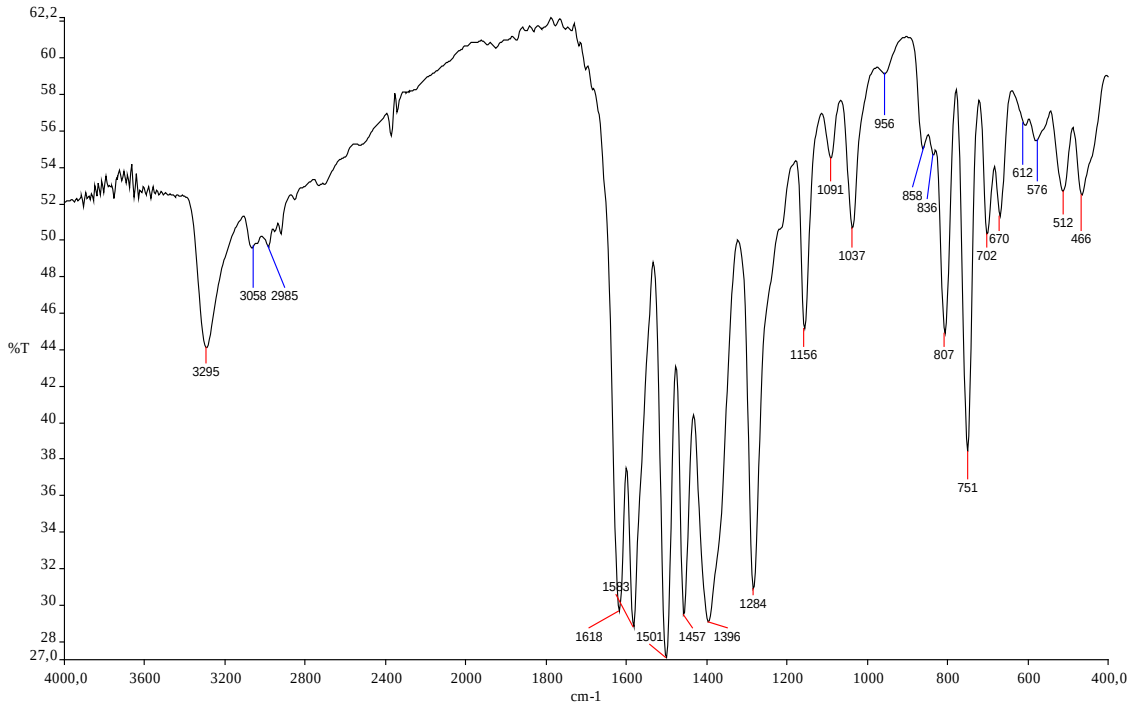

Figure VIII.18. Infrared spectrum of $Zn(MCFA)_2(H_2O)_4]$, **4**.

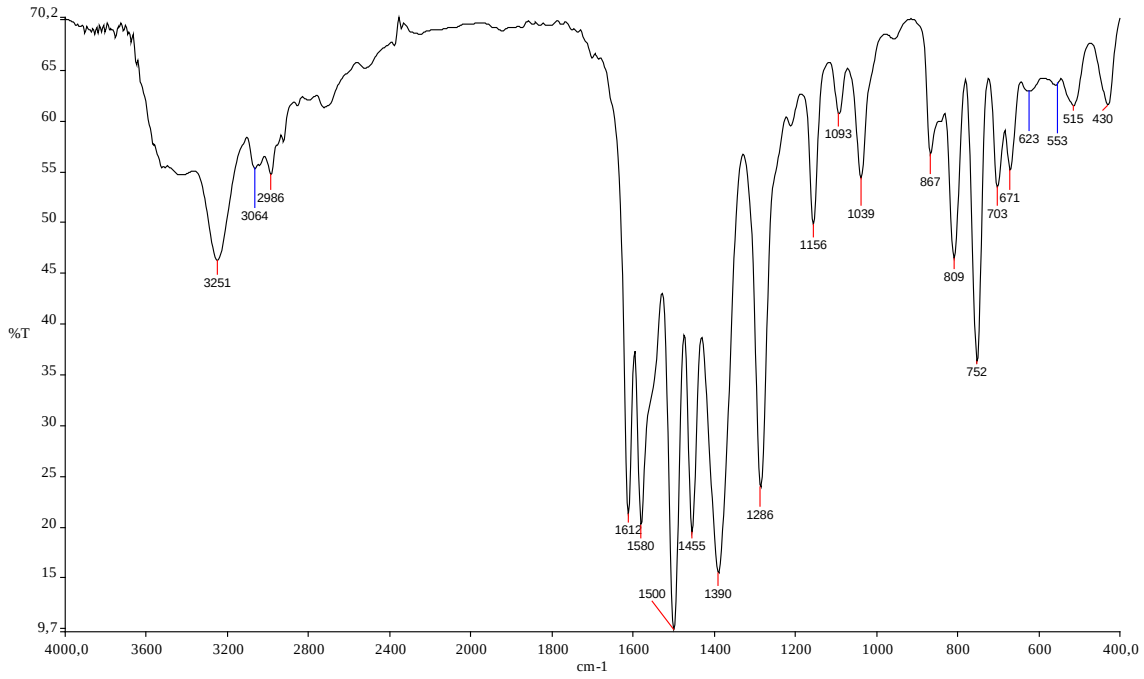

Figure VIII.19. Infrared spectrum of $Cd(MCFA)_2(H_2O)_4]$, **5**.

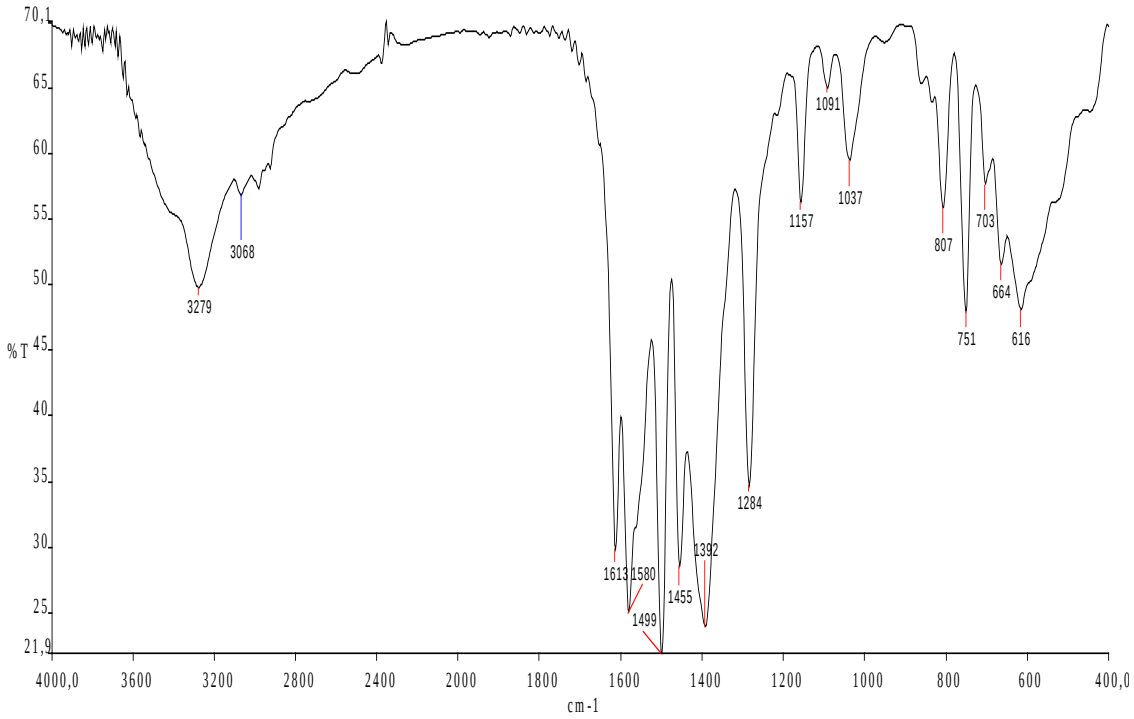

Figure VIII.20. Infrared spectrum of [Mn(AcO)(MCFA)], **6**.

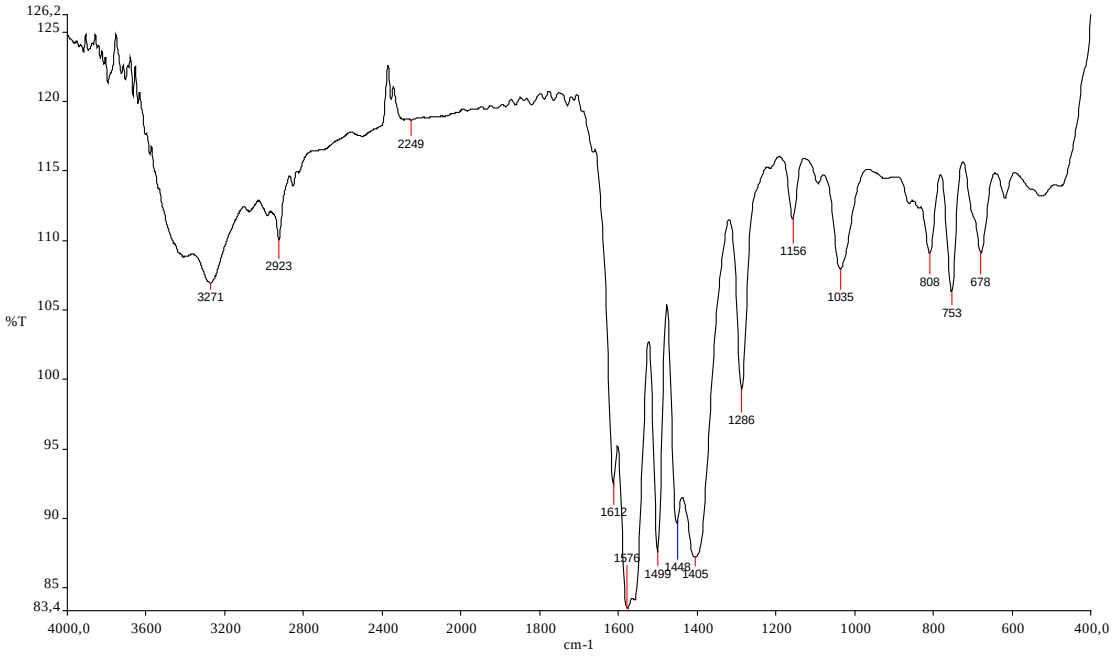

Figure VIII.21. Infrared spectrum of [Cu(AcO)(MCFA)], **7**.

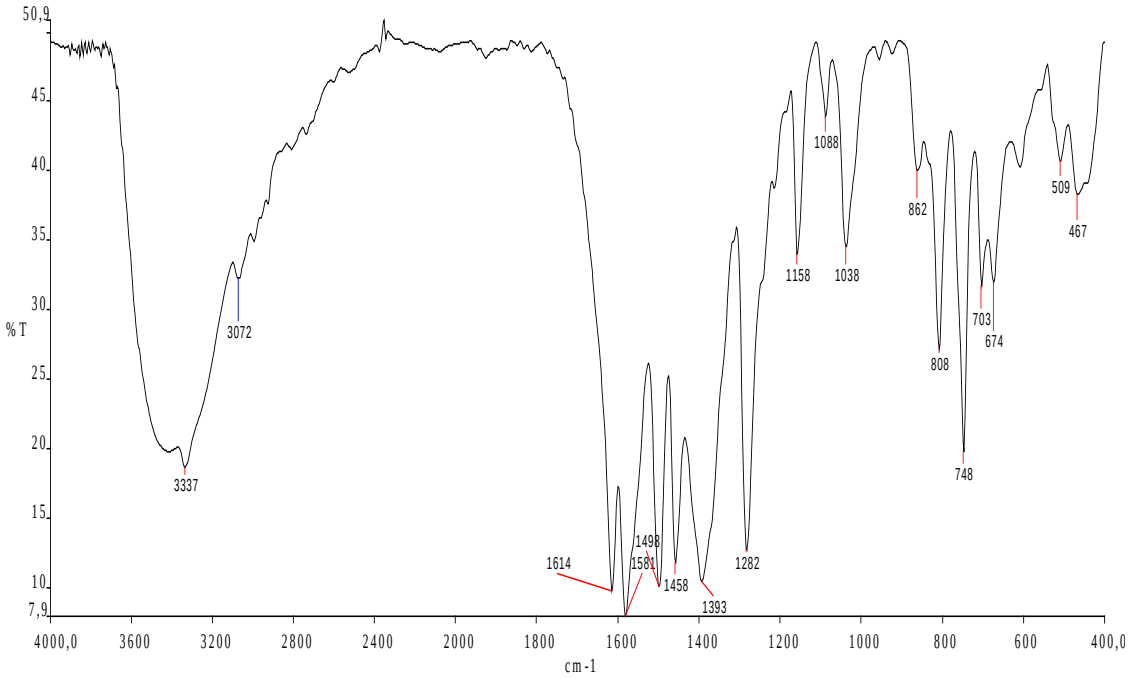

Figure VIII.22. Infrared spectrum of [Zn(AcO)(MCFA)], **8**.

VIII.3.3. Electronic spectroscopy.

Table VIII.13. Spectral data (UV-vis) for the prepared complexes **2**, **3**, **6**, **7** and the parent drug **1**.

Compounds	μ_{eff}	$CHCl_3$			DMF			Assignments
		λ (nm)	ν (cm^{-1})	log ε	λ (nm)	ν (cm^{-1})	log ε	
Meclofenamic acid (Hmcfa)		340	29.412	3.53	319	31.348	3.66	$n \rightarrow \pi^*$
		282	35.460	3.49	291	34.364	3.64	$\pi \rightarrow \pi^*$
$[Mn(MCFA)_2]$	5.66	493 (sh)	20.284	1.63	415 (sh)	24.096	1.51	$^6A_{1g} \rightarrow {}^4T_{1g}$ (G)
		381	26.247	2,46	364	27,473	2.37	$^6A_{1g} \rightarrow {}^4T_{2g}$ (G)
		337	29.674	3.84	321	31.153	4.10	$n \rightarrow \pi^*$
		283	35.336	3.85	294	34.014	4.08	$\pi \rightarrow \pi^*$
$[Cu(MCFA)_2(H_2O)]$	1.94	682	14.663	1.83	733	13.643	2.25	d – d
		339	29.499	4.07	321	30.581	4.13	$n \rightarrow \pi^*$
		281	35.587	4.07	281	35.587	4.16	$\pi \rightarrow \pi^*$
[Mn(AcO)(MCFA)]	5.53	448	22.321	2.47	485	20.619	2.47	$^6A_{1g} \rightarrow {}^4T_{1g}$ (G)
		337	29.674	3.64	314	31.847	3.71	$n \rightarrow \pi^*$
		279	35.842	3.73	299	33.445	3.71	$\pi \rightarrow \pi^*$
[Cu(AcO)(MCFA)]	2.03	702	14.246	1.78	664	15.060	2.11	d – d
		335	29.851	2.87	374	26.738	3.07	$n \rightarrow \pi^*$
		281	35.587	2.93	307	32.573	3.63	$\pi \rightarrow \pi^*$

sh = shoulder

The electronic spectra of the ligand **1** and the complexes **2**, **3**, **6**, **7** were recorded in DMF and $CHCl_3$ solution and absorption maxima in the uv-visible region are listed in **table VIII.13.** along with suggested assignments[8-11]. Practically, the overall spectra in both solvents are alike but they differ in some cases for some nm.The UV spectra of the meclofenamic acid complexes in DMSO and in $CHCl_3$ solution are alike (strong absorptions occur at ca. 280 – 300 nm) as well as for parent drug. The band at 319 nm in free Hmcfa, **1** is shifted by an extent of 2 nm in the case of $[Mn(MCFA)_2]$, **2** and 5 nm in the case of [Mn(AcO)(MCFA)], **6**. The Mn(II) complex of the type $[Mn(MCFA)_2]$, **2** exhibit strong-high energy bands at 24.096 cm^{-1} 27,473 cm^{-1} 31.153 cm^{-1} 34.014 cm^{-1} and are assigned to the transitions to the transitions $^6A_{1g} \rightarrow {}^4T_{1g}$ (G), $^6A_{1g} \rightarrow {}^4T_{2g}$ (G), $n \rightarrow \pi^*$, $\pi \rightarrow \pi^*$. A high intensity band at 27,473 cm^{-1} (**2**) and at 31.847 cm^{-1} (**6**) are assigned to the matal ligand charge transfer. The electronic spectra of the Mn(II) complexes, **2**, **6** can be assigned six coordinate stereochemistry[11]. The absorption of the organic ligand tailing into the visible region obscure the very weak d-d absorption bands of the manganese (II) complexes[9,11,12]. The d-d spectra of the solvated **2**, **6** can be assigned to transitions in pseudo-octahedral structures or sixcoordinated tetragonally distorted stereochemistries. The electronic spectra of $[Cu(MCFA)_2(H_2O)]$, **3** [Cu(AcO)(MCFA)], **7** show a broad absorption band in the visible region at 733 nm, 664 nm which could be assigned to the $d_{xz,yz} \rightarrow d_{x2y2}$ transition, respectively. Moreover, the spectra display band at about 330 - 370 nm, in turn, is assigned to metal ligand charge transfer.

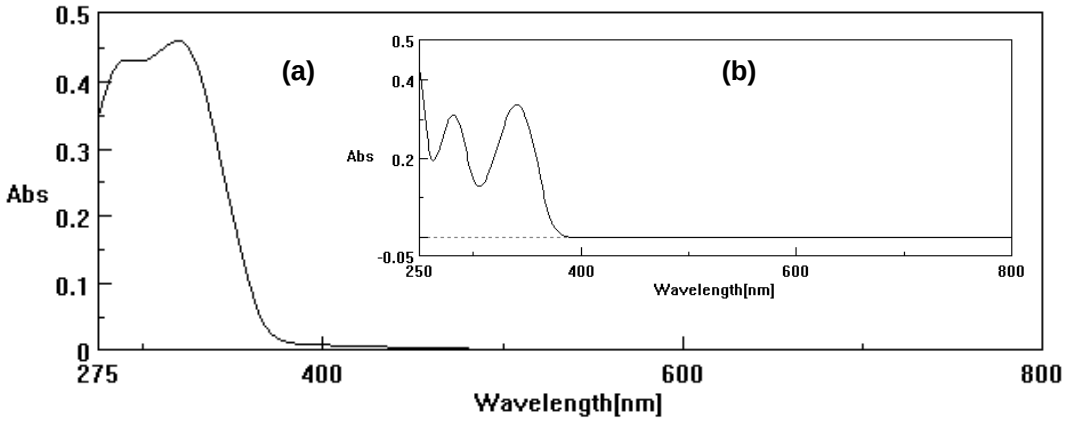

Figure VIII.23. UV-vis absorption spectra of Hmcfa, **1**,(a) 10^{-4} M in DMF, (b) 10^{-4} M in $CHCl_3$.

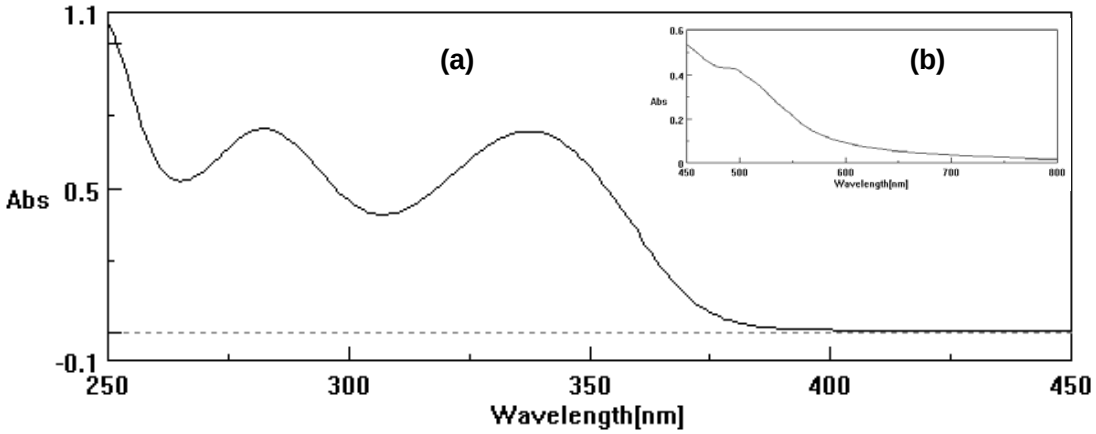

Figure VIII.24. UV-vis absorption spectra of [$Mn(MCFA)_2$], **2**, (a) 10^{-4} M in $CHCl_3$, (b) 10^{-2} M in $CHCl_3$.

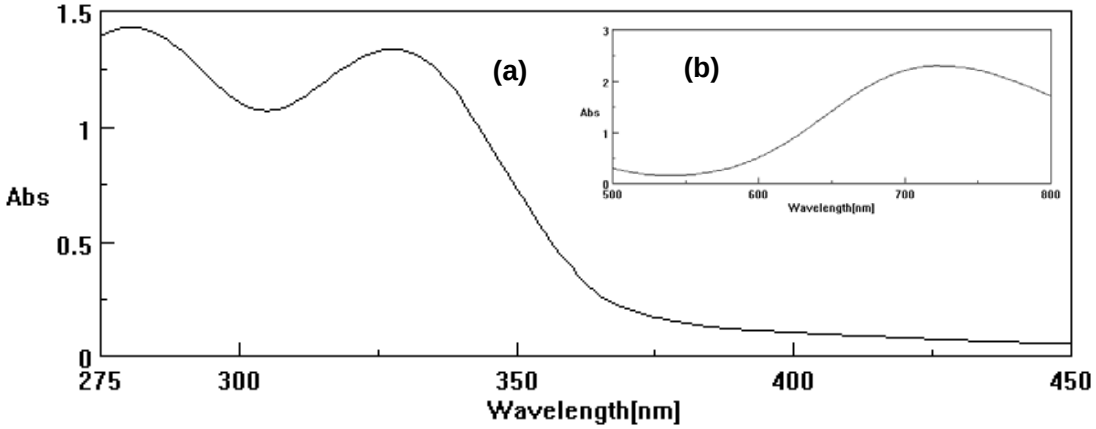

Figure VIII.25. UV-vis absorption spectra of [$Cu(MCFA)_2(H_2O)$], **3**, (a) 10^{-4} M in DMF, (b) 10^{-2} M in DMF.

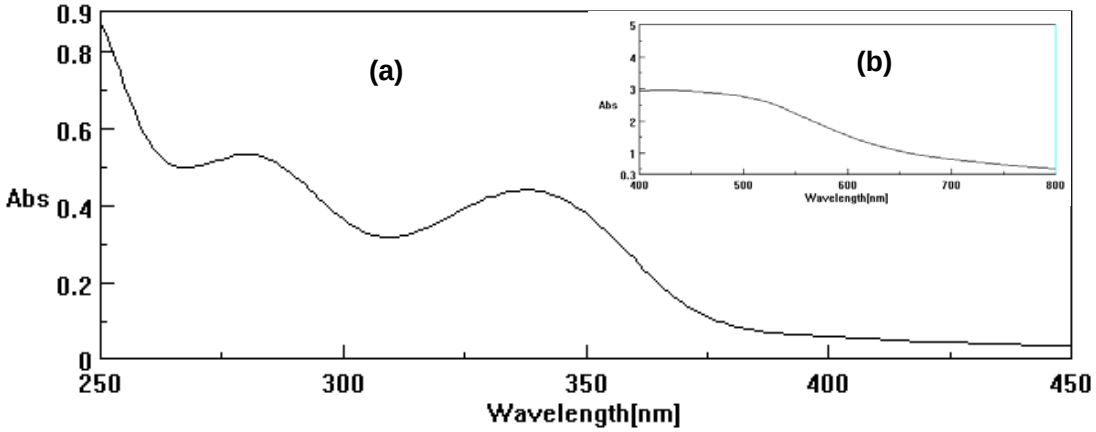

Figure VIII.26. UVi-vis absorption spectra of [Mn(AcO)(MCFA)], **6**, (a) 10^{-4} M in $CHCl_3$, (b) 10^{-2} M in $CHCl_3$.

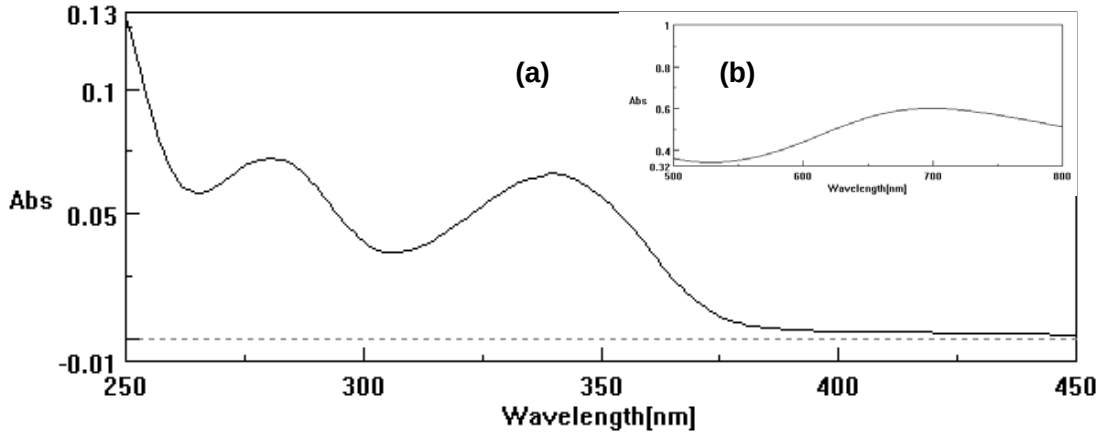

Figure VIII.27. UV-vis absorption spectra of [Cu(AcO)(MCFA)], **7**, (a) 10^{-4} M in $CHCl_3$, (b) 10^{-2}M in $CHCl_3$.

VIII.3.4. Mass spectroscopy.

ESI and APCI generate primarily: molecular ions M^+ or M^-, protonated molecules $[M + H]^+$, simple adduct ions $[M + Na]^+$, ions representing simple losses such as the loss of a water $[M + H - H_2O]^+$ The techniques requires polar solvents. For ionization eithre acetonitrile, methanol or mixtures of acetonitrile/water, methanol/water, were used. The ESI-MS spectrum of $[Cu(MCFA)_2]$ (653.8) shows peak at m/z = 652.3. In the case of $[Cu(AcO)(MCFA)(H_2O)_2]$ (453.7), m/z = 454.1 has been found. Moreover $[Zn(MCFA)_2(H_2O)_4]$ (727.6) formula is confirmed by molecular ion peak at m/z = 728.2

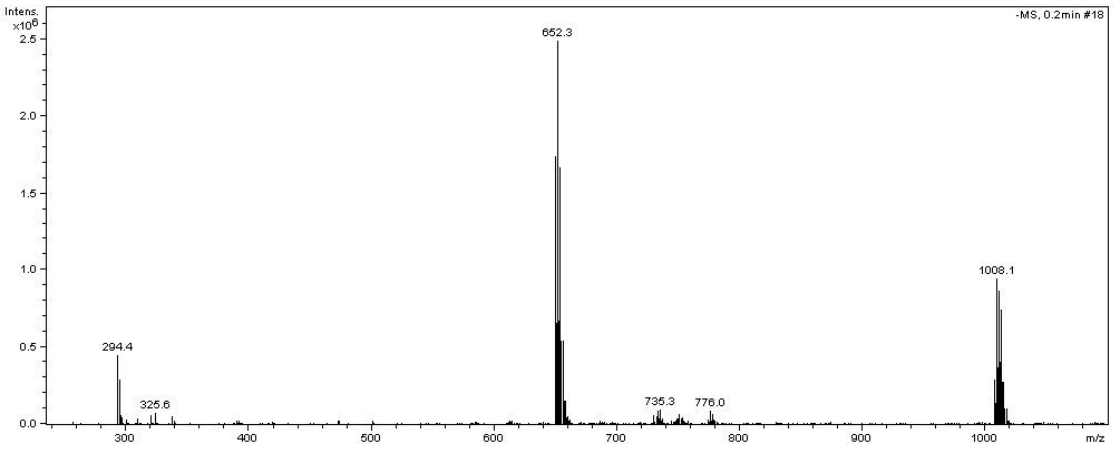

Figure VIII.28. ESI-MS spectrum of deprotonated complex $[Cu(MCFA)_2]$, **3** in CH_3OH.

Conclusions (Chapter VIII)

The synthesis and characterization of eight new meclofenamic acid complexes with Mn^{2+}, Cu^{2+}, Zn^{2+}, Cd^{2+} have been reported. In all complexes, meclofenamic acid acts as bidentate ligand bound to the metal ion through the oxygen atoms of the carboxylate group. In the series of complexes with 1:2 metal to ligand molar ratio two meclofenamic acid molecules and solvent molecules are coordinated to the metal ions. In the series of complexes with 1:1 metal to ligand molar ratio one meclofenamic acid molecule, acetate group and solvent molecules are coordinated to the metal ions. The presence of acetate group is confirmed by one singlet at ca. 1.85 ppm in ^{1}H–NMR spectra of complexes **8** and **9** and by two resonances attributed to the acetate carbons at ca. 22. ppm and 176 -178 ppm in ^{13}C-NMR spectra of complexes **8** and **9**. Monomeric six-coordinated species were isolated in the solid state for $[Mn(MCFA)_2]$, **2**, $[Zn(MCFA)_2(H_2O)_4]$, **4** and $[Cd(MCFA)_2(H_2O)_4]$, **5,** monomeric five-coordinated species for $[Cu(MCFA)_2(H_2O)]$, **3**.

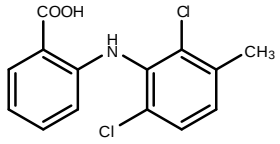

Meclofenamic acid
RCOOH

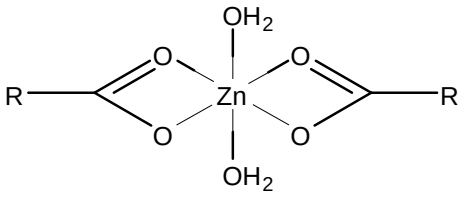

4

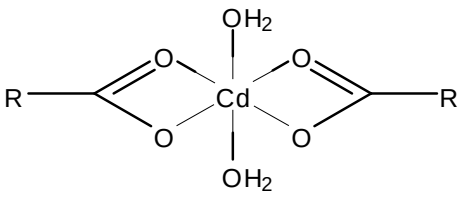

5

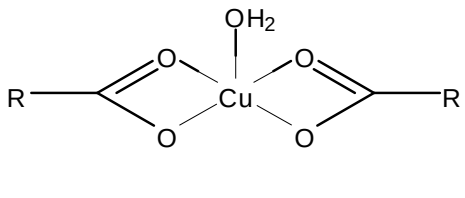

3

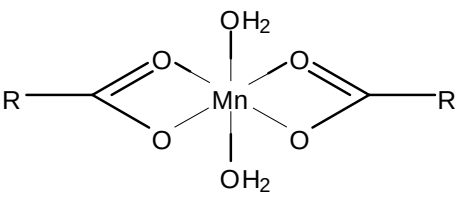

2

References

1. Kaltenbrom, J.S., Scherrer, R.A., Short, F.W., Beatty, H.R., Saka, M.M., Winder, C.W., Wax, J., Williamson, W.R.N. *Arzneim. Forsch.* **33,** 621 (1983).
2. Kovala-Demertzi, D., Dokorou, V., Primikiri, A., Vargas, R, Silvestru, C., Russo, U., Demertzis, M.A., *Journal of Inorganic Biochemistry* **103,** 738–744 (2009).
3. a) Kovala-Demertzi, D.,Hadjipavlou-Litina, D., Staninska, M., Primikiri, A., Kotoglou, C. Demertzis, M.A, *Journal of Enzyme Inhibition and Medicinal Chemistry* **24,**742 — 752 (2009)
   b) Kovala-Demertzi, D.,Hadjipavlou-Litina, D., Primikiri, A., Staninska, M., Kotoglou, C. Demertzis, M.A, *Chemistry&Biodiversity* **6,** 948-960 (2009).
4. a) Munro, S.L.A., Craik, D.J. *Magnetic resonance in chemistry* **32,** 335-342 (1994).
   b) Kovala-Demertzi, D., Kourkoumelis, N., Koutsodimou, A., Moukarika, A., Horn, E., Tiekink, E.R.T. *Journal of Organometallic Chemistry* **620 ,** 194–201 (2001).
5. Stamatatos, T.C., Vlahopoulou, J.C., Tangoulis, V., Raptopoulou, C.P.,, Terzis, A., Papaefstathiou, G.S., Perlepes, S.P., *Polyhedron* **28,** 1656–1663 (2009).
6. Lörinc, S., Švorec, J., Melník, M. Koman, M., *Polyhedron* **27,** 3545–3548(2008).
7. a) Lazarou, K.N., Psycharis, V., Perlepes, S.P., Raptopoulou , C.P. *Polyhedron* **28,** 1085–1096 (2009).
   b) Stamatatos, T.S., Vlahopoulou, J.C., Tangoulis, V., Raptopoulou , C.P., Terzis, A., Papaefstathiou, G.S.,Perlepes, S.P., *Polyhedron* **28,** 1656–1663 (2009).
   c) Stoumpos, C.C., Gass, I.A., Milios, C.J., Lalioti, N., Terzis, A., Simon , G.A., Teat, J., Brechin, E.K., Perlepes, S.P.,*Dalton Trans.* 307–317 (2009).
8. Kovala-Demertzi, D., Theodorou, A., Demertzis, M.A., Raptopoulou, C.,, Terzis, A. *J. Inorg.Biochem.* **5,** 151 (1997).
9. Kovala-Demertzi, D., Hadjikakou, S.K., Demertzis, M.A., Deligiannakis, Y., *J. Inorg. Biochem.* **69,** 223 (1998).
10. Nakamoto K. *Infrared and Raman spectra of inorganic and coordination compounds.* 4th ed. New York: Wiley;1986
11. Szymanska, B. Skrzypek, D., Kovala-Demertzi D, Staninska M., Demertzis M.A. *Spectrochimica Acta Part A* **63,** 518–523 (2006).
12. Lever, A.B.P. *Inorganic Electronic Spectroscopy* **2nd edn**., Elsevier, Amsterdam 480–505 (1984).
13. Bury, A.,Underhill, A.E. *Inorganica Chimica* Acta, **52,** 171-175 (1988).

IX Synthesis and characterization of manganese(II), copper(II), zinc(II) and cadmium(II) complexes with (N-[3-(trifluoromethyl)-phenyl]-anthranilic acid), flufenamic acid (10).

IX.1. General

The synthesis of first and second row-block-d divalent metal ion complexes with ''fenamates'' family anti-inflammatory drugs were previously reported.[1,2] The reactions of manganese(II)-, copper(II)-, zinc(II)-, cadmium(II)-acetates and/or cadmium(II)-chloride with the anti-inflammatory drug flufenamic acid, (Hffa), (N-[3-(trifluoromethyl)-phenyl]-anthranilic acid) in methanol produced micro-crystalline solids, powder-like solids, **table IX.1** (metal to ligand molar ratio 1:2), (**table IX.2**) (metal to ligand molar ratio 1:1).

Table IX.1. Analytical and physical data of the flufenamic acid complexes.

	Compounds	M.W g/mol	mp(˚C)	Colour	C%	H%	M%
10	Hffa	281.23	130-132°C	white			
11	$[Mn(FFA)_2(H_2O)]$	615.352	85°C	pale yellow	53.10 (52.78)	3.18 (3.43)	8.67 (10.7±1.4)
12	$[Cu(FFA)_2]$	623.960	230°C (dec)	blue	53.90 (53.77)	2.90 (2.79)	10.18 (11.2±1.1)
13	$[Zn(FFA)_2(H_2O)_2]$	629.822	170°C	white	50.82 (49.61)	3.35 (2.81)	9.88 (8.7±1.6)
14	$[Cd(FFA)_2(H_2O)_2]$	708.840	80°C	white	47.44 (47.21)	2.69 (3.13)	15.86 (14.0±2.7)

Results of elemental analysis: calculated, (found).

Table IX.2. Analytical and physical data of the flufenamic acid complexes.

	Complexes	M.W g/mol	mp ˚C	Colour	C%	H%	M%
15	$[Mn(FFA)(AcO)(H_2O)_3]$ [a]	448.200	110°C	off white	42.88 (42.93)	4.04 (3.76)	12.26 (10.0±1.0)
16	$[Cu(AcO)(FFA)]$[a]	402.784	>300°C (dec)	green			16.78 (16.9±2.0)
17	$[Zn(AcO)(FFA)]$[a]	404.618	79-81°C	off white			16.16 (19.2±3.0)
18	$[Cd(AcO)(FFA)]$[a]	451.648	>300°C (dec)	white			24.89 (20.4±2.9)

Results of elemental analysis: calculated, (found).

[a] Ac = CH_3CO

The complexes$[Mn(FFA)_2(H_2O)]$ **11**, $[Cu(FFA)_2]$ **12**, $[Zn(FFA)_2(H_2O)_2]$ **13**, $[Cd(FFA)_2(H_2O)_2]$ **14**, were synthesized according to the reactions (a) – (d). The complexes [Mn(AcO)(FFA)] **15**, [Cu(AcO)(FFA)] **16**, $[Zn(AcO)(FFA)(H_2O)_4]$ **17**, $[Cd(AcO)(FFA)(H_2O)_4]$ **18**, were synthesized according to the reactions (e) – (h). The complexes are stable in the air. All the complexes are insoluble in water, except of cadmium complexes **14**, **18** which are slight soluble in water. All the

complexes are soluble in polar solvents as DMFand DMSO and are slightly soluble in nonpolar solvents as $CHCl_3$, CH_2Cl_2.

$Mn(AcO)_2 + 2\ Hffa \rightarrow [Mn(ffa)_2(H_2O)] + 2\ AcOH$ (a)

$Cu(AcO)_2 \cdot H_2O + 2\ Hffa \rightarrow [Cu(ffa)_2] + 2\ AcOH + H_2O$ (b)

$Zn(AcO)_2 \cdot 2\ H_2O + 2\ Hffa \rightarrow [Zn(ffa)_2(H_2O)_2] + 2\ AcOH$ (c)

$Cd(AcO)_2 \cdot 2\ H_2O + 2\ Hffa \rightarrow [Cd(ffa)_2(H_2O)_2] + 2\ AcOH$ (d)

$Mn(AcO)_2 + Hffa \rightarrow [Mn(AcO)(ffa)(H_2O)_3] + AcOH$ (e)

$Cu(AcO)_2 \cdot H_2O + Hffa \rightarrow [Cu(AcO)(ffa)] + AcOH + H_2O$ (f)

$Zn(AcO)_2 \cdot 2\ H_2O + Hffa \rightarrow [Zn(AcO)(ffa)] + AcOH$ (g)

$Cd(AcO)_2 \cdot 2\ H_2O + Hffa \rightarrow [Cd(AcO)(ffa)] + AcOH$ (h)

Table IX.3. Solubility test of **11** – **18** complexes and parent drug **10**.

	H_2O	n-pentane	n-hexane	Et_2O	CH_3NO_2	CH_3CN	cyclohexane	methanol	ethanol	acetone	toluene	benzene	THF	DMF	DMSO	CH_2Cl_2	$CHCl_3$
10	-	-	-	-	+/-	+/-	-	+	+	+/-	+/-	+/-	+/-	+	+/-	+/-	+/-
11	-	+/-	+/-	+/-	+/-	+/-	+/-	+	+/-	+	+	+	+	+	+	+	+
12	-	+/-	+/-	+/-	+	+	+/-	+	+	+/-	+	+	+	+	+	+/-	+/-
13	-	-	-	-	-	-	-	-	-	-	-	-	-/+	+	+	+/-	+/-
14	+/-	-	-	-	-	-	-	-	-	-	-	-	+/-	+	+	+/-	+/-
15	-	+/-	+/-	+/-	+/-	+/-	+/-	+/-	+/-	+/-	+/-	+/-	+	+	+	+/-	+/-
16	-	-	-	-	+/-	+/-	-	+	+/-	+/-	+/-	+/-	+/-	+	+	+/-	+/-
17	-	-	-	-	-	-	-	-	-	-	-	-	-	+/-	+	+/-	+/-
18	+/-	-	-	-	-	-	-	-	-	-	-	-	+/-	+	+	+/-	+/-

+ soluble; +/- slightly soluble; - insoluble.

IX.2. Spectroscopic characterization of Mn(II), Cu(II), Zn(II) and Cd(II) complexes with flufenamic acid (10).

IX.2.1. Nuclear Magnetic Resonance

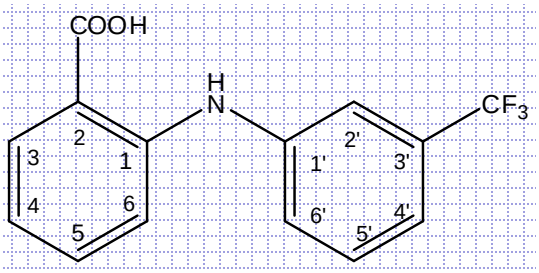

Figure IX.1. Structural formule of flufenamic acid, **10**.

The ^{1}H and ^{13}C signals were assigned using one- and two-dimensional $^{1}H–^{1}H$ COSY, $^{1}H–^{13}C$ HSQC, $^{1}H–^{13}C$ HMBC spectra. The ^{1}H and ^{13}C NMR data for flufenamic acid (**figure IX.1.**) and the complexes are summarized in **table IX.4.** and **table IX.5.** These results, together with the published data[3] on flufenamic acid allowed complete assignment of all signals in the spectra of both the flufenamic acid and its zinc complexes. In order to investigate the behaviour of the compounds in solution similar to those, used for the biological studies, all solutions were prepared mostly in DMSO-d_6. The downfield chemical shift for HN in flufenamic acid indicates that this proton is involved in hydrogen bonding. The crystal structure of flufenamic acid suggests the presence of hydrogen-bonded dimers linked by two intermolecular O–H–O hydrogen bonds and an intramolecular hydrogen bond between the HN group and the carbonyl group of the carboxyl acid.The NH peak is a sharp singlet at approximately 10.0 ppm in the ^{1}H–NMR spectra of flufenamic acid.The existence of the HN resonance indicates that the nitrogen atoms remain protonated in **13**, **17** and **14**, **18**.[3] The small downfield shift (0.25 ppm) of the NH resonance in $CDCl_3$ solution suggests that no significant participation in intermolecular hydrogen-bonding takes place.The greatest downfield shift by 1.19 ppm and 1.10 ppm occurs for NH resonance in DMSO-d_6 solution for cadmium complexes **14** and **18** respectively. The furthest downfield peak is assigned as H-3 due to its proximity to the carboxylic acid group in the ^{1}H spectrum of free drug. In ^{1}H-NMR spectra of **13**, **17** and **14**, **18** H(4), H(6), signals shift are upfield. The resonance H(3), by contrast, shifts downfield in ^{1}H spectrum of zinc complexes **13**, **17** and cadmium complexes **14**, **18** in DMSO-d_6. For **17** and **18** one singlet appears at 2.07 ppm and 1.86, thus in the region of proton of acetate group. Two resonances attributed to the acetate carbons are found at 23.4 ppm, 181.1 ppm in ^{13}C-NMR spectrum of **17** and also are found at 22.0 ppm, 178.0 ppm in ^{13}C-NMR spectrum of **18**. Involvement of the carboxyl group in bonding to Zn and Cd atoms is confirmed by the resonance ascribed to C1, which exhibits shift upon coordination.[10] The remaining resonances due to the aromatic carbon atoms for **13**, **17** and **14**, **18** do not shift considerably after binding to Zn and Cd atoms with C4 exhibiting the greatest downfield shift (2.5 ppm) for **13** and with C2 exhibiting the greatest downfield shift (2.6 ppm) for **17**. In ^{13}C spectrum of flufenamic acid and its zinc and cadmium complexes **13**, **17** and **14**, **18** in the case of the signal emerging at approximately 122-124 ppm, which is attributed to carbon of CF_3 group.

Table IX.4. ^{1}H NMR shifts of **13**, **14**, **17**, **18** complexes and parent drug **10** (δ in ppm and *J* in Hz).

	10[a]	**10**[b]	**13**[a]	**13**[b]	**17**[a]	**17**[b]	**14**[a]	**18**[a]

OH	13.11s	d	**-**	**-**		**-**	-	-
NH	9.68s	9.39s	10.64s	9.64s	10.60s	9.75s	10.87s	10.78s
H – C(3)	7.94dd J(3-4)=7.9 J(3-5)=1.5	8.09dd J(3-4)=8.1 J(3-5)=1.4	8.08d J(3-4)=7.6	8.00d J(3-4)=7.6	8.02d J(3-4)=7.2	7.98d J(3-4)=6.0	8.10d J(3-4)=7.5	8.05d J(3-4)=7.5
H – C(4)	6.88t J(4-5)=7.7	6.84t J(4-5)=7.7	6.84t J(4-5)=6.9	6.63t	6.83t	6.57m	6.85t J(4-5)=5.8	6.83t J(4-5)=6.6
H – C(6)	7.29d	7.29d J(6-5)=6.9	7.20d J(6-5)=5.6	7.20d J(6-5)=6.7	7.21s	6.84m	7.22d J(6-5)=6.4	7.22d J(6-5)=5.9
H – C(5)	7.27 – 7.55m[c]	7.32 – 7.51m[c]	7.31 – 7.34m[c]	7.21 – 7.34m[c]	7.21 – 7.50m[c]	7.00 – 7.33m[c]	7.31– 7.51m[c]	7.29– 7.47m[c]
H – C(2')								
H – C(4')								
H – C(5')								
H – C(6')								
CH_3 COO	**-**	**-**	**-**	**-**	2.07s	2.07s	-	1.86s

[a] Spectrum recorded in DMSO-d_6
[b] Spectrum recorded in $CDCl_3$
[c] Resonances are heavily overlapped, forming a complex multiplet.
[d] Carboxyl proton exchanged in $CDCl_3$

Table IX.5. ^{13}C NMR shifts (ppm) of **13**, **14**, **17**, **18** complexes and parent drug **10**.

	10[a]	**10[b]**	**13[a]**	**13[b]**	**17[a]**	**17[b]**	**14[a]**	**18[a]**
COOH	169.6	174.0	173.2	175.4	173.1	175.5	173.3	173.3
C1	145.4	147.5	144.6	146.0	144.8	145.5	144.4	144.3
C2	114.4	111.4	114.5	114.1	114.8	114.0	114.3	114.4
C3	132.8	132.8	132.4	132.0	132.6	132.9	132.1	132.1
C4	116.2	118.4	118.7	118.1	117.8	117.3	117.3	117.3
C5	134.1	136.5	132.9	133.7	133.1	133.6	133.0	132.9
C6	114.8	114.2	115.0	116.2	115.2	116.4	114.6	114.5
C1'	141.9	141.2	143.0	141.8	143.2	142.1	143.0	142.9
C2'	118.7	118.4	119.4	118.6	119.0	117.9	118.6	118.6
C3'	131.9	132.0	130.7	131.0	130.9	130.7	130.5	130.6
C4'	121.8	120.2	122.1	121.8	119.8	121.9	119.5	119.6
C5'	130.5	130.0	130.5	129.6	130.4	129.3	130.1	130.0
C6'	126.2	125.3	126.5	126.1	126.1	126.2	126.3	126.3
CF_3	123.7	121.7	122.6	124.2	122.8	123.5	122.3	122.3
CH_3COO	-	-	-	-	22.9 177.6	23.4 181.1	-	22.0 178.0

[a] Spectrum recorded in DMSO-d_6
[b] Spectrum recorded in $CDCl_3$

Figure IX.2. ^{1}H-NMR spectrum of [Zn(FFA)$_2$(H$_2$O)$_2$], **13** recorded in dmso-d_6.

Figure IX.3. ^{13}C-NMR spectrum of [Zn(FFA)$_2$(H$_2$O)$_2$], **13** recorded in dmso-d_6.

Figure IX.4. ^{1}H-NMR spectrum of [Zn(AcO)(FFA)], **17** recorded in $CDCl_3$.

Figure IX.5. ^{13}C-NMR spectrum of [Zn(AcO)(FFA)], **17** recorded in $CDCl_3$.

Figure IX.6. ^{1}H-NMR spectrum of [Cd(FFA)$_2$(H$_2$O)$_2$], **14** recorded dmso-d_6.

Figure IX.7. ^{13}C-NMR spectrum of [Cd(FFA)$_2$(H$_2$O)$_2$], **14** recorded dmso-d_6.

Figure IX.8. ^{1}H-NMR spectrum of [Cd(AcO)(FFA)], **18** recorded dmso-d_6.

Figure IX.9. ^{13}C-NMR spectrum of [Cd(AcO)(FFA)], **18** recorded in dmso-d_6..

2D $^{1}H–^{1}H$ shift correlated spectra (COSY), 2D cross-peaking of heteronuclear single quantum correlation (HSQC) and heteronuclear multiple bond correlation (HMBC) gradient-assisted spectra of **13** were performed in order to completely assign the resonances in zinc complex of flufenamic acid.

A listing of 2D $^{1}H–^{1}H$ (COSY), 2D $^{1}H–^{13}C$ (HSQC), 2D $^{1}H–^{13}C$ (HMBC) connectivity for complex **13** is provided in **table IX.6**, **table IX.7**, **table IX.8**. The ^{1}H-NMR spectra of **13** shows five distinct signals, respectively. In the region characteristic of aromatic protons (6.63–8.10 ppm) signals are found. In the region corresponding to the signals of aromatic rings carbons (110-150 ppm) signals are observed. However it is not possible to assign explicitly the signals to each of all aromatic systems present in the molecule. In complex, there is one signal due to the imine proton NH resonance at ca. 10.6 ppm in ^{1}H NMR spectrum. The carbon of CF_3 group is confirmed by ^{13}C-NMR spectra.

2D $^{1}H–^{1}H$ (COSY) spectrum shows correlation between coupled protons thus give rise to off-diagonal or cross-peaks for all protons that have significant(measurable) J-J coupling. In the COSY spectrum of **13**, as expected H(4) is coupled to both H(5) and H(3), H(6) is coupled to H(5) as well C. Beside it is not possible to assign explicitly cross-peaks because the resonances of the aromatic protons are heavily overlapped, forming a complex multiplet.

2D $^{1}H–^{13}C$ (HSQC) spectrum shows correlation between directly attached (one-bond) proton-carbon. C In the 2D $^{1}H–^{13}C$ (HSQC) spectrum of **13** the signals of the H(3) and H(4) protons ard detected at ca. 133 ppm and ca. 118 ppm, respectively and assigned through the shift correlation peaks with C3 and C4 carbon atoms. Moreover correlation peaks of C2 and H(2), C6 and H(6), C2’ and H(2’), C3’ and H(3’), C4’ and H(4’), C5’ and H(5’),are observed.

2D $^{1}H–^{13}C$ (HMBC) spectrum shows correlation between long-range (two, three and four-bonds) proton-carbon couplings.C In the 2D $^{1}H–^{13}C$ (HMBC) spectrum of **4** carbon atom C1’ (at ca. 143 ppm) of carboxyl-bearing ring displayed a coupling to H(6) proton of the methyl-bearing ring. Imine proton NH connect through aromatic ring to the carbons C1, C1’, C2, C2’, C3, C5, C6 of both aromatic rings followed on the basis of coupling patterns The remaining carbons of the aromatic rings may then be assigned to protons in the fashion described above.In general, the carbons of each aromatic ring showed connectivity to protons of each aromatic ring.

Table IX.6. 2D$^{1}H,^{1}H$-COSY NMR data of $[Zn(FFA)_2(H_2O)_2]$, **13**[a].

1	2	3	4	5	6
H4 – H5	H4 – H3	H6 – H5	H4 – H6	H4’ – H6’	H3 – H5

[a] spectrum recorded in DMSO-d_6

Table IX.7. 2D$^{1}H,^{13}C$-HSQC NMR data of $[Zn(FFA)_2(H_2O)_2]$, **13**[a].

1	2	3	4	5	6
C2 – H2 C6 – H6	C4 – H4	C2’ – H2’	C4’ – H4’	C3’ – H3’ C5’ – H5’	C3 – H3

[a] spectrum recorded in DMSO-d_6

Table IX.8. 2D^{1}H,^{13}C-HMBC NMR data of[Zn(FFA)$_2$(H$_2$O)$_2$], **13**[a].

1	C2 – H5 C6 – H5	12	C1' – H4' C1' – H5' C1' – H2' C1' – H6'
2	C2 – H4 C6 – H4	13	C1 – H3
3	C4 – H5	14	C1 – H5
4	C2' – H4' C2' – H6'	15	C2 – H(NH)
5	C4 – H4	16	C2' – H(NH)
6	C6' – H4' C6' – H5' C6' – H2'	17	C6 – H(NH)
7	C3 – H4 C5 – H4	18	C3 – H(NH) C5 – H(NH)
8	C3 – H5	19	C1' – H(NH)
9	C5 – H3	20	C1 – H(NH)
10	C1 – H4	21	C2 – H3
11	C1' – H6	22	C4 – H3

[a] spectrum recorded in DMSO-d_6

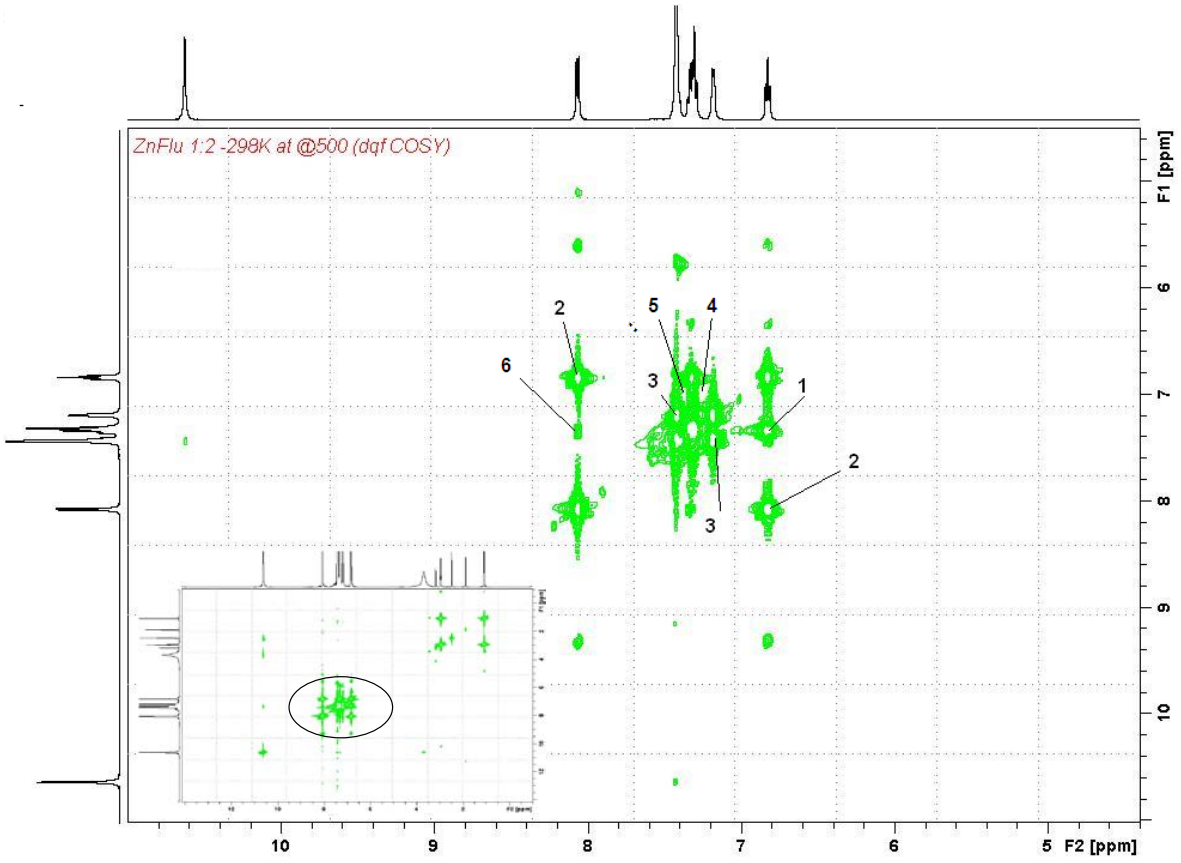

Figure IX .10. 2D^{1}H,^{1}H-COSY NMR spectrum of [Zn(FFA)$_2$(H$_2$O)$_2$], **13** recorded in dmso-d_6.

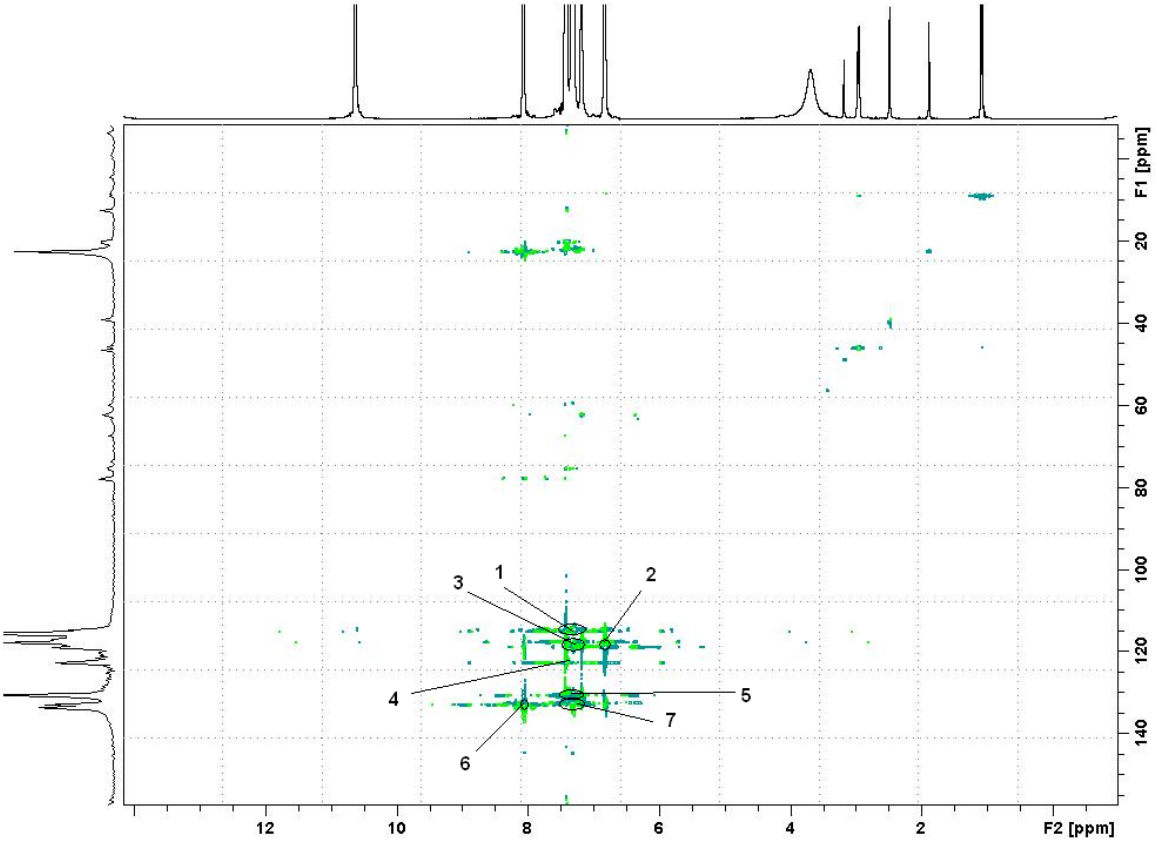

Figure IX.11. 2D^{1}H,^{13}C-HSQC NMR spectrum of [Zn(FFA)$_2$(H$_2$O)$_2$], **13** recorded in dmso-d_6.

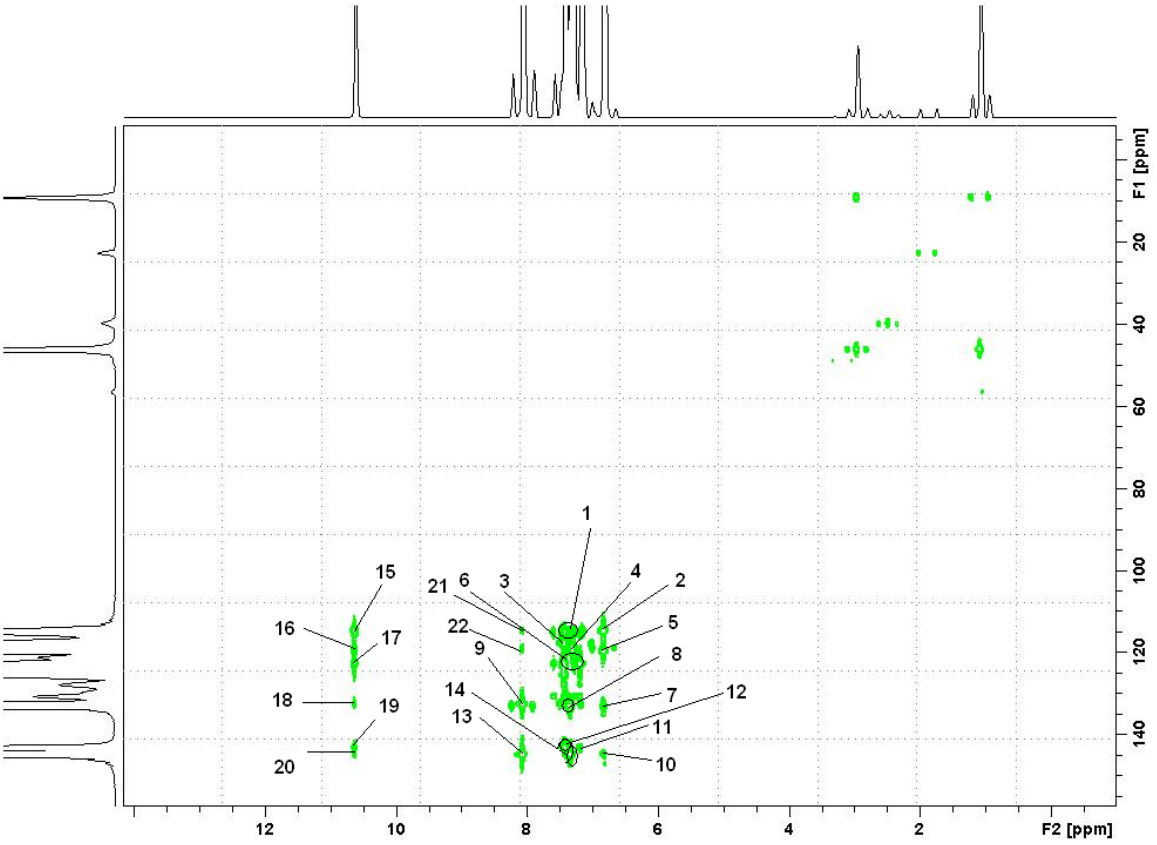

Figure. IX.12. 2D^{1}H,^{13}C-HMBC NMR spectrum of [Zn(FFA)$_2$(H$_2$O)$_2$], **13** recorded in dmso-d_6.

IX.2.2. Infrared spectroscopy.

Table IX.9. IR-data (cm^{-1}) for the prepared complexes **11 – 14**.

Compounds	νNH	Carboxylic groups		Δν	νM - O_{OCO}	νM – O_{H20}
		ν_{asym} (COO^-)	ν_{sym} (COO^-)			
Hffa	3322s	1655s	1493m	162	-	-
$[Mn(FFA)_2(H_2O)]$	3278m	1583m	1462m	121	248ms	399mw
$[Cu(FFA)_2]$	3332m	1583m	1458m	125	248mw	394m
$[Zn(FFA)_2(H_2O)_2]$	3314s	1583m	1462m	121	249ms	399mw
$[Cd(FFA)_2(H_2O)_2]$	3332s	1584s	1460m	124	253ms	398mw

s = strong, m = medium, w = weak, sh = sharp, br = broad

Table IX.10. IR-data (cm^{-1}) for the prepared complexes **15 - 18**.

Compounds	νNH	Carboxylic groups		Δν	νM - O_{OCO}	νM – O_{H20}
		ν_{asym} (COO^-)	ν_{sym} (COO^-)			
$[Mn(AcO)(FFA)(H_2O)_3]$	3339m	1584s	1459m	125	245ms	398ms
[Cu(AcO)(FFA)]	3270m	1582s	1451m	131	247m	396m
[Zn(AcO)(FFA)]	3296m	1587s	1460m	127	249ms	398mw
[Cd(AcO)(FFA)]	3520w	1581s	1457m	124	253ms	396mw

s = strong, m = medium, w = weak, sh = sharp, br = broad

The infrared spectra for all the metal derivatives exhibit remarkable similarity. In the IR spectrum of Hffa, the strong band at 3322 cm^{-1} was assigned to the N–H stretching motion, and the broad band at ca. 2867 cm^{-1} to the ν(NH•••O) and ν(OH•••O) mode due to intra- and intermolecular H-bonding[3]. The IR spectra of **11 – 14** and **15 – 18** show two absorption bands at approximately 3300 and 3100 cm^{-1}. These bands correspond to the antisymmetric and symmetric OH stretch and confirm the presence of water in the complexes. Moreover, the IR spectrum exhibits characteristic bands at approximately 860 and 560 cm^{-1} assigned to the rocking and wagging mode of the coordinated water molecule[4]. As the carboxyl hydrogen is more acidic than the amino hydrogen the deprotonation occurs in the carboxylic group. This is confirmed by the IR spectra of the complexes, showing the characteristic bands for the secondary amino groups and for the coordinated carboxylato group. The absence of large systematic shifts of the ν(NH) and δ(NH) bands in the spectra of the complexes **11 – 14** and **15 – 18** compared with those of the ligand indicates that there is no interaction between the NH group and the metal ions[3]. Each complex showed carboxylate stretching frequencies, $\nu_{asym}(COO^-)$ and $\nu_{sym}(COO^-)$ are in the expected region (**table IX.9. table IX.10.**).The $\nu_{asym}(COO^-)$ and $\nu_{sym}(COO^-)$ bands of the prepared complexes **11 – 14 and 15 – 18** appear at 1611-1583 and at 1515-1450 cm^{-1} respectively. The difference between the asymmetric and symmetric stretching vibration $\Delta\nu = [\nu_{asym}(COO^-) - \nu_{sym}(COO^-)]$ (**Table**) gives information on the carboxylate bonding mode. However, splitting of the bands assigned to $\nu_s(COO^-)$ indicates that the fenamate anion as a ligand in **11 – 14** and **15 – 18 c**omplexes is coordinated through bidentate carboxyl group. Δν value for **11 – 14** complexes is significantly less than the ionic value (for sodium mefenamic the Δν value is 180cm^{-1}), as expected for the bidentate chelating mode of carboxylate ligation. The

medium bands at approximately 400 cm^{-1} is attributed to the $\nu(M\text{-}O_{H2O})$ stretching mode, while the bands at 250-280cm^{-1} are assigned to the $\nu(M\text{-}O_{oco})$ stretching mode.[1,2,4]. The fluorinated alkane group CF_3 absorbs strongly in the region 1350-1120 cm^{-1}.

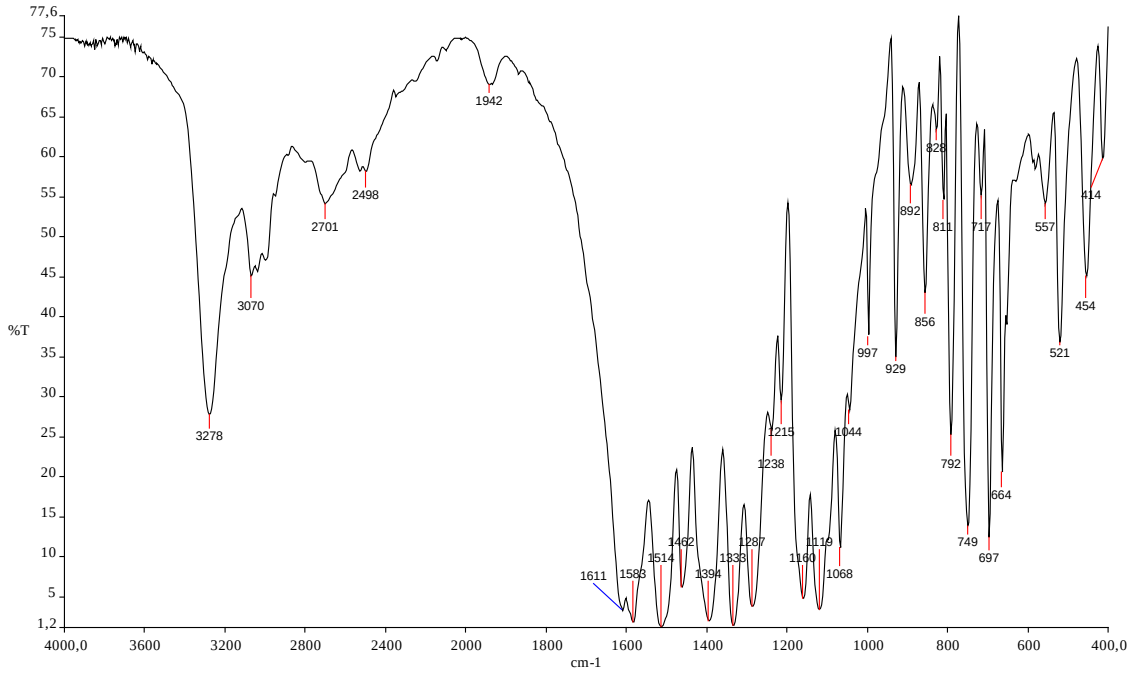

Figure IX.13. Infrared spectrum of $[Mn(FFA)_2(H_2O)]$, **11**.

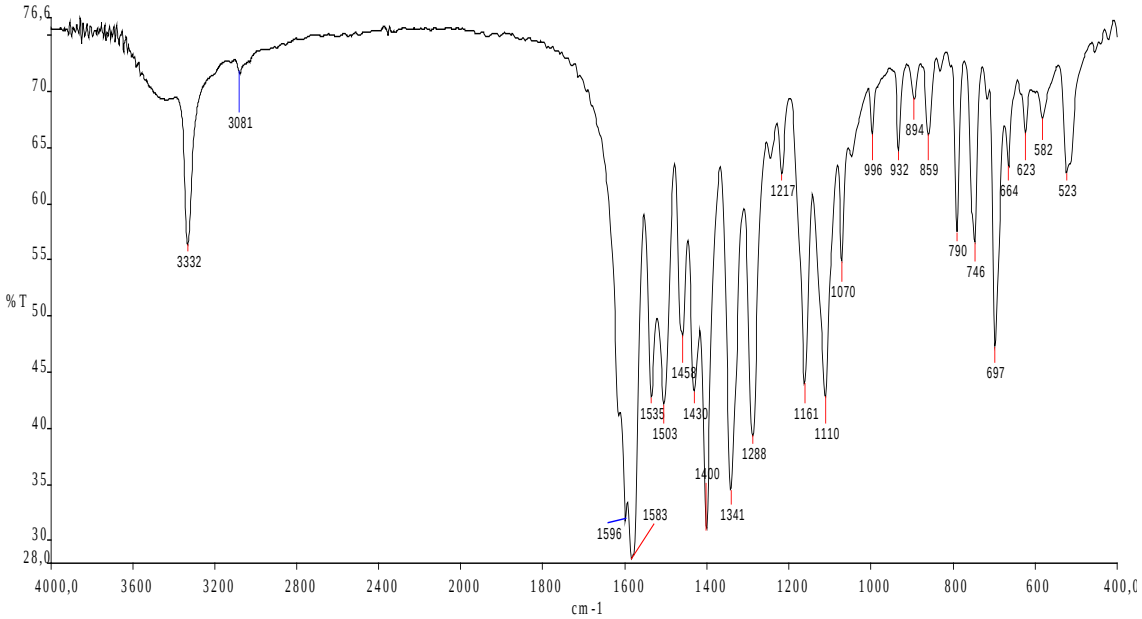

Figure IX.14. Infrared spectrum of $[Cu(FFA)_2]$, **12**.

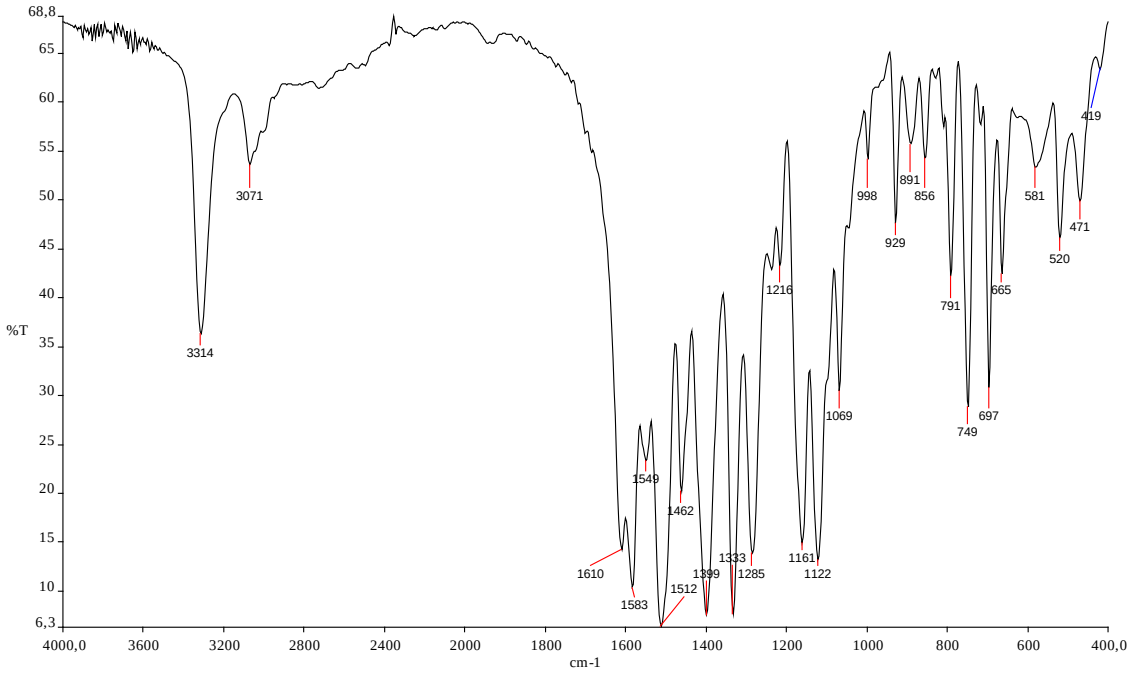

Figure IX.15. Infrared spectrum of $[Zn(FFA)_2(H_2O)_2]$, **13**.

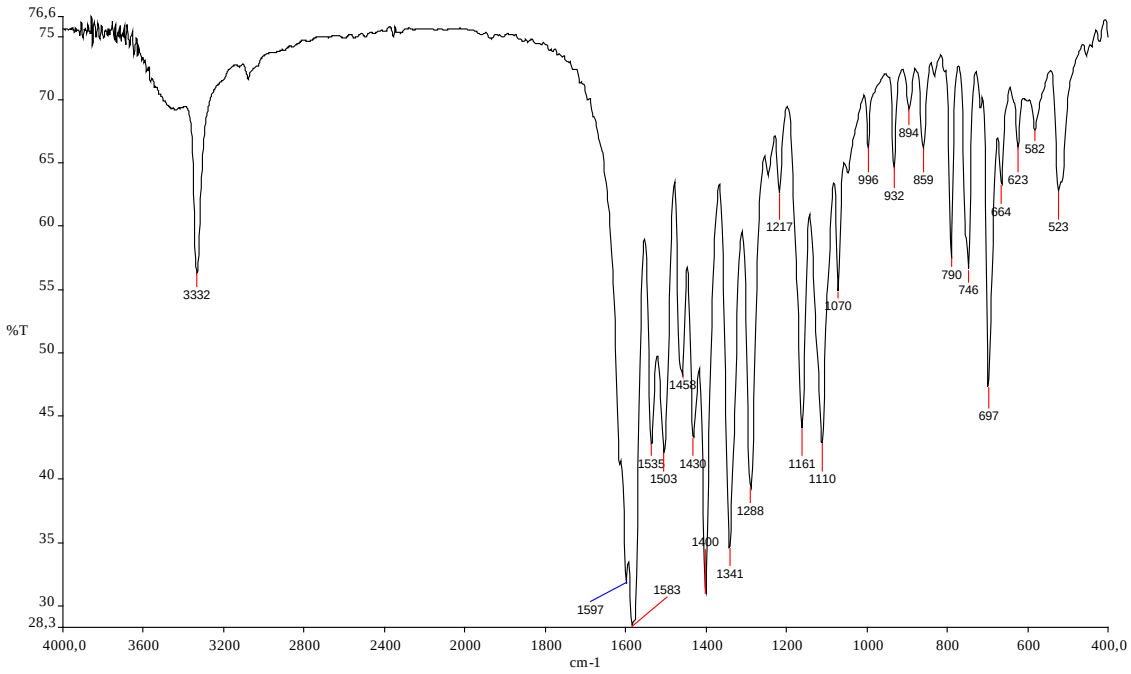

Figure IX.16. Infrared spectrum of $[Cd(FFA)_2(H_2O)_2]$, **14**.

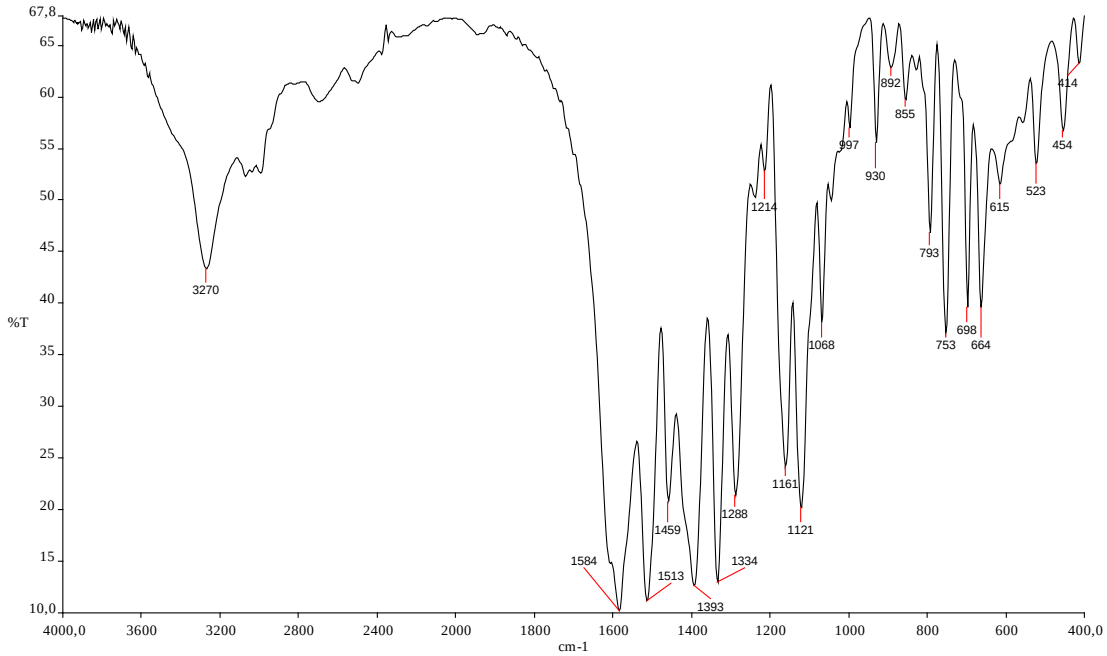

Figure IX.17. Infrared spectrum of [Mn(AcO)(FFA)(H_2O)$_3$], **15**.

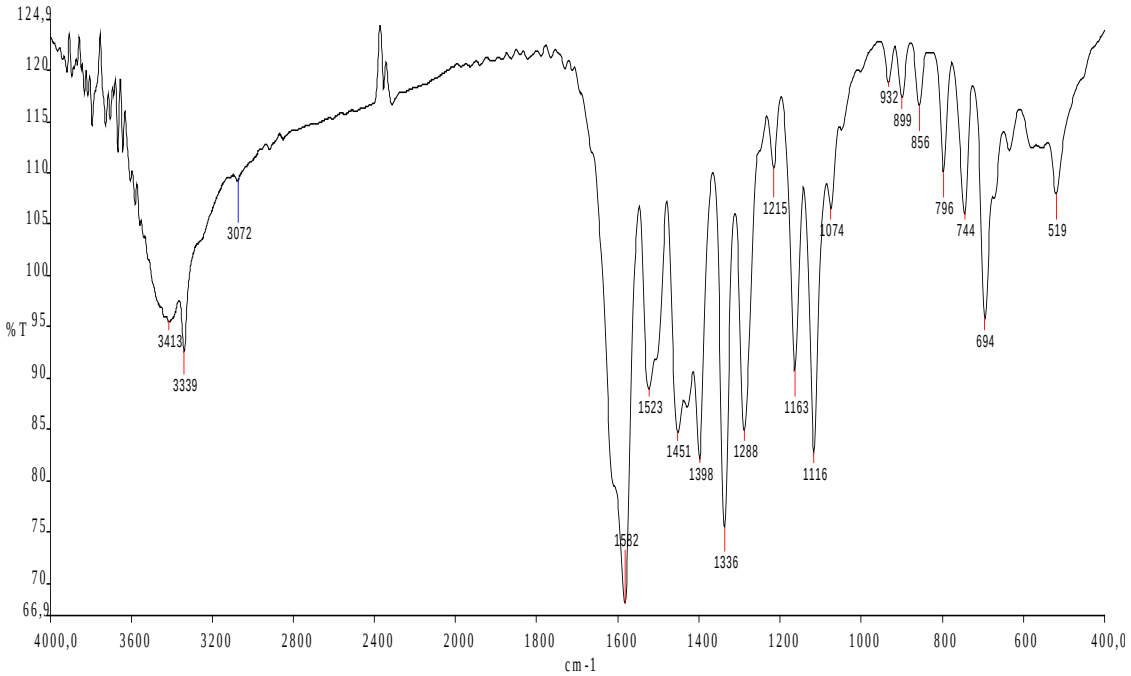

Figure IX.18. Infrared spectrum of [Cu(FFA)(AcO)], **16**.

IX.2.3. Electronic spectroscopy.

Table IX.11. Spectral data (UV-vis) for the prepared complexes **11**, **12**, **15**, **16** and the parent drug **10**.

Compounds	μ_{eff}	$CHCl_3$			DMF			Assignments
		λ (nm)	ν (cm^{-1})	log ε	λ (nm)	ν (cm^{-1})	log ε	
Flufenamic acid (Hffa)		351	28.490	3.76	338 (sh)	29.586	3.89	n → π*
		290	34.483	4.01	291	34.364	4.21	π → π*
$[Mn(FFA)_2(H_2O)]$	6.02	492 (sh)	20.325	1.64	483	20.704	1.64	$^6A_{1g} \rightarrow {}^4T_{2g}$ (G)
		347	28.818	4.11	362 (sh)	27.624	3.36	n → π*
		291	34.364	4.39	294	34.014	4.52	π → π*
$[Cu(FFA)_2]$	2.19	697	14.347	1.94	741	13.495	2.26	d – d
		345	28.986	3.09	334 (sh)	29.940	4.20	n → π*
		291	34.364	4.19	293	34.130	4.49	π → π*
$[Mn(FFA)(AcO)(H_2O)_3]$	5.74	498 (sh)	20.080	1.91	489	20.450	1.74	$^6A_{1g} \rightarrow {}^4T_{2g}$ (G)
		345	28.986	3.96	351	28.490	3.63	n → π*
		292	34.247	4.24	297	33.670	4.28	π → π*
[Cu(AcO)(FFA)]	1.83	690	14.493	1.92	717	13.947	2.30	d – d
		350	28.571	1.92	335 (sh)	29.851	3.94	n → π*
		290	34.483	2.18	294	34.014	4.21	π → π*

sh = shoulder

UV–Vis spectra of the ligand **10** and the complexes **11**, **12**, **15**, **16** were recorded in DMSO and $CHCl_3$ solution. Practically, the overall spectra in both solvents are alike but they differ in some cases for some nm. Absorption maxima in the UV/VIS region are listed in **table IX.11.** along with suggested assignments.[5-8] The UV spectra of the flufenamic complexes in DMSO and in $CHCl_3$ solution are alike (strong absorptions occur at ca. 290 – 297 nm) as well as for parent drug. The band at 290 nm is attributed to π → π* transition and the shoulder band at 338 nm is attributed to n → π* for **10**. The band at 338 nm in free Hffa, **10** is shifted by an extent of 13 – 24 nm in the case of manganese complexes **11**, **15** and 3 – 4 nm in the case of copper complexes **12**, **16**. The spectra of $[Mn(FFa)_2(H_2O)]$, **11** and $[Mn(FFA)(AcO)(H_2O)_3]$, **15** and exhibits one intense band that can be attributed to d–d transitions at λ = 483 and λ = 489 assigned as a $^6A_{1g} \rightarrow {}^4T_{2g}$ (G) transition. The electronic spectra of the complex $[Mn(FFa)_2(H_2O)]$ **11** and $[Mn(FFA)(AcO)(H_2O)_3]$, **15** can be assigned to six-coordinate configuration.[7-8] The absorption of the organic ligand tailing into the visible region obscures the very weak d-d absorption bands of the Mn^{II} complexes. The d-d spectra of the solvated manganese complex **11** and **15** can be assigned to transitions in pseudo-octahedral structures or sixcoordinated tetragonally distorted configurations. Cu(II) complexes exhibit low-energy bands at ca. 13.500-14.500 cm^{-1} and high-energy band at ca. 28.500-30,000 cm^{-1}, 34.000-34.500 cm^{-1}, assigned to the transitions d – d and n → π* , π → π*. The solution spectra of $[Cu(FFA)_2]$, **12** and [Cu(AcO)(FFA)], **16** complexes are similar to that of the free ligand spectrum except for a band having maxima at ca.13,500-

14,500 cm^{-1}. It is recognized that band is assigned to a ligand field transition $d_{xz}, d_{yz} \rightarrow d_{x2-y2}$. A high intense band at 28.500-30,000 cm^{-1} is assigned to metal ligand cherge transfer. The same pattern of spectrum is shown when compounds are dissolved in $CHCl_3$ and DMF[4]. The electronic spectra of all complex, and of flufenamic acid itself, are quite similar.

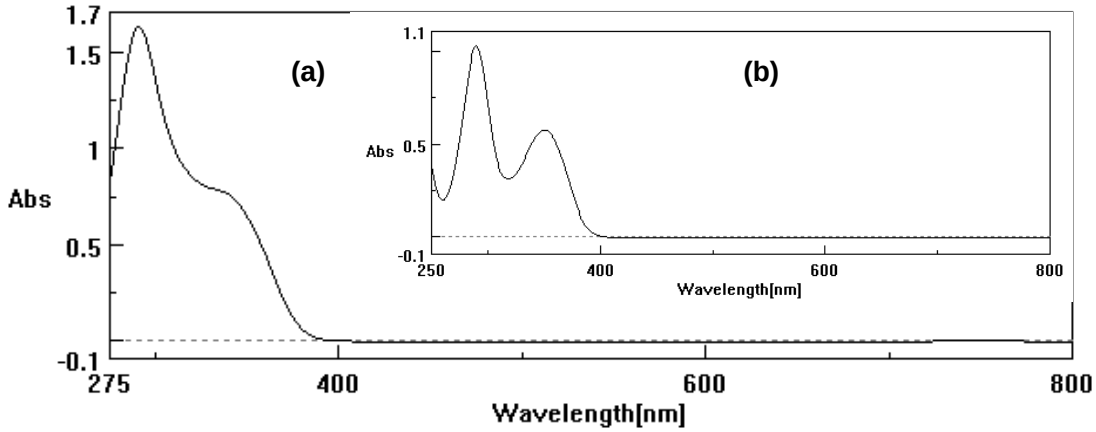

Figure IX.19. UV-vis absorption spectra of **10**, (a) 10^{-4} M in DMF, (b) 10^{-4} M in $CHCl_3$.

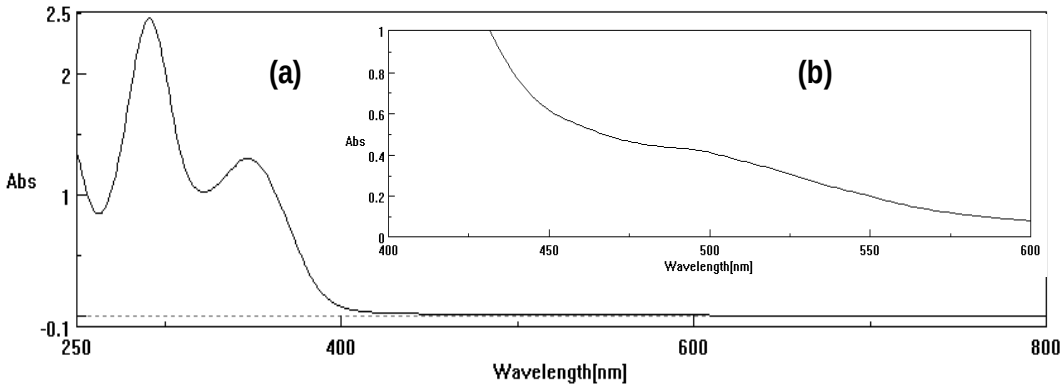

Figure IX.20. UV-vis absorption spectra of **11**, (a) 10^{-4} M in $CHCl_3$, (b) 10^{-2} M in $CHCl_3$.

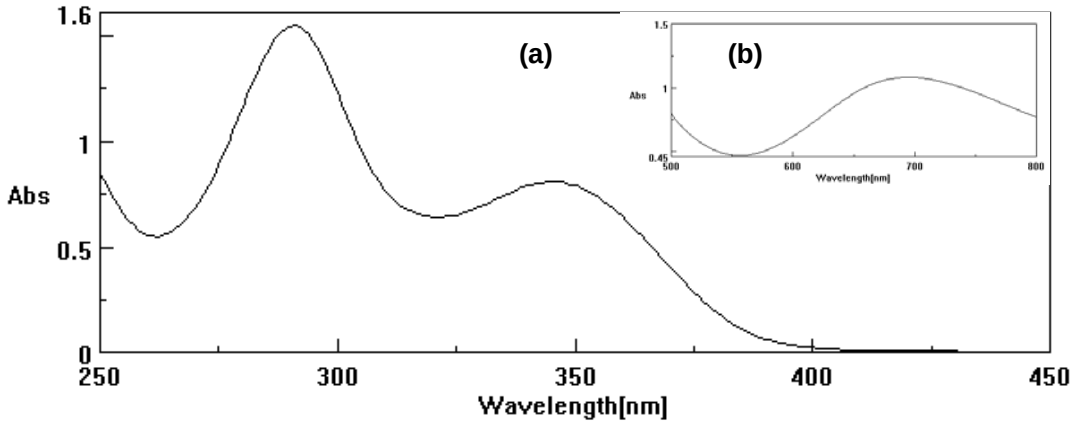

Figure IX.21. UV-vis absorption spectra of **12**, (a) 10^{-4} M in $CHCl_3$, (b) 10^{-2} M in $CHCl_3$.

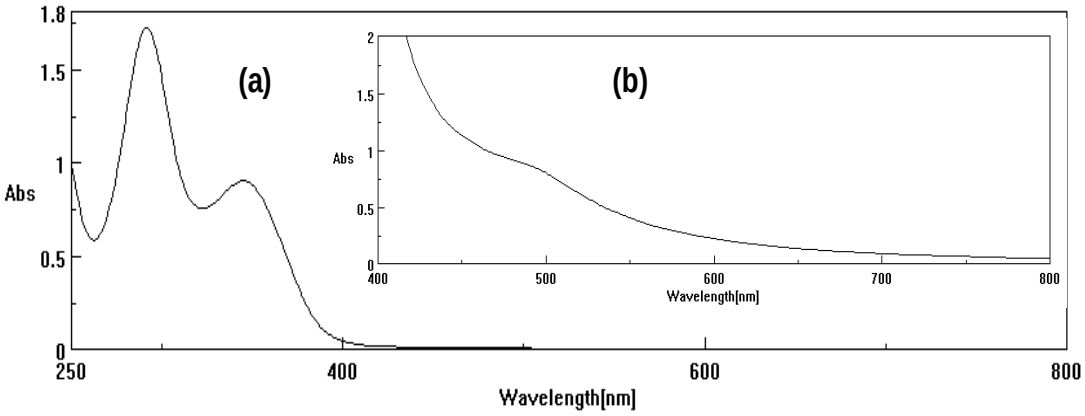

Figure IX.22. UVivis absorption spectra of **15**, (a) 10^{-4} M in $CHCl_3$, (b) 10^{-2} M in $CHCl_3$.

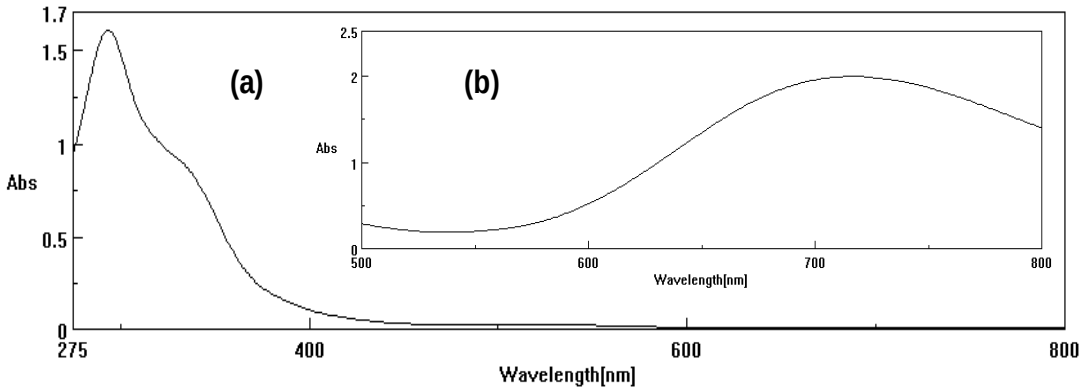

Figure IX.23. UV-vis absorption spectra of **16**, (a) 10^{-4} M in DMF, (b) 10^{-4} M in $CHCl_3$.

IX.2.4 Mass spectroscopy.

ESI and APCI generate primarily: molecular ions M^+ or M^-, protonated molecules $[M + H]^+$, simple adduct ions $[M + Na]^+$, ions representing simple losses such as the loss of a water $[M + H - H_2O]^+$ The techniques requires polar solvents. For ionization eithre acetonitrile, methanol or mixtures of acetonitrile/water, methanol/water, were used. The MS-ESI spectrum (**figure IX.24.**) of $[Cu(FFA)_2]$ (623.9) shows peak at m/z = 622.5.

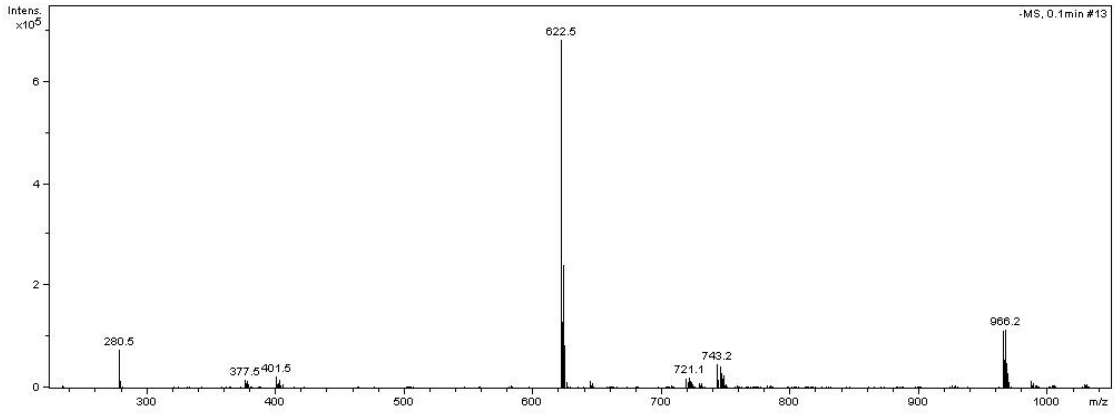

Figure IX.24. ESI-MS spectrum of deprotonated complex $[Cu(FFA)_2]$, **3** in CH_3OH.

Conclusions (Chapter IX)

The synthesis and characterization of eight new flufenamic acid, **10** complexes with Mn^{2+}, Cu^{2+}, Zn^{2+}, Cd^{2+} have been realized with physicochemical and spectroscopic methods. In all complexes, flufenamic acid acts as bidentate ligand bound to the metal ion through the oxygen atoms of the carboxylate group. In the series of complexes with 1:2 metal to ligand molar ratio two flufenamic acid molecules and solvent molecules are coordinated to the metal ions. In the series of complexes with 1:1 metal to ligand molar ratio one flufenamic acid molecule, acetate group and solvent molecules are coordinated to the metal ions. The presence of acetate group is confirmed by one singlet at ca. 1.8 – 2.1 ppm in ^{1}H–NMR spectra of complexes **17** and **18** and by two resonances attributed to the acetate carbons at ca. 22 - 23 ppm and 178 -181 ppm in ^{13}C-NMR spectra of complexes **17** and **18**. Monomeric six-coordinated species were isolated in the solid state for $[Zn(FFA)_2(H_2O)_2]$, **13** and $[Cd(FFA)_2(H_2O)_2]$, **14**, monomeric five-coordinated species for $[Mn(MCFA)_2(H_2O)]$, **11**, monomeric four-coordinated species for $[Cu(MCFA)_2]$,**12**.

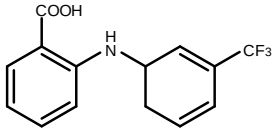

Flufenamic acid
RCOOH

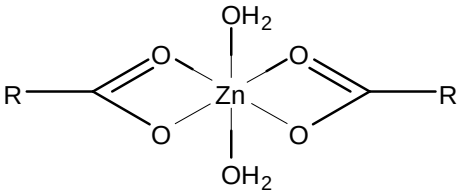

13

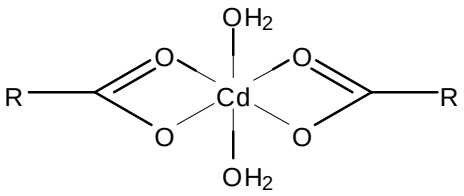

14

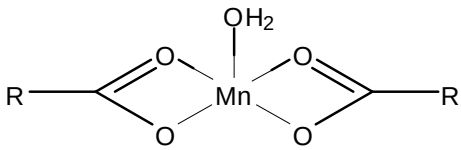

11

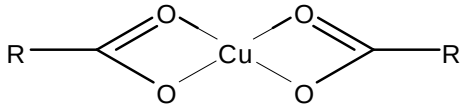

12

References

1. Kovala-Demertzi, D.,Hadjipavlou-Litina, D., Staninska, M., Primikiri, A., Kotoglou, C. Demertzis, M.A, *Journal of Enzyme Inhibition and Medicinal Chemistry* **24,**742 — 752 (2009)
2. Kovala-Demertzi, D.,Hadjipavlou-Litina, D., Primikiri, A., Staninska, M., Kotoglou, C. Demertzis, M.A, *Chemistry&Biodiversity* **6,** 948-960 (2009).
3. a) Kovala-Demertzi, D., Dokorou, V.N., Jasinski, J.P., Opolski, A. Wiecek, J., Zervou, M., Demertzis, M.A. *Journal of Organometallic Chemistry* **690 ,** 800–1806 (2005).
   b) Munro, S.L.A., Craik, D.J. *Magnetic resonance in chemistry* **32,** 335-342 (1994).
4. Lörinc, S., Švorec, J., Melník, M., Koman, M. *Polyhedron* **27,** 3545–3548(2008)
5. Kovala-Demertzi, D., Galani, A., Demertzis, M.A., Skoulika, S., Kotoglou, C. *J. Inorg. Biochem*. **98,** 358 (2004).
6. Kovala-Demertzi, D., Theodorou, A., Demertzis, M.A. Raptopoulou, C., Terzis, A. J. Inorg. Biochem. **5,** 151 (1997).
7. Kovala-Demertzi, D., Hadjikakou, S.H., Demertzis, M.A., Deligiannakis, Y. *J. Inorg. Biochem.* **69,** 223 (1998).
8. Lever, A.B.P. *Inorganic Electronic Spectroscopy* **2nd edn**.,Elsevier, Amsterdam, 480–505 (1984).
9. Bury, A., Underhill, A.E., *Inorganica Chimica* Acta **52,** 171-175 (1988).
10. Kovala-Demertzi, D., kourkoumelis, N., Koutsodimou, A., Moukarika, A., Horn, E., Tiekink, E.R.T. *Journal of Organometallic Chemistry* **620 ,** 4–201 (2001).

X. Synthesis and characterization of manganese(II), copper(II), zinc(II) and cadmium(II) complexes with (6-chloro-4-hydroxy-2-methyl- 2-pyridyl-2*H*-thieno[2,3-*e*]-1,2-thiazine-3-amide-1,1-dioxide), lornoxicam (19).

X.1. General

The complexes have been synthesized at high yield (70–80%) via the addition of an alcoholic solution of metal acetates or chlorides to an alcoholic solution of lornoxicam, (Hlorn), (6-chloro-4-hydroxy-2-methyl- 2-pyridyl-2*H*-thieno[2,3-*e*]-1,2-thiazine-3- amide-1,1-dioxide), **19**. The reaction mixture has been either stirred or refluxed for a few hours. The resulting microcrystalline or powder-like products have been obtained after filtration. Further purification through re-crystallization procedures from DMSO, produced pure compounds in the form of crystals suitable for X-ray diffraction analyses.

Table X.1. Analytical and physical data of the lornoxican complexes **20 – 23** and parent drug, **19**.

.

	Compounds	M.W g/mol	mp ˚C	Colour	M%
19	HLorn	371.82	225°C	yellow	-
20	$[Mn(Lorn)_2]$	796.488	231°C	yellow	6.90 (7.5±1.4)
21	$[Cu(Lorn)_2]$	805.096	>300°C (dec)	pale yellow	7.87 (7.4±11.7)
22	$[Zn(Lorn)_2]$	806.930	229°C	yellow	8.10 (7.6±0.7)
23	$[Cd(Lorn)_2]$	853.960	219°C	yellow	13.16 (15.8±1.9)

Results of XRF: calculated, (found).

Table X.2. Analytical and physical data of the lornoxican complexes **24 – 26**.

.

	Complexes	M.W g/mol	mp ˚C	Colour	M%
24	[Mn(AcO)(Lorn)][a]	484.744	234°C	pale orange	11.33 (10.6±1.4)
25	[Cu(AcO)(Lorn)][a]	493.352	239-240°C	pale green	12.88 (14.4±1.2)
26	[Zn(AcO)(Lorn)][a]	495.186	232°C	yellow	13.20 (12.3±1.1)
27	[Cd(AcO)(Lorn)][a]	542.216	230°C(dec)	yellow	20.73 (20.8±2.4)

Results of XRF: calculated, (found).

[a] Ac = CH_3CO

The complexes $[Mn(Lorn)_2]$ **20**, $[Cu(Lorn)_2]$ **21**, $[Zn(Lorn)_2]$ **22**, $[Cd(Lorn)_2]$ **23**, **table X.1** were synthesized according to the reactions (a) – (d). The complexes [Mn(AcO)(Lorn)] **24**, [Cu(AcO)(Lorn)] **25**, [Zn(AcO)(Lorn)] **26**, [Cd(AcO)(Lorn)] **27**, **table X.2** were synthesized according to the reactions (e) – (h).

The complexes are stable in the air. All the complexes are slightly soluble in water, except of parent drug **19** and cadmium complex **23** which is insoluble in water. Moreover all complexes are insoluble in n-pentane and n-hexane. All the complexes are solouble in polar solvents as DMFand DMSO. Besides the parent drug and manganese complexes, complexes **22** a **23** are soluble in nonpolar solvent as THF.

$Mn(AcO)_2 + 2\ HLorn \rightarrow [Mn(Lorn)_2] + 2\ AcOH$ (a)

$Cu(AcO)_2 \cdot H_2O + 2\ HLorn \rightarrow [Cu(Lorn)_2] + 2\ AcOH + H_2O$ (b)

$Zn(AcO)_2 \cdot 2\ H_2O + 2\ HLorn \rightarrow [Zn(Lorn)_2] + 2\ AcOH + 2\ H_2O$ (c)

$Cd(AcO)_2 \cdot 2\ H_2O + 2\ HLorn \rightarrow [Cd(Lorn)_2] + 2\ AcOH + 2\ H_2O$ (d)

$Mn(AcO)_2 + HLorn \rightarrow [Mn(AcO)(Lorn)] + AcOH$ (e)

$Cu(AcO)_2 \cdot H_2O + HLorn \rightarrow [Cu(AcO)(Lorn)] + AcOH + H_2O$ (f)

$Zn(AcO)_2 \cdot 2\ H_2O + HLorn \rightarrow [Zn(AcO)(Lorn)] + AcOH + 2\ H_2O$ (g)

$Cd(AcO)_2 \cdot 2\ H_2O + HLorn \rightarrow [Cd(AcO)(Lorn)] + AcOH + 2\ H_2O$ (h)

Table X.3. Solubility test of **20** – **27** complexes and parent drug **19**.

	H_2O	n-pentane	n-hexane	Et_2O	CH_3NO_2	CH_3CN	methanol	ethanol	acetone	toluene	benzene	THF	EtOAc	DMF	1,4-dioxane	DMSO	CH_2Cl_2	$CHCl_3$
19	-	-	-	-	+	+/-	+/-	+/-	+/-	+/-	+/-	+	+/-	+	+	+	+	+/-
20	+/-	-	-	-	+/-	-	+/-	+/-	+	+/-	+/-	+	+/-	+	+/-	+	+/-	+/-
21	+/-	-	-	+/-	+/-	+/-	+/-	+/-	+/-	+/-	+/-	+/-	+/-	+	+/-	+/-	+/-	+/-
22	+/-	-	-	-	+/-	+/-	+/-	+/-	+/-	+/-	+/-	+	+/-	+	+/-	+	+/-	+/-
23	-	-	-	+/-	+/-	+/-	+/-	+/-	+/-	+/-	+/-	+	+/-	+	+/-	+	+/-	+/-
24	+/-	-	-	-	+/-	+/-	+/-	+/-	+/-	+/-	+/-	+	+/-	+	+/-	+	+/-	+/-
25	+/-	-	-	+/-	+/-	+/-	+/-	+/-	+/-	+/-	+/-	+/-	+/-	+	+/-	+	+/-	+/-
26	+/-	-	-	+/-	+/-	+/-	+/-	+/-	+/-	+/-	+/-	+/-	+/-	+	+/-	+	+/-	+/-
27	+/-	-	-	+/-	+/-	+/-	+/-	+/-	+/-	+/-	+/-	+/-	+/-	+	+/-	+	+/-	+/-

+ soluble; +/- slightly soluble; - insoluble.

X.2. X-Ray crystallography

X.2.1. X-Ray structure of [$M^{II}(lorn)_2(O\text{-}dmso)_2$] (M = Mn 20a, Cu 21a, Cd 22a,)

The molecular structure of complexes [$Mn(lorn)_2(O\text{-}dmso)_2$] **20a**, [$Cu(lorn)_2(O\text{-}dmso)_2$] **21a**, [$Cd(lorn)_2(O\text{-}dmso)_2$] **22a**, are depicted in **Figures X.1, X.2, X.3.** Selected interatomic distances and angles for compound are listed and selected hydrogen bonds are given in **Table X.4 – X.9** Complexes crystallize in the monoclinic space group P 21/n (**20a**, **22a**) and P 21/c (**21a**)**.** Each metal center is coordinated by two ligands and two DMSO groups. The experimental data suggest that lornoxicam acts as a bidentate ligand in **20a**, **21a**, **22a** complexes and is coordinated to the metal ion through the pyridine nitrogen and the carbonyl oxygen. The complex molecules **20a**, **21a** and **23a** are isostructural. The co-ordination spheres are pseudooctahedral and the metal ions sit on the inversion centres. The $lorn^-$ anions act as chelators through the N(11) nitrogen atoms of the pyridine ring and through the O(18) carbonyl oxygen atoms at the equatorial positions (with a *trans* arrangement). The apical co-ordination sites are occupied by the O(1D) oxygen atoms of the two dmso ligands. M–O(apical) bond distances are 2.181(3) **20a,** 2.420(2) **21a**, 2.318(17)Å **22a** and the effect being the largest for **21a**. The M–N(11) bond distances are 2.252(4) **20a**, 2.021(3) **21a** and 2.307(2) **22a** Å, whereas the M–O(18) bond lengths are 2.135(3) **20a**, 1.920(2) **21a** and 2.245(16) **22a** Å, for **20a**, **21a** and **22a**, respectively. The bond distance found for **21a** can be compared to the values previously found for the octahedral [$Cu(pir)_2(O\text{-}dmso)_2$], where Cu–O, Cu–N, Cu–O(apical) were 1.9422(14), 2.0494(17), 2.4092(19). The lornoxicam ligand is deprotonated at O(23) **20a**, **21a**, O(24) **22a** and adopts *ZZZ* conformation. The chelating anion is stabilised by a strong intramolecular hydrogen bond which involves the O(23) **20a**, **21a**, O(24) **22a** and the N(17) atom (O•••N, 2.622 **20a**, 2.692 **21a**, 2,.616 **22a** Å; O•••H–N, 1.81for **20a**, 1.95 for **21a**, 1.81 for **22a**). The ambidentate dmso ligand co-ordinates the metal centre through the oxygen atom (O(1D)) for **20a**, **21a** and **22a**.

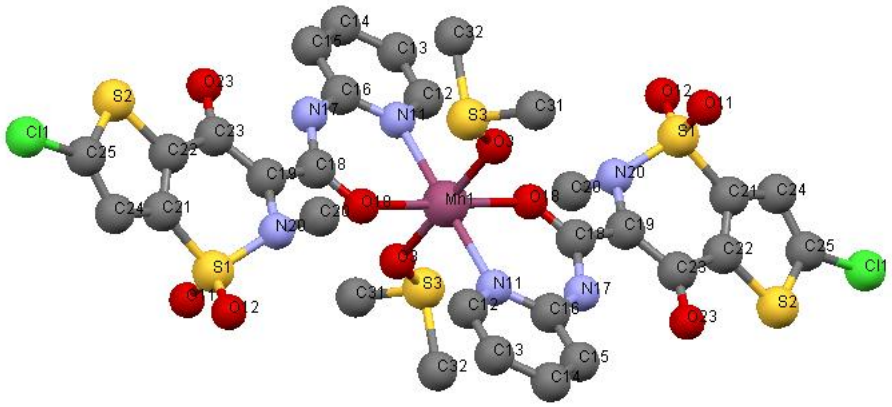

Figure X.1. Crystal structure of [$Mn(lorn)_2(DMSO)_2$].

Table X.4. Selected bond lengths [Å] and angles [º] for $[Mn(lorn)_2(DMSO)_2]$.

Vector	Length	Vector	Angle
Mn(1)-O(18)	2.135(3)	O(18)#1-Mn(1)-O(18)	180.0
Mn(1)-O(3D)	2.181(3)	O(18)#1-Mn(1)-O(3)#1	88.89(12)
Mn(1)-N(11)	2.252(4)	O(18)-Mn(1)-O(3)#1	91.11(12)
O(18)-C(18)	1.245(5)	O(18)#1-Mn(1)-O(3)	91.11(12)
N(11)-C(16)	1.343(6)	O(18)-Mn(1)-O(3)	88.89(12)
N(11)-C(12)	1.345(6)	O(3)#1-Mn(1)-O(3)	180.0
N(17)-C(18)	1.381(6)	O(18)#1-Mn(1)-N(11)#1	83.09(13)
N(17)-C(16)	1.405(6)	O(18)-Mn(1)-N(11)#1	96.91(13)
N(20)-C(19)	1.453(6)	O(3)#1-Mn(1)-N(11)#1	85.90(13)
C(18)-C(19)	1.434(7)	O(3)-Mn(1)-N(11)#1	94.10(13)
C(19)-C(23)	1.414(7)	O(18)#1-Mn(1)-N(11)	96.91(13)
S(1)-O(11)	1.429(3)	O(18)-Mn(1)-N(11)	83.09(13)
S(1)-O(12)	1.441(4)	O(3)#1-Mn(1)-N(11)	94.10(13)
S(1)-N(20)	1.638(4)	O(3)-Mn(1)-N(11)	85.90(13)
O(23)-C(23)	1.271(6)	N(11)#1-Mn(1)-N(11)	180.0
N(20)-C(20)	1.475(6)		
C(21)-C(22)	1.374(7)		
C(22)-C(23)	1.466(7)		
C(12)-C(13)	1.373(7)		
C(13)-C(14)	1.377(7)		
C(14)-C(15)	1.376(7)		
C(15)-C(16)	1.397(7)		

Table X.5. Selected hydrogen bonds for $[Mn(lorn)_2(DMSO)_2]$.

Atoms D,H,A	Dist. D, H [A]	Dist. H, A [A]	Dist. D,A [A]	Angle D,H,A [º]
N(17)-H(17A)...O(23)	0.89	1.81	2.622(5)	149.4

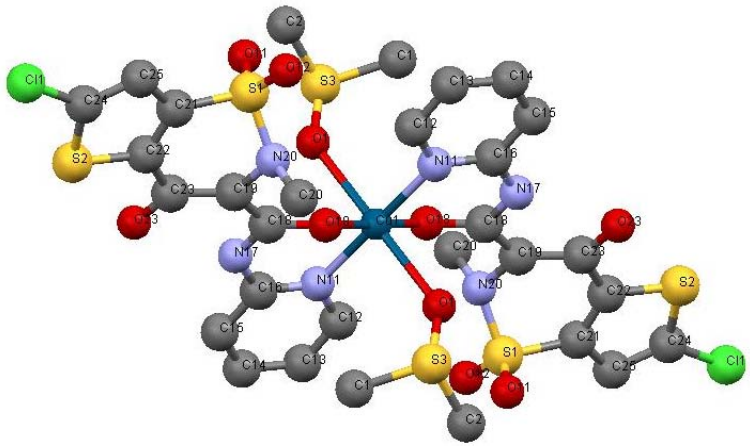

Figure X.2. Crystal structure of $[Cu(lorn)_2(DMSO)_2]$.

Table X.6. Selected bond lengths [Å] and angles [º] for $[Cu(lorn)_2(DMSO)_2]$.

Vector	Length	Vector	Angle
Cu(1)-O(18)	1.920(2)	O(18)#1-Cu(1)-O(18)	180.00(17)
Cu(1)-N(11)	2.021(3)	O(18)#1-Cu(1)-N(11)#1	87.76(10)
Cu(1)-O(1D)	2.420(2)	O(18)-Cu(1)-N(11)#1	92.24(10)
O(18)-C(18)	1.267(4)	O(18)#1-Cu(1)-N(11)	92.24(10)
N(11)-C(16)	1.347(4)	O(18)-Cu(1)-N(11)	87.76(10)
N(11)-C(12)	1.359(4)	N(11)#1-Cu(1)-N(11)	180.0(2)
N(17)-C(18)	1.368(4)	O(18)#1-Cu(1)-O(1)#1	87.62(9)
N(17)-C(16)	1.399(4)	O(18)-Cu(1)-O(1)#1	92.38(9)
N(20)-C(19)	1.446(4)	N(11)#1-Cu(1)-O(1)#1	88.86(9)
C(18)-C(19)	1.418(4)	N(11)-Cu(1)-O(1)#1	91.14(9)
C(19)-C(23)	1.408(4)	O(18)#1-Cu(1)-O(1)	92.38(9)
S(1)-O(11)	1.434(2)	O(18)-Cu(1)-O(1)	87.62(9)
S(1)-O(12)	1.435(2)	N(11)#1-Cu(1)-O(1)	91.13(9)
S(1)-N(20)	1.629(3)	N(11)-Cu(1)-O(1)	88.87(9)
O(23)-C(23)	1.255(4)	O(1)#1-Cu(1)-O(1)	180.0
N(20)-C(20)	1.476(4)		
C(21)-C(22)	1.369(5)		
C(22)-C(23)	1.490(4)		
C(12)-C(13)	1.371(5)		
C(13)-C(14)	1.381(5)		
C(14)-C(15)	1.380(4)		
C(15)-C(16)	1.387(4)		

Table X.7. Selected hydrogen bonds for $[Cu(lorn)_2(DMSO)_2]$.

Atoms D,H,A	Dist. D, H [A]	Dist. H, A [A]	Dist. D,A [A]	Angle D,H,A [º]
N(17)-H(17A)...O(23)	0.85	1.95	2.692(3)	144.8

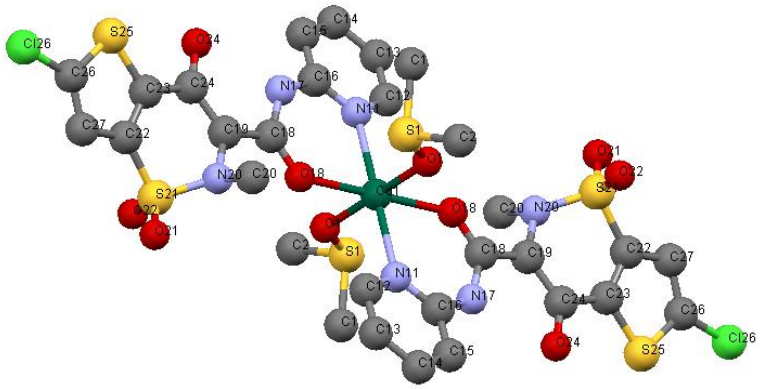

Figure X.3. Crystal structure of $[Cd(lorn)_2(DMSO)_2]$.

Table X.8. Selected bond lengths [Å] and angles [º] for $[Cd(lorn)_2(DMSO)_2]$.

Vector	Length	Vector	Angle
Cd(1)-O(18)	2.2452(16)	O(18)#1-Cd(1)-O(18)	180.0
Cd(1)-O(1D)	2.3018(17)	O(18)#1-Cd(1)-O(1)	90.83(6)
Cd(1)-N(11)	2.307(2)	O(18)-Cd(1)-O(1)	89.17(6)
O(18)-C(18)	1.246(3)	O(18)#1-Cd(1)-O(1)#1	89.17(6)
N(11)-C(16)	1.341(3)	O(18)-Cd(1)-O(1)#1	90.83(6)
N(11)-C(12)	1.356(3)	O(1)-Cd(1)-O(1)#1	180.0
N(17)-C(18)	1.372(3)	O(18)#1-Cd(1)-N(11)#1	81.62(6)
N(17)-C(16)	1.398(3)	O(18)-Cd(1)-N(11)#1	98.38(6)
N(20)-C(19)	1.451(3)	O(1)-Cd(1)-N(11)#1	96.37(7)
C(18)-C(19)	1.443(3)	O(1)#1-Cd(1)-N(11)#1	83.63(7)
C(19)-C(24)	1.410(3)	O(18)#1-Cd(1)-N(11)	98.38(6)
S(21)-O(21)	1.4309(18)	O(18)-Cd(1)-N(11)	81.62(6)
S(21)-O(22)	1.4316(18)	O(1)-Cd(1)-N(11)	83.63(7)
S(21)-N(20)	1.629(2)	O(18)-Cd(1)-N(11)	96.37(7)
O(24)-C(24)	1.267(3)	N(11)#1-Cd(1)-N(11)	180.0
N(20)-C(20)	1.477(3)		
C(22)-C(23)	1.366(4)		
C(23)-C(24)	1.474(3)		
C(12)-C(13)	1.367(4)		
C(13)-C(14)	1.387(4)		
C(14)-C(15)	1.374(4)		
C(15)-C(16)	1.396(3)		

Table X.9. Selected hydrogen bonds for $[Cd(lorn)_2(DMSO)_2]$.

Atoms D,H,A	Dist. D, H [A]	Dist. H, A [A]	Dist. D,A [A]	Angle D,H,A [º]
N(17)-H(17)...O(24)	0.90	1.81	2.616(3)	149.4

X.3. Spectroscopic characterization of Mn(II), Cu(II), Zn(II) and Cd(II) complexes with lornoxicam.

X.3.1. Nuclear Magnetic Resonance.

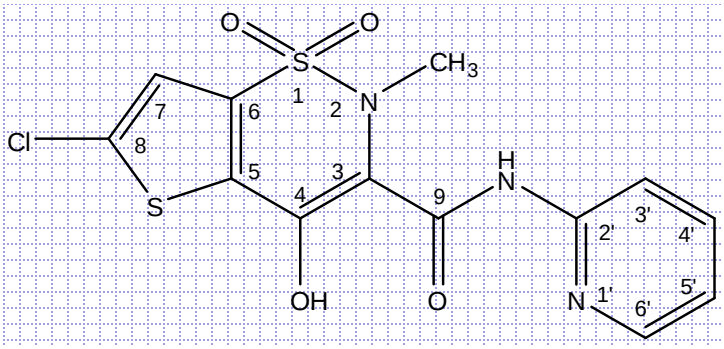

Figure X.4. Structural formule of lornoxicam **19**.

^{1}H and ^{13}C NMR spectra of Hlorn (**19**), its zinc complexes **22**, **26** and cadmium complexes **23**, **27** complexes were recorded in DMSO-d_6 solutions. Assignment of every signal of the aromatic rings in spectrum of the complex **22** has been achieved with the aid of 2D NMR techniques [^{1}H–^{1}H COSY (correlation spectroscopy), ^{1}H–^{13}C HSQC (heteronuclear single quantum correlation)] and the results are shown in **table X.10** and **table X.11**. The analysis of the chemical shifts for the signals of **22** shows that the peaks attributable to the pyridyl system C(3')H, C(4')H, C(5')H and C(6')H protons occur at 7.80 ppm (singlet, 1H), 8.28 ppm (doublet, 1H), 7.07 (triplet, 1H) 8.31 (singlet, 1H) respectively[1]. The resonances due to the pyridyl ring proton atoms for **23**, **26, 27** occure in the spectral region around 7.00 – 8.30 ppm and are shifted when compared to that found for free Hlorn.The most significant chemical shift difference between the ^{1}H spectrum of the free drug and **22**, **26** is observed for the H(5') atom. The signal for the C(5')H proton undergoes upfield shift (0.26 ppm,) upon complexation and deprotonation when compared to the spectrum of free Hlorn , whereas the signals for the C(3')H, C(4')H and C(6')H protons experience some downfield shifts.The changes of the chemical shifts of the pyridyl protons signals indicate that the pyridyl ring is bound to Zn and Cd atoms through the N atom. The signal relevant to the thiofuran C(7)H proton for **22** (7.49 ppm, singlet, 1H), for **26** (7.50 ppm, singlet, 1H), is shifted downfield when compared to that found for free Hlorn. Small perturbations of the chemical shifts ~ 0.06 ppm) are observed for H7 thiazole proton, which lie far away from the coordination center of the ligand. In all complex, H(CH_3) resonance is appeared as a singlet. The remaining resonances due to the CH_3 proton atoms for all complexes do not shift considerably after binding to metal ion. The shifts are similar for all zinc and cadmium complexes. The presence of methyl group is also confirmed by ^{13}C-NMR spectra. It has to be noted that the largest effect upon complexation is experienced by the signal (broad peak) for the OH proton which occurs at 13.43 ppm (1H) and 14.10 ppm (1H) for **22** and Hlorn, respectively. A downfield shift is also observed for the OH proton (**26**) 13.42 ppm (1H) while resonance shifts found for **23**,

27 are 13.05 ppm and 13.00 ppm, respectively. No signal was observed in the region 9–11 ppm for the spectrum of Hlorn.[1,4] Involvement of the intramolecular hydrogen bond is confirmed by the resonance ascribed to NH proton, which either disappears for **23** and **27** cadmium complexes or exhibits very weak, almost invisible peak at 9.03 ppm (1H) for **22** and **26** zinc complexes. This hydrogen bond is formed between the hydrogen in the amide group NH and the oxygen in the ketone functionality formed after ligand reduction and complexation.[8] The ^{13}C NMR spectrum of the complexes **22**, **23**, **26, 27** shows differences in chemical shifts for lornoxicam and **22**, **23**, **26, 27** which imply coordination of the pyridine nitrogen as well as the carbonyl oxygen. The signals of the pyridyl carbons are significantly shifted upon complexation with the chemical shifts of C6' and C4' shifted upfield by 5 ppm and 6 ppm, respectively for **22**, while the other pyridyl carbons are shifted towards higher field. The overall changes in the NMR spectra of **22**, **23**, **26, 27** are indicative of coordination of lornoxicam to Zn and Cd through N_{pyr} and O_{amide} atoms. For **26** and **27** one singlet appears at ca. 1.86 ppm, thus in the region of proton of acetate group. Two resonances attributed to the acetate carbons are found at 22.0 ppm and 175 ppm in ^{13}C-NMR spectrum of **26** and **27**.

Table X.10. ^{1}H NMR shifts of **22**, **23**, **26**, **27** complexes and parent drug **19** (δ in ppm and *J* in Hz).

	HLorn[a]	**22**[a]	**26**[a]	**23**[a]	**27**[a]
CH_3	2.91s	2.89s	2.89s	2.86	2.85s
H – C(3')	7.69d J(3'-4')=8.7	7.80s	7.80s	7.69t	7.71t
H – C(4')	8.22td J(4'-5')=8.0 J(4'-6')=1.6	8.28d	8.27d	7.89s	7.94s
H – C(5')	7.33t J(5'-6')=6.7	7.07t	7.07t	7.00t	6.97t
H – C(6')	8.30dd J(6'-5')=6.0 J(4'-6')=1.1	8.31s	8.29s	8.20d	8.19d
H – C(7)	7.55s	7.49s	7.50s	7.44s	7.43s
N – H	-	9.03br[b]	9.03br[b]	-	-
O – H	14.10 br[b]	13.43 br[b]	13.42 br[b]	13.05	13.00
CH_3COO			1.85s		1.87s

[a] Spedtrum recorded in DMSO-d_6
[b] br = broad

Table X.11. ^{13}C NMR shifts (ppm) of **22**, **23**, **26**, **27** complexes and parent drug **19**.

	HLorn[a]	22[a]	26[a]	23[a]	27[a]
CH_3	-	21.1	21.7	-	21.9
C2'	149.1	147.0	147.3	153.6	153.7
C3'	116.0	114.4	113.8	113.6	113.6
C4'	142.5	136.5	136.9	146.0	147.7
C5'	118.0	118.1	117.7	117.5	117.6
C6'	144.8	139.8	138.6	147.6	146.1
C3	107.0	107.7	107.8	108.2	108.1
C4	163.4	153.0	153.2	162.0	162.1
C5	137.1	131.1	132.8	135.7	135.7
C6	134.4	127.9	128.0	132.7	132.7
C7	122.6	122.4	122.2	122.2	122.2
C8	138.5	133.8	133.6	138.4	138.3
C9	164.9	165.7	166.9	164.6	164.6
CH_3COO			21.8 174.8		22.0 175.0

[a] Spedtrum recorded in DMSO-d_6

Figure X.5 . ^{1}H-NMR spectrum of **22** recorded in dmso-d_6.

Figure X.6. ^{13}C-NMR spectrum of **22** recorded in dmso-d_6.

Figure X.7. ^{1}H-NMR spectrum of **26** recorded in dmso-d_6.

Figure X.8. ^{1}H-NMR spectrum of **23** recorded in dmso-d_6.

Figure X.9. ^{13}C-NMR spectrum of **23** recorded in dmso-d_6.

Figure X.10. ^{1}H-NMR spectrum of **27** recorded in dmso-d_6.

Figure X.11. ^{13}C-NMR spectrum of **27** recorded in dmso-d_6.

Table X.12. 2D^{1}H,^{1}H-COSY NMR data for **26**[a].

1	2	3
H3' – H5'	H4' – H5' H5' – H6'	H3' – H4'

[a] spectrum recorded in DMSO-d_6

Table X.13. 2D^{1}H,^{13}C-HSQC NMR data for **26**[a].

1	2	3
C5' – H5'	C7' – H7	C4' – H4'

[a] spectrum recorded in DMSO-d_6

2D ^{1}H–^{1}H shift correlated spectra (COSY), 2D cross-peaking of heteronuclear single quantum correlation (HSQC) spectra of **22** were performed in order to completely assign the resonances in zinc complex of meclofenamic acid. 2D ^{1}H–^{1}H (COSY), 2D ^{1}H–^{13}C (HSQC), 2D ^{1}H–^{13}C (HMBC) data for complex **22** are summarized in **tables X.12** and **X.13.**

The ^{1}H-NMR spectra of **22**, in the region characteristic of aromatic protons (6.50–8.50 ppm) five signals are found. In the region corresponding to the signals of aromatic rings carbons (110-150 ppm) three signals are observed.

2D ^{1}H–^{1}H (COSY) spectrum shows correlation between coupled protons thus give rise to off-diagonal or cross-peaks for all protons that have significant (measurable) J-J coupling. In the COSY spectrum of **22**, as expected, the aromatic protons show ortho coupling between H(4') and H(5'), H(5') and H(6'), H(4') and H(3').Interestingly proton H(3') are coupled to H(5').

2D ^{1}H–^{13}C (HSQC) spectrum shows correlation between directly attached (one-bond) proton-carbon. In the 2D ^{1}H–^{13}C (HSQC) spectrum of **22** three correlations peaks are found.The ^{13}C signal of C4', C5', C7 are detected and assigned through the shift correlation peaks with H(4'), H(5'), H(7), respectively.

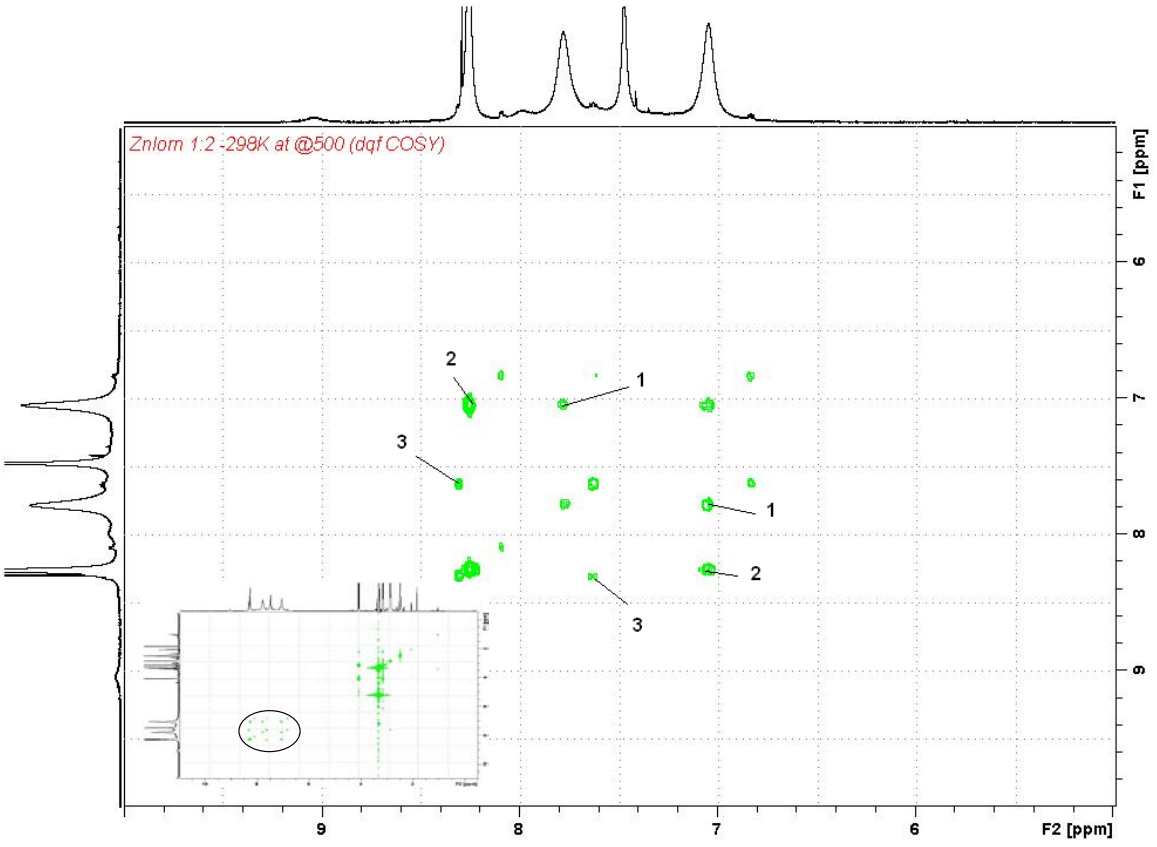

Figure X .13. 2D^{1}H,^{1}H-COSY NMR spectrum of **22** recorded in dmso-d_6.

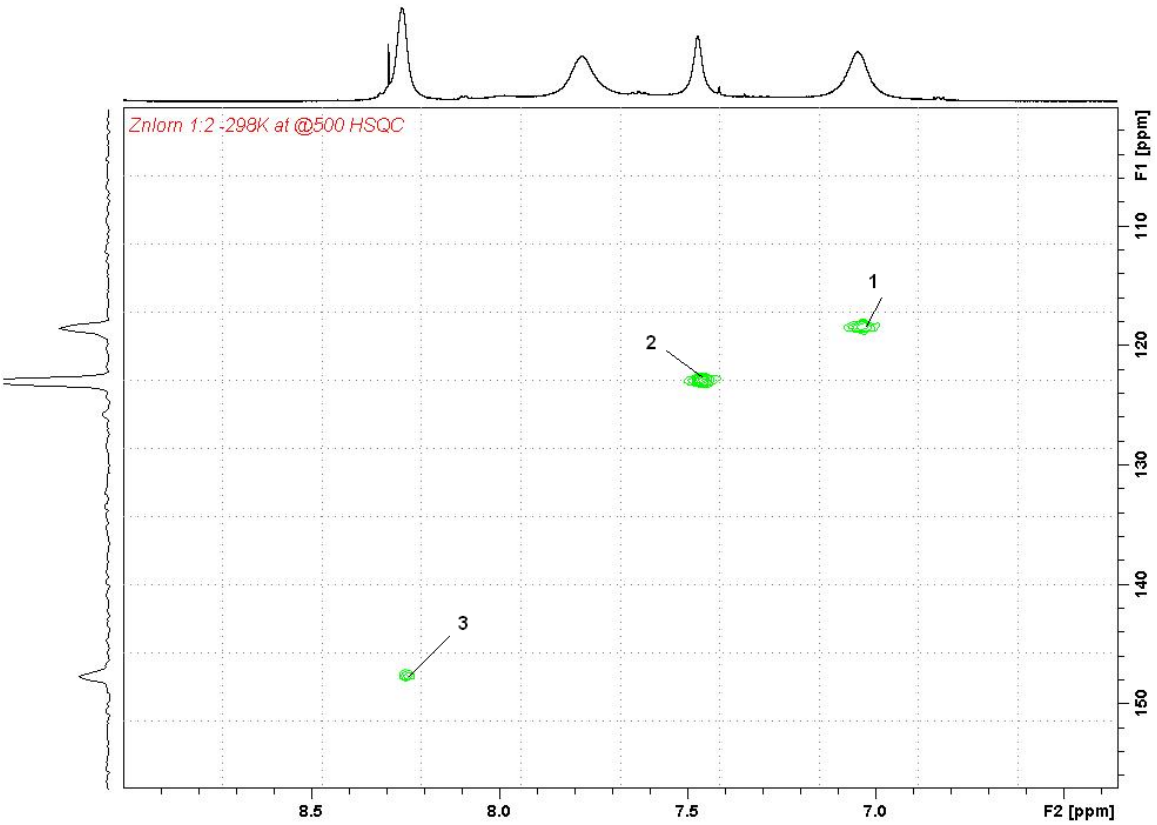

Figure X.14. 2D^{1}H,^{13}C-HSQC NMR spectrum of **22** recorded in dmso-d_6.

X.3.2. Infrared Spectroscopy.

Table X.14. IR-data (cm^{-1}) for the prepared complexes **20 – 23** and parent drug **19**.

		ν(O–H)	ν(N–H)	ν(C=O) amide	ν(C=N)	ν_{asym} (SO_2)	ν_{sym} (SO_2)	ν(M–O)	ν(M–N)
HLorn	Lornoxicam	3439w	3068s	1621w	1594s	1382s	1187w	-	-
20	[Mn(Lorn)$_2$]	3195m,br	3095m	1607w	1580s	1334s	1157s	361m	622mw 267mw
21	[Cu(Lorn)$_2$]	3355m,br	3099m	1608w	1576s	1338s	1160s	342m	652mw 271mw
22	[Zn(Lorn)$_2$]	3227m,br	3097m	1608w	1581s	1336s	1159s	355m	670mw 297mw
23	[Cd(Lorn)$_2$]	3221m,br	3097m	1609w	1580s	1335s	1157s	352m	287mw

s = strong, m = medium, w = weak, sh = sharp, br = broad

Table X.15. IR-data (cm^{-1}) for the prepared complexes **24 – 27**.

		ν(O–H)	ν(N–H)	ν(C=O) amide	ν(C=N)	ν_{asym} (SO_2)	ν_{sym} (SO_2)	ν(M–O)	ν(M–N)
24	[Mn(AcO)(Lorn)]	3209m,br	3096m	1605w	1581s	1334s	1157s	363m	653mw 273mw
25	[Cu(AcO)(Lorn)]	3356m,br	3099m	1603w	1577s	1338s	1159s	351m	653mw 272mw
26	[Zn(AcO)(Lorn)]	3226m,br	3096m	1609w	1581s	1335s	1164s	368m	640mw 299mw
27	[Cd(AcO)(Lorn)]	3213m,br	3097m	1607w	1580s	1334s	1157s	358m	288mw

s = strong, m = medium, w = weak, sh = sharp, br = broad

The infrared spectra for all the metal derivatives exhibit remarkable similarity. **Tables X.14** and **X.15** list and compare the infrared spectra for the free ligand **19** and the metal complexes **20 – 23** and **24 – 27**. [8] Characterization of metal complexes with lornoxican, focus on the most typical vibrations that are characteristic of the coordination mode of lornoxicam. The ligand, Hlorn, shows a broad absorption band centred at ca. 3500 and 3400 cm^{-1} that is characteristic of an O–H stretching vibration. The broad signal observed in this region for the metal complexes could come from a strong intramolecular hydrogen bond. This hydrogen bond is formed between the hydrogen in the amide group NH and the oxygen in the ketone functionality formed after ligand reduction and complexation.[8] The band at 3068 cm^{-1} for lornoxicam is attributed to the N–H stretching vibration. The low frequency of these two bands may be explained by inter- and intramolecular hydrogen bonds involving the nitrogen and two oxygen atoms.The sharp bands observed at 1621 cm^{-1} and the band at 1594 cm^{-1} in lornoxicam are assigned to the carbonyl $\nu(C=O)_{amide}$ and the $\nu(C=N)$ vibrations.[7] Upon complexation, the shift of $\nu(C=O)_{amide}$ is indicative of the coordination mode and the number of coordination sites of lornoxicam. Lornoxicam acts as a bidentate chelating ligand via N_{pyr} and O_{amide} in metal complexes **20** – **23** $\nu(C=O)_{amide}$ is shifted to slightly lower wavenumbers, in the range 1603–1609 cm^{-1}.[4] In any case, coordination of the N_{pyr} is usually indicated by a 3–26 cm^{-1} shift to a higher wave number. For complexes **20** – **23** and **24** – **27** $\nu(C=O)_{amide}$ appears in the range 1603 – 1610 cm^{-1} and the $\nu(C=N)_{pyr}$ absorption is shifted to lower wavenumbers indicating coordination of lornoxicam through N_{pyr} and O_{amide}.[4] The shift of the N–H amide group vibration from 3068 cm^{-1} to higher wavenumbers up to 3099

cm^{-1} is indicative of the weakening of the N–H bond due to an intramolecular H-bond between the deprotonated enolic oxygen atom and the hydrogen of the amide N–H group.[4] The vibrations for the SO_2 group give bands at 1382 cm^{-1} (asymmetric stretching) and 1186 cm^{-1} (symmetric stretching) in the spectrum of free H_2lorn[1]. The band in the lornoxicam spectrum attributable to $\nu(SO_2)_{asym}$ vibration undergoes a shift at higher energies up to 50 cm^{-1} upon complexation even though the SO_2 group does not interact with the metal ion. The overall spectrum pattern of the complexes indicates that in complexes **20** – **23** lornoxicam acts as a bidentate ligand bound to the metal ions through the O_{amide} and N_{pyr} atoms. The appearance of a broad peak in the range 3500–3550 cm^{-1} in the spectra of complexes all complexes is indicative of the existence of water molecule bound to the metal ion.[4]

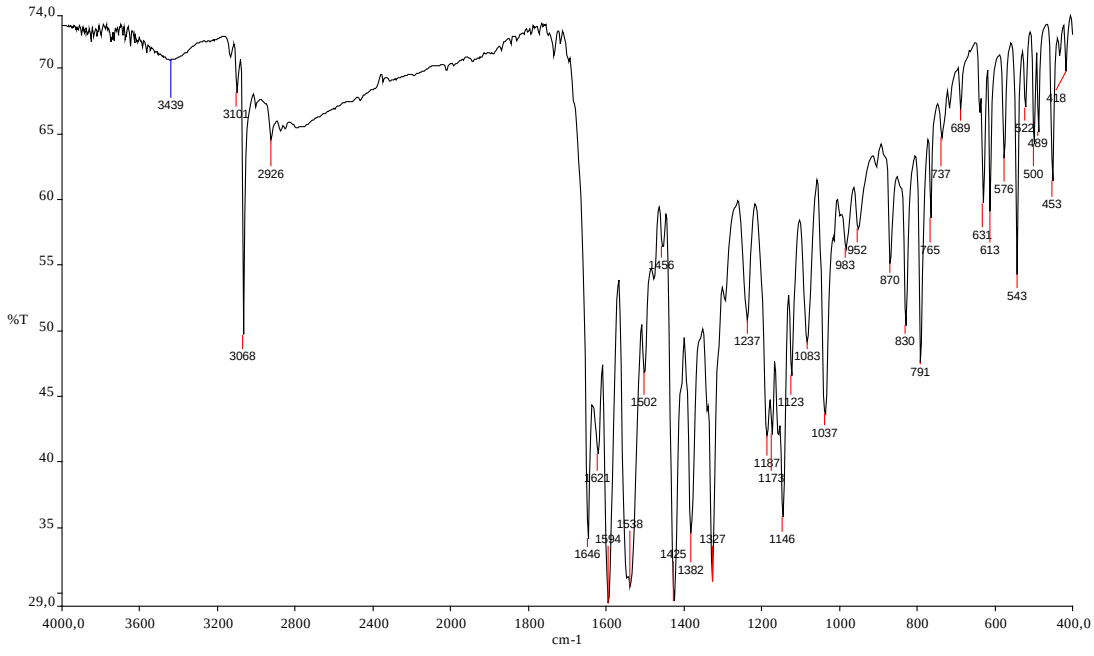

Figure X.15. Infrared spectrum of Lornoxicam, **19**.

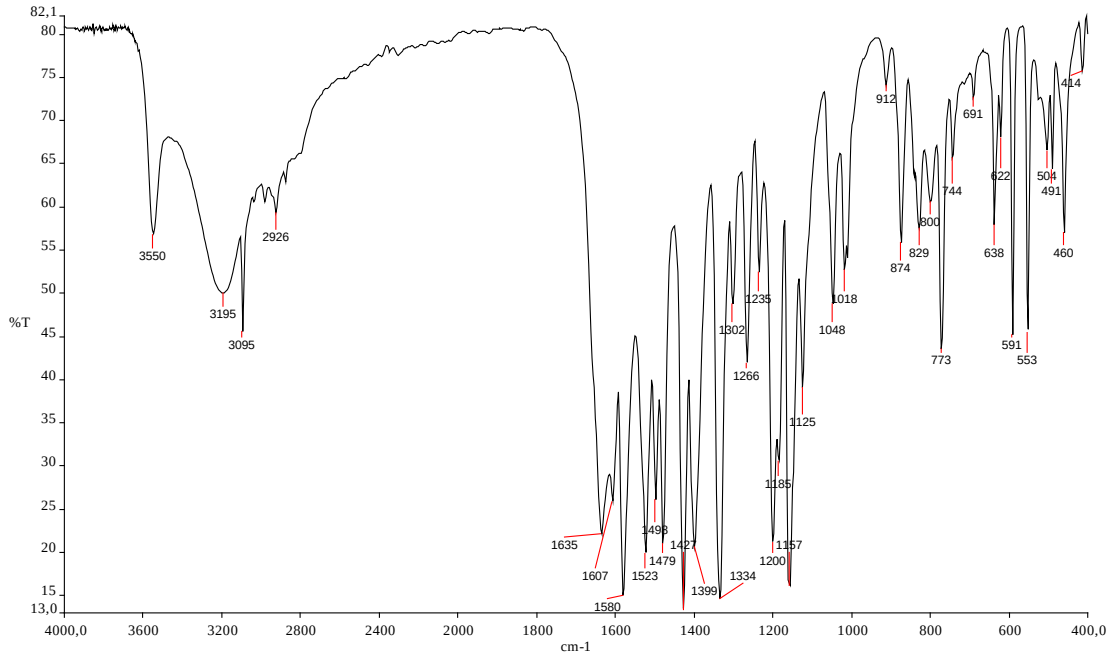

Figure X.16. Infrared spectrum of [Mn(Lorn)$_2$], **20**.

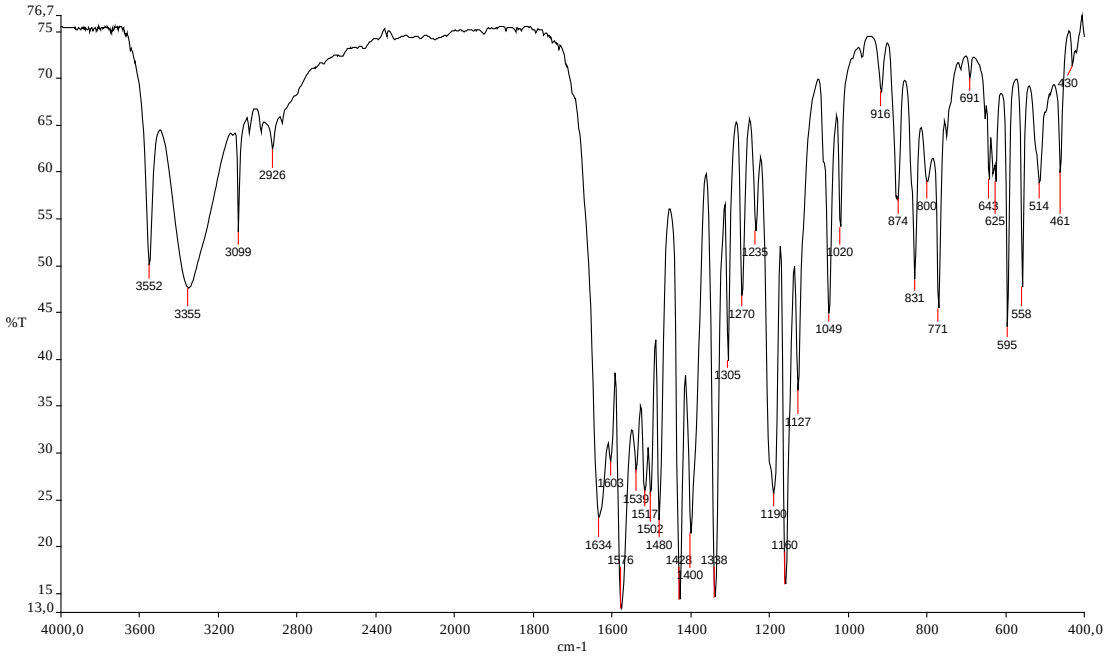

F
igure X.17. Infrared spectrum of [Cu(Lorn)$_2$], **21**.

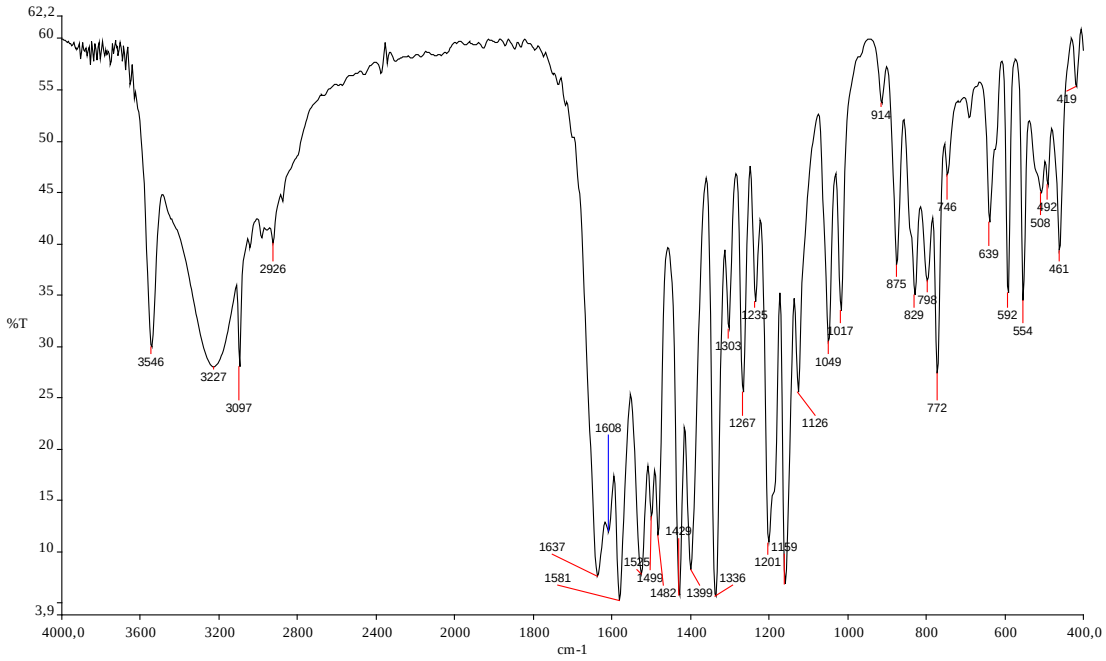

Figure X.18. Infrared spectrum of [Zn(Lorn)$_2$], **22**.

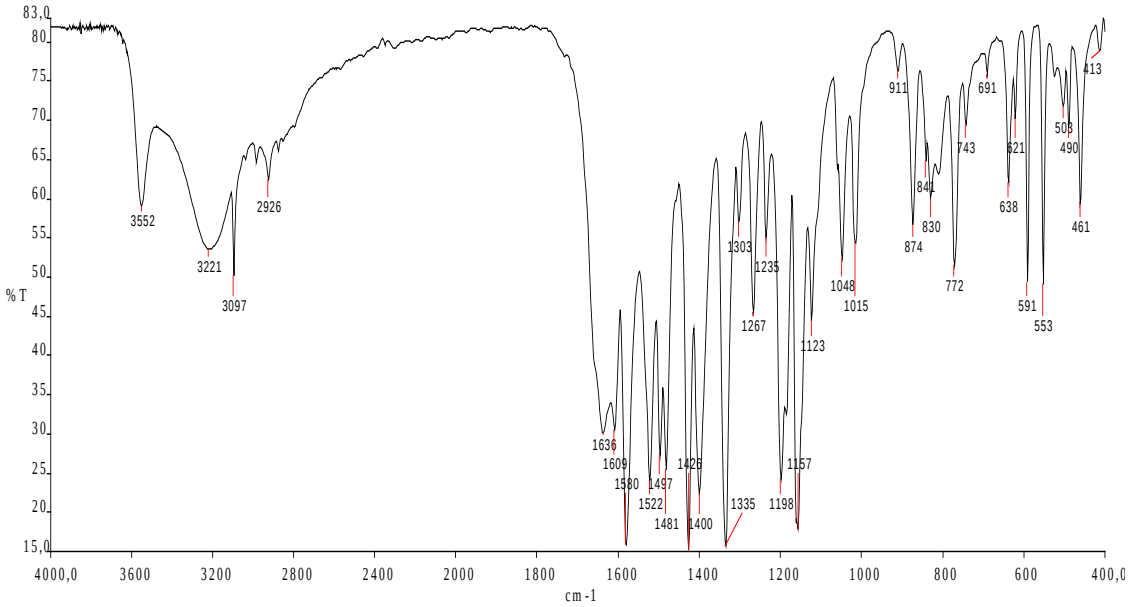

Figure X.19. Infrared spectrum of [Cd(Lorn)$_2$], **23**.

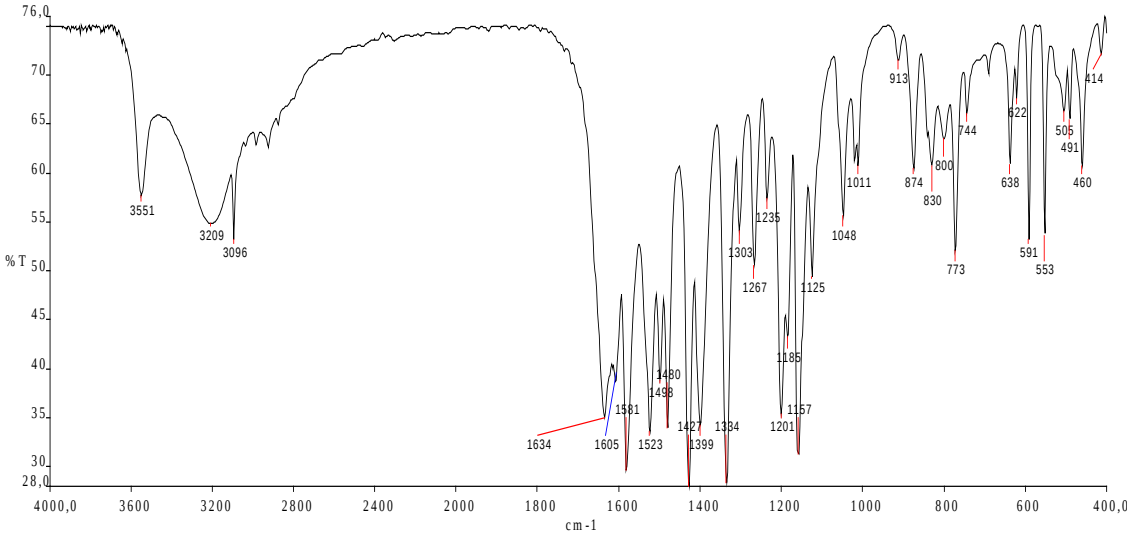

Figure X.20. Infrared spectrum of [Mn(AcO)(Lorn)], **24**.

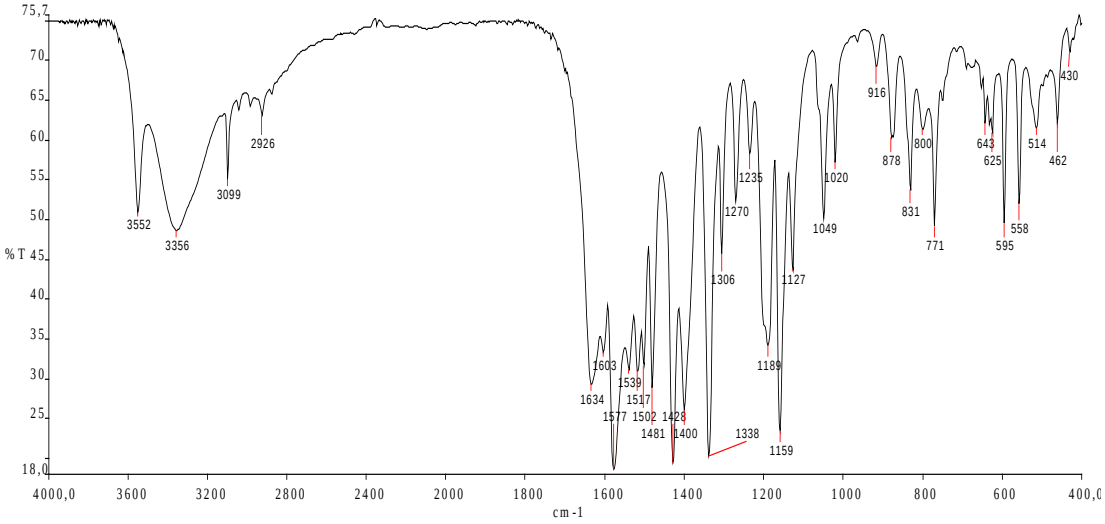

Figure X.21. Infrared spectrum of [Cu(AcO)(Lorn)], **25**.

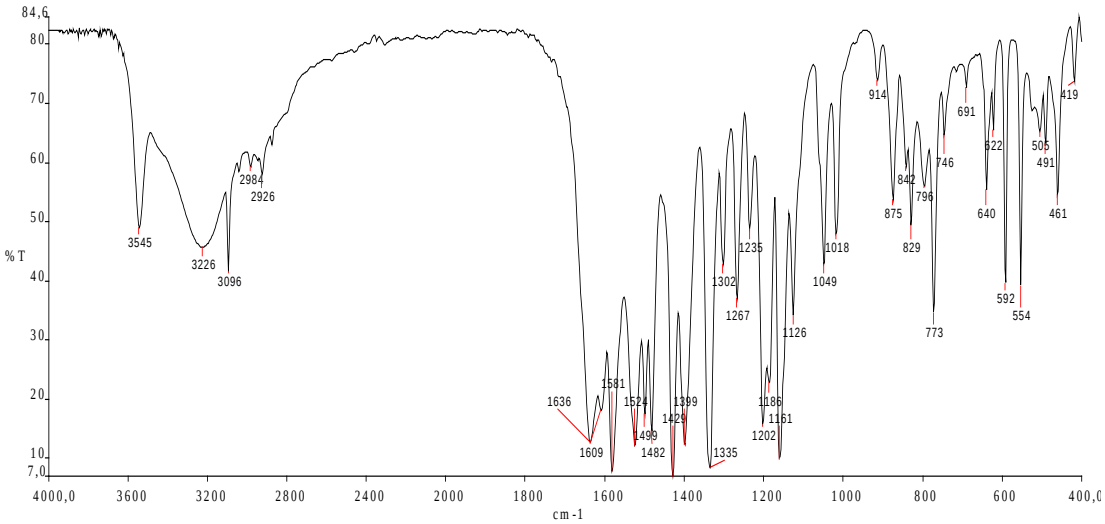

Figure X.22. Infrared spectrum of [Zn(AcO)(Lorn)], **26**.

X.3.3. Electronic spectroscopy.

Table X.16. Spectral data (UV-vis) for the prepared complexes **20**, **21**, **24**, **25** and the parent drug **19**.

Compounds	μ_{eff}	$CHCl_3$			DMF			Assignments
		λ (nm)	ν (cm^{-1})	log ε	λ (nm)	ν (cm^{-1})	log ε	
Lornoxicam		355 273	28.169 36.630	4.02 3.62	395 282	25.316 34.602	4.08 4.11	$n \rightarrow \pi^*$ $\pi \rightarrow \pi^*$
$[Mn(Lorn)_2]$	5.83	421(sh) 411(sh) 349 287	23.753 24.331 28.653 34.843	2.69 2.73 2.89 3.10	446(sh) 404 394 289	22.422 24.752 25.380 34.602	3.12 4.27 4.36 4.37	$^6A_{1g} \rightarrow {}^4T_{1g}$ (G) $^6A_{1g} \rightarrow {}^4T_{2g}$ (G) $n \rightarrow \pi^*$ $\pi \rightarrow \pi^*$
$[Cu(Lorn)_2]$	1.92	405 397 268	24.691 25.189 37.313	3.90 3.87 3.86	475(sh) 394 -	21.882 25.188 -	3.55 4.37 -	$^6A_{1g} \rightarrow {}^4T_{1g}$ (G) $n \rightarrow \pi^*$ $\pi \rightarrow \pi^*$
[Mn(AcO)(Lorn)]	5.58	436 358 278	22.936 27.933 35.971	3.43 3.05 3.17	461 396 276	21.692 25.253 36.232	3.43 4,10 4.16	$^6A_{1g} \rightarrow {}^4T_{1g}$ (G) $n \rightarrow \pi^*$ $\pi \rightarrow \pi^*$
[Cu(AcO)(Lorn)]	1.96	501 396 268	19.960 25.253 37.313	2.53 2.74 2.68	425 399 -	23,592 25.069 -	3.49 3.77 -	d-d $n \rightarrow \pi^*$ $\pi \rightarrow \pi^*$

sh = shoulder

The electronic spectra of the lornoxicam **19** and the complexes **20**, **21**, **24**, **25** were recorded in DMF and $CHCl_3$ solution and absorption maxima in the uv-visible region are listed in **table X.16** along with suggested assignments. **Figure X.23.** shows the absorption spectra observed for drug alone. For lornoxicam, **19** (UV absorption spectra recorded in $CHCl_3$) , an absorbance maximum is observed at 355 nm, a smaller one at 273 nm The maximum at 355 nm undergoes shift in DMF solutions towards 395 nm and the maximum at 273 nm shows shift to 282 nm, increasing the absorbance.[10] The shoulder band at ca. 282 nm attributed to $n \rightarrow \pi^*$ transition of the C=O group of amide moiety in the free H_2Lorn is shifted to 289 nm in the manganese complex 20 revealing the involvement of the C=O of amide group in complexation. The band at 395 nm in free HLorn assigned to $n \rightarrow \pi$ transition of the pyridyl nitrogen is shifted by an extent of 1 – 6 nm in the case of manganese complexes **20**, **24** and 1 – 40 nm in the case of copper complexes **21**, **25**. This shift can be assigned to the donation of the lone pair of the pyridyl nitrogen atom of HLorn to the metal ion ($N \rightarrow M$). The changes in the UV spectra of the complexes in comparison with that of lornoxicam may be attributed to the donation of the lone pair of electrons of O_{amide} and N_{pyr} atoms to the metal ions centers ($O \rightarrow M$ and $N \rightarrow M$) suggesting coordination of lornoxican through N_{pyr} and O_{amide} atoms.[4] The spectra of the complexes $[Cu(Lorn)_2]$ and [Mn(AcO)(Lorn)] exhibit band at 21.882 cm^{-1} and 21.692 cm^{-1} which can be assigment as a $^6A_{1g} \rightarrow {}^4T_{1g}$ (G) transition. The Mn(II) complex of type $[Mn(Lorn)_2]$ exhibits two sholder bands at 22.422 cm^{-1} 24.752 cm^{-1} that can be assigned as $^6A_{1g} \rightarrow {}^4T_{1g}$ (G) and $^6A_{1g} \rightarrow {}^4T_{1g}$ (G) transitions, respectively.

In the visible region, bands are observed for **20**, **24** and both copper complexes **21** and **25**. For the complexes low-intensity bands at 446 nm (**20**), 475 nm (**21**), 461 nm (**24**) and 425 (**25**) nm are attributed to d–d transitions. Bands at 446 nm (**20**), 475 nm (**21**) are also observed as a weak shoulder and can be attributed to a $d_{xy} \rightarrow d_{z2}$ transition. In electronic spectrum of $[Mn(Lorn)_2]$

and [Cu(Lorn)$_2$] in $CHCl_3$ those bands lie under the much stronger ligand-to-metal charge-transfer transition at λ = 420 nm and λ = 405 nm, respectively.These bands are typical for distorted octahedral stereochemistries.[4] **Figure X.24** shows the absorption spectra of the [Cu(Lorn)$_2$] in DMF solution.The spectra exhibit a behavior very similar to that of the free drug instead of new low intensity shoulder at 475 nm (responsible for the yellow color of the solutions).[10] Moreover the spectrum of [Mn(Lorn)$_2$] exhibits another band that can be attributed to d–d transitions at 404 nm assigned as $^6A_{1g} \rightarrow {}^4T_{2g}$ (G).

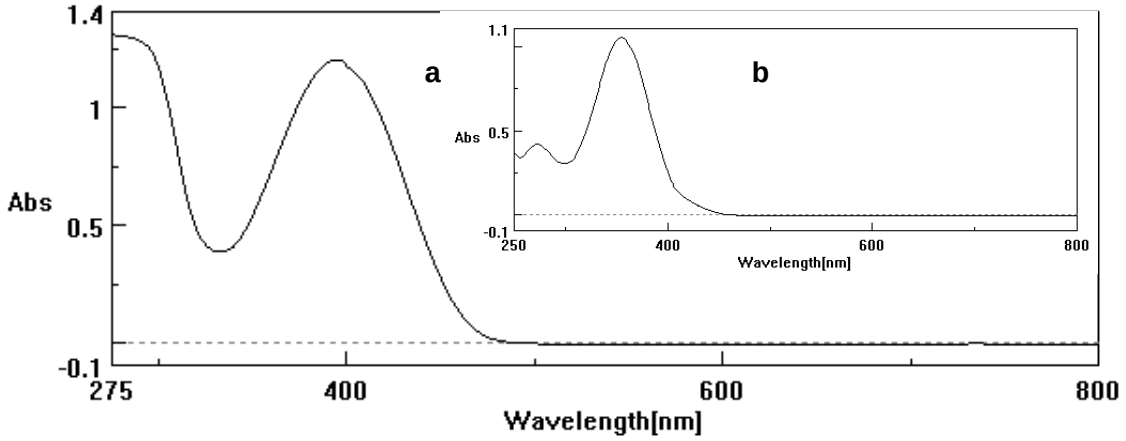

Figure X.23. UVi-vis absorption spectra of Lornoxicam, **19**, (a) 10^{-4}M in DMF, (b) 10^{-4}M in $CHCl_3$.

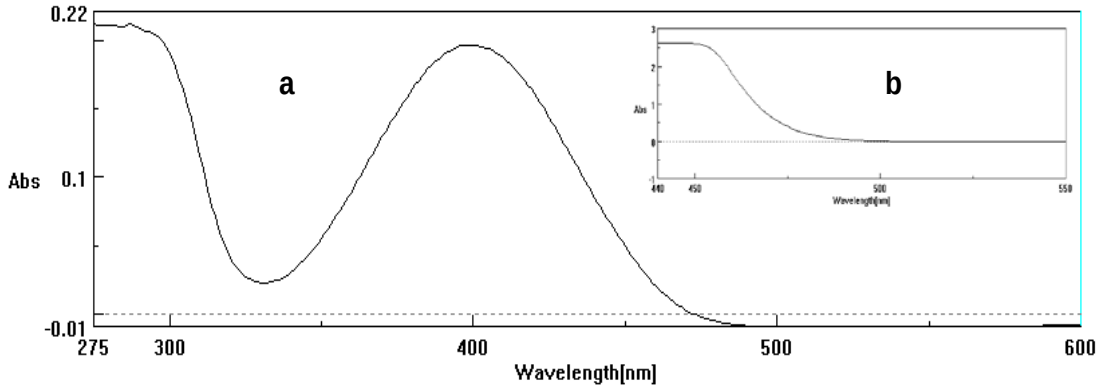

Figure X.24. UVi-vis absorption spectra of [Mn(Lorn)$_2$], **20**, (a) 10^{-5} M in DMF, (b) 10^{-3} M in DMF.

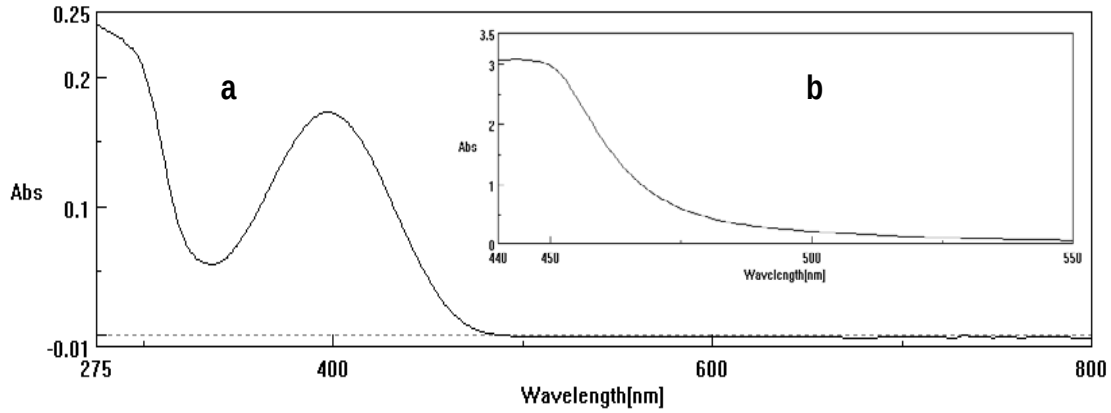

Figure X.25. UVi-vis absorption spectra of $[Cu(Lorn)_2]$ **21**, (a) 10^{-5} M in DMF, (b) 10^{-3} M in DMF.

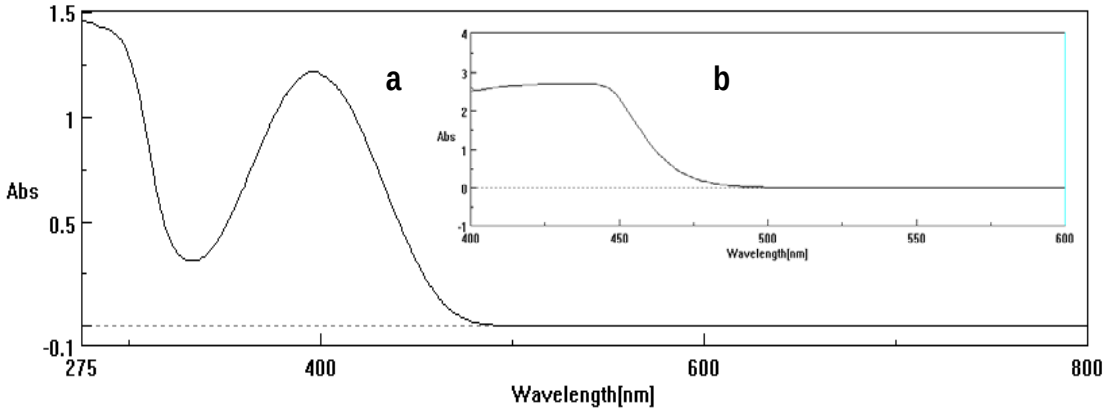

Figure X.26. UVi-vis absorption spectra of [Mn(AcO)(Lorn)] **24**, 10^{-4} M in DMF, (b) 10^{-3} M in DMF.

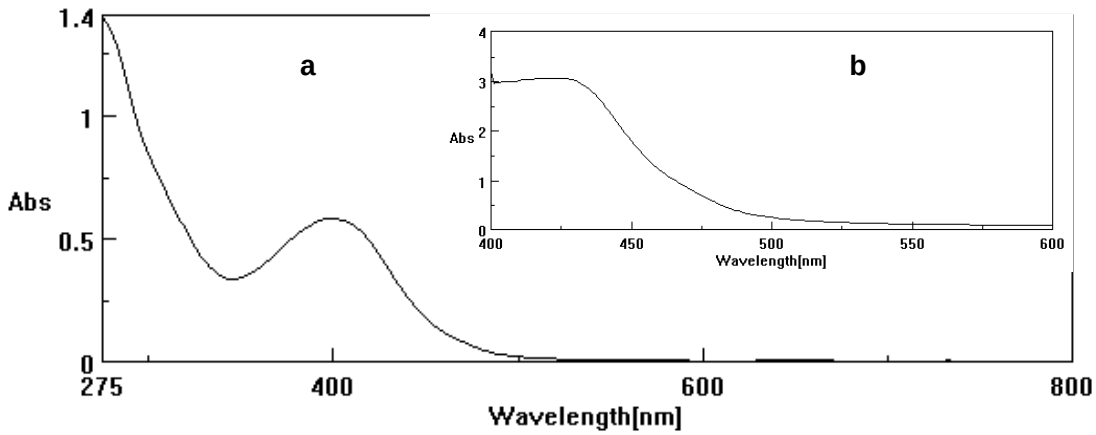

Figure X.27. UVi-vis absorption spectra of [Cu(AcO)(Lorn)] **25**, (a) 10^{4} M in DMF, (b) 10^{-3} M in DMF.

X.3.4. MS

ESI and APCI generate primarily: molecular ions M^+ or M^-, protonated molecules $[M + H]^+$, simple adduct ions $[M + Na]^+$, ions representing simple losses such as the loss of a water $[M + H - H_2O]^+$ The techniques requires polar solvents. For ionization eithr acetonitrile, methanol or mixtures of acetonitrile/water, methanol/water, were used. The formula of $[Cd(Lorn)_2(H_2O)_2]$ (891.3) is confirmed by molecular ion peak at m/z = 890.2

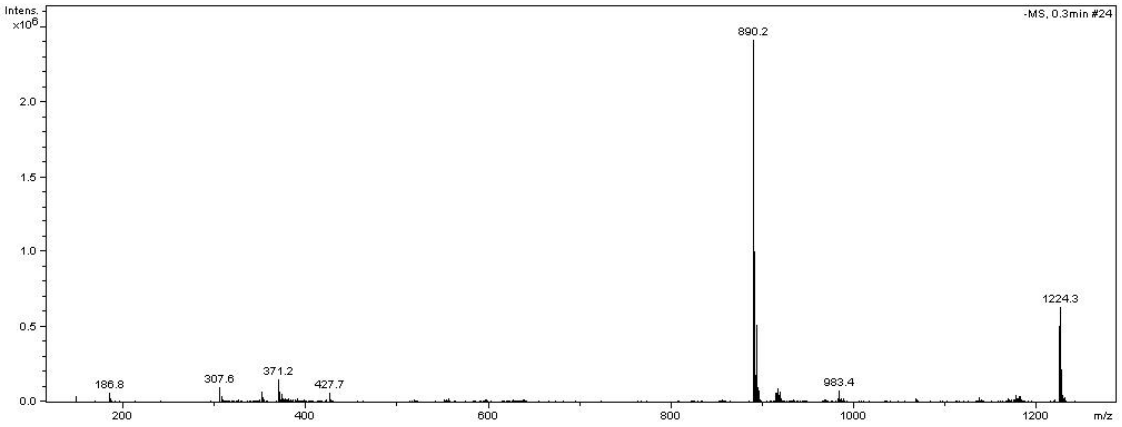

Figure X.28. ESI-MS spectrum of deprotonated complex of $[Cd(Lorn)_2(H_2O)_2]$, **23** in CH_3OH.

Conclusions (Chapter X).

The synthesis and characterization of eight new lornoxicam **19**, complexes with Mn^{2+}, Cu^{2+}, Zn^{2+}, Cd^{2+} have been realized with X-ray diffraction analysis, physicochemical and spectroscopic methods. In all complexes, lornoxicam is on deprotonated mode and acts as bidentate ligand bound to the metal ion through the carbonyl oxygen and pyridine nitrogen atoms. Each metal (complexes **20-23**, metal to ligand molar ratio 1:2) is six-coordinate and the environment around each metal could be described as pseudooctahedral. The structures of manganese(II), copper(II) and cadmium(II) complexes is confirmed by X-ray diffraction analysis.

In the series of complexes **24- 27** with 1:1 metal to ligand molar ratio one lornoxicam molecule, one acetate group and solvent molecules are coordinated to the metal ions. The presence of acetate group is confirmed by one singlet at ca. 1.86 ppm in ^{1}H–NMR spectra of complexes **26** and **27** and by two resonances attributed to the acetate carbons at ca. 22. ppm and 175 ppm in ^{13}C-NMR spectra of complexes **26** and **27**.

References

1. Defazio, S., Cini, R. Dalton *J. Chem. Soc., Dalton Trans.,* 1888–1897 (2002).
2. Tamasi, G., Serinelli, F., Consumi, M., Magnani, A., Casolaro, M., Cini , R. *Journal of Inorganic Biochemistry* **102,** 1862–1873 (2008).
3. Bordner, J., Hammen, P.D., Whipple, E.B. *J. Am. Chem. Soc.*,**111,** 6572-6578 (1989).
4. Katsarou, C.P. Papakyriakou, M., Sanakis, A., Katsaros, Y., Psomas, N.,*Journal of Inorganic Biochemistry* **99,** 2197–2210 (2005).
5. Galani, A., Demertzis, M.A., Kubicki, M., Kovala-Demertzi, D., *Eur. J. Inorg. Chem.*1761-1767 (2003).
6. Mendez-Rojas, M.A.,, Cordova-Lozano, F., Gojon-Zorrilla, G., Gonzalez-Vergara, E., Quiroz., M.A. *Polyhedron* **18,** 2651– 2658 (1999).
7. Cini, R., Tamasi, G., Defazio, S., Hursthouse, M.B. *Journal of Inorganic Biochemistry* **101,** 1140–1152 (2007).
8. Moya-Hernandez, M.R., Mederos, A., Domınguez, S. Orlandini , A., Ghilardi, C.A., Cecconi, F., Gonzalez-Vergara, E., Rojas-Hernandez, A., *Journal of Inorganic Biochemistry* **95,** 131–140 (2003).

XI. Synthesis and characterization of manganese(II), copper(II), zinc(II) and cadmium(II) complexes with [7-(D-2-amino-2-phenylacetamido)-3-chloro-3-cepham-4-carboxylic acid], cefaclor (28).

XI.1. General

All metal complexes **29 – 32** and **33 – 36** were prepared by the stoichiometric reaction of the corresponding metal(II) salts as acetate or metal(II) chloride with the cefaclor, **Hcef**, [7-(D-2-amino-2-phenylacetamido)-3-chloro-3-cepham-4-carboxylic acid] in a molar ratio M:L of 1:2 (**table XI.1**) and 1:1 (**table XI.2**). The reaction mixture has been either stirred or refluxed for a few hours. The resulting microcrystalline or powder-like products have been obtained after filtration.

Table XI.1.. Analytical and physical data of the cefaclor complexes **29 – 32**.

	Compounds	M.W g/mol	mp ˚C	Colour	C%	H%	N%	S%	M%
28	Hcef	367.81	>300°C (dec)	yellow					
29	$[Mn(Cef)_2]$	797.076	180°C (dec)	brown					6.97 (6.2±0.5)
30	$[Cu(Cef)_2]$	788.468	>300°C (dec)	brown	45.21 (45.53)	3.28 (4.14)	10.54 (10.52)	8.04 (10.68)	8.52 (10.3±1.4)
31	$[Zn(Cef)_2]$	798.910	>300°C (dec)	yellow					8.18 (7.1±1.5)
32	$[Cd(Cef)_2]$	845.940	246°C	yellow					13.29 (12.9±1.4)

Results of elemental analysis: calculated, (found).
Results of XRF: calculated, (found).

Table XI.2. Analytical and physical data of the lornoxican complexes **33 – 36**.

	Complexes	M.W g/mol	mp ˚C	Colour	M%
33	[Mn(AcO)(Cef)][a]	480.734	>300°C (dec)	brown	11.43 (12.7±1.6)
34	[Cu(AcO)(Cef)][a]	447.312	180°C (dec)	brown	12.99 (12.3±1.1)
35	[Zn(AcO)(Cef)][a]	449.146	>300°C (dec)	orange	13.31 (12.9±1.4)
36	[Cd(AcO)(Cef)][a]	538.206	>300°C (dec)	brown	20.89 (21±1.3)

Results of XRF: calculated, (found).

[a] Ac = CH_3CO

The complexes $[Mn(Cef)_2]$ **29**, $[Cu(Cef)_2]$ **30**, $[Zn(Cef)_2]$ **31**, $[Cd(Cef)_2]$ **32**, were synthesized according to the reactions (a) – (d). The complexes [Mn(AcO)(Cef)] **33**, [Cu(AcO)(Cef)] **34**, [Zn(AcO)(Cef)] **35**, [Cd(AcO)(Cef)] **36**, were synthesized according to the reactions (e) – (h).
The complexes are stable in atmospheric conditions. All the complexes are slightly soluble in water, except of parent drug **34** and cadmium complexes **32** and **36** which are insoluble in water.

Moreover all complexes are solouble in polar solvent as DMSO, parent drug **28** and 29, 30, 31, 33 are also soluble in DMF. Besides cefaclor and copper complexes, complexes **30** a **31** are soluble in nonpolar solvent as THF.

$Mn(AcO)_2 + 2\ HCef \rightarrow [Mn(Cef)_2] + 2\ AcOH$ (a)

$Cu(AcO)_2 \cdot H_2O + 2\ HCef \rightarrow [Cu(Cef)_2] + 2\ AcOH + H_2O$ (b)

$Zn(AcO)_2 \cdot 2\ H_2O + 2\ HCef \rightarrow [Zn(Cef)_2] + 2\ AcOH + 2\ H_2O$ (c)

$Cd(AcO)_2 \cdot 2\ H_2O + 2\ HCef \rightarrow [Cd(LCef)_2] + 2\ AcOH + 2\ H_2O$ (d)

$Mn(AcO)_2 + HCef \rightarrow [Mn(AcO)(Cef)] + AcOH$ (e)

$Cu(AcO)_2 \cdot H_2O + HCef \rightarrow [Cu(AcO)(Cef)] + AcOH + H_2O$ (f)

$Zn(AcO)_2 \cdot 2\ H_2O + HCef \rightarrow [Zn(AcO)(Cef)] + AcOH + 2\ H_2O$ (g)

$Cd(AcO)_2 \cdot 2\ H_2O + HCef \rightarrow [Cd(AcO)(Cef)] + AcOH + 2\ H_2O$ (h)

Table XI.3 Solubility test of **29** – **36** complexes and parent drug **28**.

	H_2O	n-pentane	n-hexane	Et_2O	CH_3NO_2	CH_3CN	cyclohexane	methanol	ethanol	acetone	toluene	benzene	THF	DMF	DMSO	CH_2Cl_2	$CHCl_3$
28	+/-	+/-	+/-	-	+/-	+/-	+/-	+/-	+/-	+/-	+/-	+/-	+	+	+	+/-	+/-
29	+/-	+/-	+/-	+/-	+/-	+/-	+/-	+/-	+/-	+/-	-	+/-	+	+	+	+/-	+/-
30	+/-	+/-	+/-	-	+/-	+/-	+/-	+/-	+/-	+/-	+/-	+/-	+	+	+	+/-	+/-
31	+/-	+/-	+/-	+/-	+/-	+/-	+/-	+/-	+/-	+/-	+/-	+/-	+	+	+	+/-	+/-
32	-	+/-	+/-	+/-	+/-	+/-	+/-	+/-	+/-	+/-	+/-	+/-	+/-	+/-	+	+/-	+/-
33	+/-	+/-	+/-	+/-	+/-	+/-	+/-	+/-	+/-	+/-	+/-	+/-	+	+	+	+/-	+/-
34	-	-	-	-	+/-	+/-	-	+/-	-	+/-	-	-	+/-	+/-	+	+/-	+/-
35	+/-	+/-	+/-	+/-	+/-	+/-	+/-	+/-	+/-	+/-	+/-	+/-	+/-	+/-	+	+/-	+/-
36	-	+/-	+/-	+/-	+/-	+/-	+/-	+/-	+/-	+/-	+/-	+/-	+/-	+/-	+	+/-	+/-

+ soluble; +/- slightly soluble; - insoluble.

XI.1. Spectroscopic characterization of Mn(II), Cu(II), Zn(II) and Cd(II) complexes with cefaclor.

XI.1.1. Nuclear magnetic resonance

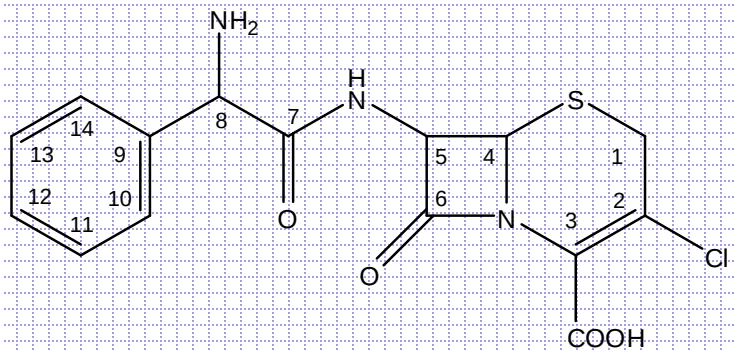

Figure XI.1. Structural formule of cefaclor, **28**.

The proton and carbon signals were assigned using ^{1}H and ^{13}C specra and DEPT-135 spectra. The data have been interpreted based on literature data reported.[1,2] The ^{1}H NMR and ^{13}C–NMR shifts of zinc complexes, **31**, **35** and cadmium complexes **32**, **36** and free cefaclor (HCef), **28** are presented in **table XI.4** and **table XI.5.** All the protons were found to be in their expected region. ^{1}H and ^{13}C specra and DEPT spectra of the free ligand and its diamagnetic Zn (II) and cadmium (II) complexes were taken in DMSO-*d6*.[5] Cefaclor has a several potentaial donor atoms nitrogen, oxygen and sulfur.[3,4] However the presence of the peak at ca. 11,1 ppm and 11.4 ppm for zinc complexes, **31**, **35** and cadmium complexes **32**, **36**, attributed to the proton of the carboxylate group, elimnates the involvement of the carboxyl oxygen in complexation. The signal relevant to the proton of the carboxylate group for complexes shifted upfield when compared to that found for free Hcef.The ^{1}H NMR spectra of the complexes **31**, **35**, **32**, **36** are compared with this of cefaclor, **28**. The broad peaks are probably due to the presence of CI in the molecule.[1] All signals are shifted toward higher fields, except signals of H(1), which are shifted downfield relative to cefaclor, **28**. The most significant chemical shift difference (0.22 ppm) between the H(1) proton of the free drug and complex is observed for **32**. The analysis of the chemical shifts for the signals of **28** shows that the peaks attributable to the β-lactam H(4), H(5),protons occur at 5.08 ppm (doublet 1H), 5.91 ppm (triplet, 1H), 7.07, respectively. The signals for those protons undergo upfield shift (ca. 0.1 ppm) upon complexation when compared to the spectrum of free Hcef , whereas the signals for the H(8) proton also experience upfield shifts by 0.13 ppm and 0.10 ppm, for zinc complexes, **31**, **35** and cadmium complexes **32**, **36**.The changes of the chemical shifts of the β-lactam protons and CH proton signals indicate that the Zn and Cd atoms are bounded to the cefaclor molecule through the O atoms of amide groups and β-lactam sysytem. The resonances due to the aromatic proton atoms for **36** occure at 7.31 ppm as a

singlet. Besides the cadmium complex **36**, the spectral region around 7.20 – 7.50 ppm is complex and overlapping for **31**, **32**, **35** and it is assigned to protons in aromatic rings. For **35** and **36** one singlet appears at ca. 1.85 ppm, thus in the region of proton of acetate group. Two resonances attributed to the acetate carbons are found at 22.5 ppm and 175 ppm in ^{13}C-NMR spectrum of **35**, **36**, respectively, confirm the presence of acetate group in the complexes.

Involvement of the oxygen atoms of amide groups and β-lactam sysytem in bonding to Zn or Cd is confirmed by the resonance ascribed to C6, C7, C8, which exhibits the greatest shift upon coordination. Figure XI.7. shows DEPT-135 spectra of cefaclor, **28** and Cd(Cef)$_2$], **32,** methylene carbon C1 can be assigned with the help of DEPT-135 experiments, where methylene carbon (CH_2) and remaining carbons (CH, CH_3) signals appear as negative and positive phase, respectively. In the ^{13}C-NMR spectra of all complexes, the greatest downfield shift is exhibited by the C7 atom (2.8 ppm for the cadmium complex, **35**) while the carbonyl C shifts downfield by ca 1.0 ppm. The C9 resonance, by contrast, shifts upfield. The remaining resonances due to the aromatic carbon atoms for all complexes do not shift considerably after binding to metal atoms. Moreover the spectral region around 128 – 130 ppm ppm is complex and overlapping. In all ^{1}H-NMR spectra of zinc and cadmium complexes with cefaclor, **28** one triplet appear at ca. 1.0 ppm and one quartet at ca. 2.5 ppm. These peaks are assign to protons of triethylamine (CH_3 and CH_2), respectively. The presence of triethylamine is confirmed by two peaks ca. at 12 ppm and 45 ppm in ^{13}C-NMR of complexes.

Table XI.4. ^{1}H NMR shifts of **31**, **32** and **35**, **36** complexes and parent drug **28** (δ in ppm and *J* in Hz).

	28[a]	**31**[a]	**35**[a]	**32**[a]	**36**[a]
OH	11.45s	11.11s	11.08s	11.38	11.30
HN	9.23s	9.10	9.12	9.29	11.11
NH_2 – C(8)	5.73s	-	-	-	-
H – C(1)	3.40s	3.35s	3.43s	3.62s	3.61s
H – C(4)	5.08d	4.95m	4.98m	5.00m	4.95m
H – C(5)	5.91t	5.79m	5.82s	5.88t	5.84s
H –C(8)	4.99s	4.87m	4.85m	4.91m	4.90m
H – C(10)	7.20 – 7.50m	7.31 – 7.48m	7.32 – 7.50m	7.27 – 7.44m	7.31s
H –C(11)					
H –C(12)					
H –C(13)					
H –C(14)					
CH_3COO			1.85s		1.86s

[a] spectrum recorded in DMSO-d_6
[b] disappears upon coordination

Table XI.5. ^{13}C NMR shifts (ppm) of **31**, **32** and **35**, **36** complexes and parent drug **28**.

	28[a]	**31**[a]	**35**[a]	**32**[a]	**36**[a]
COOH	166.8	166.0	165.5	165.9	166.2
C1	29.8	29.2	-	23.1	30.7
C2	133.4	133.7	133.6	133.5	133.4
C3	125.1	124.6	126.0	126.3	126.2
C4	57.0	56.7	56.6	58.8	56.1
C5	58.7	59.6	59.7	59.2	59.2
C6	167.6	168.7	168.1	166.8	166.1
C7	168.2	170.4	171.0	167.8	166.6
C8	55.1	50.5	50.9	50.7	51.1
C9	134.6	134.5	134.6	135.1	134.5
C10	128.7	128.1	128.3	128.8	128.5
C11	127.9	127.3	127.5	128.1	128.0
C12	126.3	126.0	126.9	126.6	126.6
C13	128.1	127.8	128.0	128.6	128.2
C14	129.3	128.8	129.0	129.4	128.6
CH_3COO	-	-	22.5 174.9	-	22.5 174.6

[a] Spectrum recorded in DMSO-d_6
[b] disappears upon coordination

Figure XI.2. ^{1}H-NMR spectrum of Cefaclor, **28** recorded in dmso-d_6..

Figure XI.3. ^{1}H-NMR spectrum of [Zn(Cef)$_2$], **31** recorded in dmso-d_6.

Figure XI.4. ^{1}H-NMR spectrum of [Zn(AcO)(Cef)] , **35** recorded in dmso-d_6.

Figure XI.5. ^{1}H-NMR spectrum of [Cd$(Cef)_2$], **32** recorded in dmso-d_6.

Figure XI.6. ^{1}H-NMR spectrum of [Cd(AcO)(Cef)], **36** recorded in dmso-d_6.

Figure XI.7. DEPT spectrum of Cefaclor, **28** recorded in dmso-d_6.

Figure XI.8. ^{13}C-NMR spectrum of [Cd(Cef)$_2$], **32** recorded in dmso-d_6.

Figure XI.9. DEPT spectrum of [Cd(Cef)$_2$], **32** recorded in dmso-d_6.

Figure XI.10. ^{13}C-NMR spectrum of [Zn(AcO)(Cef)] , **35** recorded in dmso-d_6.

Figure XI.11. ^{13}C-NMR spectrum of [Cd(AcO)(Cef)], **36** recorded in dmso-d_6.

XI.1.2. Infrared spectroscopy.

Table XI.6. IR-data (cm^{-1}) for the prepared complexes **29 – 32** and parent drug **28**.

		νN–H	ν(C=O) β-lactam	ν(C=O) amide	ν_{asym}(COO)	ν_{sym}(COO)	ν(C–N) β-lactam	ν(M–O)
28	HCef	3331m	1779s	1700s	1607s	1458w	1359m	-
29	$[Mn(Cef)_2]$	3403m 3216m	1775s	1698s	1602m	1455w	1352s	238mw
30	$[Cu(Cef)_2]$	3435m 3213m	1773s	1697s	1607m	1457w	1352s	231mw
31	$[Zn(Cef)_2]$	3327m 3224m	1777s	1636w	1606w	1436w	1369m	381mw
32	$[Cd(Cef)_2]$	3435m 3201mw	1773s	1636m	1610s	1435w	1368s	382mw

s = strong, m = medium, w = weak, sh = sharp, br = broad

Table XI.7. IR-data (cm^{-1}) for the prepared complexes **33 – 36**.

		νN–H	ν(C=O) β-lactam	ν(C=O) amide	ν_{asym} (COO)	ν_{sym}(COO)	ν(C–N) β-lactam	ν(M–O)
33	[Mn(AcO)(Cef)]	3364s	1732m,	1638m,	1638m	1437w	1385w	386mw
34	[Cu(AcO)(Cef)]	3418s	1723m	1608m	1608m	1446w	1385w	363mw
35	[Zn(AcO)(Cef)]	3247m	1635m,	1635m	1592w	1434w	1385w	365mw
36	[Cd(AcO)(Cef)]	3250m	1636m,	1636m,	1608s	1453w	1387m	376mw

s = strong, m = medium, w = weak, sh = sharp, br = broad

The coordination chemistry of some β-lactam antibiotics with transition metal ions has been reported.[4,5] Cefaclor molecule has several potential donor atoms but probably due to steric constraints, the molecule can provide only some of donor sites to the metal atom. Cefaclor molecule could coordinate through the carboxylate, lactam ring and/or nitrogen of NH amide group or NH_2 amine group.[4,5] IR spectra of cefaclor and its metal complexes are reported in **table XI.6** and **table XI.7.** The investigated of cefaclor has a number of similar functional groups and, thus IR spectra shoved several common absorption bands, *i.e*. in the carbonyl region. All of the complexes showed a β-lactam carbonyl band in a range 1725 – 1780 cm^{-1}. A comparison between the IR spectra of cefaclor and those of its transition metal complexes **29 – 32** and **33 – 36** provides evidence regarding the bonding sites in the cefaclor complexes.[5] The infrared spectrum of cefaclor shows an NH amide stretching band at 3331 cm^{-1}, a β-lactam stretching at about 1779 cm"[1], and an amide carbonyl band at 1700 cm^{-1}.[1] The complexes **29**, **30** having a molar ratio of metal:cefaclor as 1:2 exhibit unchanged amide and lactam bands. These observations suggest that cefaclor is not coordinated to the metal ions through amide or lactam oxygens for **29**, **30** complexes. In metal complexes **33** – **36** ν(C=O) $_{\beta\text{-lactam}}$ is shifted to lover wavenumbers in the range 1640 – 1608 cm^{-1}.[5] Although cefaclor contains a number of potentail donor atoms (nitrogen, oxygen and sulfur), the pattern of spectra show that cefaclor could acts as a bidentate and could bond with metal atoms either through its oxygens (amide and β-lactam) for **33** – **36** complexes or carboxyl oxygens and/or nitrogen of β-lactam for **29, 30** complexes.

A comparative scrutiny of the infrared spectral data of the complexes **30 – 36** with those of uncomplexef ligand indicates that a strong stretching vibration of carbonyl at 1607 cm^{-1} in the ligand is not effected upon complexation. However, the complexes showed two charaecteristic bands (not observed in the free ligand) in the region 360 – 380 cm^{-1} attributed to (M–O) modes respectively, which hint at the coordination of the ligand to metal atoms through the oxygens. [3,6,7.]

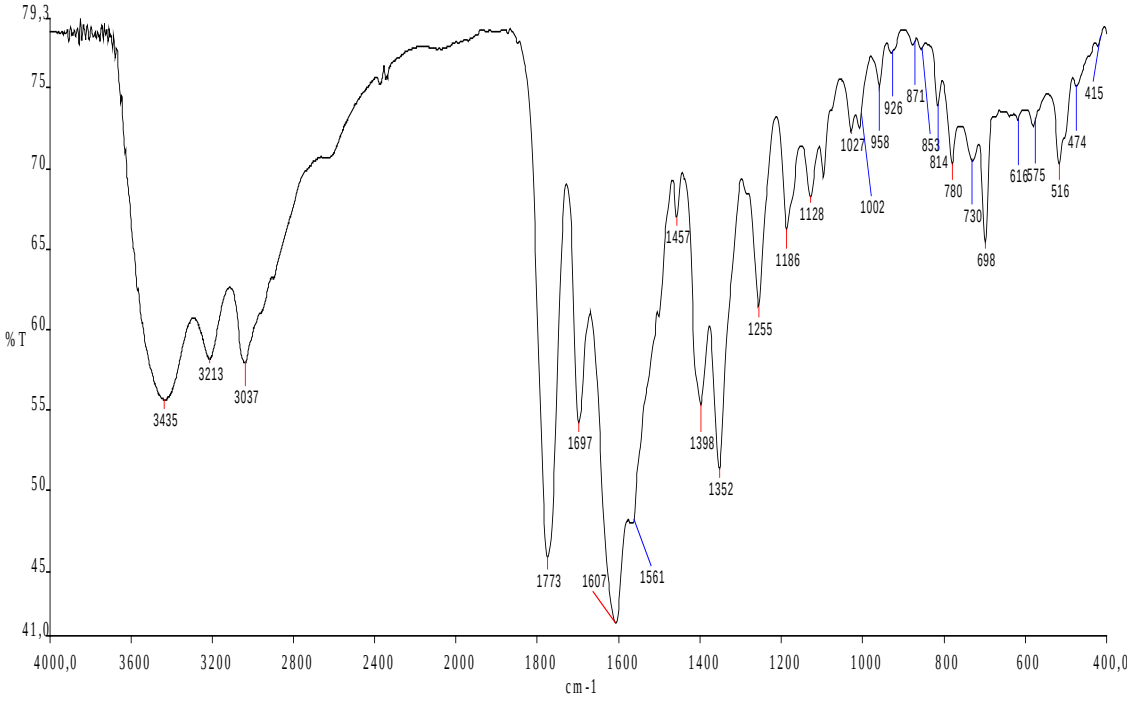

Figure XI.12. Infrared spectrum of [Cu(Cef)], **30**.

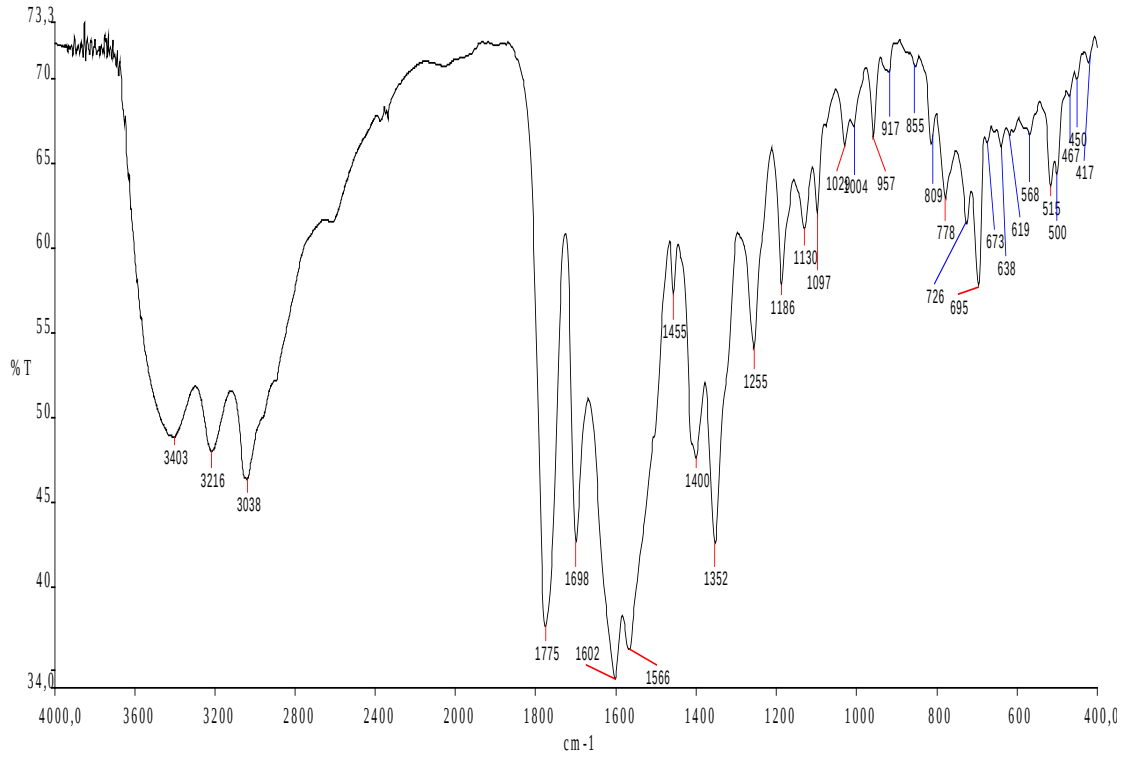

Figure XI.13. Infrared spectrum of [Mn(Cef)], **29**.

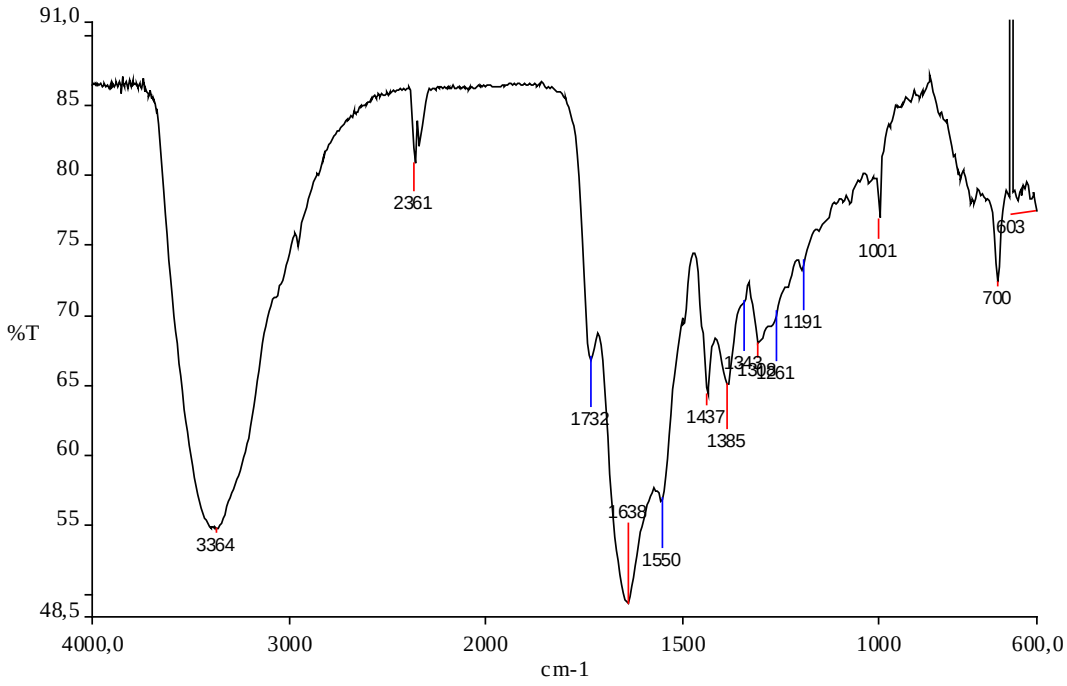

Figure XI.15. Infrared spectrum of [Mn(AcO)(Cef)], **33**.

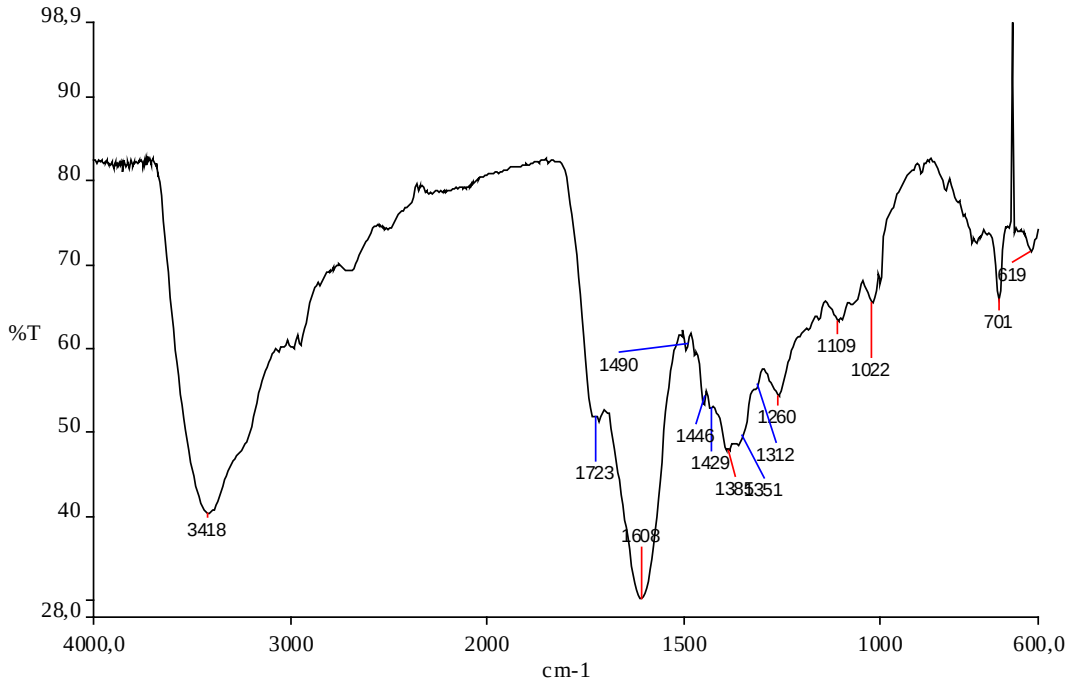

Figure XI.16. Infrared spectrum of [Cu(AcO)(Cef)], **34**.

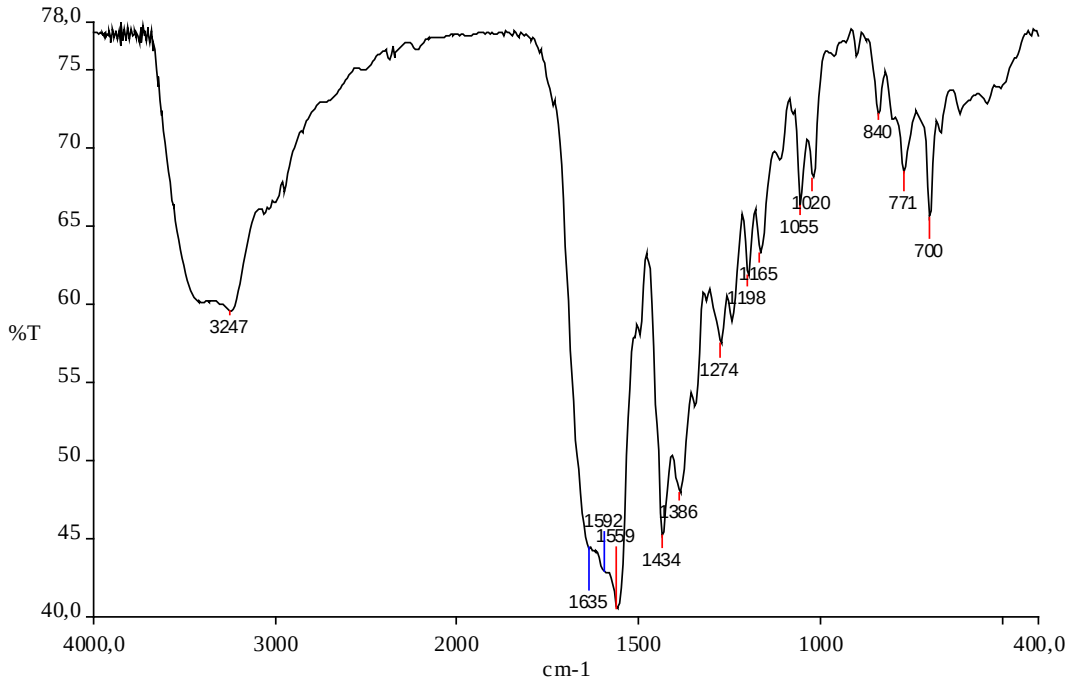

Figure XI.16. Infrared spectrum of [Zn(AcO)(Cef)], **35**.

XI.1.3. Electronic spectroscopy.

Table XI.8. Spectral data (UV-vis) for the prepared complexes **29**, **30**, **33**, **34** and the parent drug **28**.

Compounds	μ_{eff}	$CHCl_3$			DMF			Assignments
		λ (nm)	ν (cm^{-1})	log ε	λ (nm)	ν (cm^{-1})	log ε	
Cefaclor		351 290	28,490 34.483	3.76 4.01	370 282	27.027 35.461	3.65 3.88	$n \rightarrow \pi^*$ $\pi \rightarrow \pi^*$
$[Mn(Cef)_2]$	6.02	612 445 341 288	16.340 22.472 29,326 34,720	2,72 2.83 3.37 3.61	663 457sh 338sh -	15.083 21.882 29.586 -	2.29 3.02 3.63 -	d – d $^6A_{1g} \rightarrow {}^4T_{1g}$ (G) $n \rightarrow \pi^*$ $\pi \rightarrow \pi^*$
$[Cu(Cef)_2]$	1.80	416 339 271	24.038 29.499 36.900	2.19 3.28 3.36	483 364 -	20.704 27.473 -	3.19 3.56 -	$^6A_{1g} \rightarrow {}^4T_{1g}$ (G) $n \rightarrow \pi^*$ $\pi \rightarrow \pi^*$
[Mn(AcO)(Cef)]	5.72	415 272	24.096 36.765	3.38 3.40	434 -	23.041 -	3.4 -	d – d $\pi \rightarrow \pi^*$
[Cu(AcO)(Cef)]	1.88	567 401 342 288	17.637 24.938 29.239 34.722	2.10 2.85 3.60 4.63	617 412 339 -	16.207 24.272 29.499 -	2.57 3.24 3.44 -	d – d $^6A_{1g} \rightarrow {}^4T_{1g}$ (G) $n \rightarrow \pi^*$ $\pi \rightarrow \pi^*$

sh = shoulder

The electronic spectra of the lornoxicam **28** and the complexes **29**, **30**, **33**, **34** were recorded in DMF and $CHCl_3$ solution and absorption maxima in the uv-visible region are listed in **table XI.8.** along with suggested assignments. **Figure XI.17.** shows the absorption spectra observed for drug alone. For cefaclor, **28**, an absorbance maximum is observed at 370 nm, a another one at 282 nm The band at ca. 370 nm is attributed to $n \rightarrow \pi^*$ transition and the band at 282 is assigned to $\pi \rightarrow \pi^*$, respectively.

The spectrum of $[Mn(Cef)_2]$, **29** exhibits two bands that can be attributed to d-d trnasitions, one at 617 nm, and sholder band at 457, which can be assigned as $^6A_{1g} \rightarrow {}^4T_{1g}$ (G) transition. Additionally a band at λ = 338 observed as a shoulder can be attributed to $n \rightarrow \pi^*$ transition. The electronic spectra of the Cu(II) complexe, **30** exhibits band at λ = 483 that can be attributed to d-d trnasition which can be assigned as $^6A_{1g} \rightarrow {}^4T_{1g}$ (G) transition. Moreover a band at 27.473 cm^{-1} can be attributed to $n \rightarrow \pi^*$ transition. The spectra of [Mn(AcO)(Cef)], **33** display band at about 434 nm, in turn, is assigned to d-d transition. The Cu(II) complex of the type [Cu(AcO)(Cef)], **34** showed low-energy band at 17.637 cm^{-1} and exhibit strong-high energy bands at 24.938 cm^{-1} 29,239 cm^{-1} 34.722 cm^{-1} and are assigned to the transitions $^6A_{1g} \rightarrow {}^4T_{1g}$ (G), $n \rightarrow \pi^*$, $\pi \rightarrow \pi^*$.

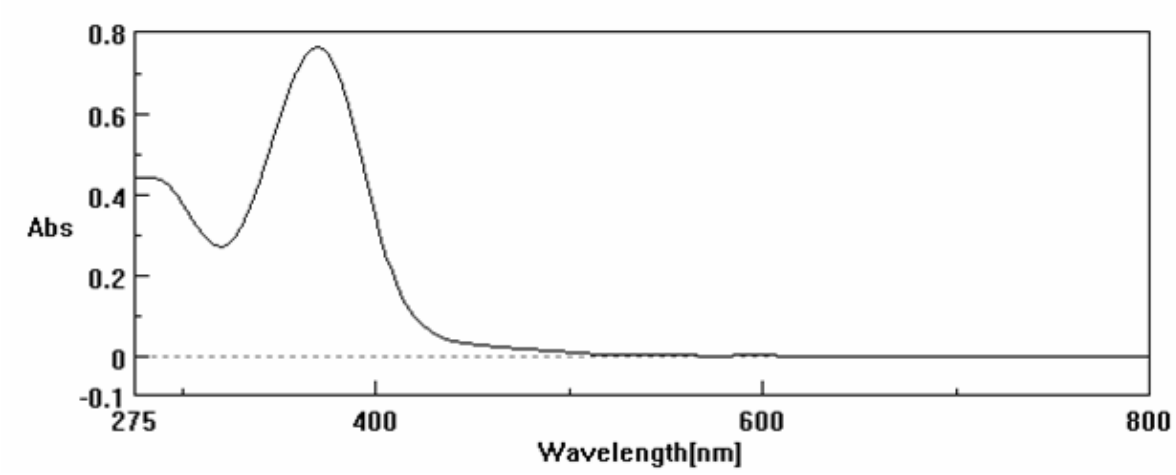

Figure XI.17. UVi-vis absorption spectra of cefcalor (Hcef), **28**, 10^{-4} M in DMF.

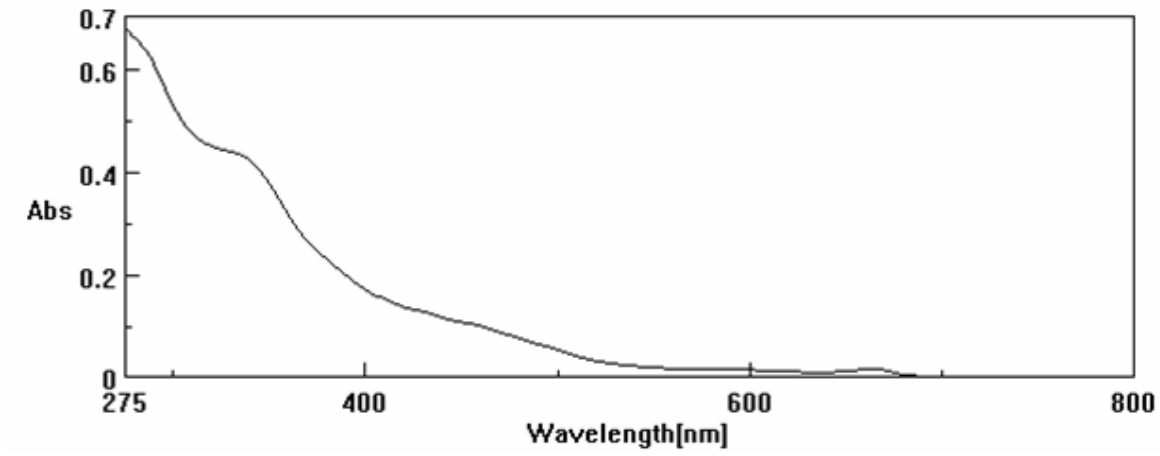

Figure XI.18. UVi-vis absorption spectra of [Mn(Cef)$_2$], **29**,10^{-4} M in DMF.

.

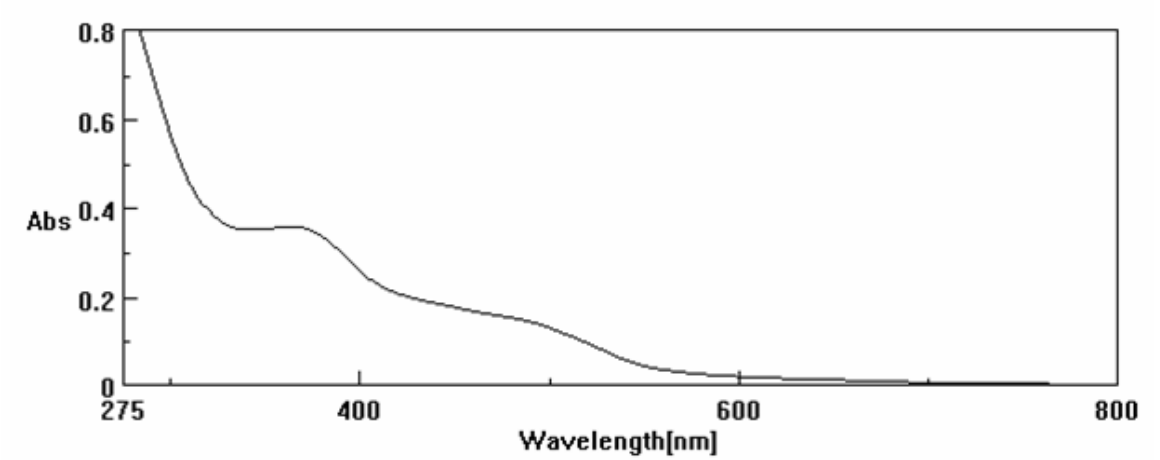

Figure XI.19. UVi-vis absorption spectra of [Cu(Cef)$_2$], **29**, $^{-4}$ M in DMF.

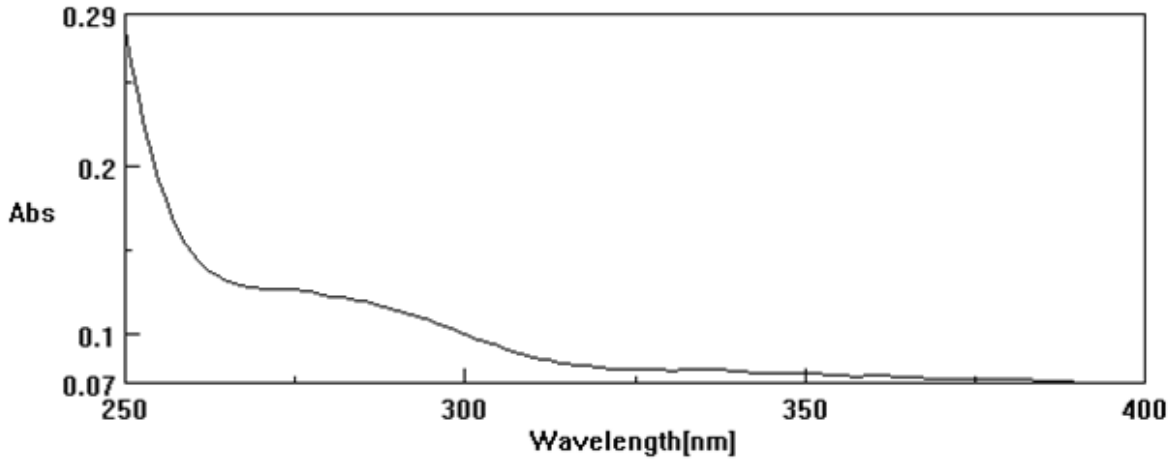

Figure XI.20. UVi-vis absorption spectra of Mn(AcO)(Cef)] **33**,10^{-4} M in DMF.

Conclusions (Chapter XII)

The synthesis and characterization of eight new cefaclor complexes with Mn^{2+}, Cu^{2+}, Zn^{2+}, Cd^{2+} have been realized with physicochemical and spectroscopic methods. In zinc and cadmium complexes (1:2 and 1:1 metal to ligand molar ratio), manganese and copper complexes with 1:1 metal to ligand molar ratio, cefaclor acts as bidentate ligand and preferentially bond through its oxygen atoms of amide group and β-lactam system. In manganese and copper complexes with 1:2 metal to ligand molar ratio cefaclor bond through either oxygen atoms of carboxyl group or oxygen atom of carboxyl group and nitrogen atom of β-lactam system. In the series of complexes with 1:2 metal to ligand molar ratio two cefaclor molecules. In the series of complexes with 1:1 metal to ligand molar ratio one cefaclor molecule, one acetate group. The presence of acetate group is confirmed by one singlet at ca. 1.85 ppm in ^{1}H–NMR spectra of complexes **35** and **36** and by two resonances attributed to the acetate carbons at ca. 22.5 ppm and 178 ppm in ^{13}C-NMR spectra of complexes **35** and **36**.

References

1. Martinez, H., Byrn, S.R., Pfeiffer, R., *Pharmaceutical Research,* **7,** 147-153 (1990).
2. Vilanova, B., Donoso, J., Muiioz, F., Garcia-Blanco, F. *Helvetica Chimica Acta* **79,** 1793 (1996)
3. Chohan, Z.H., *Chem. Pharm. Bull*. **39,** 1578-1580 (1991).
4. Chohan, Zahid H., Supuran, Claudiu T. and Scozzafava, A. *Journal of Enzyme Inhibition and Medicinal Chemistry* **19,** 79 — 84 (2004).
5. Chohan, Z.H., Supuran, C.,T. *Journal of Enzyme Inhibition and Medicinal Chemistry* **21,** 441 — 448 (2006).
6. Fazakerley, G. V., Jackson, G.E. *J. inorg, nuck Chem..* **37,** 2371-2375 (1975).
7. Moratal, J.M., Borras, J., Donaire, A. In*organica Chimica Acta,* **162,** 113-119 (1989)

XII. Antiproliferative activity *in vitro* of of Mn(II), Cu(II), Zn(II) and Cd(II) complexes with meclofenamic acid, flufenamic acid, lornoxicam and cefaclor.

Platinum is a non-endogenous toxic heavy metal, whereas copper, manganese and zinc are an essential elements that is required for several key processes in the body. A wellknown example is Cu,Zn–superoxide dismutase enzyme that showed an important role in taking control on the inflammations and rheumatic diseases. On the other side, the ligands **1**, **10**, **19** and mostly the copper-complexes are well established anti-inflammatory drugs that passed scrupulous screening toxicity tests. Therefore, it is supposable that the administration of drugs like 1 and possibly 2 and 3, and 4, might hopefully produce beneficial effects as anticancer agents (through anti-proliferative activity) and anti-inflammatory and anti-rheumatic agents (through the specific activity of the NSAIDs ligands, and the oxygen radical scavenging activity of copper complexes).[1] Part of the project including studies aimed to cefaclor and its complexes were inspired by the successful introduction of metal based compounds of β-lactam antibiotics to stop and/or heal bacterial infections.

The results of cytotoxic activity *in vitro* are expressed as IC_{50} , i.e., the concentration of compound (in mm) that inhibits a proliferation rate of the tumor cells by 50% as compared to control untreated cells. Manganese(II), copper(II) zinc(II) and cadmiu complexes of meclofenamic acid, flufenamic acid, lornoxicam and cefaclor and free ligands were tested for their antiproliferative activity *in vitro* against the cells of three human cancer cell lines, MCF-7 (breast cancer cell line), T24 (bladder cancer cell line), and A-549 (non-small-cell lung carcinoma), and a mouse fibroblast L-929 cell line, and the results are compared with those of the known chemotherapeutic cisplatin. Since the complexes were diluted in dmso, its effect in MCF-7, T24, A-549, L-929 cancer cells at its highest concentration was also tested and found that the amount of dmso used in all experiments did not have such a significant cytotoxic effect, that could interfere with the rest of the results.

Table XII.1. The antiproliferative activity *in vitro* of meclofenamic acid **1** and **2 -7** (expressed as IC_{50} (μM) against MCF-7, T-24, A-549 and L-929 cancer cell lines.

	Compounds	L-929	A-549	T-24	MCF-7
1	Hmcfa	133.0 ± 0.8	139.1 ± 0.7	70.2 ± 0.3	63.1 ± 0.4
2	$[Mn(MCFA)_2]$	25.3 ± 2.4	27.4 ± 3.2	3.8 ± 1.3	39.8 ± 2.4
3	$[Cu(MCFA)_2(H_2O)]$	61.9 ± 3.9	41.2 ± 5.6	5.3 ± 0.6	38.2 ± 0.9
4	$[Zn(MCFA)_2(H_2O)_4]$	24.2 ± 2.8	>244 (32%)*	3.2 ± 1.0	32.5 ± 2.1
5	$[Cd(MCFA)_2(H_2O)_2]$	22.7 ± 2.2	29.8 ± 1.4	3.3 ± 1.6	5.1 ± 1.2
6	[Mn(AcO)(MCFA)]	61.1 ± 4.9	>137 (41%)*	1.7 ± 0.7	65.2 ± 1.4
7	[Cu(AcO)(MCFA)]	57.4 ± 6.8	107.7 ± 4.8	26.3 ± 2.4	85.4 ± 5.5
	Cisplatin[2]	0.69 ± 0.02	1.53 ± 0.02	41.7 ± 0.41	8.00 ± 0.21

* inhibition for the final concentration 50 μg/ml

IC_{50} value of metal complexes with meclofenamic acid are correlated with the related parent drug and cisplatin in the **table XII.1,** Hmcfa **1** is less cytotoxic than its metal complexes and cisplatin towards four cancer cell lines, except for $[Zn(MCFA)_2(H_2O)_4]$, **4**, [Mn(AcO)(MCFA)], **6** against A-

549 cancer cell line, are no effective and [Mn(AcO)(MCFA)], **6**, [Cu(AcO)(MCFA)], **7** against MCF-7 are less cytotoxic compared to drug alone. A significant cytotoxic activity from **6** was found for T-24 cancer cell line , only 1.7 μM. The complex **6,** against T-24 cell line, is 24.5 times more cytotoxic than cisplatin. Additionaly the complex **6** has shown selectivity towards T-24 cell line. In the case of T-24, the IC_{50} value for **2**, **3**, **4**, **7** are 3.8 μM, 5.3 μM, 3.2 μM, 26.3 μM and compared to cisplatin are 11, 7.9, 13, 16 times, respectively, more cytotoxic while the parent drug Hmcfa is 1.7 times less cytotoxic than cisplatin. As regards to the cell lines L929 all the complexes are less effective than cisplatin. IC_{50} value of **3**, **6**, **7** complexes in the range 20 – 28 μM and **2, 4**, **5** complexes in the range 20 – 28 μM, thus **3**, **6**, **7** are ca. 60 times less cytotoxic than cisplatin and **2, 4**, **5** are ca. 24 times less effective compared to cisplatin. $[Cd(MCFA)_2(H_2O)_2]$, **5** shows a higher anti-proliferative activity against MCF-7 when compared to cisplatin, free drug and its metal complexes, the IC_{50} value being 5.1 μM, respectively. However , it has to be emphasized that the toxicity of the cadmium can eliminate its complexes in the therapies on the humans. The cytotoxic activity shown by Mn(II), Cu(II) and Zn(II) compounds **2**, **3**, **4**, **6**, **7** against T24 cell line indicate that coupling of **1** to the metal center result in metallic complexes with important biological properties and remarkable cytotoxic activity, since they display IC_{50} values in a μM range better to that of the antitumor drug cis-platin. Thus, the Mn(II), Cu(II) and Zn(II) Zn(II) compounds **2**, **3**, **4**, **6**, **7** are considered as agents with potential antitumor activity, and can therefore be candidates for further stages of screening *in vitro* and/or in vivo.

Table XII.2. The antiproliferative activity *in vitro* of flufenamic acid **10** and **11 -16** (expressed as IC_{50} (μM) against MCF-7, T-24, A-549 and L-929 cancer cell lines.

	Compounds	L-929	A-549	T-24	MCF-7
10	Hffa	192.0 ± 15.1	106.80 ± 3.1	99.6± 9.4	120.9 ± 9.3
11	$[Mn(FFA)_2(H_2O)]$	44.7 ± 1.6	13.7 ± 3.7	0.4 ± 0.05	30.9 ± 5.9
12	$[Cu(FFA)_2]$	44.9 ± 4.5	32.7 ± 5.1	14.8 ± 2.7	>160 (38%)*
13	$[Zn(FFA)_2(H_2O)_2]$	41.3 ± 1.6	28.6 ± 9.7	41.3 ± 11.1	63.5 ± 3.2
14	$[Cd(FFA)_2(H_2O)_2]$	20.6 ± 2.8	23.0 ± 4.4	27.2 ± 1.8	4.8 ± 0.3
15	$[Mn(FFA)(Ac)(H_2O)_3]$	64.0 ± 4.6	67.8 ± 3.4	0.4 ± 0.1	84.8 ± 8.9
16	[Cu(AcO)(FFA)]	47.5 ± 7.8	>248 (35%)*	63.8 ± 5.9	89.4 ± 9.3
	Cisplatin[2]	0.69 ± 0.02	1.53 ± 0.02	41.7 ± 0.41	8.00 ± 0.21

* 10^{-5}, inhibition for the final concentration 50 μg/ml

The antiproliferative activity *in vitro* (defined by IC_{50} (μM)) of flufenamic acid **10** and its complexes **11 -16** are listed in **table XII.2**. The metal(II) complexes of flufenamic acid **10** exhibited a enhancement activity compared to the drug alone against all the tested cell lines. The metal complexes with two flufenamic acid molecules coordinated to the one central metal atom **11 – 14** are more cytotoxic than the complexes having one flufenamic molecule attached with the metal atom **15 – 18**, except for $[Mn(FFA)(Ac)(H_2O)_3]$, **15** towards T-24 cell line and $[Cu(FFA)_2]$ against MCF-7 cell line. However, the IC_{50} value for **15** against T24 cell line was found 0.4 μM

and compared to cisplatin is 104.3 times more cytotoxic, **12** is no effective against MCF-7. A significant cytotoxic activity from **15** against T-24 is in μM range similar to [Mn(FFA)$_2$(H$_2$O)], **11** only 0.4 μM, thus **11** is 104 times more cytotoxic than ciplatin, respectively. Besides manganese (II) complexes of flufenamic acid, copper and cadmium complexes **12**, **14** are more effective for T-24 cell line, 5.3 and 3.3 times more cytotoxic, respectively. However , it has to be emphasized that the toxicity of the cadmium can eliminate its complexes in the therapies on the humans. A similar range (41 – 42 μM) of IC_{50} was observer for [Zn(FFA)$_2$(H$_2$O)$_2$], **13** and cisplatin for T-24 cell line. For the cell lines L929, all the complexes are less effective than cisplatin nevertheless more cytotoxic than the parent drug **10**. As regards to the cell lines A-549, the most significant enhancement of antiproliferative effect of Hffa, **10** is observed for [Mn(FFA)$_2$(H$_2$O)], **11** towards A-549 cancer cell lines, is 9 times less cytotoxic than ciplatin. The IC_{50} value for **11**, **12**, **15** against T-24 cell line are significantely smaller than IC_{50} for cisplatin that was seleced as reference in this study. These results indicate that coupling of flufenamic acid to Mn(II) and Cu(II) metal center result in a metallic complex with important biological properties.

Table XII.3.. The antiproliferative activity *in vitro* of lornoxicam **19** and **20 -27** (expressed as IC_{50} (μM) against MCF-7, T-24, A-549 and L-929 cancer cell lines.

	Compounds	L-929	A-549	T-24	MCF-7
19	H$_2$Lorn	79.6 ± 7.3	>269 (41%)*	1.7 ± 0.6	26.9± 2.6
20	[Mn(Lorn)$_2$]	>125 (20%)*	>125 (36%)*	36.0 ± 0.1	7.9 ± 2.9
21	[Cu(Lorn)$_2$]	>124 (30%)*	>124 (22%)*	38.1 ± 3.6	>124 (20%)*
22	[Zn(Lorn)$_2$]	>124 (35%)*	>124 (10%)*	6.3 ± 1.8	>124 (12%)*
23	[Cd(Lorn)$_2$]	46.0 ± 3.0	>112 (36%)*	1.8 ± 0.2**	40.0 ± 4.5
24	[Mn(AcO)(Lorn)]	>235 (11%)*	>235 (35%)*	13.5 ± 0.3	29.0 ± 3.6
25	[Cu(AcO)(Lorn)]	>230 (39%)*	>233 (39%)*	0.3 ± 0.1	54.8 ± 7.0
	Cisplatin[2]	0.69 ± 0.02	1.53 ± 0.02	41.7 ± 0.41	8.00 ± 0.21

* inhibition for the final concentration 50 μg/ml

** tested for the final concentration 20, 10, 1, 0.1 μg/ml

The anti-proliferative activity of tests *in vitro* by lornoxicam and its metal complexes as defined by the inhibition factor IC_{50} for the L-929, A-549, T-24 and MCF-7 cancer cell line is reported in **table XII.3** IC_{50} value of metal complexes with lornoxicam are correlated with the related parent drug and cisplatin. Cellular proliferation was found to be inhibited in the case of all complexes and lornoxicam, **19** alone towards T-24 cell line. Lornoxicam, **19** and **22**, **23**, **24**, **25** complexes show significant citotoxic effect, against T-24 cancer cell line, IC_{50} in the range ca. 0.3 – 13. 5 μM, 24.5 times (**19**), 6.6 times (**22**), 23.2 times (**23**), 3.1 times (**24**), 157 times (**25**) more cytotoxic than cisplatin. A similar range (ca. 36 – 38 μM) of IC_{50} was observer for [Mn(H$_2$Lorn)$_2$], **20** and [Cu(H$_2$Lorn)$_2$], **21**, comparable with IC_{50} of cisplatin (41.7 μM) for T-24 cell line, cisplatin was lees effective. Additionaly, free drug and its complexes, except [Mn(H$_2$Lorn)$_2$], **20** have shovn selectivities towards T-24 cell line. However, it has to be emphasized that, apart form the effective IC_{50} value of cadmium complex, **23** it can be eliminated in the therapies on the humans,

because of its toxic effect. As regards to the cell lines MCF-7, the most significant enhancement of antiproliferative effect of H_2Lorn, **19** is observed for [Mn(H_2Lorn)$_2$], **20** towards MCF-7 cancer cell lines, is 1 time less cytotoxic than ciplatin. The cytotoxic activity was not found from lornoxicam and its metal complexes for A-549 cancer cell line. In the case of L-929 only free drug and cadmium complex show cytotoxic effect. The cytotoxic activities shown by **20**, **21**, **22**, **24**, **25** against T-24 cancer call line and 20 also towards MCF-7 cancer cell line indicate that coupling of H_2Lorn to Cu^{II} and Mn^{II} centers results in complex with important biological properties since they display IC_{50} values in a molar range similar or better to that of the antitumor drug cisplatin.

Table XII.4. The antiproliferative activity *in vitro* of cefaclor **28** and **29 -36** (expressed as IC_{50} (μM) against MCF-7, T-24, A-549 and L-929 cancer cell lines.

	Compounds	L-929	A-549	T-24	MCF-7
28	HCef	>272 (8%)*	>272 (6%)*	>272 (21%)*	>272 (11%)*
29	Mn(Cef)$_2$	>127 (31%)*	>127 (10%)*	0.3 ± 0.08	>127 (25%)*
30	Cu(Cef)$_2$	44.8 ± 2.8	>125 (15%)*	>126 (19%)*	>126 (13%)*
31	Zn(Cef)$_2$	28.3 ± 2.0	>125 (7%)*	7.9 ± 2.8	>125 (5%)*
32	Cd(Cef)$_2$	22.9 ± 1.3	22.4 ± 0	>118 (26%)*	47.3 ± 2.1
33	[Mn(AcO)(Cef)]	>208 (33%)*	>208 (14%)*	44.4 ± 1.2	>237 (43%)*
34	[Cu(AcO)(Cef)]	54.4 ± 1.2	61.8 ± 1.3	40.1 ± 7.5	47.6 ± 2.4
	Cisplatin[2]	0.69 ± 0.02	1.53 ± 0.02	41.7 ± 0.41	8.00 ± 0.21

* inhibition for the final concentration 50 μg/ml

All the newly synthesized complexes **29 – 34** of cefaclor were screened for their antiproliferative activity. **Table XII.4** gives the results of the tests *in vitro*. The metal(II) complexes exhibited enhancement in cefaclor activity against all the tested cell lines, while cefaclor alone did not have any significant effect. Cellular proliferation was found to be inhibited in the case of all complexes for certain cancer cell lines. As regards to the cell lines T-24, obteined results showed a significant cytotoxic effect of Mn(Cef)$_2$, **29**. The IC_{50} values for the complexes **29** and **31** towards T-24 cell line are 0.3 μM and 7.9 μM, thus are 139 and 5.3 times, more cytotoxic than cisplatine respectively. Moreover the complexes Mn(Cef)$_2$, 29 and Zn(Cef)$_2$, 31 have shovn selectivities towards T-24 cell line.The metal complexes **29** and **31** with two cefaclor molecules coordinated to the one central metal atom were found more effective than the complexes having one cefaclor molecule attached with the metal atom for T-24 cell line. [Mn(AcO)(Cef)], **33** and [Cu(AcO)(Cef)], **34** display IC_{50} values in a μM range similar to that of the antitumor drug cis-platin. However **33** is 1.2 times less cytotoxic than ciplatin, 34 is 1 times more cytotoxic than cisplatin, respectively. Cellular proliferation was found to be inhibited in the case of four cell lines only for [Cu(AcO)(Cef)], **34,** on the other hand **34** did not have such significant citotoxic effect. As regards to the cell lines L929 all the complexes are less effective than cisplatin. IC_{50} value of **31**, **32** complexes in the range ca. 20 – 30 μM and **30**, **34** complexes in the range ca. 44 – 54 μM, thus **31** is 41 times less effective compared to cisplatin.

Table XII.4. The antiproliferative activity *in vitro* of metal acetates and $CdCl_2$ (expressed as IC_{50} (μM) against MCF-7, T-24, A-549 and L-929 cancer cell lines.

Compounds	L-929	A-549	T-24	MCF-7
$Mn(Ac)_2$	> 577.9	> 577.9	53.4 ± 9.6	> 577.9
$Cu(Ac)_2 *H_2O$	233.7± 15.3	> 501	50.1 ± 10.0	> 501
$Zn(Ac)_2 *2H_2O$	> 455.6	> 455.6	95.7 ± 16.2	> 455.6
$Cd(Ac)_2 *2H_2O$	157.6 ± 19.5	> 375.2	13.6 ± 1.9	> 375.2
$CdCl_2 *2H_2O$	> 455.9	> 455.9	130.7 ± 7.0	> 455.9

References

1. Cini, R., Tamasi, G., Defazio, S., Hursthouse, M.B. *Journal of Inorganic Biochemistry* **101,** 1140–1152 (2007).
2. Kovala-Demertzi, D., Dokorou, V., Primikiri, A., Vargas, R., Silvestru, C., Russo, U., Demertzis, M.A. *Journal of Inorganic Biochemistry* 103, 738–744 (2009).

XIII. Superoxide dismutation activity of of Mn(II), Cu(II), Zn(II) and Cd(II) complexes with meclofenamic acid, flufenamic acid, lornoxicam and cefaclor.

The superoxide dismutase activity (defined by IC_{50} (μM)) of mecloenamic acid, **1** flufenamic acid, **10** lornoxican, **19** and cefaclor, **28** and metal complexes complexes are listed in **table**. According to the method originally developed by Beauchamp and Fridovich[1], the superoxide dismutase activity was examined indirectly using the nitro blue tetrazolium assay at pH 7.8. The indirect determination of SOD activity by monitoring the reduction of NBT by O_2^- involves the generation of O_2^- in vitro by using xanthine/xanthine oxidase. As the reaction proceeds, the farmazan colour is developed and a colour change from yellow to blue/mauve is appeared, which is associated with an increase in the absorption spectrum at 560 nm. When a chemical inhibitor is added, the reduction reaction proceeds slowly or is totally inhibited in which instance the solution remains yellow and the rate of increase was reduced with increasing concentration. concentration required to produce 50% inhibition (IC_{50}) be obtained by graphing the rate of NBT reduction versus the concentration or the log of the concentration of the test solution. Many low-molecular metal complexes, mainly copper, manganese complexes, have been synthesized and their SOD-like activity examined in vitro and in vivo. The IC_{50} results for a Cu(II) salicylate using NBT assay were investigated Complexes exhibited SOD activity with IC_{50} values ranging from 1 to 28 μM. In the reported study a number of different assays were performed, including the NBT reduction and the inhibition of cytochrome reduction. All complexes exhibited SOD activity in these assays but, the order of activity of the complexes was not preserved across the different assays. The IC_{50} values of $[Cu_2(Indo)_4 (DMSO)_2]$ ranged from 25 μM in acetonitrile to 2 μM in dimethylsulfoxide, DMSO. SOD activity was also observed for other Cu-NSAIDs although IC_{50} values were not determined.[2] Several complexes containing transition metal are known to give good SOD activity, although, their structures are totally unrelated with native enzyme.[3] The lowest values for a manganese superoxide dismutase mimic were reported by Nagano and coworkers (0.75 μM) and Rajan (0.75 μM). In both of these complexes manganese is in the divalent form. However, in dismutases containing manganese the metal is normally in the trivalent state, but can be reduced to the divalent state without any loss of enzymic activity. It is also worth noting that many of the high activity complexes are neutral rather than anionic. This may be an indication that maintaining the manganese in a neutral state leads to improved catalytic activity.[4]

Generaly the metal complexes with two lignds molecules coordinated to the one central metal atom was found more effective than the complexes having one ligand molecule attached with the metal atom, however did ot have so significant effect in the reduction suproxide anion. Out of the synthesized complexes, copper and manganes complexes of meclofenamic acid, flufenamic acid, lornoxicam and cefaclor exhibited SOD activity with IC_{50} values ranging from ca. 1.8 to 15 μM, besides [Mn(AcO)(Cef), **33**. Zinc and cadmium complexes of all four ligands and ligands themselves were found to be inactive towards superoxide dismutase. All the studied copper(II) and manganese(II) complexes presented a relatively low SOD-like activity, higher than

1 μM, however it was noted that the IC_{50} values for [Cu(MCFA)$_2$(H$_2$O)] and [Cu(AcO)(MCFA)] lay at the region, where are considered as potent SOD mimics.

SOD assay of manganese(II) and copper(II) complexes with meclofenamic acid (1).

Table XIII.1. The superoxide dismutase activity (expressed as IC_{50}) of meclofenamic acid complexes **2 – 7** and parent drug **1**.

	Complexes of Meclofenamic Acid	IC_{50} (μM)
1	Hmcfa	44%*
2	[Mn(MCFA)$_2$]	6.48 ± 0.81
3	[Cu(MCFA)$_2$(H$_2$O)][a]	1.78 ± 0.16
4	[Zn(MCFA)$_2$(H$_2$O)$_4$]	20%*
5	[Cd(MCFA)$_2$(H$_2$O)$_2$]	44%*
6	[Mn(AcO)(MCFA)]	8.40 ± 1.49
7	[Cu(AcO)(MCFA)]	2.91 ± 0.80

* inhibition for the final concentration 40 μM
[a] IC_{50} values were calculated from regression lines, where c was log of tested compound concentration and y was percent inhibition of enzyme activity; where b (b = 34.41±4.68) is the slope of the regression line and R (R = 0.94105) is the correlation coefficient and N = 9.

In **table XIII.1** the complexes of meclofenamic acid were organized for IC_{50} values. The complexes [Cu(MCFA)$_2$(H$_2$O)], **3** shows an IC_{50} value of 1.78 ± 0.16 μM, **Figure XIII.1.** ,respectively. [Cu(AcO)(MCFA)], **5** presented the second lowest IC_{50} value of 2.91 ± 0.80μM while the parent drug alone did not show any significant SOD activity. These values indicate that, **3** and **7** are potent superoxide dismutase mimics. The inhibition of the NBT reduction by superoxide in the presence of [Cu(MCFA)$_2$(H$_2$O)], **3** reached a maximum value of about 72% concentration 40 μM, and for [Cu(AcO)(MCFA)], **5** the maximum value was 83%. Similar results have been obtained for copper complexes. The IC_{50} value is the concentration of the complex which exerts activity equal to one unit of that of native SOD. Following the usual criteria advanced by Roberts and Robinson[5], the present complexes are considered as potent SOD mimics.The IC_{50} of [Cu(MCFA)$_2$(H$_2$O)], **3** is corresponded closely to that regarding the [Cu(AcO)(MCFA)], **5** complex. The IC_{50} values of both the [Mn(MCFA)$_2$], **2** and [Mn(AcO)(MCFA)], **6** (6.48 ± 0.81 μM, 8.40 ± 1.49 μM, respectively) showed that these were less active than that of copper meclofenamic acid complexes.

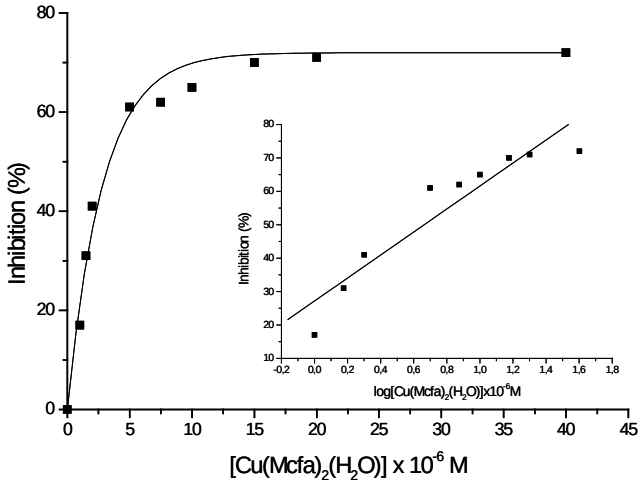

Figure. **XIII.1.** Dependence of the inhibition of NBT reduction by superoxide on the concentration of $[Cu(MCFA)_2(H_2O)]$ **3** and on the logarithm of **3**. Incubation time was 20 min.

SOD assay of manganese(II) and copper(II) complexes with flufenamic acid (10).

Table XIII.2. The superoxide dismutase activity (expressed as IC_{50}) of flufenamic acid complexes **11 -16** and parent drug **10** .

	Complexes of Flufenamic Acid	IC_{50} (μM)
10	Hffa	39%*
11	$[Mn(FFA)_2(H_2O)]$	11.86 ± 0.54
12	$[Cu(FFA)_2]$	11.82 ± 0.97
13	$[Zn(FFA)_2(H_2O)_2]$	20%*
14	$[Cd(FFA)_2(H_2O)_2]$	19%*
15	$[Mn(FFA)(Ac)(H_2O)_3]$	10.76 ± 0.65
16	[Cu(AcO)(FFA)]	7.74 ± 0.76

* inhibition for the final concentration 40 μM

Table XIII.2. gives the results of SOD assay for flufenamic alone and its metal complexes. The SOD activity of complexes $[Mn(FFA)_2(H_2O)]$, **11**, $[Cu(FFA)_2]$, **12**, $[Mn(FFA)(Ac)(H_2O)_3]$, **15** indicated 50% inhibition at the range ca. 11 – 12 μM, on the other hand flufenamic acid , **10** alone did not have any sod activity, respectively.[Cu(AcO)(FFA)], **16** presented the ca. 1.5 times lowest IC_{50} value, however following the usual criteria advanced by Roberts and Robinson[5], the complex **16** are not considered as potent SOD mimic. The inhibition of the NBT reduction by superoxide in the presence of $[Mn(FFA)_2(H_2O)]$, **11**, $[Cu(FFA)_2]$, **12**, $[Mn(FFA)(Ac)(H_2O)_3]$, **15** reached a maximum value of about 67%, 60%, 64% concentration 40 μM, and for [Cu(AcO)(FFA)], **16** the maximum value was 85%, respectively.

SOD assay of manganese(II) and copper(II) complexes with lornoxicam (19).

Table XIII.3. The superoxide dismutase activity (expressed as IC_{50}) of lornoxicam complexes **20 – 25** and parent drug **19**.

	Complexes of Lornoxicam	IC_{50} (μM)
19	H_2Lorn	35%*
20	[Mn(Lorn)$_2$]	10.35 ± 1.43
21	[Cu(Lorn)$_2$]	8.04 ± 0.47
22	[Zn(Lorn)$_2$]	35%*
23	[Cd(Lorn)$_2$]	41%*
24	[Mn(AcO)(Lorn)]	10.12 ± 1.88
25	[Cu(AcO)(Lorn)]	3.19 ± 1.19

* inhibition for the final concentration 40 μM

IC_{50} value for lornoxicam complexes and parent drug are reported in **table XIII.3.** [Cu(Lorn)], **25** exhibited the highiest sod activity (IC_{50} = 3.19μM) among four lornoxicam complexes. Lornoxicam alone did not have any effect. The SOD activity of complexes [Mn(Lorn)$_2$], **20**, [Mn(Lorn)], **24**, indicated 50% inhibition at the range ca. 10 μM. Furthermore, the IC_{50} value for the complex [Mn(Lorn)$_2$], **20** is 10.35 μM. The IC_{50} value shown by [Cu(Lorn)$_2$], **21** is in the similar range, 8.04 μM respectively. The inhibition of the NBT reduction by superoxide in the presence of [Cu(Lorn)], **25** reached a maximum value of about 83% concentration 40 μM.

SOD assay of manganese(II) and copper(II) complexes with cefaclor (28).

Table XIII.4. The superoxide dismutase activity (expressed as IC_{50}) of cefaclor complexes **29 – 34** and parent drug **28**.

	Complexes of Cefaclor	IC_{50} (μM)
28	HCef	24%*
29	Mn(Cef)$_2$	15.15 ± 1.49
30	Cu(Cef)$_2$	6.16 ± 0.81
31	Zn(Cef)$_2$	20%*
32	Cd(Cef)$_2$	16%*
33	[Mn(AcO)(Cef)]	46%*
34	[Cu(AcO)(Cef)]	5.43 ± 0.80

* inhibition for the final concentration 40 μM

In order to compare the SOD-like activity of the copper(II) and manganese(II) complexes with cefaclorthe IC_{50} values of the above were measured and listed in **table XIII.4.** Copper cefaclor complexes Cu(Cef)$_2$, **30** gave slightly higher value, 6.16 μM than the , [Cu(AcO)(Cef)], **34**, 5.43 μM, respectively. Furthermore it was found that only Mn(Cef)$_2$, **29** posses SOD-like activity (15.15 μM) unlike [Mn(AcO)(Cef)], **33** did not show any sod activity. The inhibition of the NBT reduction by superoxide in the presence of Cu(Cef)$_2$, **30** reached a maximum value of about 57% concentration 40 μM, and for [Cu(AcO)(Cef)], **34** the maximum value was 63%, respectively.

References

1. Beauchamp, C., Fridovich, I ., *Anal. Biochem*. **44,** 276-286 (1971).
2. Kovala-Demertzi, D., Galani, A., Demertzis, M.A., Skoulika, S., Kotoglou, C., *J. Iorg. Biochem.* **98**, 358 (2004).
3. Siddiqi, Z.A., Shahid, M., Khalid, M., Kumar, S. *European Journal of Medicinal Chemistry* **44,** 2517–2522 (2009).
4. a) Rajan, R., Rajaram, R., Nair, B.U., Ramaswami, T., Mandal, S.K. *J. Chem. Soc., Dalton Trans.* 2019–2030 (1996).
   b) Osawa, K.N., Tamura, M.N., Moro-oka, Y., Hirano, T., Hirobe, M., Nagano, T. *Inorg. Chem.* **32,** 1879.(1993).
5. Roberts, N.A., Robinson, P.A., *Br. J. Rheumatol*. **24,** 128 (1985).
6. Christofis, P., Katsarou, M., Papakyriakou, A., Sanakis, Y., Katsaros, N., Psomas, G. *Journal of Inorganic Biochemistry* **99,** 2197–2210 (2005).
7. Galani, A., Demertzis, M.A., Kubicki, M., Kovala-Demertzi, D. *Eur. J. Inorg. Chem.* 1761-1767 (2003)

Experimental

XIV. General

Materials

Manganese(II) acetate, $Mn(CH_3COO)_2$ (Aldrich); Copper(II) acetate monohydrate, $Cu(CH_3COO)_2 \cdot H_2O$ (Sigma); Zinc(II) acetate dihydrate, $Zn(CH_3COO)_2 \cdot 2H_2O$ (Merck); Cadmium(II) acetate dihydrate, $Cd(CH_3COO)_2 \cdot 2H_2O$ (Merck); Diphenyliodonium-2-carboxylate monohydrate (Lancaster); 2,6-dichloro-3 mehyl aniline (Acros organics); 2-Bromobenzoic acid (Merck), sodium hydroxide (Merck). All the chemicals were used as purchased without further purification. Lornoxicam was a gift from ‘‘NYCOMED’’ NYCOMED DENMARK A/S.
Dimethylsulfoxide (DMSO, Merck), ethanol 99% (EtOH, Merck), methanol (MeOH, Merck), diethyl ether (Et_2O, Prolaro), N,N-Dimethylformamid (DMF, Merck), Triethylamine (Et_3N, Merck)

Instrumental

NMR spectra were recorded on a Bruker AV-400 spectrometer operating at 400 and 100 MHz for ^1H and ^{13}C acquisitions, respectively, or on a Bruker AV-250 spectrometer operating at 250.13 and 62.90 MHz for ^1H and 13C acquisitions, respectively. 2D NMR spectra were recorded on a Bruker AV-500 spectrometer operating at 500 and 100 MHz for ^1H and ^{13}C acquisitions, respectively, The spectra were acquired at room temperature (298 K). The splitting of proton resonances in the reported ^1H NMR spectra are defined as s = singlet, d = doublet, t = triplet and m = multiplet. The chemical shifts are reported in ppm for ^1H and ^{13}C NMR). Samples were dissolved in dimethylsulfoxide-d_6 and chloroform D. Spectra were obtained at room temperature with the signal of free dimethylsulfoxide-d_6 (at 2.50 ppm ^1H NMR, 39.5 ppm ^{13}C NMR) and free $CDCl_3$ (at 7.26 ppm ^1H NMR, 77.16 ppm ^{13}C NMR) as a reference.

Infrared and far-infrared spectra were recorded on a Perkin Elmer Spectrum GX Fourier transform spectrophotometer using KBr pellets (4000–400 cm^{-1}) and nujol mulls dispersed between polyethylene disks (400–40 cm^{-1}).

UV spectra were acquired with a JASCO V-570 spectrophotometer UV/VIS/NIR.

Mass spectra were measured on an Agilent 1100 Series LC-MSD-Trap-SL spectrometer. Techniques: atmospheric pressure chemical ionization (APCI) and electrospray ioanization (ESI).

Metal compositions were determined using an energy-dispersive X-ray fluorescence (EDXRF) spectroscopy arrangement, operating in ambient air. Photons emitted from an annular ^{109}Cd or ^{241}Am source were used for sample excitation. The source was fixed coaxially above a CANBERRA SL80175 Si(Li) detector (5 mm crystal thickness, 80 mm^2 area), with a 25 μm-thick Be window and an

energy resolution of 171 eV at the 5.9 keV Mn (K_α) peak. Samples were placed on top of the assembly with their surface perpendicular to the detector axis. Data acquisition was performed through a PC card (ORTEC TRUMP-PCI), controlled by the MAESTRO-32 software, while spectral analysis was carried out using the WinQxas software package (IAEA 1997-2002). Samples were measured in the form of thin pellets, 12 mm in diameter, typically obtained by mixing 30 mg of sample with cellulose. Standard pellets were also prepared and used to generate calibration curves, in order to calculate metal compositions of the unknown samples.

Magnetic moments: at r.t. by the Evans method with mercuric tetrathiocyanocobaltate(II) as the susceptibility standard with a Sherwood Scientific Magnetic Susceptibility Balance; the effective magnetic moments (μ_{eff}) values calculated by using the Curie equation: $\mu_{eff} = 2.83 (\chi_M^{corr})^{1/2}T^{1/2}$.

Elemental analyses were carried out by the microanalytical service of the University of Ioannina, Greece.

Melting points were determined in open capillaries.

XV. X-Ray crystallography

XV.1. Crystal structures determination

A green needle crystal of $[Cu_4(AcMCFA)_6(OH)_2(DMSO)_2].2DMSO$ **3a**, a yellow needle crystal of $[Mn(lorn)_2(DMSO)_2]$ **20a**, a brown prismatic crystal of $[Cu(lorn)_2(DMSO)_2]$ **21a** A yellow prismatic crystal of $[Cd(lorn)_2(DMSO)_2]$ **23a** was mounted on a glass fiber and used for data collection. Crystal data were collected at 100.0 K, using a Bruker X8 KappaAPEXII diffractometer. Graphite monochromated MoK(alpha) radiation (lambda = 0.71073 angstrom's) was used throughout. The data were processed with APEX2[3] and corrected for absorption using SADABS (transmissions factors: 1.000 - 0.0.904, **20a**, 1.000 - 0.794, **20a**, 1.000 - 0.790, **21a**, 1.000 - 0.856 **23a**[4], The structure was solved by direct methods using the program SHELXS-97[5] and refined by full-matrix least-squares techniques againts F^2 using SHELXL-97[6]. Positional and anisotropic atomic displacement parameters were refined for all nonhydrogen atoms. For **3a** the C atoms of the methyl groups in each ligand showed disorder and was refined using a split with 50% occupancy for each "meta" position (C24/C25, C44/C45 and C64/C65). Hydrogen atoms were located in difference maps and included as fixed contributions riding on attached atoms with isotropic thermal parameters 1.2 times those of their carrier atoms.For **3a** the H atoms of methyl groups and isotropically refined atoms were included in geometrically idealized positions. Criteria of a satisfactory complete analysis were the ratios of "rms" shift to standard deviation less than 0.001 and no significant features in final difference maps. Atomic scattering factors from "International Tables for Crystallography".[7] Molecular graphics from PLATON[8]

and SCHAKAL.[9] Selected crystallographic data are listed in tables table XV.1, table XV.2, table XV.3, table XV.4.

XV.2. Crystal data and structure refinement

Table XV.1.1. Crystal data and structure refinement for $[Cu_4(MCFA)_6(OH)_2(DMSO)_2].2DMSO$.

Empirical formula	C92 H80 Cl12 Cu4 N6 O18 S3
Formula weight	937.04
Temperature/K	110(2)
Wavelength/Å	0.71073
Crystal system	triclinic
Space - group	P -1
Cell dimensions	
a/Å	8.6917(17)
b/Å	9.2754(18)
c/Å	24.612(5)
α/°	85.617(3)
β/°	83.067(3)
γ/°	73.185(3)
Cell volume/$Å^3$	1883.7(6)
Z	2
Calculated density/mg cm^{-3}	1.652
Absorption coefficient/mm^{-1}	1.080
F(000)	952
Crystal size/mm	0.27 x 0.23 x 0.06
The range for data collection/º	0.83 to 26.37
Limiting indices	10<=h<=10, -11<=k<=11, 0<=l<=30
Reflections collected/unique	21646 / 7683 [R(int) = 0.0348]
Completeness to theta = 26.37	99.5 %
Absorption correction	Empirical
Max. and min. transmission	0.9380 and 0.7592
Refinement method	Full-matrix least-squares on F^2
Data / restraints / parameters	7683 / 0 / 460
Goodness-of-fit on/F^2	1.091
Final R indices [I>2σ(I)]	R1 = 0.0558, wR2 = 0.1100
R indices (all data)	R1 = 0.0801, wR2 = 0.1218
Largest diff. peak and hole/e $Å^{-3}$	2.445 and -1.684

Table XV.1.2. Crystal data and structure refinement for $[Cd(MCFA)_2(DMSO)_2]$.

Empirical formula	C34 H38 Cl4 Cd N2 O7 S4
Formula weight	2365.42
Temperature/K	100(2)
Wavelength/Å	0.71073
Crystal system	monoclinic
Space - group	P 21/n
Cell dimensions	
a/Å	8.4916(5)
b/Å	25.2754(17)
c/Å	23.1572(16)
α/°	90
β/°	93.224(3)
γ/°	90
Cell volume/$Å^3$	4962.3(6)
Z	2
Calculated density/mg cm^{-3}	1.58298
Absorption coefficient/mm^{-1}	1.322
F(000)	2404
Crystal size/mm	0.47 x 0.05 x 0.05
The range for data collection/º	1.19 to 26.02
Limiting indices	10<=h<=10, 0<=k<=31, 0<=l<=28
Reflections collected/unique	74833 / 9796 [R(int) = 0.0671]
Completeness to theta = 26.02	100.0 %
Absorption correction	Empirical
Max. and min. transmission	0.9369 and 0.5755
Refinement method	Full-matrix least-squares on F^2
Data / restraints / parameters	9796 / 0 / 640
Goodness-of-fit on/F^2	1.022
Final R indices [I>2σ(I)]	R1 = 0.0517, wR2 = 0.1061
R indices (all data)	R1 = 0.1033, wR2 = 0.1300
Largest diff. peak and hole/e $Å^{-3}$	0.876 and -0.687

Table XV.2. Crystal data and structure refinement for $[Mn(lorn)_2(DMSO)_2]$.

Empirical formula	C30 H30 Cl2 Mn N6 O10 S6
Formula weight	952.80
Temperature/K	100(2)
Wavelength/Å	0.71073
Crystal system	Monoclinic
Space - group	P 21/n
Cell dimensions	
a/Å	7.6513(7)
b/Å	14.8471(14)
c/Å	17.1030(14)
α/°	90
β/°	97.015(4)
γ/°	90
Cell volume/$Å^3$	1928.4(3)
Z	2
Calculated density/mg cm^{-3}	1.641
Absorption coefficient/mm^{-1}	0.869
F(000)	974
Crystal size/mm	0.16 x 0.05 x 0.02
The range for data collection/º	1.82 to 26.38
Limiting indices	-9<=h<=9, 0<=k<=18, 0<=l<=21
Reflections collected/unique	19034 / 3956 [R(int) = 0.0648]
Completeness to theta = 26.02	99.9 %
Absorption correction	Empirical
Max. and min. transmission	0.9828 and 0.8735
Refinement method	Full-matrix least-squares on F^2
Data / restraints / parameters	3956 / 0 / 250
Goodness-of-fit on/F^2	0.998
Final R indices [I>2σ(I)]	R1 = 0.0590, wR2 = 0.1000
R indices (all data)	R1 = 0.1414, wR2 = 0.1256
Largest diff. peak and hole/e $Å^{-3}$	0.499 and -0.533

Table XV.3. Crystal data and structure refinement for $[Cu(lorn)_2(DMSO)_2]$.

Empirical formula	C30 H30 Cl2 Cu N6 O10 S6
Formula weight	961.40
Temperature/K	100(2)
Wavelength/Å	0.71073
Crystal system	Monoclinic
Space - group	P 21/c
Cell dimensions	
a/Å	10.0054(3)
b/Å	16.5683(6)
c/Å	11.2051(4)
α/°	90
β/°	94.203(2)
γ/°	90
Cell volume/$Å^3$	1852.50(11)
Z	2
Calculated density/g cm^{-3}	1.724
Absorption coefficient/mm^{-1}	1.137
F(000)	982
Crystal size/mm	0.10 x 0.08 x 0.04
The range for data collection/º	2.04 to 26.02
Limiting indices	-12<=h<=12, 0<=k<=20, 0<=l<=13
Reflections collected/unique	15153 / 3648 [R(int) = 0.0516]
Completeness to theta = 26.02	99.9 %
Absorption correction	Empirical
Max. and min. transmission	0.9559 and 0.8948
Refinement method	Full-matrix least-squares on F^2
Data / restraints / parameters	3648 / 0 / 250
Goodness-of-fit on/F^2	1.023
Final R indices [I>2σ(I)]	R1 = 0.0401, wR2 = 0.0798
R indices (all data)	R1 = 0.0679, wR2 = 0.0898
Largest diff. peak and hole/e $Å^{-3}$	0.513 and -0.389

Table XV.4. Crystal data and structure refinement for $[Cd(lorn)_2(DMSO)_2]$.

Empirical formula	C30 H30 Cd Cl2 N6 O10 S6
Formula weight	1010.26
Temperature/K	100(2)
Wavelength/Å	0.71073
Crystal system	Monoclinic
Space - group	P 21/n
Cell dimensions	
a/Å	7.6815(3)
b/Å	14.8628(4)
c/Å	17.1980(6)
α/°	90
β/°	98.129(2)
γ/°	90
Cell volume/$Å^3$	1943.74(11)
Z	2
Calculated density/g cm^{-3}	1.726
Absorption coefficient/mm^{-1}	1.084
F(000)	1020
Crystal size/mm	0.20 x 0.10 x 0.06
The range for data collection/º	1.82 to 26.38
Limiting indices	-9<=h<=9, 0<=k<=18, 0<=l<=21
Reflections collected/unique	22430 / 3988 [R(int) = 0.0392]
Completeness to theta = 26.02	100.0 %
Absorption correction	Empirical
Max. and min. transmission	0.9378 and 0.8124
Refinement method	Full-matrix least-squares on F^2
Data / restraints / parameters	3988 / 0 / 250
Goodness-of-fit on/F^2	1.022
Final R indices [I>2σ(I)]	R1 = 0.0288, wR2 = 0.0607
R indices (all data)	R1 = 0.0394, wR2 = 0.0646
Largest diff. peak and hole/e $Å^{-3}$	0.462 and -0.422

X.VI. Synthesis

*Synthesis of N-(2,6-dichloro-3-methylphenyl) anthranilic acid, meclofenamic acid (**1**)[1].*

A solution off 3.0g (9.27 mmol) of (2-carboxyphenyl)phenyliodonium, inert salt, 1.36 (7.72 mmol) of 2,6-dichloro-3-methylbenzenamine and 0.06 g of cupric acetate in 12 ml of 2-propanol was heated at reflux for 29h. The solvent was removed under reduced pressure, the residue taken up in 2 N sodium hydroxide, extracted with ether, and acidified with dilute hydrochloric acid. The white precipitate was collected giving 1.7 g (70% yield) of the crude product. Recrystallization from ethanol gave 1.0 g (44% yield) of pure product m.p 252-253°C .

Synthesis of [$Mn(MCFA)_2$], ***(2).***

Manganese(II) acetate anhydrous (0.0216 g, 0.125 mmol) was dissolved in methanol (2 ml) and this solution was added to a solution of Meclofenamic Acid (0.0740 g, 0.25 mmol) in methanol (2 ml). Drops of triethylamine ($N(eth)_3$) were added to the reaction mixture till the apparent pH value was ~ 7. After 4 hours stirring at the room temperature, the reactiom mixture was stored in the refrigerator overnight. Cold water was added dropwise till desired precipitate appeared. Off white powder (0.0375 g, 46.5% yield) was collected by filtration, subsequently washed with cold methanol:water (1:1) and dried under vacuum.

IR (cm^{-1}): 3226m, ν(NH); 3070m 2943m, ν(CH3); 1615s, ν_{asym}(COO); 1501s, ν_{sym}(COO); 1581s, ν_{asym}(COO); 1456s, ν_{sym}(COO); 438ms, ν(Mn-O_{H2O}); 281ms, ν(Mn-O_{oco}).

Synthesis of [$Cu(MCFA)_2(H_2O)$], ***(3).***

Copper(II) acetate monohydrate (0.0250 g, 0.125 mmol) was dissolved in methanol (2 ml) and this solution was added to a solution of Meclofenamic Acid (0.0740g, 0.25 mmol) in methanol (2 ml). Drops of triethylamine ($N(eth)_3$) were added to the reaction mixture till the apparent pH value was ~ 7. After 4 hours stirring at the room temperature, the reactiom mixture was stored in the refrigerator overnight. The obteined desire precipitate (0.0579 g, 69% yield) was filtered off, subsequently washed with cold methanol and dried under vacuum. The product was re-crystallised from dmso. The Cu(II) derivative gave green crystals (**3a**) , respectively.

IR (cm^{-1}): 3310m, ν(NH); 3070m 2923m, ν(CH3); 1616s, ν_{asym}(COO); 1501s, ν_{sym}(COO); 1583s, ν_{asym}(COO); 1455 ν_{sym}(COO); 375m, ν(Cu-O_{H2O}); 246m ν(Cu-O_{oco}).

Synthesis o f[$Zn(MCFA)_2(H_2O)_4$], ***(4).***

Zinc(II) acetate dihydrate (0.0274 g, 0.125 mmol) was dissolved in methanol (3ml) and this solution was added to a solution of Meclofenamic Acid (0.0740 g, 0.25 mmol) in methanol (3 ml). Drops of

triethylamine ($N(eth)_3$) were added to the reaction mixture till the apparent pH value was ~ 7 After 3 hours of reflux, the reactiom mixture was stored in the refrigerator overnight. Cold water was added dropwise till desired precipitate appeared. Off white powder (0.0263 g, 29.4% yield) was collected by filtration subsequently washed with cold methanol:water (1:1) and dried under vacuum.

IR (cm^{-1}): 3295m, ν(NH); 3058m 2985m, ν(CH3); 1618s, ν_{asym}(COO); 1501m, ν_{sym}(COO); 1583s, ν_{asym}(COO); 1457s, ν_{sym}(COO); 438m, ν(Zn-O_{H2O}); 289ms, ν(Zn-O_{oco}).

Synthesis of [$Cd(MCFA)_2(H_2O)_2$] ***(5)***.

Cadmium(II) Chloride dihydrate (0.0.1097 g, 0.25 mmol) was dissolved in methanol (3 ml) and this solution was added to a solution of Meclofenamic Acid (0.1481g, 0.5 mmol) in methanol (3 ml). Drops of triethylamine ($N(eth)_3$) were added to the reaction mixture till the apparent pH value was ~ 7. After 4 hours stirring at the room temperature, the reactiom mixture was stored in the refrigerator overnight. Cold water was added dropwise till desired precipitate appeared. Off white powder (0.1766 g, 95% yield) was collected by filtration subsequently washed with cold methanol:water (1:1) and dried under vacuum.

IR (cm^{-1}): 3251m, ν(NH); 3064m 2986m, ν(CH3); 1612s, ν_{asym}(COO); 1500s, ν_{sym}(COO); 1580s, ν_{asym}(COO); 1455s, ν_{sym}(COO); 430m, ν(Cd-O_{H2O}); 246s, ν(Cd-O_{oco}).

Synthesis of [Mn(AcO)(MCFA)] ***(6)***.

Manganese(II) acetate anhydrous (0.0952 g, 0.55 mmol) was dissolved in methanol (3 ml) and this solution was added to a solution of Meclofenamic Acid (0.1481 g, 0.50 mmol) in methanol (3 ml). Drops of triethylamine ($N(eth)_3$) were added to the reaction mixture till the apparent pH value was ~ 9. After 4 hours stirring at the room temperature, the reactiom mixture was stored in the refrigerator overnight. The obteined desire precipitate (0.0926 g, 70.4% yield) was filtered off, subsequently washed with cold methanol and dried under vacuum.

IR (cm^{-1}): 3279m ν(NH); 3068w 2982w, ν(CH3); 1613s, ν_{asym}(COO); 1499s, ν_{sym}(COO); 1580s, ν_{asym}(COO); 1455m, ν_{sym}(COO); 398m, ν(Mn-O_{H2O}); 246m, ν(Mn-O_{oco}).

Synthesis of [Cu(AcO)(MCFA)] ***(7)***.

Copper(II) acetate monohydrate (0.0732 g, 0.36 mmol) was dissolved in methanol (2 ml) and this solution was added to a solution of Meclofenamic Acid (0.0987 g, 0.33 mmol) in methanol (2 ml). Drops of triethylamine ($N(eth)_3$) were added to the reaction mixture till the apparent pH value was ~ 9. After 4 hours stirring at the room temperature, the reactiom mixture was stored in the refrigerator overnight. The obteined desire precipitate (0.0565 g, 40.6% yield) was filtered off, subsequently washed with cold methanol and dried under vacuum.

IR (cm^{-1}): 3271m, ν(NH); 3062w 2923w, ν(CH3); 1612s, ν_{asym}(COO); 1499s, ν_{sym}(COO); 1576s, ν_{asym}(COO); 1448s, ν_{sym}(COO); 394mw, ν(Cu-O_{H2O}); 246m, ν(Cu-O_{oco}).

Synthesis of [Zn(AcO)(MCFA)] ***(8)***.

Zinc(II) acetate dihydrate (0.0804 g, 0.37 mmol) was dissolved in methanol (1ml) and this solution was added to a solution of Meclofenamic Acid (0.0987 g, 0.33 mmol) in methanol (2 ml). Drops of triethylamine ($N(eth)_3$) were added to the reaction mixture till the apparent pH value was ~ 9. After 3 hours of reflux, the reactiom mixture was stored in the refrigerator overnight. Cold water was added dropwise till desired precipitate appeared. Off white powder (0.1242 g, 88% yield) was collected by filtration subsequently washed with cold methanol:water (1:1) and dried under vacuum.

IR (cm^{-1}): 3337m, ν(NH); 3072w 2924w, ν(CH3); 1614s, ν_{asym}(COO); 1501m, ν_{sym}(COO);1581s, ν_{asym}(COO); 1458m, ν_{sym}(COO); 499mw, ν(Zn-O_{H2O}); 247ms, ν(Zn-O_{oco}).

Synthesis of [Cd(AcO)(MCFA)] ***(9)***.

Cadmium(II) acetate dihydrate (0.1466 g, 0.55 mmol) was dissolved in methanol (3 ml) and this solution was added to a solution of Meclofenamic Acid (0.1481 g, 0.50 mmol) in methanol (3 ml). Drops of triethylamine ($N(eth)_3$) were added to the reaction mixture till the apparent pH value was ~ 9. After 4 hours stirring at the room temperature, the reactiom mixture was stored in the refrigerator overnight. The obteined desire precipitate (0.0565 g, 24.2% yield) was filtered off, subsequently washed with cold methanol and dried under vacuum.

IR (cm^{-1}): 3524m, ν(NH); 3067s 2943s, ν(CH3); 1610s, ν_{asym}(COO); 14598s, ν_{sym}(COO); 1579s, ν_{asym}(COO); 1455m, ν_{sym}(COO); 397mw, ν(Cd-O_{H2O}); 251ms, ν(Cd-O_{oco}).

Synthesis of [Mn$(FFA)_2(H_2O)$] ***(11)***.

Manganese(II) acetate anhydrous (0.0865 g, 0.5 mmol) was dissolved in methanol (2 ml) and this solution was added to a solution of Flufenamic Acid (0.2812 g, 1 mmol) in methanol (2 ml). Drops of triethylamine ($N(eth)_3$) were added to the reaction mixture till the apparent pH value was ~ 7. After 4 hours stirring at the room temperature, the reactiom mixture was stored in the refrigerator overnight. Cold water was added dropwise till desired precipitate appeared. Off white powder (0.1079 g, 35.1% yield) was collected by filtration and dried under vacuum.

IR (cm^{-1}): 3278m, ν(NH); 3079w 2940w, ν(CH3); (COO); 1583m, ν_{asym}(COO); 1462m, ν_{sym}(COO); 399mw, ν(Mn-O_{H2O}); 248ms, ν(Mn-O_{oco}).

Synthesis of $[Cu(FFA)_2]$ ***(12).***

Copper(II) acetate monohydrate (0.0998 g, 0.5 mmol) was dissolved in methanol (5 ml) and this solution was added to a solution of Flufenamic Acid (0.2812 g, 1 mmol) in methanol (5 ml). Drops of triethylamine ($N(eth)_3$) were added to the reaction mixture till the apparent pH value was ~ 7. After 3 hours stirring at the room temperature, the reactiom mixture was stored in the refrigerator overnight. The obteined desire precipitate (0.1051 g, 33.7% yield) was filtered off, subsequently washed with cold methanol and dried under vacuum.

IR (cm^{-1}): 3332m, ν(NH); 3081w; ν(CH3); 1583m, ν_{asym}(COO); 1503m, 14587, ν_{sym}(COO); 34m, ν(Cu-O_{H2O}); 394w, ν(Cu-O_{oco}).

Synthesis of $[Zn(FFA)_2(H_2O)_2]$ ***(13).***

Zinc(II) acetate dihydrate (0.1084 g, 0.5 mmol) was dissolved in methanol (3 ml) and this solution was added to a solution of Flufenamic Acid (0.3094 g, 1.1 mmol) in methanol (5 ml). Drops of triethylamine ($N(eth)_3$) were added to the reaction mixture till the apparent pH value was ~ 7. After 3 hours of reflux, the reactiom mixture was stored in the refrigerator overnight. Cold water was added dropwise till desired precipitate appeared. White powder (0. 2001 g, 57.7% yield) was collected by filtration, subsequently washed with cold methanol:water (2:1) and dried under vacuum.

IR (cm^{-1}): 3314s, ν(NH); 3057m 2953m, ν(CH3); 1583m, ν_{asym}(COO); 1462m, ν(Zn-O_{H2O}); 399mw, 246mw, ν(Zn-O_{oco}).

Synthesis of $[Cd(FFA)_2(H_2O)_2]$ ***(14).***

Cadmium(II) Chloride dihydrate (0.1097 g, 1 mmol) was dissolved in methanol (4 ml) and this solution was added to a solution of Flufenamic Acid (0.3678 g, 1 mmol) in methanol (4 ml). Drops of triethylamine ($N(eth)_3$) were added to the reaction mixture till the apparent pH value was ~ 9. After 4 hours stirring at the room temperature, the reactiom mixture was stored in the refrigerator overnight. Cold water was added dropwise till desired precipitate appeared. White powder (0.1383 g, 30% yield) was collected by filtration and dried under vacuum.

IR (cm^{-1}): 3332s, ν(NH); 3067m 2943m, ν(CH3); 1584m, ν_{asym}(COO); 1460m, ν(Cd-O_{H2O}); 398mw, 253ms, ν(Cd-O_{oco}).

Synthesis of [Mn(AcO)(FFA)] ***(15).***

Manganese(II) acetate anhydrous (0.1903 g, 1.1 mmol) was dissolved in methanol (3 ml) and this solution was added to a solution of Flufenamic Acid (0.2812 g, 1 mmol) in methanol (3 ml). Drops of triethylamine ($N(eth)_3$) were added to the reaction mixture till the apparent pH value was ~ 9. After 4

hours stirring at the room temperature, the reactiom mixture was stored in the refrigerator overnight. Cold water was added dropwise till desired precipitate appeared. Beige powder (0.1997 g, 44.5% yield) was collected by filtration and dried under vacuum.

IR (cm^{-1}): 3330s, ν(NH); 3081w 2945w, ν(CH3); 1584s, ν_{asym}(COO); 1459m, ν_{sym}(COO); 254ms, ν(Mn-O_{H2O}); 398ms, ν(Mn-O_{oco}).

Synthesis of [Cu(AcO)(FFA)] ***(16)***.

Copper(II) acetate monohydrate (0.2196 g, 1.1 mmol) was dissolved in methanol (5 ml) and this solution was added to a solution of Flufenamic Acid (0.2812 g, 1 mmol) in methanol (5 ml). Drops of triethylamine ($N(eth)_3$) were added to the reaction mixture till the apparent pH value was ~ 9. After 3 hours stirring at the room temperature, the reactiom mixture was stored in the refrigerator for several days. The obteined desire precipitate (0.1455 g, 36.1% yield) was filtered off, subsequently washed with cold methanol and dried under vacuum

IR (cm^{-1}): 3270s, ν(NH); 3082w; ν(CH3); 1582s, ν_{asym}(COO); 1451m, ν_{sym}(COO); 396m, ν(Cu-O_{H2O}); 247m, ν(Cu-O_{oco}).

Synthesis of [Zn(AcO)(FFA)] ***(17)***.

Zinc(II) acetate dihydrate (0.2414 g, 1.1 mmol) was dissolved in methanol (4 ml) and this solution was added to a solution of Flufenamic Acid (0.2812 g, 1 mmol) in methanol (5 ml). Drops of triethylamine ($N(eth)_3$) were added to the reaction mixture till the apparent pH value was ~ 9. After 3 hours of reflux, the reactiom mixture was stored in the refrigerator overnight. Cold water was added dropwise till desired precipitate appeared. Off white powder (0.1242 g, 30.7% yield) was collected by filtration and dried under vacuum.

IR (cm^{-1}): 3296, ν(NH); 3058m 2954m, ν(CH3); 1587s, ν_{asym}(COO); 1460m, ν_{sym}(COO); 398mw, ν(Zn-O_{H2O}); 349ms, ν(Zn-O_{oco}).

Synthesis of [Cd(AcO)(FFA)] ***(18)***.

Cadmium(II) acetate dihydrate (0.1333 g, 0.5 mmol) was dissolved in methanol (4 ml) and this solution was added to a solution of Flufenamic Acid (0.3094 g, 1 mmol) in methanol (4 ml). Drops of triethylamine ($N(eth)_3$) were added to the reaction mixture till the apparent pH value was ~ 7. After 4 hours stirring at the room temperature, the reactiom mixture was stored in the refrigerator overnight. Cold water was added dropwise till desired precipitate appeared. White powder (0.1383 g, 28.4% yield) was collected by filtration and dried under vacuum.

IR (cm^{-1}): 3520s, ν(NH); 3066m 2944m, ν(CH3); 1581s, ν_{asym}(COO); 1457m, ν_{sym}(COO); 396mw, ν(Cd-O_{H2O}); 253ms, ν(Cd-O_{oco}).

Synthesis of [Mn(Lorn)$_2$], (***20).***

Manganese(II) acetate anhydrous (0.0216 g, 0.125mmol) was dissolved in methanol (3 ml) and this solution was added to a solution of Lornoxicam (0.0930g, 0.25 mmol) in methanol (3 ml). Drops of triethylamine (N(eth)$_3$) were added to the reaction mixture till the apparent pH value was ~ 7. After 24 hours stirring at the room temperature, the reactiom mixture was stored in the refrigerator overnight. The obteined desire precipitate (0.0782 g,, 75% yield) was filtered off, subsequently washed with cold methanol and dried under vacuum.The product was re-crystallised from dmso. The Mn(II) derivative gave pale orange crystals (**20a**), respectively.

IR (cm^{-1}): 3195m, ν(OH); 3095m, ν(NH); 1607w, ν(C=O); 1580s, ν(C=N); 1334s, $\nu_{asym}(SO_2)$; 1157s, $\nu_{sym}(SO_2)$; 361, ν(Mn-O); 622mw, 267mw, ν(Mn-N).

Synthesis of [Cu(Lorn)$_2$] (***21).***

Copper(II) acetate monohydrate (0.0250 g, 0.125 mmol) was dissolved in methanol (3 ml) and this solution was added to a solution of Lornoxicam (0.0930 g, 0.25 mmol) in methanol (3 ml). Drops of triethylamine (N(eth)$_3$) were added to the reaction mixture till the apparent pH value was ~ 7. After 24 hours stirring at the room temperature, the reactiom mixture was stored in the refrigerator overnight. The obteined desire precipitate (0.0754 g, 72% yield) was filtered off, subsequently washed with cold methanol and dried under vacuum. The product was re-crystallised from dmso. The Cu(II) derivative gave pale yellow crystals (**21a**), respectively.

IR (cm^{-1}): 3355m, ν(OH); 3099m, ν(NH); 1608w, ν(C=O); 1576s, ν(C=N); 1338s, $\nu_{asym}(SO_2)$; 1160, $\nu_{sym}(SO_2)$; 324m, ν(Cu-O); 652mw, 271mw ν(Cu-N).

Synthesis of [Zn(Lorn)$_2$] (***22).***

Zinc(II) acetate dihydrate (0.0274g, 0.0125 mmol) was dissolved in methanol (3 ml) and this solution was added to a solution of Lornoxicam (0.0930g, 0.25mmol) in methanol (2 ml). Drops of triethylamine (N(eth)$_3$) were added to the reaction mixture till the apparent pH value was ~ 7. After 3 hours of reflux, the reactiom mixture was stored in the refrigerator overnight. The obteined desire precipitate (0.0879 g, 83% yield) was filtered off, subsequently washed with cold methanol and dried under vacuum. The product was re-crystallised from dmso. The Zn(II) derivative gave yellow crystals (**22a**), respectively.

IR (cm^{-1}): 3227m, ν(OH); 3097m, ν(NH); 1608w, ν(C=O); 1581s, ν(C=N); 1336s, $\nu_{asym}(SO_2)$; 1159m, $\nu_{sym}(SO_2)$; 355m, ν(Zn-O); 610mw, 297mw, ν(Zn-N).

Synthesis of [Cd(Lorn)$_2$] (***23)***.

Cadmium(II) Chloride dihydrate (0.0229 g, 0.125mmol) was dissolved in methanol (3 ml) and this solution was added to a solution of Lornoxicam (0.0930g, 0.25mmol) in methanol (2 ml). Drops of triethylamine (N(eth)$_3$) were added to the reaction mixture till the apparent pH value was ~ 7. After 24 hours stirring at the room temperature, the reactiom mixture was stored in the refrigerator overnight. The obteined desire precipitate (0.0900 g, 80% yield) was filtered off, subsequently washed with cold methanol and dried under vacuum. The product was re-crystallised from dmso. The Cd(II) derivative gave pale yellow crystals (**23a**), respectively.

IR (cm^{-1}): 3221m, ν(OH); 3097m, ν(NH); 1609w, ν(C=O); 1580s ν(C=N); 1335s, $\nu_{asym}(SO_2)$; 1157s, $\nu_{sym}(SO_2)$; 352m, ν(Cd-O); 289mw, ν(Cd-N).

Synthesis of [Mn(AcO)(Lorn)] (***24)***.

Manganese(II) acetate anhydrous (0.0476 g, 0.275 mmol) was dissolved in methanol 3 ml) and this solution was added to a solution of Lornoxicam (0.0930 g, 0.25 mmol) in methanol (3 ml). Drops of triethylamine (N(eth)$_3$) were added to the reaction mixture till the apparent pH value was ~ 9. After 24 hours stirring at the room temperature, the reactiom mixture was stored in the refrigerator overnight. The obteined desire precipitate (0.0750 g, 70.4% yield) was filtered off, subsequently washed with cold methanol and dried under vacuum.

IR (cm^{-1}): 3209m ν(OH); 3096m, ν(NH); 1605w, ν(C=O); 1581s, ν(C=N); 1334s, $\nu_{asym}(SO_2)$; 1157s, $\nu_{sym}(SO_2)$; 363m ν(Mn-O); 653m, 273mw ν(Mn-N).

Synthesis of [Cu(AcO)(Lorn)] (***25)***.

Copper(II) acetate monohydrate (0.0549 g, 0.275 mmol) was dissolved in methanol (3 ml) and this solution was added to a solution of Lornoxicam (0.0930 g, 0.25 mmol) in methanol (3 ml). Drops of triethylamine (N(eth)$_3$) were added to the reaction mixture till the apparent pH value was ~ 9. After 24 hours stirring at the room temperature, the reactiom mixture was stored in the refrigerator overnight. The obteined desire precipitate (0.1068 g, 98% yield) was filtered off, subsequently washed with cold methanol and dried under vacuum.

IR (cm^{-1}): 3209M, ν(OH); 3099M, ν(NH); 1609W, ν(C=O); 1577s, ν(C=N); 1338s, $\nu_{asym}(SO_2)$; 1159S, $\nu_{sym}(SO_2)$; 351M, ν(Cu-O); 653mw, 272mw ν(Cu-N).

Synthesis of [Zn(AcO)(Lorn)] (***26)***

Zinc(II) acetate dihydrate (0.0604 g, 0.275 mmol) was dissolved in methanol (3 ml) and this solution was added to a solution of Lornoxicam (0.0930 g, 0.25 mmol) in methanol (3 ml). Drops of triethylamine ($N(eth)_3$) were added to the reaction mixture till the apparent pH value was ~ 9. After 3 hours of reflux., the reactiom mixture was stored in the refrigerator overnight. The obteined desire precipitate (0.0930 g, 85.2% yield) was filtered off, subsequently washed with cold methanol and dried under vacuum.

IR (cm^{-1}): 3226m, ν(OH); 3096m, ν(NH); 1609w, ν(C=O); 1581s, ν(C=N); 1335s, $\nu_{asym}(SO_2)$; 1164m, $\nu_{sym}(SO_2)$; 368m, ν(Zn-O); 640mw, 20mw, ν(Zn-N).

Synthesis of [Cd(AcO)(Lorn)] (***27)***

Cadmium(II) acette dihydrate (0.0733 g, 0.275 mmol) was dissolved in methanol (3 ml) and this solution was added to a solution of Lornoxicam (0.0930 g, 0.25 mmol) in methanol (3 ml). Drops of triethylamine ($N(eth)_3$) were added to the reaction mixture till the apparent pH value was ~ 9. After 24 hours stirring at the room temperature, the reactiom mixture was stored in the refrigerator overnight. The obteined desire precipitate (0.1008 g, 72.7% yield) was filtered off, subsequently washed with cold methanol and dried under vacuum.

IR (cm^{-1}): 3213m, ν(OH); 3097m, ν(NH); 1607w, ν(C=O); 1581ss, ν(C=N); 1334s, $\nu_{asym}(SO_2)$; 1157s, $\nu_{sym}(SO_2)$; 358m, ν(Cd-O); 288mw, ν(Cd-N).

Synthesis of $[Mn(Cef)_2]$ (***29)***

Manganese(II) acetate anhydrous (0.0216 g, 0.125 mmol) was dissolved in methanol (2 ml) and this solution was added to a solution of Cefaclor (0.0919 g, 0.25 mmol) in methanol (4 ml). Drops of triethylamine ($N(eth)_3$) were added to the reaction mixture till the apparent pH value was ~ 7. After 4 hours stirring at the room temperature, the reactiom mixture was stored in the refrigerator overnight. The obteined desire precipitate (0.0349 g, 35.4% yield) was filtered off, subsequently washed with cold methanol and dried under vacuum.

IR (cm^{-1}): 3403m, 3216m, ν(NH); 1775s, $\nu(C=O)_{\beta\text{-lactam}}$; 1698s, $\nu(C=O)_{amide}$; 1602m, $\nu_{asym}(C=O)$; 1455w, $\nu_{sym}(C=O)$; 1352s, $\nu(CN)_{\beta\text{-lactam}}$; 238mw, ν(Mn-O);

Synthesis of $[Cu(Cef)_2]$ (***30)***

Copper(II) acetate monohydrate (0.0998 g, 0.5 mmol) was dissolved in methanol (5 ml) and this solution was added to a solution of Cefaclor (0.3678 g, 1 mmol) in methanol (10 ml). Drops of triethylamine ($N(eth)_3$) were added to the reaction mixture till the apparent pH value was ~ 7. After 3

hours stirring at the room temperature, the reactiom mixture was allowed to cool down in the refrigerator. The obteined desire precipitate (0.1588 g, 40% yield) was filtered off, subsequently washed with cold methanol and dried under vacuum.

IR (cm^{-1}): 3435m, 3213m ν(NH); 1773s, $\nu(C=O)_{\beta\text{-lactam}}$; 1697s, $\nu(C=O)_{amide}$; 1607m, $\nu_{asym}(C=O)$; 1457w, $\nu_{sym}(C=O)$; 1352s, $\nu(CN)_{\beta\text{-lactam}}$; 231mw, ν(Cu-O);

Synthesis of $[Zn(Cef)_2]$ (***31)***

Zinc(II) acetate dihydrate (0.2195 g, 0.5 mmol) was dissolved in methanol (4 ml) and this solution was added to a solution of Cefaclor (0.3678 g, 1 mmol) in methanol (6 ml). Drops of triethylamine ($N(eth)_3$) were added to the reaction mixture till the apparent pH value was ~ 7. After 3 hours of reflux, the reactiom mixture was stored in the refrigerator overnight. The obteined desire precipitate (0.2807 g, 70.3% yield) was filtered off, subsequently washed with cold methanol and dried under vacuum.

IR (cm^{-1}): 3327m, 3224m ν(NH); 1777s, $\nu(C=O)_{\beta\text{-lactam}}$; 1636w, $\nu(C=O)_{amide}$; 1606w, $\nu_{asym}(C=O)$; 1436w, $\nu_{sym}(C=O)$; 1369m, $\nu(CN)_{\beta\text{-lactam}}$; 381mw, ν(Zn-O);

Synthesis of $[Cd(Cef)_2]$ (***32)***

Cadmium(II) Chloride dihydrate (0.0274 g, 0.125 mmol) was dissolved in methanol (3 ml) and this solution was added to a solution of Cefaclor (0.0919 g, 0.25 mmol) in methanol (3 ml). Drops of triethylamine ($N(eth)_3$) were added to the reaction mixture till the apparent pH value was ~ 7. After 24 hours stirring at the room temperature, the reactiom mixture was stored in the refrigerator overnight. The obteined desire precipitate (0.0280 g, 26.5% yield) was filtered off, subsequently washed with cold methanol and dried under vacuum.

IR (cm^{-1}): 3435m, 3201mw ν(NH); 1773s, $\nu(C=O)_{\beta\text{-lactam}}$; 1636m, $\nu(C=O)_{amide}$; 1610s, $\nu_{asym}(C=O)$; 1436w, $\nu_{sym}(C=O)$; 1369s, $\nu(CN)_{\beta\text{-lactam}}$; 382mw ν(Cd-O);

Synthesis of [Mn(AcO)(Cef)] (***33)***

Manganese(II) acetate anhydrous (0.0640 g, 0.37 mmol) was dissolved in methanol (2 ml) and this solution was added to a solution of Cefaclor (0.1226 g, 0.33 mmol) in methanol (4 ml). Drops of triethylamine ($N(eth)_3$) were added to the reaction mixture till the apparent pH value was ~ 7. After 4 hours stirring at the room temperature, the reactiom mixture was stored in the refrigerator overnight. The obteined desire precipitate (0.0662 g, 47.5% yield) was filtered off, subsequently washed with cold methanol and dried under vacuum.

IR (cm^{-1}): 3364s, ν(NH); 1732m, $\nu(C=O)_{\beta\text{-lactam}}$; 1638m, $\nu(C=O)_{amide}$; 1638m, $\nu_{asym}(C=O)$; 1437w, $\nu_{sym}(C=O)$; 1385w, $\nu(CN)_{\beta\text{-lactam}}$; 386, ν(Mn-O);

Synthesis of [Cu(AcO)(Cef)] (***34)***

Copper(II) acetate monohydrate (0.2196 g, 1.1 mmol) was dissolved in methanol (5 ml) and this solution was added to a solution of Cefaclor (0.3678 g, 1 mmol) in methanol (5 ml). Drops of triethylamine ($N(eth)_3$) were added to the reaction mixture till the apparent pH value was ~ 9. After 4 hours stirring at the room temperature, the reactiom mixture was stored in the refrigerator for several days. The obteined desire precipitate (0.0826 g, 20% yield) was filtered off, subsequently washed with cold methanol and dried under vacuum.

IR (cm^{-1}): 3418s, ν(NH); 1723m, $\nu(C=O)_{\beta\text{-lactam}}$; 1638m, $\nu(C=O)_{amide}$; 1638w, $\nu_{asym}(C=O)$; 1437w, $\nu_{sym}(C=O)$; 1385w, $\nu(CN)_{\beta\text{-lactam}}$; 368mw ν(Cu-O);

Synthesis of [Zn(AcO)(Cef)] (***35)***

Zinc(II) acetate dihydrate (0.2414 g, 1.1 mmol) was dissolved in methanol (4 ml) and this solution was added to a solution of Cefaclor (0.3678 g, 1 mmol) in methanol (6 ml). Drops of triethylamine ($N(eth)_3$) were added to the reaction mixture till the apparent pH value was ~ 9. After 3 hours of reflux, the reactiom mixture was stored in the refrigerator overnight. The obteined desire precipitate (0.2807 g, 65% yield) was filtered off, subsequently washed with cold methanol and dried under vacuum.

IR (cm^{-1}): 3247m, ν(NH); 1635, $\nu(C=O)_{\beta\text{-lactam}}$; 1635m, $\nu(C=O)_{amide}$; 1592w, $\nu_{asym}(C=O)$; 1434w, $\nu_{sym}(C=O)$; 1386w, $\nu(CN)_{\beta\text{-lactam}}$; 345mw, ν(Zn-O);

Synthesis of [Cd(AcO)(Cef)] (***36)***

Cadmium(II) Chloride dihydrate (0.0603 g, 0.275 mmol) was dissolved in methanol (3 ml) and this solution was added to a solution of Cefaclor (0.0919 g, 0.25 mmol) in methanol (3 ml). Drops of triethylamine ($N(eth)_3$) were added to the reaction mixture till the apparent pH value was ~ 9. After 4 hours stirring at the room temperature, the reactiom mixture was stored in
the refrigerator overnight. The obteined desire precipitate (0.0875 g, 73% yield) was filtered off, subsequently washed with cold methanol and dried under vacuum.

IR (cm^{-1}): 3340m, ν(NH); 1636s, $\nu(C=O)_{\beta\text{-lactam}}$; 1635s, $\nu(C=O)_{amide}$; 1608s, $\nu_{asym}(C=O)$; 1453w, $\nu_{sym}(C=O)$; 1386m, $\nu(CN)_{\beta\text{-lactam}}$; 376mw, ν(Cd-O);

XVII Biological studies

Materials

SOD assay

Nitrotetrazolium blue chloride (Sigma-Aldrich); Xanthine, 2,6-Dihydroxypurine (Sigma); Potassium phosphate monobasic, H_2KO_4P (Fluka); Xanthine oxidase, Xanthine: oxygen oxidoreductase, grade I: from buttermilk (Sigma);

Antiproliferative Assay in vitro.

Trizma base, (Tris[hydroxymetyl]aminomethane) (Sigma); Hepes (Sigma); Sodium dodecyl sulfate (Sigma); Thiazolyl blue tetrazolium bromide (Sigma); Sulforhodamine B sodium salt (Sigma); Trypan Blue solution (0.4%) (Sigma); RPMI 1640 (BiochromAG); Streptomycine (Streptomycin sulfate); Benzylpenicillina (Biopharma); Trichloroacetic acid (Merck); Phosphate buffered saline, pH=7.4 (Gibco), DMEM, Dulbecco's Modified Eagle Medium (Gibco); F-12 Nutrient mixture Kaighn's Modification (Gibco); MEN Non-essential aminoacid (Gibco), L-Glutamine (Sigma); Antibiotic Antimycotic (Gibco); Sodium Bicarbonate (Gibco), Penicillin Streptomycin (PAA), Fetal bovine serum (BiochromAG).

Basic laboratoty design and selection of equipment of cells in culture.

- Microbiological safety cabinet (NUAIR Biological safty cabinet)
- Inverted microscope (Microscope KRUSS OPTRONIC)
- Centrifuge (Centrifuge ROTOFIX 32)
- CO_2 incubator (Galaxy R CO_2 incubator, RS Biotech). Certain conditions are required for optimal cell growth, the preferred temperature is 36.5° ± 1°C and 5% CO_2
- Storage facilities such as liquid nitrogen tanks and fridges/freezers storing stocks of the cells lines and holding tissue culture media or serum

- 10 units Tissue culture flasks
- Nunclon 96-well plates
- Automatic piprttes
- Disposable serological pipette
- Multichannel pipette
- Repetitive pipette
- Pipette tips

- PD-Tip (repetitive tips)
- Eppendorf PCR tubes
- Centrifuge tubes
- Sterile glassware
- Hemocytometer NeuBauer (cell counting)

Methods

SOD assay

SOD assay using XO/NBT system.The reaction was initiated by the addition of XO.
The SOD-like activity was determined spectrophotometrically using superoxide radicals generated by the xanthine–xanthine oxidase system with NBT (nitroblue tetrazolium chloride) as indicator. The absorbance change at 560nm was monitored at 25ºC for 20min. The degree of the inhibition of the concentration of superoxide radical was expressed as IC_{50}, corresponding to the concentration of metal(II) complex for which the concentration of superoxide radical was reduced by 50% (determined indirectly by the indicator). In each experiment, two cuvettes were used. The first cuvette was always the reference system, the second cuvette contained solutions of the studied compound at different concentrations[10].

Antiproliferative Assay in vitro.

In the in vitro assays each experiment was performed at least in triplicate and the standard deviation of absorbance was less than 10% of the mean[11,12].

- Compounds. Test solutions of the compounds tested (1 mg/ml) were prepared by dissolving the substance in 100 ml of dimethyl sulfoxide (DMSO) completed with 900 ml of tissue culture medium[11,12]. Immediately after preparation of intermediate dilutions, 100μL aliquots of each dilution are added to the appropriate microtiter plate wells. As the microtiter wells already contain the cells in 100μL of medium, the final drug concentration tested is 50% of that in the intermediate dilutions[13]. Thus, the tested compounds were diluted in culture medium to reach the final concentrations of 100, 50, 10, 1, and 0.1 μg/ml. The solvent (DMSO) in the highest concentration used in the test did not reveal any cytotoxic activity[11,12].
- Cells. The established in vitro human cancer cell lines MCF-7 (breast cancer cell line), T24 (bladder cancer cell line), and A-549 (non-small-cell-lung carcinoma), and a mouse L-929 (a fibroblast-like cell line cloned from strain L) were applied. The cell lines are maintained in the Cell Culture Collection of the University of Ioannina. Twenty-four hours before addition of the tested agents, the cells were plated in 96-well plates at a density of 10^4 cells per well. The T-24 and MCF-7 cells were cultured in D-MEM (Dulbecco's Modified Eagle Medium) supplemented with 1%

antibiotic and 10% fetal bovine serum. L-929 cells were grown in Hepes-buffered RPMI 1640 medium supplemented with 10% fetal bovine serum, penicillin (75 U/ml), and streptomycin (75 mg/ml). A-549 cells were grown in F-12K Nutrient mixture Kaighn's Modification supplemented with 1% glutamine, 1%antibiotic/antimycotic, 2%$NaHCO_3$, and 10% fetal bovine serum. The cell cultures were maintained at 37ºC in a humid atmosphere saturated with 5% CO_2. Cell number was counted by the Trypan Blue dye exclusion method. MCF-7, L-929, and A-549 cells were determined by the sulforhodamine B assay, and T24 cells by the MTT (3-(4,5-dimethylthiazol-2-yl)-2,5-diphenyl- 2H-tetrazolium hydrobromide) assay[11-13].

- SRB (Sulforhodamine B) Assay.The cytotoxicity assay was performed after 72-h exposure of the cultured cells to varying concentrations (from 0.1 to 100 µg/ml) of the tested agents. The cells attached to the plastic were fixed by gently layering cold 80% trichloroacetic acid (TCA) on the top of the culture medium in each well. The plates were incubated at for 60 minutes at 4ºC.Afterwards, the supernatant is discarded, and the plates are washed five times with tap water and dried. The background optical density was measured in the wells filled with culture medium, without the cells. The cellular material fixed with TCA was stained for 30 min with 0.4% sulforhodamine B dissolved in 1% acetic acid. Unbound dye was removed by rinsing five times with 1% acetic acid. The protein-bound dye was extracted with 10 mM unbuffered Tris base for determination of optical density (at 540 nm) in a computer-interfaced, 96-well microtiter plate[11-13].
- MTT (Sigma). This technique was applied for cytotoxicity screening against T-24 cells growing in suspension culture. An assay was performed after 72-h exposure to varying concentrations (from 0.1 to 100 mg/ml) of the tested agents. For the last 3–4 h of incubation 20 ml of MTT solutions was added to each well (stock solutions 5 mg/ml).The MTT assay is based on the principle that living cells have the ability to convert a soluble tetrazolium salt (3-(4,5 dimethylthiazol-2-yl)-2,5-diphenyl tetrazolium bromide, MTT) to an insoluble formazan precipitate.The mitochondria of viable cells reduce a pale yellow MTT to a navy blue formazan, so, if more viable cells are present in the well, more MTT will be reduced to formazan. When the incubation time was completed, 80 ml of the lysing mixture was added to each well (lysing mixture: 225 ml of DMF, 67.5 g of sodium dodecylsulfate and 275 ml of distillated H_2O). After 24 h, when formazan crystals had dissolved, the optical densities of the samples were read on an Eliza SpectraMax 190 photometer at 540-nm wavelength. Each compound at a given concentration was tested in triplicate in each experiment, which was repeated three times[11-13].

Recerences

1. Kaltenbronn, J.S., Scherrer, R.A., Short, F.,Jones, E.M., Beatty, H.R.,Saka,M.M., Winder, C.V., Wax, J.,Williamson, W.R.N. Arzneim.-Forsch/Drug Res. 33(I) 4a (1983)
2. Bruker (2005). APEX2 Software, Bruker AXS Inc. V2.0-1, Madison, Wisconsin, USA
3. G.M. Sheldrick (1997). SADABS. Program for Empirical Absorption Correction of Area Detector Data. University of Goettingen, Germany.
4. G.M. Sheldrick (2008). Acta Cryst. A64, 112-122.
5. G.M. Sheldrick (1997). SHELXL-97. Program for the Refinement of Crystal Structures. University of Goettingen, Germany.
6. A. J. C. Wilson (1995). International Tables for Crystallography. Vol. C, Kluwer Academic Publishers: Dordrecht, The Netherlands.
7. A.L. Spek (2003). PLATON. A Multipurpose Crystallographic Tool. Utrecht University, Utrecht, The Netherlands.
8. E. Keller (1997). SCHAKAL-97. A computer program for the graphic representation of molecular and crystallographyc models. University of Freiburg i. Br., Germany.
9. Díaz, Alicia M., Villalonga, Reynaldo and Cao, R. ,Journal of Coordination Chemistry,62:1,100 — 107 (2009)
10. Kovala-Demertzi, D.,Hadjipavlou-Litina, D., Staninska, M., Primikiri, A., Kotoglou, C. Demertzis, M.A, Journal of Enzyme Inhibition and Medicinal Chemistry **24,**742 — 752 (2009)
11. Kovala-Demertzi, D.,Hadjipavlou-Litina, D., Primikiri, A., Staninska, M., Kotoglou, C. Demertzis, M.A, Chemistry&Biodiversity **6,** 948-960 (2009).

Conclusions

Chemistry

As results of first part of our work:

- Thirty two new simple synthesis of Mn(II), Cu(II), Zn(II), Cd(II) complexes with meclofenamic acid, (N-(2,6-dichloro-3-methylphenyl) anthranilic acid), flufenamic acid, (N-[3-(trifluoromethyl)-phenyl]-anthranilic acid), lornoxixam, (6-chloro-4-hydroxy-2-methyl- 2-pyridyl-2*H*-thieno[2,3-*e*]-1,2-thiazine-3-amide-1,1-dioxide) and cefaclor [7-(D-2-amino-2-phenylacetamido)-3-chloro-3-cepham-4-carboxylic acid] in metal to ligand molar ratio 1:2 and 1:1
- After repeated attempts we succeeded in isolating singiel crystals suitable for X-ray diffraction analysis thus five new crystal structures have been reported.

Recrystallization from dimethylsulfoxide (dmso) of complex **3** gave tetranuclear molecule (core consists of two, 5-coordinate Cu^{II} atoms and two, 6-coordinate Cu^{II} atoms) held together by six meclofenamic acid molecules as ligands and two DMSO groups, $[Cu_4(MCFA)_6(OH)_2(DMSO)_2].2DMSO$ (**3a**).

Recrystallization from dimethylsulfoxide (dmso) of complex **5** gave molecule held together by two meclofenamic acid molecules (meclofenamic acid acts as a deprotonated bidentate ligand and it is coordinated to the metal ion through the oxygens of the carboxyl groups) and two DMSO groups, $[Cd(MCFA)_2(DMSO)_2]$. (**5a**).

Recrystallization from dimethylsulfoxide (dmso) of complex **20**, **21**, **22** gave three isostructural molecules $[M^{II}(lorn)_2(O\text{-}dmso)_2]$ (M = Mn **20a**, Cu **21a,** Cd **22a**), held together by two lornoxicam molecules (employ the oxygene of the amide group and the pyridyl nitrogen to bond to the cation) and two DMSO groups.

- Elemental analysis, XRF, IR, UV-vis, ESI-MS – spectral data of eight new manganese(II) complexes and eight new copper(II) complexes are repoterd.
- Characterization of eight new zinc(II) complexes and eight new cadmium(II) complexes has been realized with physicochemical (elemental analysis, XRF) and spectroscopic metods (^{1}H-NMR, ^{13}C-NMR, 2D ^{1}H–^{1}H COSY, ^{1}H–^{13}C HSQC, ^{1}H–^{13}C HMBC NMR, DEPT-135, IR and ESI-MS).

Biological studies

As results of second part of our work:

- Examination of the anti-proliferative activit *in vitro* of twenty four meclofenamic acid, flufenamic acid, lornoxicam, cefaclor Mn(II), Cu(II), Zn(II), Cd(II) complexes as well as free drugs against the cells of three human cancer cell lines, MCF-7 (breast cancer cell line), T-24 (bladder cancer cell line), and A-549 (non-small-cell lung carcinoma), and a mouse fibroblast L-929 cell line, regarding cytotoxicity, has been performed.

- Among all complexes tested, the IC_{50} values shown by five complexes of meclofenamic acid*, three complexes of flufenamic acid*, three complexes of lornoxicam* and two complexes of cefaclor*, against T-24 cancer cell line, in a molar range better to that of well known chemotherapeutic cisplatin that is selected as references. Moreover all of those complexes shown selectivity towards T-24 cancer cell line.
- The IC_{50} values shown by one complex of flufenamic acid*, two complex of lornoxicam* and two complexes of cefaclor*, against T-24 cancer cell line, in a molar range similar to that of well known chemotherapeutic cisplatin that is selected as references. Moreover all of those complexes shown selectivity towards T-24 cancer cell line.
- The IC_{50} values shown by $[Mn(Lorn)_2]$, against MCF-7 cancer cell line, in a molar range similar to that of cisplatin.
- Among twenty four complexes tested for their superoxide dismutase activity, copper(II) and manganese(II) complexes presented a relatively low SOD-like activity, higher than 1 μM, however it was noted that the IC_{50} values for $[Cu(MCFA)_2(H_2O)]$ and [Cu(AcO)(MCFA)] lay at the region, where are considered as potent SOD mimics.

*cadmium(II) complexes were not taken into account

Abstract

The present PhD thesis is dealing with synthesis, crystal structures, spectroscopic study and biological activity of manganese(II), copper(II), zinc(II) and cadmium(II) complexes with drugs. For the reasons of this PhD thesis, three members of NSAIDs drugs: meclofenamic acid, (N-(2,6-dichloro-3-methylphenyl) anthranilic acid), flufenamic acid (N-[3-(trifluoromethyl)-phenyl]-anthranilic acid) and lornoxicam (6-chloro-4-hydroxy-2-methyl- 2-pyridyl-2*H*-thieno[2,3-*e*]-1,2-thiazine-3- amide-1,1-dioxide) have been choosen. Additionally, the member of cephalosporines, cefaclor [7-(D-2-amino-2-phenylacetamido)-3-chloro-3-cepham-4-carboxylic acid] has been choosen.

The PhD thesis contains three main units: Introduction (chapters I – VII), Resulta and Discussion (chapters VIII – XIII) and Experimental (chapters XIV – XVI). In the first chapters we attempted to present a review for the non-steroidal anti-inflamatory drugs (NSAIDs).The anti-inflammatory activity of NSAIDs and most of its other pharmacological effects are related to the inhibition of the conversion of arachidonic acid (AA) to prostaglandins, which are mediators of the inflammatory process. The enzymes cyclooxygenase (COX) and lipoxygenase (LOX), which catalyze the oxidative metabolism of amino acids, are useful targets for the design and the development of new drugs that substantially inhibit the generation of the final inflammatory products and the propagation of inflammation. Recent studies revealed that, in addition to arthritis and pain, cancer and neurodegenerative diseases like Alzheimer's disease could potentially be treated with Cox-2 inhibitors.

The role of selected metal ions in biological systems is studied in second chapter.

The next chapters (III and IV) are dealing with the NSAIDs metal complexes. Metal complexes with active drugs as ligands is a research area of increasing interest for inorganic and medicinal chemistry and has concentrated much attentionas an approach towards drug development. The synthesis of metal complexes with nonsteroidal anti-inflammatory drugs (NSAIDs) as ligands has acquired new impetus in the past decade. First, on the basis of pure co-ordination chemistry NSAIDs are very versatile ligands and show a huge variety of ligating modes as function of the metal and the environmental conditions. The information collected from the preparative, structural and reactivity studies have high significance for several fields which span from the bio-sciences to the material sciences. Second, NSAIDs have numerous applications as pharmaceutical agents. Third, for this type of drugs the complex formation with specific metals may improve the activity towards certain diseases and hopefully may increase the activity spectrum. The combination of two or more different species into the same compound may bring to a multitherapeutic agent. The coordination chemistry of non-steroidal anti-inflammatory drugs (NSAIDs) has been studied by several groups worldwide. Some complexes have increased pharmaceutical or biological activity with respect to the drug, or are interesting from a purely chemical point of view.

Chapter V contains short discussion about β-antibiotic, cefaclor as the member of the cephalosporines.

Short reviews concerns on the superoxide dismutation activity, SOD mimetics and cancer cells selected for the reason of presented PhD are included in chapters VI and VII. SODs enzymes have molecular weights too high to cross cell membranes and can only provide extracellular protection. In order to circumvent this difficulty, a stable non-toxic, low-molecular-weight metal complex that catalyses the dismutation of superoxide anion might be a suitable alternative to superoxide dismutase in clinical applications with the desirable qualities of low cost, cell permeability and non-immunogenicity.

The aim of this research was to extend the pharmacological profile of selected drugs, in order to search for new properties such as antioxidant and anticancer activity, to prepare new compounds, complexes of meclofenamic acid, flufenamic acid, lornoxixam and cefaclor with essential metal ions, which probably would exhibit improved or different biological properties compared to parent drugs.

In the second part of the thesis is discussed the results according to the experimental data. The synthesis of manganese(II)-, copper(II)-, zinc(II)-, cadmium(II)-acetates and/or cadmium(II)-chloride with either anti-inflammatory drugs or β-antibiotic, cefaclor in methanol, in metal to ligand molar ratio 1:2 and 1:1 are reported. All new synthesized complexes are characterized by means of, elemental analysis, XRF and spectroscopic techniques ^{1}H-NMR, ^{13}C-NMR, 2D ^{1}H–^{1}H COSY, ^{1}H–^{13}C HSQC, ^{1}H–^{13}C HMBC NMR, DEPT-135, IR, UV-vis and mass spectroscopy (ESI-MS, APCI-MS) and some of the complexes are analyzed by X-ray diffraction . We successfuly isolated some single crystals suitable for X-ray diffraction analysis. Five new crystal structures were determined: tetranuclear molecule (core consists of two, 5-coordinate Cu^{II} atoms and two, 6-coordinate Cu^{II} atoms) held together by six meclofenamic acid molecules as ligands and two DMSO groups, $[Cu_4(MCFA)_6(OH)_2(DMSO)_2].2DMSO$; $[Cd(MCFA)_2(DMSO)_2]$ held together by two meclofenamic acid molecules as ligands and two DMSO groups; three isostructural molecules $[M^{II}(lorn)_2(O\text{-}dmso)_2]$ (M = Mn, Cu Cd), held together by two lornoxicam molecules $Lorn^-$ anions act as chelators through the nitrogen atoms of the pyridine ring and through the amidic oxygen) and two DMSO groups.

Biological studies are dealing with anti-proliferative activit *in vitro* of twenty four meclofenamic acid, flufenamic acid, lornoxicam, cefaclor Mn(II), Cu(II), Zn(II), Cd(II) complexes as well as free drugs against the cells of three human cancer cell lines, MCF-7 (breast cancer cell line), T-24 (bladder cancer cell line), and A-549 (non-small-cell lung carcinoma), and a mouse fibroblast L-929 cell line. The IC_{50} values shown by new metal complexes, against T-24 cancer cell line, are in a molar range similar or better to that of well known chemotherapeutic cisplatin that is selected as references. The IC_{50} value shown by $[Mn(Lorn)_2]$, against MCF-7 cancer cell line is similar to that of cisplatin. The superoxide dismutase activity was measured, and IC_{50} value is determined by the Fridovich test. All the studied copper(II) and manganese(II) complexes presented a relatively low SOD-like activity, higher than 1 μM, however it was noted that the IC_{50} values for $[Cu(MCFA)_2(H_2O)]$ and [Cu(AcO)(MCFA)] lay at the region, where are considered as potent SOD mimics.

In the Experimental part, the procedures which was followed for the synthesis of manganese(II), copper(II), zinc(II) and cadmium(II) complexes with drugs, the experimental techniques applied for the

analysis are described. Basic requirements of sod assay and cells in culture as well as basic laboratoty design and selection of equipment of cells in culture are also described.

Περίληψη

Η παρούσα διδακτορική διατριβή περιλαμβάνει την σύνθεση και την μελέτη κρυσταλλικών δομών, φασματοσκοπικών δεδομένων και της βιολογικής δράσης συμπλόκων μαγγανίου(II), χαλκού(II), ψευδαργύρου(II) και κάδμιου(II) με φάρμακα. Για τον σκοπό αυτής της διατριβής επιλέχθηκαν τρία μέλη φαρμάκων NSAIDs: meclofenamic acid, (N-(2,6-dichloro-3-methylphenyl) anthranilic acid), flufenamic acid (N-[3-(trifluoromethyl)-phenyl]-anthranilic acid) and lornoxicam (6-chloro-4-hydroxy-2-methyl- 2-pyridyl-2*H*-thieno[2,3-*e*]-1,2-thiazine-3- amide-1,1-dioxide). Επίσης, επιλέχθηκε και η κεφαλοσπορίνη, cefaclor [7-(D-2-amino-2-phenylacetamido)-3-chloro-3-cepham-4-carboxylic acid].

Η διατριβή αποτελείται από τρεις κύριες ενότητες: την Εισαγωγή (κεφάλαια I-VII), τα Αποτελέσματα και Συζήτηση (κεφάλαια VIII-XIII) και το Πειραματικό Μέρος (κεφάλαια XIV-XVI). Στα πρώτα κεφάλαια πραγματοποιείται μία εκτενής αναφορά στα μη-στεροειδή αντι-φλεγμονώδη φάρμακα (NSAIDs). Η αντι-φλεγμονώδης δραστικότητα των NSAIDs καθώς και οι περισσότερες από τις άλλες φαρμακολογικές τους δραστικότητες σχετίζονται με την αναστολή της μετατροπής του αραχιδονικού οξέος (AA) σε προσταγλαδίνες, που αποτελούν ενδιάμεσα της φλεγμονώδους διαδικασίας. Τα ένζυμα κυκλοοξυγενάση (COX) και λιποξυγενάση (LOX), τα οποία καταλύουν τον οξειδωτικό μεταβολισμό των αμινοξέων, αποτελούν χρήσιμους στόχους για τον σχεδιασμό και την ανάπτυξη νέων φαρμάκων που ουσιαστικά αναστέλλουν την δημιουργία των τελικών φλεγμονωδών παραγώγων και την ανάπτυξη της φλεγμονής. Από πρόσφατες μελέτες προκύπτει ότι εκτός από την αρθρίτιδα και τον πόνο, ο καρκίνος και νευροεκφυλιστικές ασθένειες όπως το Alzheimer μπορούν πιθανά να θεραπευθούν με αναστολείς της COX.

Στο δεύτερο κεφάλαιο μελετάται ο ρόλος των επιλεγμένων μεταλλικών ιόντων στα βιολογικά συστήματα.

Τα επόμενα κεφάλαια (III και IV) αναφέρονται στα μεταλλικά σύμπλοκα των NSAIDs. Τα μεταλλικά σύμπλοκα με ενεργά φάρμακα ως υποκαταστάτες αποτελούν ένα ερευνητικό πεδίο αυξανόμενου ενδιαφέροντος για την ανόργανη και φαρμακευτική χημεία και έχουν συγκεντρώσει μεγάλη προσοχή ως μία προσέγγιση στην ανάπτυξη νέων φαρμάκων. Η σύνθεση μεταλλικών συμπλόκων με μη-στεροειδή αντι-φλεγμονώδη φάρμακα (NSAIDs) ως υποκαταστάτες απέκτησε νέα ώθηση τον περασμένο αιώνα. Πρώτον, στη βάση της καθαρής χημείας ένταξης τα NSAIDs αποτελούν ιδιαίτερα ευέλικτους υποκαταστάτες και δείχνουν μία τεράστια ποικιλία τρόπων υποκατάστασης ως συνέπεια των μεταλλικών και των περιβαλλοντικών συνθηκών. Οι πληροφορίες που συλλέχτηκαν από συνθετικές και δομικές μελέτες καθώς και μελέτες αντίδρασης έχουν ιδιαίτερη σημασία για διάφορα πεδία που επεκτείνονται από τις βιοεπιστήμες μέχρι τις επιστήμες υλικών. Δεύτερον, τα NSAIDs διαθέτουν πολυάριθμες εφαρμογές σαν φαρμακευτικοί παράγοντες. Τρίτον, ο σχηματισμός συμπλόκων με συγκεκριμένα μέταλλα για αυτόν τον τύπο φαρμάκων είναι πολύ πιθανό να βελτιώσει την δραστικότητα ενάντια σε συγκεκριμένες ασθένειες και να αυξήσει το φάσμα δραστικότητας. Ο συνδυασμός δύο ή περισσότερων διαφορετικών ειδών στην ίδια ένωση μπορεί να οδηγήσει σε έναν πολυ-θεραπευτικό υλικό. Η χημεία ενταξης των μη-στεροειδών αντι-φλεγμονώδων φαρμάκων (NSAIDs) έχει μελετηθεί από πολλές ερευνητικές ομάδες παγκοσμίως. Ορισμένα σύμπλοκα έχουν

αυξήσει την φαρμακευτική ή βιολογική δραστικότητα λόγω του φαρμάκου, ή είναι ενδιαφέροντα από καθαρή χημική πλευρά.

Το κεφάλαιο V περιέχει μία σύντομη συζήτηση για το β-αντιβιοτικό, cefaclor σαν μέλος των κεφαλοσπορινών.

Σύντομες αναφορές που αφορούν την δραστικότητα της υπεροξειδικής δισμουτάσης, SOD mimetics και τα καρκινικά κύτταρα που επιλέχτηκαν να μελετηθούν στην παρούσα διδακτορική διατριβή συμπεριλαμβάνονται στα κεφάλαια VI και VII. Τα SODs ένζυμα έχουν μοριακά βάρη ιδιαίτερα υψηλά για να διαπεράσουν τις κυτταρικές μεμβράνες και μπορούν μόνο να παρέχουν εξωκυττάρια προστασία. Για να παρακαμφθεί αυτή τη δυσκολία, ένα σταθερό μη-τοξικό, χαμηλού μοριακού βάρους μεταλλικό σύμπλοκο το οποίο καταλύει την αυτοοξειδοαναγωγή του υπεροξειδικού ανιόντος μπορεί να αποτελέσει μία κατάλληλη εναλλακτική λύση για την υπεροξειδική δισμουτάση σε κλινικές εφαρμογές με τις επιθυμητές ποσότητες χαμηλού κόστους, κυτταρική διαπερατότητα και μη-ανοσογονικότητα.

Σκοπός της έρευνας αυτής ήταν η επέκταση του φαρμακολογικού προφίλ επιλεγμένων φαρμάκων ώστε να ερευνηθούν νέες ιδιότητες όπως αντιοξειδωτικές και αντικαρκινικές δραστικότητες, η προετοιμασία νέων ενώσεων, συμπλόκων του meclofenamic οξέος, του flufenamic οξέος, του lornoxixam οξέος και του cefaclor με ουσιώδη μεταλλικά ιόντα, τα οποία πιθανών να επιδείξουν βελτιωμένες ή διαφορετικές βιολογικές δραστικότητες συγκρινόμενες με γονικά φάρμακα.

Στο δεύτερο μέρος της διατριβής πραγματοποιείται συζήτηση των αποτελεσμάτων σύμφωνα με τα πειραματικά δεδομένα. Αναφέρονται οι συνθέσεις με μαγγανίο(II), χαλκό(II), ψευδαργύρο(II) και οξικό κάδμιο(II) και/ή χλωριούχο κάδμιο(II) είτε με αντι-φλεγμονώδη φάρμακα είτε με το β-αντιβιοτικό, cefaclor σε μεθανόλη, σε μοριακή αναλογία μετάλλου με υποκατάστατη 1:2 και 1:1. Όλα τα νεοσυντιθέμενα σύμπλοκα μελετήθηκαν με στοιχειακή ανάλυση, XRF και τις φασματοσκοπικές τεχνικές ^{1}H-NMR, ^{13}C-NMR, 2D ^{1}H-^{1}H COSY, ^{1}H-^{13}C HSQC, ^{1}H-^{13}C HMBC NMR, DEPT-135, IR, UV-Vis και φασματοσκοπία μάζας (ESI-MS, APCI-MS) και ορισμένα σύμπλοκα αναλύθηκαν με XRD. Απομονώσαμε επιτυχώς κάποιους μονο-κρυστάλλους κατάλληλους για X-ray ανάλυση. Πέντε νέες κρυσταλλικές δομές προσδιορίστηκαν: το τετραπυηνικώ μόριο (ο πυρήνας συνίσταται από δύο, πενταενταγμένα μόρια Cu^{II} και δύο εξαενταγμένα μόρια Cu^{II}) που συγκρατούνται από έξι μόρια meclofenamic οξέος ως υποκατάστατες και δύο μόρια DMSO, $[Cu_4(MCFA)_6(OH)_2(DMSO)_2].2DMSO$; $[Cd(MCFA)_2(DMSO)_2]$ που συγκρατούνται από δύο μόρια meclofenamic οξέος ως υποκατάστατες και δύο μόρια DMSO; τρία ισοδομικά μόρια $[M^{II}(lorn)_2(O\text{-}dmso)_2]$ (M=Mn, Cu, Cd), που συγκρατούνται από δύο μόρια lornoxicam (ανιόντα $lorn^-$ δρουν χηλικά μέσω των ατόμων αζώτου του πυριδινικού δακτυλίου και του αμιδικού οξυγόνου) και δύο μόρια DMSO.

Οι βιολογικές μελέτες αφορούν την αντιπολλαπλασιαστική δράση *in vitro* των 24 συμπλόκων του meclofenamic οξέος, του flufenamic οξέος, lornoxixam οξέος και του cefaclor με Mn(II), Cu(II), Zn(II), Cd(II) καθώς και των υποκαταστατών ενάντια σε τρεις κυτταρικές καρκινικές σειρές ανθρώπου, MCF-7 (καρκίνος του μαστού), T-24 (καρκίνος ουροδόχου κύστης), A-549 (καρκίνος του πνεύμονα) και μία καρκινική κυτταρική σειρά από ινοβλάστες ποντικού L-929. Οι τιμές IC_{50} των νέων συμπλόκων, ενάντια στην κυτταρική σειρά T24, είναι παρόμοιες ή και καλύτερες από εκείνες του γνωστού χημειοθεραπευτικού cisplatin το οποίο επιλέχθηκε ως ένωση αναφοράς. Η τιμή IC_{50} του συμπλόκου

[$Mn(Lorn)_2$] ενάντια στην MCF-7 σειρά είναι παρόμοια με αυτή του cisplatin. Επίσης μετρήθηκε και η δράση της υπεροξειδικής δισμουτάσης και η τιμή IC_{50} προσδιορίστηκε με το Fridovich test. Όλα τα σύμπλοκα χαλκού(II) και μαγγανίου(II) παρουσίασαν μία σχετικά χαμηλή SOD δραστικότητα, μεγαλύτερη από 1μM, ενώ οι IC_{50} τιμές για τα [$Cu(MCFA)_2(H_2O)$] και [Cu(AcO)(MCFA)] βρίσκονται στα επίπεδα όπου μπορούν να θεωρηθούν ως ικανοί SOD μιμητές.

Στο πειραματικό μέρος περιγράφονται οι διαδικασίες που ακολουθήθηκαν για την σύνθεση των συμπλόκων μαγγανίου(II), χαλκού(II), ψευδαργύρου(II) και καδμίου(II) με φάρμακα καθώς και οι πειραματικές τεχνικές που εφαρμόστηκαν για την ανάλυσή τους. Επίσης περιγράφονται και οι βασικές απαιτήσεις για την μέθοδο SOD και την καλλιέργεια των κυττάρων καθώς και ο βασικός εργαστηριακός σχεδιασμός και η επιλογή του εξοπλισμού για την καλλιέργεια των κυττάρων.